The University Of Sheffield.

Development of a Composite Tissue Engineered Alveolar Bone–Mucosal Model Using Conventional and 3D Printed Scaffolding Techniques

Thafar Almela

A thesis submitted in partial fulfilment of the requirements for the degree of Doctor of Philosophy

School of Clinical Dentistry

Faculty of Medicine, Dentistry and Health

University of Sheffield

United Kingdom

September 2018

DECLARATION

The work referred to in this thesis has not been submitted in support for any other qualification at this or any other University or Institute of learning.

ABSTRACT

Advances in tissue engineering have allowed the construction of various tissues of the oral and maxillofacial region for clinical and *in vitro* modelling proposes. Additive manufacturing, also known as three−dimensional printing (3DP) is an innovative technique that offers an entirely new method of fabricating geometrically precise 3D structures, allowing the opportunity to progress composite tissue engineering to the point where complex anatomical relationships can be accurately replicated. The aim of this study was to develop and characterise a novel 3D composite human alveolar bone−mucosal model (ABMM) based on conventional and 3D printed bone scaffolds.

Two types of bone scaffold were used: firstly, a conventional hydroxyapatite/tricalcium phosphate (HA/TCP) scaffold fabricated using an aqueous gel-casting method, and secondly, a 3D printed β−tricalcium phosphate (β−TCP) scaffold prepared using an extrusion−based Rapid Prototyping plotting system. In order to construct a composite bone−mucosal model, alveolar bone-derived osteoblasts were seeded into the respective scaffolds (both conventional and printed) and the resultant bone constructs were then attached to a tissue engineered, collagen−based oral mucosa. Histological, immunohistochemical, and ultrastructural features of the mucosal part as well as, the histology, genes expression, and proteins secretion of the composite models were examined to validate the ABMM as a representative analogue of combined oral hard and soft tissues.

The mucosal component demonstrated a mature epithelium undergoing terminal differentiation similar to that of native oral mucosa, as confirmed using cytokeratin immunohistochemistry. Histological evaluation of ABMM confirmed an anatomically representative tri-layer consisting of distinct epithelial, connective tissue, and bone layers.

Interrogation of osteogenic and epithelial−related gene expression within the models confirmed an osteogenic expression profile in the tri−layered model that was not observed in epithelial−stromal bilayers. Collectively, these data suggest that the developed composite model displayed characteristics similar to those of normal tissue counterparts. This novel tri−layered model, therefore, may offer great scope as a more advanced, and anatomically representative tool for a number of *in vitro* applications.

ACKNOWLEDGMENTS

"My Lord, increase me in knowledge". With this prayer, I always ask almighty God to give me the wisdom, and whoever has been given wisdom has certainly been given much good. All praise to God for the strength, support, and patience he bestowed upon me in order to satisfactorily complete this journey.

This work would not have been possible without the support of my family, supervisors, staff, and friends. I genuinely owe a debt of gratitude to all my family, particularly my parents for their love, support, and encouragement to follow my dreams and success in all of my pursuits.

I would like to express my very great appreciation to all my supervisors; Prof. Ian Brook, Dr. Keyvan Moharamzadeh, and Dr. Robert Bolt. Prof. Brook has given me his most wonderful intellectual support, constant encouragement and careful guidance throughout this project. My most sincere gratitude to Dr. Moharamzadeh for his valuable constructive suggestions during the planning and development of this research work. His understanding, patience, motivation, and willingness to teach me every research skill has continuously stimulated my passion to achieve more with confidence. My thanks extended to Dr. Bolt for his help and support in completing this project.

I would like to thank all the staff in the dental school particularly Dr. Jill T Callaghan and Mrs. Kirsty L Franklin for teaching me the tissue culture skills essential to my Ph.D. Thanks also go to Mrs. Brenka McCabe and Mr. Jason Heath for their assistance in the molecular biology laboratory work. My thanks to Mr. David Thompson for his help in the preparation of samples for histological examination. I would also like to thank Mr. Christopher J Hill at the Department of Biomedical Science for his excellent technical assistance in preparation of samples for scanning and transmission electron microscopy examination. My thanks are

further extended to Mrs. Kirsty Nicholson at the Medical School for her assistance in micro-CT imaging. Also, I would like to thank everyone in Unit of Oral and Maxillofacial Surgery, especially Mrs. Geraldine Temprell for assisting in the process of consenting patients and collecting biopsies.

My sincere thanks go to Dr. Lobat Tayebi at Marquette University School of Dentistry in the USA for offering me the opportunity to conduct part of my project in her laboratory. I am very grateful for her generosity in providing all the necessary facilities including the 3D printing machine and demonstrating the process of biomaterial printing, which is very interesting topic to me. To her excellent team members, particularly, Mr. Morteza Rasoulianboroujeni and Dr. Kimia Khoshroo who helped me during my laboratory work, I appreciate your assistance, kindness, and the warm welcome I received.

Finally, I thank the Iraqi Ministry of Higher Education and Scientific Research for supporting and funding this project.

"The roots of education are bitter, but the fruit is sweet"

Aristotle

PUBLICATIONS AND CONFERENCE ABSTRACTS

Publications

Book chapter

- **Almela, T.**, Brook, I. M. & Moharamzadeh, K. Bone Tissue Engineering in Maxillofacial Region. In: Tayebi, L. & Moharamzadeh, K. 2017. Biomaterials for oral and dental tissue engineering: Oxford: Woodhead Publishing, 2017.

Peer-reviewed journal papers

1. **Almela, T**., Brook, I. M. & Moharamzadeh, K. 2016. Development of three-dimensional tissue engineered bone−oral mucosal composite models. *Journal of Materials* Science*: Materials in* Medicine*,* 27 (4), pp 65.
2. **Almela, T**., Brook, I. M. & Moharamzadeh, K. 2016. The significance of cell−related challenges in the clinical application of tissue engineering. *Journal of Biomedical Materials Research Part A*. 104 (12), pp 3157-3163.
3. **Almela, T**., Brook, I. M., Khoshroo, K., Rasoulianboroujeni, M., Fahimipour, F., Tahriri, M., Dashtimoghadam, E., El-Awa, A., Tayebi, L. & Moharamzadeh, K. 2017. Simulation of cortico−cancellous bone structure by 3D printing of bilayer calcium phosphate−based scaffolds. *Bioprinting,* 6, pp 1-7.
4. **Almela, T**., Al-Sahaf, S., Bolt, R., Brook, I. & Moharamzadeh, K. 2017. Characterisation of multi−layered tissue engineered human alveolar bone and gingival mucosa. *Tissue Engineering Part C: Methods*, 24 (2), pp 99-107.
5. **Almela, T**., Al-Sahaf, S., Brook, I. M., Khoshroo, K., Rasoulianboroujeni, M., Fahimipour, F., Tahriri, M., Dashtimoghadam, E., Bolt, R., Tayebi, L. & Moharamzadeh, K. 2018. 3D printed tissue engineered model for bone invasion of oral cancer. *Tissue and Cell*, 52, pp 71-77.
6. Tayebi, L., Rasoulianboroujeni, M., Moharamzadeh, K., **Almela, T. K. D**., Cui, Z. & Ye, H. 2018. 3D−printed membrane for guided tissue regeneration. *Materials Science and Engineering: C*, 84, pp 148-158.

Conference abstracts

1. **Almela T**, Brook, IM and Moharamzadeh K. Development of three−dimensional models of bone and oral mucosa. British Society for Oral and Dental Research (BSODR) Annual Meeting. Cardiff, UK, September 2015. The poster won the commendation (2nd place) for Unilever Poster Prize.
2. Moharamzadeh K, **Almela T**, Tayebi L, Brook IM. Advanced Tissue−Engineered Models of Complex Human Oral Tissues. American Association of Dental Research (AADR). Los Angeles, California, USA, March 2016.
3. Tayebi L, **Almela T**, Moharamzadeh K, Jazayeri H, Rasoulianboroujeni M, Dashtimoghadam E, Bures M. An Evaluation of a PCL/Halloysite Scaffold for Maxillofacial Tissue Regeneration. American Association of Dental Research (AADR). Los Angeles, California, USA, March 2016.
4. Bures M, Tayebi L, **Almela T**, Moharamzadeh K, Jazayeri H, Rasoulianboroujeni M, Dashtimoghadam E. Halloysite Improves Properties of 3D−Printed PLA Scaffolds for Tissue Engineering. American Association of Dental Research (AADR). Los Angeles, California, USA, March 2016.
5. Tayebi L, Moharamzadeh K, **Almela T**, Cui Z, and Ye C. Design criteria and production process of 3D−printed scaffolds for application in tissue engineering of full−thickness oral mucosa. The 3rd BIRAX Regenerative Medicine Conference, Oxford, April 2016.
6. Khoshroo K, **Almela T**, Tahriri M, Fahimipour F, Metalwala Z, Moharamzadeh K, Tayebi L. 3D−printing of porous calcium phosphate cements for bone tissue engineering. Academy of Dental Materials Conference, Chicago, October 2016.
7. **Almela T**, Brook IM, Khoshroo K, Rasoulianboroujeni M, Fahimipour F, Tahriri M, Dashtimoghadam E, Tayebi L, Moharamzadeh K. 3D−printed Bilayer Cortico−cancellous Calcium Phosphate Cement-based Bone Scaffold. American Association of Dental Research (AADR). San Francisco, California., USA, March 2017.
8. **Almela T**, Brook IM, Tayebi L, Moharamzadeh K. 3D−Printed Bone Scaffold in a Tissue Engineered Human Osteo−Mucosal Model. British Society for Oral and Dental Research (BSODR) Annual Meeting. Plymouth, UK, September 2017.
9. Binaljadm T, Moorehead R, **Almela T**, Franklin K, Tayebi L, Moharamzadeh K. Biomodification of Class−V Restorative Material by Incorporation of Bioactive Agents.

International Association of Dental Research (IADR) General Session & Exhibition. London, UK, 2018.

10. Shaikh Z, Franklin K, **Almela T**, Tayebi L, Moharamzadeh K. Biological Effects of Electronic Cigarette Liquid on Oral Mucosal Cells. International Association of Dental Research (IADR) General Session & Exhibition. London, UK, 2018.

Table of Contents

LIST OF FIGURES

LIST OF TABLES

ABBREVIATIONS

µ-CT	Micro-computed tomography
µg	Microgram
µm	Micrometre
µmol	Micromole
2D	2 Dimensional
3D	3 Dimensional
3DP	Three-dimensional printing
ABC	Alveolar bone construct
ABMM	Alveolar bone-mucosal model
ALI	Air-to-liquid interface
ALP	Alkaline phosphatase enzyme
ALPL	Alkaline phosphatase gene
AM	Additive manufacturing
ANOVA	Analysis of variance
ARS	Alzarin red stain
B_2M	B-2-microglobulin
BC	Bone construct
BGLAP	Bone gamma-carboxyglutamic acid-containing protein
BMM	Bone mucosal model
BMPs	Bone morphogenic proteins
BSA	Bovine serum albumin
β−TCP	β−tricalcium phosphate
BTE	Bone tissue engineering
Ca^{2+}	Calcium ion
$CaCl_2$	Calcium chloride
CAD	Computer-aided design
CDMEM	Complete Dulbecco's modified Eagle's medium
cDNA	Complementary deoxyribonucleic acid
CK	Cytokeratin protein
CO_2	Carbon dioxide

COL1	Type I collagen protein
COL1A1	Collagen I alpha 1 gene
Conc	Concentration
Ctrl	Control
DAPI	4',6-diamidino-2-phenylindole
dH_2O	Distilled water
DMEM	Dulbecco's Modified Eagles Medium
DMSO	Dimethyl sulfoxide
DNA	Deoxyribonucleic acid
DPX	Dibutyl phthalate, polystyrene, xylene
dsDNA	Double stranded DNA
ECM	Extracellular matrix
EDTA	Ethylenediamine tetra-acetic acid
EGF	Epidermal growth factor
ELISA	Enzyme-linked immunosorbent assay
EOM	Engineered oral mucosa
FBS	Foetal bovine serum
FDA	Food and Drug Administration
FDM	Fused deposition modelling
FFPE	Formalin-fixed paraffin-embedded
FITC	Fluorescein isothiocyanate
FSP	Fibroblasts surface protein
g	Gravity
H&E	Haematoxylin and eosin
HA/TCP	Hydroxyapatite/Tricalcium phosphate
HAOBs	Human alveolar osteoblasts
HCL	Hydrochloric acid
HEPES	4-(2-hydroxyethyl)-1-piperazinethanesulfonic acid
hESCs	Human embryonic stem cells
HLA	Human leukocyte antigen
hMSCs	Human mesenchymal stem cells

i3T3	Irradiated murine 3T3 fibroblasts
IDA	Industrial denatured alcohol
IF	Immunofluorescence
Ig	Immunoglobulin
iPSCs	induced pluripotent stem cells
IU	International unit
KRT	Cytokeratin gene
kV	Kilovoltage
LAA	L-ascorbic acid 2-phosphate
LSM	Laser scanning microscopy
mg	Milligram
ml	Millilitre
mM	Millimolar
mm	Millimeter
MSCs	Mesenchymal stem cells
MTT	(3-(4,5-dimethylthiazol-2-yl)-2,5-diphenyltetrazolium bromide)
NaOH	Sodium hydroxide
ng	Nanogram
NHOFs	Normal human oral fibroblasts
NHOKs	Normal human oral keratinocytes
nm	Nanometer
NOM	Normal oral mucosa
OC	Osteocalcin
OD	Optical density
OMF	Oral and maxillofacial
OMM	Oral mucosal model
ON	Osteonectin
OP	Osteopontin
P/S	Penicillin/Streptomycin
PB	PrestoBlue
PBS	Phosphate buffered saline

PFA	Paraformaldehyde
PLGA	Poly (lactide-co-glycolide)
pNPP	*P*-nitrophenyl phosphate
qRT-PCR	Quantitative real time polymerase chain reaction
rhBMPs	Recombinant human bone morphogenetic proteins
rhPDGF-BB	Recombinant human platelet-derived growth factor-BB
RNA	Ribonucleic acid
ROI	Region of interest
ROS	Rat osteosarcoma
RP	Rapid prototyping
rpm	Revolutions per minute
SD	Standard deviation
SEM	Scanning electron microscopy
SFF	Solid free form
SLA	Stereolithography
SLS	Selective Laser sintering
SPARC	Secreted protein acidic and rich in cysteine
SPP1	Secreted phosphoprotein-1
STR	Short tandem repeat
T3	3, 3, 5- Tri-iodothyronine
TE	Tissue engineering
TEM	Transmission electron microscopy
TERT	Telomerase reverse transcriptase
US	United States
v/v	Volume per volume
VEGFs	Vascular endothelial growth factor
w/v	Weight per volume
XRD	X−ray diffraction

INTRODUCTION

Tissue engineering (TE) can be defined as the process of recreating functional biological tissues by combining cells, materials, bioactive molecules, and environmental factors (Langer and Vacanti, 1993). Since the term TE was first introduced to the broader scientific community, this field of research has continued to advance at a tremendous pace, resulting in the achievement of 3D construction of various human tissues such as liver, pancreas, skin, muscle, vasculature, and cartilage (Langer and Vacanti, 2016; Ali and Robert, 2006; Khademhosseini and Langer, 2016). With the introduction of the TE concept to dentistry, many oral and dental tissue analogues have been developed including alveolar bone, oral mucosa, and periodontal structures (Amrollahi et al., 2016; Zafar et al., 2015).

The primary aim of TE is to ultimately achieve biological substitutes capable of resolving the need for clinical transplantation, with the TE substitutes acting to restore, maintain, and even improve tissue function (Langer and Vacanti, 1993). However, there are currently many challenges to overcome in order to produce clinically and physiologically relevant tissues capable to perform this function. Many of these challenges pertain to limitations of the TE process itself, such as a paucity of immunologically acceptable cell sources, lack of biomaterials that recapitulate the normal extracellular matrix, and difficulties with the generation of large areas of adequately vascularised tissue (Berthiaume et al., 2011).

In addition to the potential clinical applications of TE, 3D models of human tissues have been developed for *in vitro* study. The models can be used in the testing of biomaterial biocompatibility (Moharamzadeh et al., 2009), as well as investigation of the mechanisms of disease initiation and progression, such as oral cancer (Colley et al., 2011) and tissue infection (Pinnock et al., 2014). Such models may offer a unique opportunity to investigate the

interactions between multiple cell types, the surrounding matrix, and numerous environmental factors that would otherwise be difficult to study in a controlled manner. TE models offer insight into cell behaviour from biological, physiological and pathological perspectives, allowing novel products, diagnostics, and treatment approaches to be developed *in vitro* (Spector, 2002). Furthermore, the use of TE constructs for *in vitro* research may minimise the need for lengthy, costly, and controversial animal studies, which can furthermore deliver misleading results, due to interspecies molecular and physiological differences (Benam et al., 2015; van der Worp et al., 2010).

Development of composite constructs represents a new avenue in TE particularly in the oral and maxillofacial (OMF) region, where a variety of tissue types are in close association with each other. This intricate relationship of heterogeneous tissues poses a considerable challenge, not only in engineering the sheer number of tissue types required in order to replicate all tissues native to the orofacial region, but also in attaching these various tissue types to each other in a manner that recreates the normal anatomical relationships observed *in vivo* (Spicer et al., 2014). As a result, to date, very few intricately-structured TE composite tissues have been developed, although some success has been reported in the fabrication of osteochondral structures (Ruan et al., 2017) and also fibro-osseous structures capable of replicating the bone-periodontal ligament complex (Park et al., 2011).

The periodontium and region of the hard palate represent two oral structures where the mucosa tightly adheres to the underlying bone (Nanci, 2013). The periodontium is comprised of root cementum, alveolar bone proper, gingiva, and periodontal ligament. These components together form the tooth-supporting apparatus that anchor the tooth root to the jaws (Lang et al., 2015). Although the engineering of bone tissue (Thavornyutikarn et al., 2014) and oral mucosal equivalents (Moharamzadeh et al., 2012) have been extensively studied for

various clinical and experimental applications, *in vitro* combination of these two components into a single construct has not been investigated to date. Development of an accurate human alveolar bone-mucosal model represents the next important step in the process of achieving a physiologically relevant and utilisable TE oral construct.

In order to faithfully imitate the complex structure of native human bone, advanced TE techniques may be required. Recently, such advances have been achieved in computational design and additive manufacturing (AM), otherwise known as 3DP, which has enabled quick and accurate fabrication of 3D porous scaffolds with a highly controlled architecture (Cox et al., 2015; Bose et al., 2018). 3DP offers an alternative to current scaffold fabrication methods and has the potential to deliver precise scaffolds of a predefined shape, size, porosity, pore size, and spatial distribution; all of which can have significant impact on cell behaviour within TE models (Ferlin et al., 2016; Cavo and Scaglione, 2016).

The work described in this thesis demonstrates the development, optimisation, and characterisation of the composite human alveolar bone-mucosal models *in vitro* using both conventional and 3DP bone scaffolding methods.

Chapter 1: Literature review

NB: The work described in this chapter has been published in:

Almela, T., Brook, I. M. & Moharamzadeh, K. 2016. The significance of cell-related challenges in the clinical application of tissue engineering. *Journal of Biomedical Material Research A,* 104 (12), pp 3157-3163.

Almela, T., Brook, I. M. & Moharamzadeh, K. Bone Tissue Engineering in Maxillofacial Region. In: Tayebi, L. & Moharamzadeh, K. 2017. Biomaterials for oral and dental tissue engineering: Oxford: Woodhead Publishing, 2017.

1.1. Normal human alveolar bone–mucosal tissue

1.1.1. Overview of alveolar bone–mucosal structure

Alveolar bone, as with all bones, is comprised of two macroscopically distinguishable layers, termed “compact” and “cancellous”. Compact (cortical) bone is a dense outer layer, which forms the external and internal alveolar plates. These plates enclave the inner cancellous (spongy) bone which consists of thin trabeculae arranged in a 3D lattice, interspersed with marrow. Compared to compact bone, cancellous bone is less dense, more porous, and highly vascularized (Nanci, 2013). These differing features reflect the fact that each of the two bone types are functionally distinct; whilst the dense cortical plates confer strength and rigidity to the bone’s overall structure, the cancellous layer offers a degree of flexibility whilst also performing an important haemopoietic function.

Microscopically, bone may be also categorised as woven or lamellar. Woven bone represents an immature tissue in which collagen fibres are of a variable diametre and are arranged randomly, giving the bone a basket-weave appearance. Woven bone is formed rapidly, has a higher cellular turnover, and is subsequently converted into organised, fine-fibred, mature, lamellar bone (Berkovitz, 2009). Lamellar bone consists of three distinct layers: circumferential, concentric, and interstitial. While circumferential lamellae enclose the bone and form its outer and inner layer, concentric lamellae make the bulk of bone and form its basic metabolic unit, called the “osteon” or “Haversian system”. Each osteon consists of a bony cylinder surrounding a Haversian canal which is lined by a single layer of living osteocytes and contains a capillary at its centre. Adjacent canals are unified by Volkmann canals; blood vessels that form anastomoses between the capillaries of neighboring Haversian systems. Interstitial lamellae fill the spaces between adjacent concentric lamellae (Figure 1.1.).

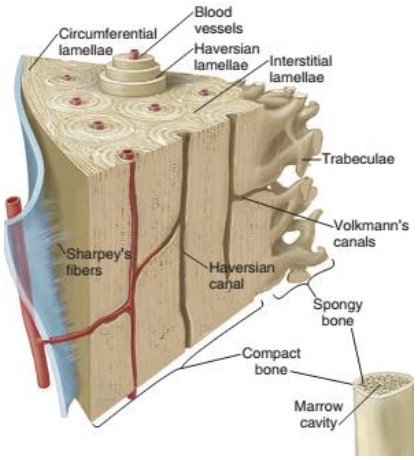

Figure 1. 1. Organisation of bone structure. The image illustrates the compact–cancellous bone structure and the arrangement of compact bone into circumferential, concentric, and interstitial layers (Nanci, 2013).

Overlying the external aspect of alveolar bone is a thin connective tissue membrane; the "periosteum". This membrane is, in fact, a bilayer comprising an outer fibrous layer that houses collagen fibrils and fibroblasts and an inner "cambium layer" that contains osteoblast progenitor cells and osteoclasts. Beyond the periosteal layer, which delineates the external boundary of the alveolar bone, a varying connective tissue layer (the lamina propria) links the bone to the overlying oral epithelium. In periodontium and hard palate, bone tightly bonds to a relatively thin lamina propria and overlaying keratinised epithelium; so-called "attached mucosa" (Nanci, 2013) (Figure 1.2.).

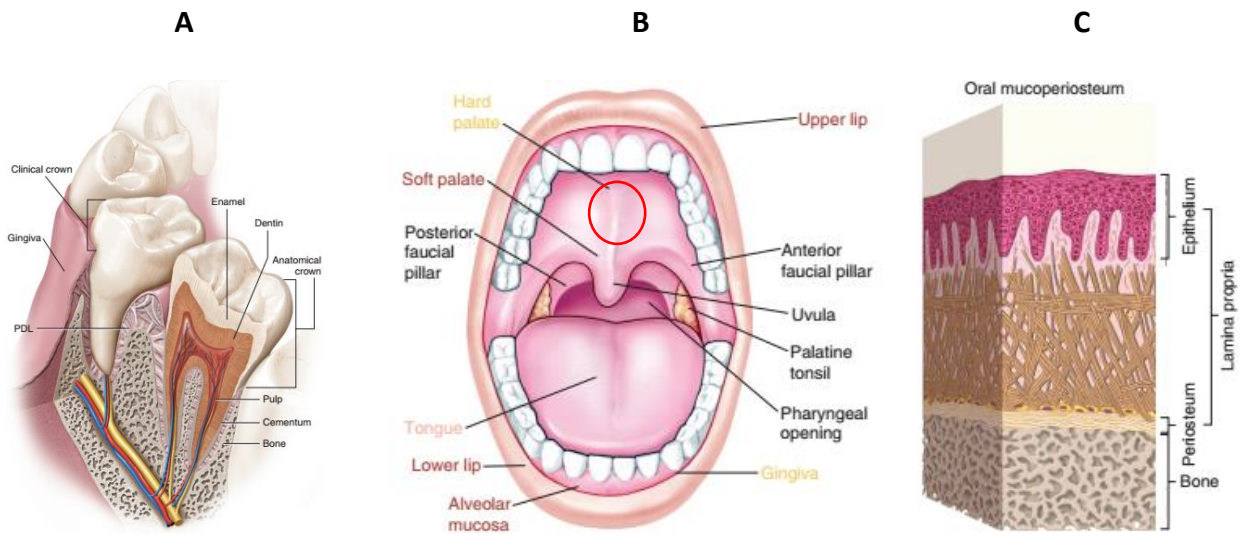

Figure 1. 2. The locations and arrangement of the native alveolar bone and associated mucosa. Images show the anatomical sites where the masticatory mucosa is firmly attached to the underlying alveolar bone; **(A)** the periodontium is comprised of alveolar bone, gingiva, cementum, and periodontal ligament; and **(B)** hard palate. **(C)** The histological arrangement of mucoperiosteum; the mucosa overlying the alveolar bone with a thin intervening layer of periosteum (Nanci, 2013).

1.1.2. Alveolar bone

1.1.2.1. Bone constituents

As with all connective tissues, bone consists of cells and extracellular matrix (ECM) (Figure 1.3.). However, two essential features distinguish it from other specialised connective tissues. The first feature is the presence of mineralisation within the ECM, which produces an extremely hard tissue capable of providing both support, protection, and storage of calcium and phosphate. The retention of adjacent non-mineralised compartments further allows the tissue to participate in haemopoesis (Ross, 2016). The second unique feature is its plasticity, which allows alteration of both its external shape "modelling" and also its internal structure "remodelling" (Berkovitz, 2009).

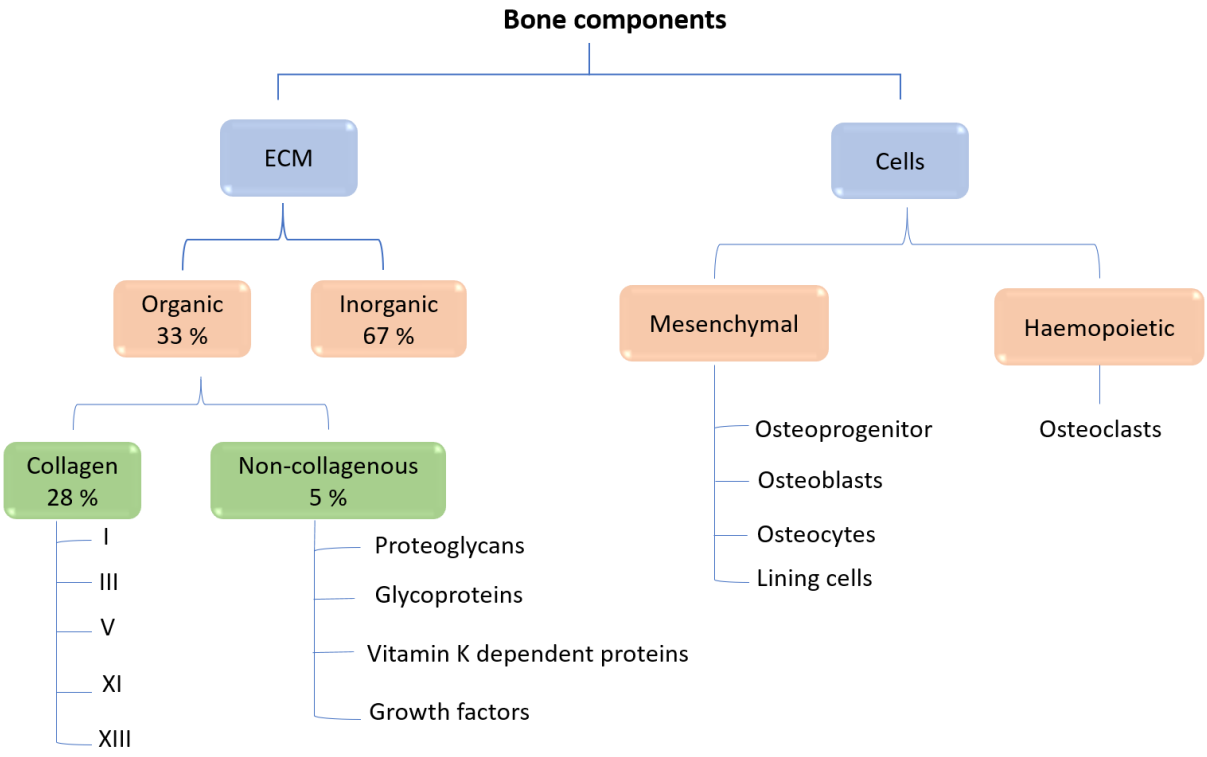

Figure 1. 3. The main components of alveolar bone.

1.1.2.1.1. Bone ECM

Bone's ECM consists by dry weight, of about 67 % inorganic phase and 33 % organic material (Nanci, 2013). The inorganic phase is composed of hydroxyapatite (HA) crystals $Ca_{10}(PO_4)_6(OH)_2$ which impart rigidity and hardness to bone. The organic matrix, or "osteoid", consists of collagen and non-collagenous proteins, of which type I collagen is the principal protein−comprising 90 % of all organic matrix. Type I collagen provides structural integrity to connective tissue and imparts resilience and tensile strength that helps bone to resist fracture. Non collagenous proteins account for the remaining 10 % of the total organic content and include four main groups, namely, proteoglycans, glycoproteins, vitamin K dependent proteins, and growth factors. Proteoglycans such as hyaluronan and chondroitin sulphate contribute to the compressive strength of bone and are responsible for binding

growth factors. Glycoproteins including osteonectin, osteopontin, and bone sialoprotein are responsible for attachment of bone cells to the matrix and gluing collagen to HA crystals. Vitamin K dependent proteins, including osteocalcin (OC), which captures calcium from the circulation and stimulates osteoclasts during bone remodelling; protein S, which assists in the removal of apoptosed cells. Growth factors and cytokines such as bone morphogenic proteins (BMPs) induce the differentiation of stem cells to osteoblasts (Ross, 2016).

1.1.2.1.2. Bone cells

Five cell types are associated with bone: osteoprogenitors, osteoblasts, osteocytes, bone lining cells, and osteoclasts. All cells except osteoclasts originate from mesenchymal stem cells which differentiate into osteoprogenitor cells, osteoblasts, and finally osteocytes and lining cells. Osteoclasts are derived from the fusion of mononuclear haemopoietic cells, namely granulocyte/monocyte progenitor cells, which differentiate into active bone resorbing cells (Ross, 2016).

Osteoprogenitor cells are renewable cells that can differentiate into *osteoblasts*−the chief cell responsible for secretion of matrix proteins, as well as calcification of unmineralised bone or osteoid. As osteoblasts progressively secrete these proteins, they ultimately become completely surrounded in a calcified matrix; whereby they are termed *osteocytes*. The main function of osteocytes is to maintain bone integrity and vitality by sensing the mechanical and biochemical environments and respond themselves or transduce signals to other cells participated in bone remodelling. Failure of this the mechanotransduction processes leads to bone sclerosis and death (Nanci, 2013). *Bone lining cells* cover the surfaces of non-remodelled bone and play a role in the metabolism of calcium and phosphate, protecting the surface of bone from the resorptive activity of osteoclasts, and may also participate in bone remodeling.

Osteoclasts are responsible for bone resorption by releasing protons and lysosomal hydrolases such as matrix metalloproteinases which degrade collagen and other matrix proteins in a concentric microenvironment of the extracellular space (Berkovitz, 2009; Ross, 2016).

1.1.2.2. Mechanism of bone formation (osteogenesis)

Osteogenesis involves the transformation of pre-existing mesenchymal tissue into bone through one of two major pathways; intramembranous ossification and endochondral ossification.

1.1.2.2.1. Intramembranous ossification

The direct conversion of mesenchymal tissue into bone is termed intramembranous ossification. The flat bones of the skull and face, the mandible, and the clavicles are formed via this pathway. During intramembranous ossification, osteogenesis is initiated by condensation of mesenchymal stem cells (MSCs) to form ossification centres. Within the ossification centres MSCs differentiate into osteoprogenitor cells, which further differentiate into osteoblasts and commence secretion of collagen and non-collagenous proteins such as osteocalcin, osteonectin, bone sialoprotein, and other matrix components; this proteinaceous secretion is termed “osteoid”. The osteoid subsequently undergoes mineralisation and the secretory osteoblasts either become osteocytes, convert to lining cells or undergo apoptosis. Mineralisation is initiated when the local concentration of calcium (Ca^{2+}) and phosphate (PO_4) ions in the matrix exceeds the normal threshold. Binding of Ca^{2+} with osteocalcin and other proteins increases the level of this ion and stimulates alkaline phosphatase (ALP) secretion by osteoblasts, which increases the concentration of PO_4. At this stage, the osteoblasts release small matrix vesicles containing ALP and pyrophosphate that

accumulate Ca^{2+} and cleave PO_4. This results in crystallisation of $CaPO_4$ which subsequently form and deposit HA crystals in the matrix. As mineralisation progresses, newly-formed bony trabeculae radiate out from the site of initial ossification and the area becomes surrounded by mitotic osteoprogenitor cells. These cells differentiate into new osteoblasts, and in turn lay down successive layers of woven bone which is subsequently replaced by lamellar bone (Ross, 2016) (Figure 1.4.). Ultimately, the matrix contains only 4−6 % osteoblasts and 1−2 % osteoclasts, whilst osteocytes comprise the vast majority of cells within the matrix (90−95 %) (McCauley and Somerman, 2012).

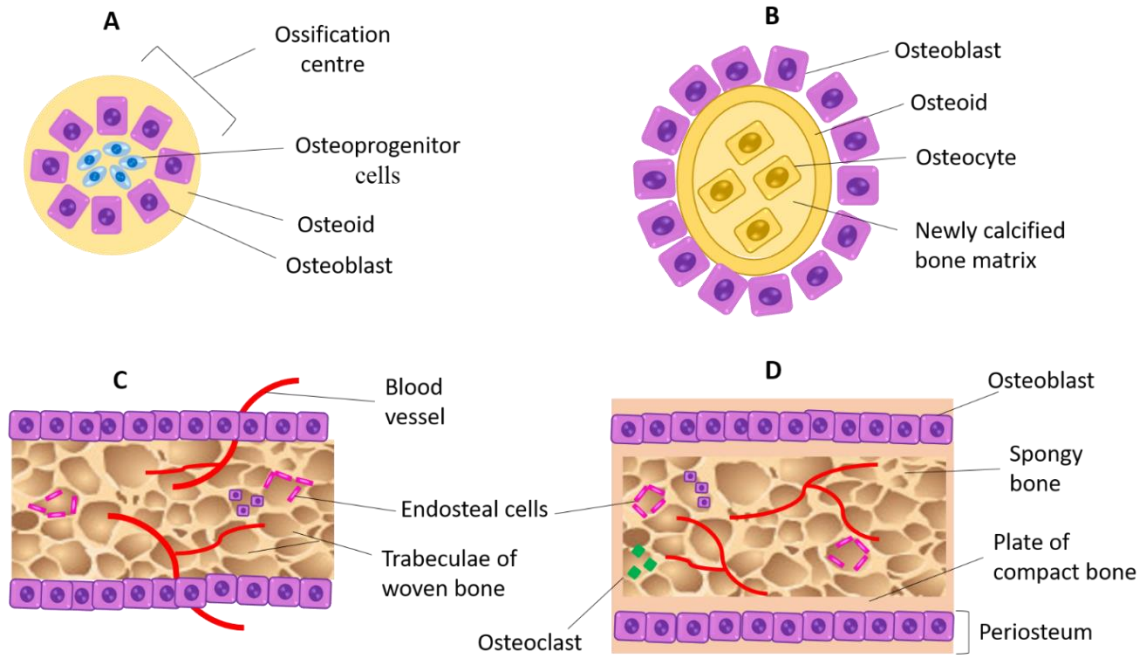

Figure 1. 4. Illustration of the mechanism of intramembranous ossification. (A) An ossification centre consists of aggregated mesenchymal osteoprogenitor cells that further differentiated to osteoblasts which begin osteoid secretion. **(B)** The osteoblasts accumulate at the periphery of the ossification centre and continue to produce and mineralise the osteoid, which traps osteoblasts to become osteocytes. **(C)** The immature woven bone has thick trabeculae lined by endosteal cells and osteoblasts. **(D)** The continued growth and remodelling of bone results in replacement of woven bone by outer and inner compact bone, with trabecular bone in between. The presence of osteoblasts, osteoclasts, and bone marrow cells that are brought by blood vessels indicates the active remodelling process.

1.1.2.2.2. Endochondral ossification

Endochondral ossification involves the production of a cartilaginous "template" which is eventually replaced by bone. All of the bones of the body, except for the flat bones of the skull, mandible, and clavicles, are formed through this pathway. The process can be divided into 5 phases.

Phases 1– Commitment: the commitment of MSCs to mature cartilage cells is induced by Sonic hedgehog which stimulates the adjacent sclerotome cells to express Pax1 transcription factor that initiates the cascade of the ossification.

Phase 2– Compaction: the committed cells then condense into compact nodules with inner and outer cells that generate cartilage and bone, respectively. BMPs are critical for driving this stage as they induce the expression of several cell adhesion molecules such as N-cadherin and neural cell adhesion molecule which are important in the initiation and maintaining of the condensations.

Phase 3– Proliferation: in the 3rd phase, chondrocytes divide rapidly and secret cartilage-specific ECM to form the cartilaginous template of the bone.

Phase 4– Growth: In the 4th phase, the proliferation ceases and the chondrocytes increase their volume to become "hypertrophic chondrocytes". This step appears to be mediated by Runt-related transcription factor 2, which is necessary for the development of both intramembranous and endochondral bone. The hypertrophic chondrocytes alter the matrix they secret by adding collagen X, fibronectin, a s well as vascular endothelial growth factor (VEGF) which induce mesenchymal cell transformation into blood vessels. In addition, at this stage, the calcification starts by secretion of numerous small, membrane-bound vesicles into the ECM. These vesicles are produced by chondrocytes and contain enzymes such as ALP that

are active in the generation of hydroxyapatite crystals, which mineralize the cartilaginous matrix in the same sequence of events occur in the intramembranous ossification.

Phase 5− Chondrocyte death and bone cell generation: The final phase involves apoptosis of the hypertrophic chondrocytes and differentiation of the cells surrounding the cartilage model into osteoblasts. In addition, the blood vessels invade the spaces and bring in osteoblasts which begin forming bone matrix on the partially degraded cartilaginous model. The cartilage matrix is then degraded by osteoclasts brought to the area via blood vessels (Gilbert, 2010).

1.1.3. Oral mucosa

Normal oral mucosa (NOM) can be divided into three types; *lining mucosa* found in lips, cheek, soft palate, floor of mouth, and the ventral surface of tongue; *masticatory mucosa* that covers the gingiva and hard palate; and *specialised mucosa* which present in the region of the tongue dorsum. For all regions of the mouth, NOM has two recognisable layers; epithelium and connective tissue (lamina propria) separated by a basement membrane. The epithelium is of stratified squamous type, which offers protection to the underlying tissue. Whilst the epithelia's principally comprises keratinocytes, there are a number of additional non−epithelial cells such as melanocytes, Langerhans cells, and lymphocytes which may be found within the layer. In masticatory mucosa (gingiva and hard palate), the epithelium is keratinised, with cells ordered into four distinct layers: the basal, prickle, granular, and keratinised layers (Figure 1.5.), whilst in non−keratinised epithelium the granular and keratinised layers are replaced by a stratum intermedium and superficial layer, respectively. Adhesion between adjacent epithelial cells is achieved via desmosomal attachments, while hemidesmosomes bind epithelium to the underlying connective tissue (Nanci, 2013).

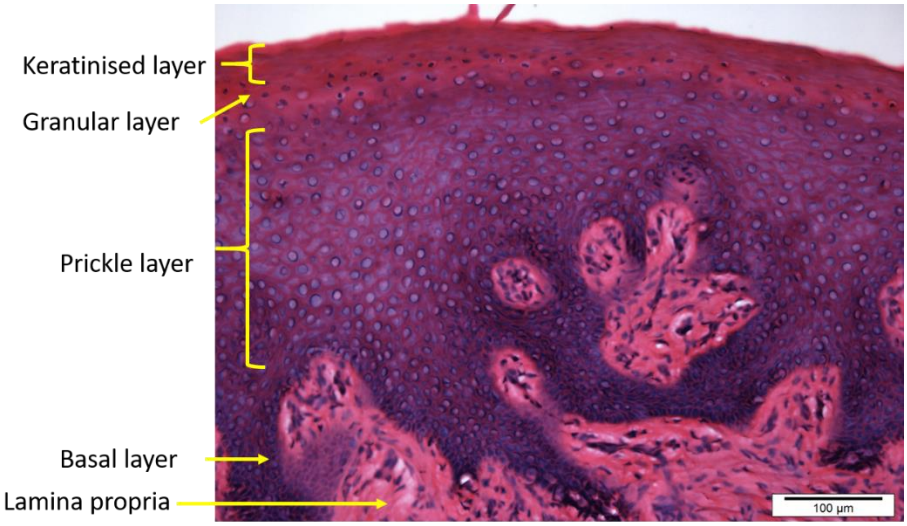

Figure 1. 5. Histologic section of keratinised oral mucosa (hard palate). Haematoxylin and eosin–stained section of palatal mucosa demonstrates the epithelial and connective tissue (lamina propria) components of keratinised oral mucosa. The mature oral epithelium in this image clearly demonstrates the respective strata, namely basal, prickle, granular, and keratinised layer (Scale bar=100 µm). This palatal gingiva was obtained with written, informed consent from a patient underwent elective oral surgery at Charles Clifford Dental Hospital, Sheffield, UK, under the ethical approval from National Research Ethics Services Committee number 15/LO/0116 (see appendix III). The detailed method of histological processing, sectioning, staining, and examination of the specimen was provided in section (2.3.6.2.).

The basement membrane is a specialised ECM containing collagen, glycoproteins, and proteoglycans, which are arranged into three distinct layers; the lamina lucida, lamina densa, and lamina reticularis. The underlying connective tissue comprises the lamina propria, which is responsible for support, nourishment, and sensation. It contains fibroblasts, mast cells, macrophages, blood vessels, nerves, and fibres embedded in ground substance. In the masticatory mucosa, the lamina propria is thick and tightly bound directly to the underlying bone “mucoperiosteum” without an intervening layer of submucosa (Avery, 2006; Berkovitz, 2009).

1.2. The need for composite alveolar bone−mucosal tissue engineering

1.2.1. Clinical need

Bone loss in the OMF region is a commonly encountered problem that can range in size from small periodontal defects to complex, difficult to manage structural defects (Elsalanty and Genecov, 2009). To illustrate the magnitude of this issue, data from the National Health and Nutrition Examination Survey showed the prevalence of severe periodontitis warranting surgery to be approximately 15 % of United States (US) population (Eke et al., 2012). In addition, the deficiency of bone and /or mucosa poses a considerable challenge in the success of the dental implant. Engineering of these tissues may provide a means to regain the bone volume and restore the integrity of mucosa to enhance the successful outcomes of dental implants while minimising complications (Wen et al., 2015). For more extensive bony defects, data from the British Association of Oral and Maxillofacial Surgeons reported that more than 4,000 facial injuries occur annually per 500,000 population (CWFI, 2010). A proportion of these fractures may require surgical revision in order to address deficits in post-treatment facial contour.

Conventional approaches in the treatment of bone defects include various types of bone grafts, guided tissue regeneration techniques, and osteodistraction. The origins of bone grafting can be traced back several centuries when the earliest xenografting procedure was reported in 1668 by Job Janszoon van Meekeren, who attempted to perform cranioplasty using dog bone. In 1821, Walther was credited with the first documented autograft procedure, although wound suppuration prevented full healing (Sanan and Haines, 1997). Sixty years later, the first published case report of successful inter−human bone transfer was performed by William MacEwen (Macewen, 1881) whereas the first introduction of synthetic

calcium phosphate as an alloplastic bone substitute material was at the turn of the 20th century (Albee, 1920).

As autografts contain all the essential elements for osteogenesis, they are considered the "gold standard". Nevertheless, autografts are on occasion associated with difficulties in obtaining adequate bone quantity to fully restore larger defects, and post−operative complications such as infection, dehiscence, and non-union may hamper the augmentation process, particularly when using non vascularised bone grafts which may have complication rates as high as 69 % (Miloro and Kolokythas, 2012). In addition, bone resorption may reach up to 50 % of the initial grafted volume (Kahnberg, 2010). Use of allograft or xenograft materials offer readily available, low−cost alternatives, although there have been some concerns with the risk of disease transmission; however the overall chance of disease transmission appears to be in the order of 1:1 million (Miloro and Kolokythas, 2012). Osteoconductive synthetic materials are another potential option, although their utility is limited by unfavourable mechanical properties and higher potential for resorption (Scheller et al., 2009).

Oral mucosal defects, as with bone defects, can be reconstructed by autografts taken from either the adjacent oral mucosa or using vascularised and non vascularised skin grafts. Direct oral mucosal grafting is limited by the availability of donor tissue, as well as donor site morbidity. Split and full thickness skin grafts are another option and have the advantage that they can be harvested in large quantities with relative ease, although there is often graft contracture and phenotypic mismatch between the mucosa and skin structure, as the latter contains skin appendages such as hair follicles and glands (Girod et al., 2009). Further limitations include the expression of different keratinisation patterns, skin being predisposed

to infection in the wet oral environment (Izumi et al., 2004), and scarring of the donor site due to healing by secondary intention (Glim et al., 2013).

1.2.2. Pre-clinical need in oral health research

In general, there are two major approaches to pre-clinical research; *in vivo* animal modelling and *in vitro* modelling. The latter is further subdivided into 2D and 3D cell culture.

1.2.2.1. Animal model

Animal models have been used to test and validate many hypotheses that have emerged from *in vitro* studies (Barré-Sinoussi and Montagutelli, 2015). However, many limitations of this approach are recognised. The first issue relates to the scope of the European Directive 2010/63/EU in animal protection and welfare. The established "three Rs rule" – ***replacement***, ***reduction***, and ***refinement*** **-** states that animals should not be used as long as non animal−based experiments are available, and that the number of animals used in experiments must be reduced to the minimum needed to reach a satisfactory conclusion, and that all provisions must be considered to minimise any harm inflicted on the animals (Kirk, 2017; Russell and Burch, 1959).

Secondly, the inter−species genetic and physiological differences between humans and animal models means any results obtained from animal work may not be reproduced in human studies and may lead to ineffective or even harmful effects (Greek and Menache, 2013). For bone engineering, a wide variety of mammalian species such as rabbit, canine, and dog have been used. However, there is no single clinically relevant animal model that can faithfully mimic human bone. The complex nature of bone is affected by a myriad of local and systemic variables, such as defect size, remodelling, age, gender, hormone levels, and

exposure to mechanical forces; this complexity leads to a gap in clinical translation, due to the difficulty of standardising such variables in animal models (Muschler et al., 2010).

1.2.2.2. *In vitro* model

1.2.2.2.1. 2D model

The majority of cell-based studies use conventional 2D cell cultures raised on flat and rigid substrates. However, monolayer culture often does not reflect the complex tissue microenvironment present *in vivo* due to the absence of a representative 3D which results in a lack of cell−to−cell communication and cell-to-matrix interaction. As a consequence, 2D cell culture tests may provide misleading data for anticipating *in vivo* responses because it does not faithfully mimic the normal structure and function of cells (Bhadriraju and Chen, 2002). Therefore, 2D does not faithfully mimic the normal structure and function of cells.

1.2.2.2.2. 3D model

To overcome the limitations associated with *in vivo* and 2D models, a growing number of studies have involved the development of physiologically relevant 3D standardised models suitable to biological, pathological, and pharmaceutical investigation (Huh et al., 2015; Linda and Melody, 2006; Peck and Wang, 2013). 3D spheroids or cell aggregates may represent the simplest example of 3D cell culture techniques. Spheroids are carrier−free microspheres in which a solid mass of cells is formed when cells are cultured on a non adherent surface (Hearnden, 2011). A number of methods can be used to create cell spheroids, including; hanging drop techniques, static liquid overlay techniques and centrifugation (Fennema et al., 2013). Spheroids may serve as a suitable model for replicating 3D relationships that cannot be achieved in 2D cultures and have been used extensively to create a model of the hypoxic tumour microenvironment (Sutherland et al., 1981). 3D spheroids have their limitations,

however, as their structure is homogenous and therefore lacks the intricacies necessary to accurately replicate a multi−layered tissue or organ.

The evolving capabilities of TE raise new opportunities to address the unmet clinical demand for more complex grafting materials as well as to create anatomically representative 3D tissue models for the study of complex physiological and pathophysiological processes *in vitro*. The following sections provide an insight into the concept of TE and the progress which has been made in the engineering of bone and oral mucosal tissues to date.

1.3. The paradigm of tissue engineering

TE applies the principles of cell biology, materials science, and engineering to create an artificial substitute for lost or damaged tissues that cannot be self−regenerated. The main strategy of TE is based on the concept that cells isolated from autologous tissue can be guided to form new tissue when placed with suitable matrices, in the presence of inductive molecules such as growth factors (Langer and Vacanti, 1993).

The cellular component of TE constructs is essential for the generation of new tissue, through the production and long−term maintenance of ECM. In fact, one of TE's great strengths over inorganic substitutes is the ability to incorporate cells capable of responding and adapting to the various mechanical and biological stimuli occurring within the recipient site to which they are exposed. Whilst non cellular material is subject to degradation and fatigue, which may then compromise its performance, an engineered construct contains cells that repair and remodel its ECM such that its properties should not degrade with time (Bonassar and Vacanti, 1998). In order to be effective for clinical purposes, cells should be easily procurable, scalable *in vitro*, and robust in both cell culture and following implantation. In addition, they should be obtained in an ethically acceptable manner, be able to functionally integrate with recipient

tissue, and be non immunogenic and safe; that is, neither tumorigenic nor contaminated by pathogens (Vacanti, 2006). Moreover, cells should ideally be capable of being processed so that they can have “off the shelf” availability, and furthermore, stem cells should have the capability to differentiate into the desired lineage (Birla, 2014).

The second component of the TE paradigm is an underlying scaffold on which to seed the cellular component. Scaffold usually provide mechanical support for cellular proliferation and differentiation (Boccaccini et al., 2014). In addition, it should fulfil the role of the normal ECM, which contributes not only to mechanical integrity, but also has an important signaling role in tissue regeneration (Juliano and Haskill, 1993). Inaccurately recapitulating the properties of the native ECM using scaffolds can result in a passive cell−matrix interface, which fails to trigger appropriate interactions, and thereby deprives cells of the substantial benefits that ECM constituents may have on cell phenotype (Birla, 2014). In order to further promote appropriate ECM formation within TE constructs, a new generation of scaffolds made from “smart biomaterials” has emerged to include a wider range of modifications, such as the incorporation of nanoparticles or bioactive molecules that can promote differentiation and attachment of cells onto the scaffold (Motamedian et al., 2015; Khan and Tanaka, 2018).

Growth factors comprise a wide range of proteins that play a key role in cellular differentiation and proliferation. The success of using bioactive molecules in TE mainly depends on the large−scale production of purified signal molecules and the development of appropriate method to deliver these molecules to their targets (Langer and Vacanti, 1993). Several delivery approaches have been attempted such as encapsulation of growth factors in biomaterial scaffold (Zhang et al., 2016) and using the gene technology to transfer the gene

encoding growth factor to specific cells which transplanted into the body where the growth factor will be released into the tissue to be engineered (Hadjizadeh et al., 2017).

1.4. Bone tissue engineering (BTE)

1.4.1. Strategies for BTE

The strategies for BTE can be broadly divided into *in vivo* and *in vitro*, depending on where tissue construction takes place (Elsalanty and Genecov, 2009). *In vivo* methods include *in situ* BTE, which involves implantation of osteoconductive, resorbable scaffolds into a bone defect to provide mechanical support for host cells (Khan et al., 2008) or *ectopic* implantation of the scaffold into muscle, which may then be transplanted as a free bone–muscle flap (Kokemueller et al., 2010). *In vitro* BTE, on the other hand, involves osteogenic cell harvesting, expansion, and seeding onto an appropriate scaffold, which should already be approved for clinical use if the engineered construct is intended for clinical applications. The seeded scaffold is then cultured *in vitro*, ideally in the presence of biophysical and biochemical signals that enhance osteogenesis (Mangano et al., 2009; Pradel and Lauer, 2012). While *in vivo* techniques provide a physiological environment that is difficult to reproduce in the laboratory, *in vitro* TE offers two distinct advantages: firstly, providing 3D geometries in a controlled culture settings that increased reproducibility and allows variability of results to be minimised, and secondly, addressing the scientific and ethical concerns related to animal tests (Gibbons et al., 2013).

1.4.2. Cell sources for BTE

Various cell types have been employed for BTE. Cells can be categorised as being derived from either human or animal sources.

1.4.2.1. Human cells

Human sources of bone cells may be either “autologous” or “allogenic”. Autologous cells are those obtained from a biopsy harvested from the individual who will subsequently receive the engineered tissue, whereas allogeneic cells are those derived from a human donor who is not the recipient of the final TE graft. Each type of cell source can be further described in terms of maturity: that is, differentiated cells and stem cells (Griffith and Naughton, 2002).

The main advantage of using differentiated primary human osteoblasts in the manufacture of bone equivalents is the elimination of interspecies differences and retaining the cell phenotype *in vitro.* However, growth and differentiation of primary human osteoblasts are affected by both donor age and site of cell origin, which may result in heterogeneous cell populations that exhibit phenotypic differences (Martínez et al., 1999). In addition, osteoblasts have a finite lifespan and limited proliferative potential which gradually declines until growth is irreversibly arrested as cells progress to senescence. This poses the risk that cell expansion may be insufficient to create a clinically relevant tissue should inadequate cells originally be harvested (Fisher, 2013).

Stem cells, in contrast, which include human mesenchymal stem cells (hMSCs), human embryonic stem cells (hESCs), and induced pluripotent stem cells (iPSCs), have a unique capacity for self−renewal, potency, and differentiation into various specialised cell types (Bhagavati, 2015). hMSCs are self−renewing and have the potential to be harvested and differentiated into bone−forming cells if cultured in the presence of β−glycerophosphate,

dexamethasone and ascorbic acid (Jaiswal et al., 1997; Coelho and Fernandes, 2000). Their potential in clinical applications has been investigated in a number of *in vivo* and *in vitro* studies, whereby regeneration of bone has been observed (Khojasteh et al., 2017; Weinand et al., 2016; Yuan et al., 2016). However, despite the many encouraging results, hMSCs carry several limitations from a tissue engineering perspective. The availability of hMSCs is extremely limited; the amount in bone marrow, for instance, is 1: 100,000 nucleated cells (El Tamer and Reis, 2009). In addition, progressive loss of functionality upon *in vitro* expansion has been reported (Wagner et al., 2008; Kim et al., 2009). Moreover, several studies have pointed out that certain culture conditions may affect the osteodifferentiation of hMSCs, including: seeding density (Zhou et al., 2011), co-culture with different cell types ((Seebach et al., 2010; Henrich et al., 2013), tissue source (Niemeyer et al., 2010; Yang et al., 2013),), and presence of specific growth factors (Biver et al., 2012).

Pluripotent hESCs derived from discarded human embryos (Shamblott et al., 1998; Thomson et al., 1998) also carry the potential to deliver an unlimited source of homogenous cells for bone engineering applications (Bielby et al., 2004; Bigdeli et al., 2010). However, the use of these cells appears to carry a number of risks, including teratoma formation and failure to consistently form bone (Przyborski, 2005), immune rejection following transplantation (Tan et al., 2014), and the ethical/ legal concerns associated with hESCs (Santos and Ventura-Junca, 2012); each of these risks hampers the potential use of hESCs in the clinical setting. Progenitor cells derived from hESCs may provide an alternative to hESCs for construction of bone substitutes (de Peppo et al., 2013b; Kim et al., 2008). However, the long-term safety and stability of bone engineered from these cells remain questionable.

Recently, iPSCs derived from the genetic reprogramming of somatic cells (Takahashi et al., 2007; Yu et al., 2007) have been introduced as an attractive source of stem cells and have displayed an osteogenic capability similar to, or higher than, hMSCs (Bastami et al., 2017; de Peppo et al., 2013a; Jin et al., 2013). The major concern in the clinical application of iPSCs remains the possibility of tumorigenesis associated with using genetically modified cells (Uri and Nissim, 2011).

In addition to normal human cells, human cell lines have been used in TE models, although their use has been limited to basic bone research. They have the advantages of carrying a relatively stable phenotype, are easy to maintain in culture compared to primary cells, allow large cell numbers obtained, and lack the need for isolation. Many bone−related cell lines have been developed and characterised, including human osteosarcoma cell lines SaOs−2 and MG-63 (Czekanska et al., 2012). However, progressive phenotypic changes induced by extensive passaging of the cell lines presents a limiting factor for their utility in tissue engineered models (Leis et al., 1997). In addition, cell lines cannot carry all phenotypic features of conventional bone cells, as they are normally stage arrested. Moreover, the proliferation of malignant cells is non-physiologic due to the disturbances of contact inhibition mechanisms and the genetic and epigenetic aberrations of cell cycle control. Although cell lines demonstrate a number of similarities with primary human osteoblasts, particularly in terms of genetic expression and mineralisation, no bone−derived cell line has been found to faithfully reproduce the characteristics of normal osteoblasts when used in TE models (Czekanska et al., 2014).

1.4.2.2. Animal cells

Due to the limitations associated with bone cells sourced from human, normal bone cells isolated from other species such as rat, bovine, and pig provide an alternative for *in vitro*

research model. The main advantage, compared to human cells, is their ease of accessibility and attainability so as they can be obtained from different sites. In addition, the selection of age, sex, and weight of the donor animal can be more controlled. The interspecies differences, on the other hand, represent a distinct disadvantage that makes extrapolation difficult (Pearce et al., 2007).

In addition to the normal animal cells, animal cell lines such as mouse cell line (MC3T3E1) (Czekanska et al., 2012) and rat osteosarcoma (ROS) cell line (Machida et al., 1995) were established and considered a popular choice for *in vitro* studies due to ease of culture and large cell yield. Nevertheless, the decline in proliferation and inconsistency in cell cycling which associated with high passage constitute a limiting factor (Grigoriadis et al., 1985).

1.4.3. Scaffold in BTE

1.4.3.1. Role and requirements of bone scaffold

According to the interaction between the biomaterial and its biological environment, three generations of biomaterials have been developed, namely, *bioinert*, *bioactive*, and *smart* or *gene-activating material* (Hench and Polak, 2002).

Contrary to what was thought for many years that scaffolds are a mechanical construct that acts as a carrier for cells and should be bioinert to avoid any foreign body reaction or scar formation, trend has shifted toward the concept of bioactive materials that have bio instructive role in stimulating the body's own repair process through guiding stem cell proliferation and differentiation to regenerate lost tissues (Ben-Nissan et al., 2014). The third generation is being designed to elicit specific cellular responses at a genetic level through a molecular modification of material. Such an informative role of "smart scaffold" can be achieved through control of the structural design or modifying surface properties by, for

example, adding nanoparticles, growth factors, or ECM-like molecules (Motamedian et al., 2015).

Ideally, several characteristics should be available in the chosen material to serve as a scaffold for BTE (Table 1.1.). However, no absolute advantageous biomaterial could be used for scaffold fabrication because every type has inherent drawbacks, instead, the selection depends on the particular application.

Table 1. 1. The ideal characteristics of scaffold for BTE.

	Criterion	***Definition***	***Reference***
1	Biocompatible	Capable of supporting normal cellular activity without local or systemic side effect.	(Williams, 2008)
2	Biodegradable	Varies according to the application. For example, 3−6 months in the craniomaxillofacial area or 9 months in spinal fusion	(Lichte et al., 2011)
3	Porous	Porosity is the ratio of the volume of open space to the total volume of the sample. Multiscale porosity is required with an optimal size of 300−500 μm for cell penetration, vascular invasion, and nutrients delivery.	(Thavornyutikarn et al., 2014; Tellis et al., 2009)
4	Interconnected	Interconnectivity is the degree of communication between pores in a 3D environment	(Yao et al., 2006)
5	Non-homogeneous	Multi-layered or gradient scaffolds that better mimic its original structure.	(Atesok et al., 2016)

6	Osteoconductive	Allows cells adherence, proliferation, and matrix secretion.	(Daculsi et al., 2013)
7	Osteoinductive	Induces progenitor cells recruitment and differentiation via biomolecules signalling	(Daculsi et al., 2013)
8	Mechanical properties	Comparable to the natural compressive strength of cancellous (2−20 MPa) and compact (100−200MPa) bones.	(Olszta et al., 2007)
9	Induce vasculogenesis	Forms new blood plexuses following the implantation and supports nutrient transport	(Gu et al., 2013)
10	Sterilisable	Can be sterilized without altering its properties	(Thavornyutikarn et al., 2014).

1.4.3.2. Biomaterials for bone scaffold

The current available biomaterials used for BTE can be grouped into ceramics and glass, natural and synthetic polymers, metal, or composite scaffold that is made up of two or more biomaterials such as a scaffold comprised of both ceramic and polymer (Bose et al., 2012) (Table 1.2.). Calcium phosphate bioceramics including HA, tricalcium phosphate (TCP), and biphasic calcium phosphate are promising candidates in BTE as their structure, chemical composition and properties in term of osteoconductivity and biocompatibility reflect the mineral component of bone matrix (Sulaiman et al., 2013; Feng et al., 2014). However, the brittleness, difficulty in processing, and a slow degradation rate are considered the main drawbacks (Ferracane et al., 2014b). Biodegradable polymers, by contrast, such as collagen and polylactic acid are biocompatible, versatile, and flexible therefore they can be processed easily (Jafari et al., 2017). Nevertheless, the weakness and the possibility of sudden loss of

their mass and mechanical integrity are among the major concerns regarding the use of biodegradable polymers as a scaffold, particularly in hard tissue applications (Yarlagadda et al., 2005). Biodegradable metals such as magnesium alloys that possess mechanical properties comparable to those of bone and degrade naturally within an aqueous environment may have higher mechanical properties and fracture toughness in comparison to biodegradable polymers (Yusop et al., 2012).

Table 1. 2. Types of biomaterials used as a scaffold in BTE.

Class	*Example*	*Advantages*	*Disadvantage*	*Reference*
Ceramic	HA	• Biocompatible. • Osteoconductive • Similar to the chemical structure of inorganic phase of bone.	• Slow biodegradation • Difficult to shape due to hardness, fragility, and brittleness	(Petrovic et al., 2012)
	TCP	Same to above	• Rigid and fragile • Faster resorption rate	(Miño Fariña et al., 2012)
	Bioglass	• Biocompatible • Osteoconductive • Bioactive • Promote angiogenesis • Enhance cell adhesion and proteins adsorption • Easy to control the chemical composition • Controlled degradation rate	• Brittleness • Low resistance to crack due to low strength and fracture toughness	(Fu et al., 2011)
Polymers– Natural proteins	Collagen, fibrin, alginate, silk fibroin, Hyaluronic Acid	• Biocompatible • Biodegradable without inflammation bioactive	• Poor mechanical strength • Rapid resorption	(Polo-Corrales et al., 2014)

Class	*Example*	*Advantages*	*Disadvantage*	*Reference*
Polymers– Natural Polysaccharides	Chitosan	• Biodegradable biocompatible • Has an antibacterial and bioadhesive properties • Promote wound healing	• Poor mechanical strength • Rapid resorption	(Polo-Corrales et al., 2014)
Polymers– Synthetic	Polyglycolic acid (PGA)	• Versatile • Reproducible • Thermoplastic so it can be shaped easily	• Inflammatory or immune reaction due to acid release in enzymatic biodegradation • Mechanical stability is of limited duration • Less biocompatible than natural • Not bioactive • Rapid resorption • Low solubility in organic solvent	(Carletti, 2011)
	poly-L-lactide acid (PLLA)	• Degrades slower and dissolves easier than PGA • Reproducible	• The potential to cause immune and foreign-body reactions because it does nor degrade completely • The mechanical stability is of limited duration	
	poly-ε-caprolactone (PCL)	• Slow degradation rate • Reproducible • Good workability	• Inflammatory or immune reaction • Mechanical stability is of limited duration	

Class	*Example*	*Advantages*	*Disadvantage*	*Reference*
Polymers– Synthetic	Hydrogel	• Modified easily • Biocompatible Biodegradable	• Contracted • Lack stiffness	(Polo-Corrales *et al*., 2014)
Metal	Titanium mesh	• High mechanical strength and fracture toughness • Biocompatible	• Corrosion may release toxic particles affecting the biocompatibility and induce an inflammatory reaction • Poor stimulation of new bone formation due to the elastic moduli which does not correspond with natural bone	(Chen et al., 2007)
Composite	PGA/β–TCP	• Better ability for osteogenesis, mineralization and biodegradation than HA	• Lack of osteoinductivity	(Cao and Kuboyama, 2010)
	Bioglass 45S5 and poly (D, L-lactide) polymer	Improved mechanical properties and resorption rate	Reaction with polymer changes the bioglass surface properties and compromised its bioactivity	(Abdollahi et al., 2013)

Class	*Example*	*Advantages*	*Disadvantage*	*Reference*
Composite	Poly (b-hydroxybutyrate-co-b-hydroxyvalerate) (PHBV) microsphere and poly (L-lactic-coglycolic acid) (PLGA).	• Supports drugs and growth factors delivery	• Changes in the surface topography and decrease porosity due to dehydration shrinkage	(Huang et al., 2010)
	hyaluronic acid-gelatine	• Good mechanical property Biocompatible • High porosity • Hydrophilic	• Suboptimal cell adhesion due to negative cell-scaffold interaction	(Linh et al., 2013)
	Nano HA/polymer	• Promote better cell adhesion and distribution • No significant inflammatory response • Biocompatible Improved mechanical properties	Unknown mechanism of cellular proliferation and differentiation	(Sun et al., 2011)

1.4.3.3. Manufacturing technologies for bone scaffold

To date, numerous techniques have been developed to fabricate 3D scaffolds. These techniques can be categorized into two principal groups: conventional fabrication technologies and solid free form (SFF) techniques; otherwise termed as rapid prototyping (RP). Each of these methods produces different characteristic features such as mechanical properties, porosity, and interconnectivity (Bose et al., 2018; Thavornyutikarn et al.). The following sections review the main conventional and SFF approaches used in BTE.

1.4.3.3.1. Conventional fabrication technologies

In these techniques, the desired conformation of the scaffold is obtained by subtracting parts of the material from the initial block (Thavornyutikarn et al., 2014).

1.4.3.3.1.1. Solvent-casting and particle leaching

In this technique, a polymer solution is dissolved in a solvent with uniformly distributed porogen particles of a particular size. Following solvent evaporation, a salt particles−embedded matrix is left behind, which is then immersed in water for salt leaching. The major advantages of this method are simplicity, high scaffold porosity, and the feasibility to control pore size and mechanical properties through adjusting the size of the particles (Annabi et al., 2010). For example, a nanohydroxyapatite−nylon composite scaffold was fabricated by using particle leaching. The resultant scaffold possessed high porosity with 200−500 μm pore size and mechanical properties comparable to native cancellous bone (Mehrabanian and Nasr-Esfahani, 2011). However, the main limitation of this technique is the very limited control of the interconnectivity of the pores in terms of degree and orientation. In addition, the need for removing the solid particles implies a limitation in shape which is restricted to thin sheets or tubes that are assembled later to a large construct. Finally, the use

of cytotoxic organic solvents requires a lengthy washing time to ensure complete removal of solvent and to reduce the risk of cell death (Annabi et al., 2010).

1.4.3.3.1.2. Freeze−drying

Freeze-drying, or lyophilization, involves dissolving a synthetic polymer in a suitable solvent then cooling the polymer solution down below its freezing point to produce thermodynamic instability that causes phase separation. The solvent is then removed by sublimation, leaving behind voids in the regions it previously occupied. The benefits of this method are the ability to incorporate biological factors due to the absence of high temperature and the possibility to use a wide range of natural and synthetic polymer (Roseti et al., 2017). However, irregular pores, lengthy processing time, high energy consumption, and the use of cytotoxic solvents limit the use of this technique (Ho et al., 2004).

1.4.3.3.1.3. Gas foaming

In this technique, a polymer mould is pressurized with inert gas foaming agents such as nitrogen or carbon dioxide until it is saturated with gas bubbles. The bubbles consequently form pores due to the thermodynamic instability that follows pressure dropping. This process produces a sponge−like scaffold with pore size ranging from 30 to 700 µm and 85 % total porosity. Although this method eliminates the need for cytotoxic solvent, the excessive heating during compression and closed, non-interconnected pores which may pose diffusion limitations constitute the main drawbacks (Thavornyutikarn et al., 2014).

1.4.3.3.1.4. Thermally induced phase separation

This low-temperature process involves the use of a volatile organic solvent of a low melting point to quench a polymer solution and to induce phase separation. This forms a polymer−rich phase that solidifies and a polymer-poor phase that evaporates; leaving a porous nanoscale network (Roseti et al., 2017). The principal advantage of this method is that various

architectures and high porosity can be obtained by controlling several parameters such as separation temperature, polymer concentration, and types of polymer and solvent (Molladavoodi et al., 2013). Despite high porosity, the small pore size of 50−500 nm limits the usefulness of such scaffolds in BTE and makes them more suitable for growth factors or drug delivery (Smith et al., 2009; Qiu et al., 2016).

1.4.3.3.1.5. Sol-gel technique

The sol−gel process is based on the polymerization of metal alkoxide and the formation of sol by the addition of surfactant followed by condensation and gelation reaction. This technique allows for the fabrication of ceramic or glass materials with different forms, including spherically shaped powder, ceramic fibres, thin-film coating, inorganic membrane, and porous aerogel materials (Thavornyutikarn et al., 2014). In addition, it produces an open interconnected porosity and pore sizes in the range of 300−600 μm. However, the poor mechanical properties associated with this method constitute the main disadvantage (Goudouri et al., 2016). To overcome this problem, (Chung et al., 2016) developed a hybrid bioactive glass scaffold by adding self−hardening copolymers with different architectures that significantly improved the mechanical properties without compromising biocompatibility.

1.4.3.3.1.6. Electrospinning

Electrospinning utilizes an electrical charge and polymer solution to draw fine micro or nanofibres and creates a highly porous scaffold with interconnected pores. The diameter and pattern of the fibres can be adjusted through a number of factors, including the viscosity, molecular weight and charge density of polymer, as well as the strength of the electrical field (Pham et al., 2006). The high surface area/volume ratio of nanoscale fibres allows for efficient delivery of loaded bioactive factors. Li et al. (2015) developed nanoparticle−embedded electrospun nanofibre for dual delivery of BMP−2 and dexamethasone. The scaffold strongly

induced osteogenic differentiation *in vitro* and enhanced the repair of a bone defect *in vivo*. However, the disadvantage of his method is the use of a cytotoxic organic solvent (Pham et al., 2006).

1.4.3.3.2. Limitation of conventional fabrication techniques

Although conventional methods have been widely used in BTE, they are incapable of producing scaffold with full interconnectivity and precisely controlled pores in terms of size, morphology and spatial distribution. In addition, some of these methods are manual based. Therefore, they are labour intensive and difficult to reproduce. Another limitation is the need for organic solvent and porogens, which are cytotoxic, and their residues may cause inflammatory responses (Hutmacher, 2000).

1.4.3.3.3. Solid free−form (SFF) techniques

This technology is based on a computer-aided design to fabricate a custom-made construct. Unlike subtractive conventional methods, SFF is an additive process in which scaffold is manufactured in a layer−by−layer manner built according to its computerised 3D image (Bose et al., 2018). SFF offers a number of substantial benefits that counteract the limitations associated with conventional methods. First, a customised, patient−specific design can be obtained by using computerised modelling. Second, a scaffold with high porosity (>90 %), full interconnectivity and consistent pore morphology can be easily achieved with high accuracy and minimum labour (Thavornyutikarn et al., 2014). Third, a functionally graded scaffold of different porosities and mechanical properties can be produced (Kawai et al., 2017). Finally, it is solvent and porogen−free, which makes the incorporation of some bioactive molecules such as VEGF feasible (Akkineni et al., 2015). To date, the main SFF techniques are stereolithography (SLA), selective laser sintering (SLS), fused deposition modelling (FDM), 3D printing (3DP) and bioprinting (Roseti et al., 2017).

1.4.3.3.3.1. Stereolithography (SLA)

This process is based on the solidification of a photosensitive liquid resin by photopolymerisation. Although this technique shows excellent reproducibility and high accuracy and resolution, the toxicity and irritation caused by photosensitive materials and the shrinkage of the polymer due to polymerisation are considered to be the main limitations of this process (Melchels et al., 2010).

1.4.3.3.3.2. Selective laser sintering (SLS)

SLS employs a CO_2 laser beam to sinter or fuse selected regions of a tightly compacted powder made of a thermoplastic material forming a material layer. Compared with SLA, SLS enables the processing of powder−based material by melting and does not use any cytotoxic chemicals or organic solvent. In addition, no supporting structures are required for the model during processing since support is provided by the unprocessed powder (Mazzoli 2013). Nevertheless, the heat generated by the laser beam and the time that the polymer powder is exposed can lead to the deterioration of the powder's properties (Pham et al., 2008). Another problem with this technique is the extreme difficulty in removing powder trapped inside the small pores, which may adversely affect cell growth or induce an inflammatory reaction (Thavornyutikarn et al., 2014).

1.4.3.3.3.3. Fused deposition modelling (FDM)

In FDM, the filament material is placed into two rotating rollers and the molten thermoplastic material is extruded from a movable nozzle in XY directions and deposited on to a platform. When a layer is completed, the platform (Z axis) is lowered and the process is repeated. Low cost, lack of organic solvent, the ability to form a construct with high porosity and full interconnectivity are considered to be the advantages of this technique (Roseti et al., 2017). However, the main difficulty of FDM is the material selection, which needs to be in the form

of fibres with a specified size. Furthermore, the effect of high temperature on the raw material and inadequate resolution constitute another limiting factor (Chen et al, 2007).

1.4.3.3.3.4. 3D printing (3DP)

3DP enables layer−by−layer scaffold fabrication by using one of three main technologies: inkjet, extrusion or laser-assisted printing (Mandrycky et al., 2016; Obregon et al., 2015). This available range of techniques facilitates precise fabrication of 3D scaffolds with a defined shape, size, porosity and pore size distribution, which can have a significant impact on cell proliferation, differentiation, and vascularisation (Cavo and Scaglione, 2106; Ferlin et al., 2016; Wang et al., 2015). They also allow for scalable fabrication of complex designs using various biocompatible materials; thereby providing an optimal cell microenvironment. In addition, the physical properties of the scaffolds such as compressive strength, toughness and elastic modulus can be optimised by adjusting the layer thickness and printing orientation (Farzadi et al., 2014). Moreover, it enables the incorporation of growth factors such as the vascular endothelial growth factor to enhance vasculogenesis (Fahimipour et al., 2017). However, to date, the clinical translation of construct containing growth factors is limited by rapid clearance from the implanted site, short effective half-life, low protein stability and rapid deactivation by enzymes at body temperature (Zhenming et al., 2017). Research is being conducted to design a delivery system for optimal control of spatial release and to reduce the dose such as micro and nanocontact printing, layered and gradient scaffold, and modular assembly (Samorezov and Alsberg, 2015). The rough surface finish, which may affect the resolution of the scaffold, is considered to be the main limitation of the 3DP method.

1.4.3.3.3.5. Bioprinting

In bioprinting, cell−laden biomaterials are dispensed with micrometre precision to form tissue-like structures. It offers scalability, cost−effectiveness, high−resolution cell deposition

and great precision relating to the spatial distribution of cells, proteins, growth factors and drug particles. These advantages have led to the development and subsequent applications of this technology to include broad applications such as clinical transplantation, drug screening and high−throughput assays, cancer research, and tissue engineering and regenerative medicine (Ozbolat et al., 2016).

Bioprinting of vascular and clinically relevant organs remains elusive due to several challenges such as the need to incorporate various cell types, limited mechanical and structural integrity, and difficulties in integrating a vascular network down to the level of capillaries (Ozbolat and Yin Yu, 2013). However, some thin, avascular tissues have been successfully bioprinted such as skin, hollow blood vessels and avascular cartilage (Aljohani et al., 2017).

Efforts to bioprint bone are ongoing towards the fabrication of scalable and composite constructs containing skin, muscle, nerve, and cartilage, although the mechanical properties of these constructs are still inferior to native bone and require more extensive investigation (Datta et al., 2017). Recently, successful bioprinting of composite constructs comprised of mandibular bone with open vascular channels and osteochondral tissue has been demonstrated (Hyun-Wook et al., 2016). Moreover, attempts are in progress to enhance angiogenesis and osteogenesis through culturing stem cells with osteogenic or angiogenic growth factors such as BMP−2 and VEGF, respectively. Cunniffe et al. (2017) demonstrated the dual delivery of therapeutic genes encoding bone morphogenic protein and transforming growth factor from gene−activated bioink prepared from alginate and nanohydroxyapatite (nHA) combined with bone marrow−derived MSCs. Fourteen days post bioprinting, cultured cells displayed robust osteogenesis and matrix deposition *in vitro* as well as superior vascularisation and mineralisation *in vivo.*

1.4.3.3.4. Limitations of SFF techniques

In spite of the advantages of SFF, there are some technical limitations that should be addressed for future improvements. First, each technique utilises a specific form of material. For example, fine powder is used for SLS, whilst thermoplastics are useful for FDM. Using the material can be challenging if the material is deemed suitable for a particular application but cannot be easily prepared to meet the required process. Second, printability of any material does not necessarily guarantee its usefulness for scaffold fabrication because successful RP relies on the bonding strength between layers. Therefore, the material needs to be self−supporting for layer-by-layer fabrication. Third, for bioprinting, new methods of material solidification should be developed that preserve the integrity of the printed construct without compromising cell survival (An et al., 2015). For example, in extrusion printing, hydrogels are solidified through either thermal processes or post-print cross-linking, which may have potentially harmful effects on the cells. Lastly, the flexibility of printing parameters such as temperature or dispensing pressure (shear stress) have become limited when using cell-laden materials, as because sudden changes in the environment around the cells may significantly reduce cell viability (Nair et al., 2009).

1.4.4. Bioactive factors in BTE

The role of numerous bioactive molecules such as fibroblast growth factors, insulin-like growth factors, and VEGFs in bone formation has been investigated (Allori et al., 2008). However, only two recombinant human proteins have been widely used and approved by the Food and Drug Administration (FDA) for clinical purposes: bone morphogenic protein−2,−7 (rhBMP-2,-7) and platelet−derived growth factor−BB (rhPDGF-BB) (Lynch, 2008).

BMPs, which belong to the transforming growth factor−B superfamily, are group of 30 members family with various cellular effects. For example, BMP−2, 4, 6, 7 and 9 showed evidence to induce mineralisation, OC production, and orthotopic ossification. However, BMP−3 negatively regulates bone formation and exerts an inhibitory effect of orthotopic ossification induced by BMP−2, 6 and 7 (Carreira et al., 2014). Platelet-derived growth factors, by contrast, are the strongest chemotactic factors relating to osteoblasts and stem cell precursors and have a potent mitogenic and activating effect on osteoclasts, fibroblasts, and endothelial cells (Allori et al., 2008).

Although these bioactive cues have an advantageous effect on bone formation, their application in BTE may be complicated by two factors. First: evidence indicates that the significant effect of these biomolecules is dose and duration dependent, which may be difficult to achieve, particularly with regard to the clinical aspect (Lieberman et al., 2002). For example, a high risk of cancer has been associated with the clinical use of concentrated BMP products (AMPLIFY^{TM}, rhBMP-2, 40mg), which may suggest the relation of high dose with carcinogenic effect (Devine et al., 2012). Second: in order to recapitulate the complex process of embryonic bone formation or bone regeneration, a simultaneous and/or stepwise delivery of a combination or cocktail of factors is required because these molecules act synergistically rather than solely. For example, insulin-like growth factors enhance bone cells' migration whereas BMPs induce osteoprogenitor cells' differentiation and proliferation (Allori et al., 2008).

To support prolonged release and activity of multiple growth factors, several delivery strategies have been envisioned. A multilayer fibrous scaffolds incorporating more than one growth factor achieve a better result by simultaneous and sustained delivery of multiple biological signals (Shah et al, 2014; Yilgor et al., 2009). Microsphere carriers and

nanostructured colloidal gelatine gels loaded with numerous bioactive cues are another controlled release strategy (Van Der Stok et al., 2013).

1.4.5. Environmental factors in BTE

In BTE, the concept of emulating the native environment is gleaned from an understanding of normal cell behaviour. Normally, to survive and grow, cells must be able to import nutrients from their surroundings and regulate the concentration of various inorganic ions. This could be achieved by *simple diffusion*, through which only a few small non-polar molecules can transfer across the cell membrane while the vast majority cannot. Instead, their movement depends on *active transport*, which needs a driving force with an expenditure of energy to move the solute "uphill" against its concentration gradient (Alberts, 2013).

Static cell culture techniques rely on diffusion transport which is sufficient to nourish only a thin superficial layer approximately 100−200 μm, in contact with the medium. As the cells increase in number so does metabolic demand and the build−up of waste products. Consequently, the cells in the tissue interior are deprived of oxygen and a nutrient source. As such, maintenance of cells' viability entails an effective vascular supply replicating the normal convective-diffusive transport. To circumvent this problem, several bioreactor technologies have been developed such as a spinner flask, rotating wall vessels, and the perfusion system (Chen and Hu, 2006; Dermenoudis and Missirlis, 2010; Zhong, 2010). A comparison of the three systems carried out by (Goldstein et al., 2001) showed that the perfusion bioreactor yielded the most uniform cell distribution throughout the scaffold with a significant expression of ALP, while in the spinner and rotating vessels the cell density demonstrated preferential distribution towards the scaffold exterior. In BTE, the bioreactor provides another advantage of exposing the cells to mechanical conditioning caused by fluid shear

stress and this enhances osteogenic expression and produces more minerals and proteins (Gaspar et al., 2012; Martina and Giuseppe Maria de, 2014).

1.5. Oral mucosa engineering

1.5.2. Strategies of engineered oral mucosa (EOM)

EOM has offered an opportunity to bypass the shortcomings associated with autografts through many strategies which aim to emulate normal tissue, both anatomically and physiologically. As the normal oral mucosa consists of epithelium and lamina propria, EOM consequently falls into one of two categories: split thickness (epithelium only) or full thickness, which reconstructs both epithelium and connective tissue layers separated with a continuous basement membrane (Moharamzadeh et al., 2007).

1.5.2.1. Split−thickness EOM

After the serial cultivation of human epidermal keratinocytes on a murine 3T3 feeder cell layer was first described by Rheinwald and Green (1975) many clinical studies have shown the advantages of cultured autologous epithelial sheets for the treatment of skin wounds (Navsaria et al., 1995; Ronfard et al., 2000). The method was then translated for culturing gingival epithelium, which was useful as an autograft for the correction of mucosal defects such as peri−implant soft tissue loss or defects resulting from pathological resection (Ueda et al., 1998; Bodner and Grossman, 2003).

In order to exclude xenogenous products, the original culture method has been modified to a feeder−cell free culture (Lauer, 1994; Ilmarinen et al., 2013). In addition, a temperature responsive polymer poly (*N*-isopropyl acrylamide) approach has been developed to control cell detachment and harvesting via temperature changes instead of enzymatic treatment (Nishida et al., 2004). However, the intraoral grafting of epithelial sheets encountered many

drawbacks that included a relatively long keratinocyte growth time, low graft acceptance rate, wound contraction, handling difficulty due to a thin, friable layer, and blister formation following minor mechanical forces (Izumi and Feinberg, 2002).

1.5.2.2. Full−thickness EOM

An ideal full−thickness EOM that resembles normal oral mucosa comprises a lamina propria, a continuous basement membrane separating the lamina propria and the epithelium, and a stratified squamous epithelium. The lamina propria can be formed by using a fibroblast −infiltrated 3D scaffold. It has been shown that fibroblasts play an important role in keratinocyte adhesion, epithelial morphogenesis, and the formation of an epithelial−connective tissue junction (Saintigny et al., 1993). In addition, fibroblasts influence the phenotype and keratin expression of the overlying epithelial cells (Okazaki et al., 2003). A stratified squamous epithelium, on the other hand, can be achieved by culturing oral keratinocytes at the air-liquid interface in a medium containing the keratinocytes' growth factors such as the epidermal growth factors (Dongari-Bagtzoglou and Kashleva, 2006a; Izumi et al., 2000).

1.5.2. Components of EOM

1.5.2.1. Cells for EOM

The type of cell is an important factor in the construction of EOM. Human oral fibroblasts can be obtained from the connective tissue of oral mucosa while oral keratinocytes can be isolated from the hard palate (Cho et al., 2000), gingiva (Yoshizawa et al., 2004) or buccal mucosa (Bhargava et al., 2004). In addition to normal human cells, immortalised human keratinocytes such as HaCaT cells (Boelsma et al., 1999) and OKF6/Telomerase reverse transcriptase (TRET) (Dongari-Bagtzoglou and Kashleva, 2006a) as well as TR146 tumour−derived cells (Schmalz et al., 2000) have been used in the construction of oral mucosa

test models. Although these cell lines can be utilised through extended passages, the ultimate steps of terminal differentiation do not occur (Boelsma et al., 1999) and tumour derived−cells cannot be used for clinical purposes.

1.5.2.2. Scaffold for EOM

Scaffolds used in oral mucosa reconstruction fall into three different categories: “naturally derived” such as acellular dermis, “synthetic” such as polymer-based scaffolds, or “hybrid”, which are a combination of natural and synthetic matrices (Moharamzadeh et al, 2017).

Acellular cadaveric dermis (AlloDerm) (Izumi et al., 2013; Izumi et al., 2003) and deepidermalised dermis (DED) (Cho et al., 2000; Hildebrand et al., 2002) have been extensively used for the preparation of oral mucosal constructs. An *ex vivo* oral mucosa equivalent has been successfully produced by Izumi et al. (2003; 2013) through growing autologous oral keratinocytes on AlloDerm without incorporation of fibroblasts. The main advantage of this technique is the use of a chemically defined culture that precludes serum or any animal−derived constituents, which makes this method consistent with the FDA’s regulatory guidelines for clinical use. However, this technique may be deemed suboptimal for many reasons. First, from a development standpoint, epithelial−mesenchymal interaction is essential for the morphogenesis, differentiation, and complete maturation of oral mucosal epithelium (Liu et al., 2011). Second, fibroblasts present in the oral mucosa may participate in its unique scarless healing due to the role of fibroblasts in collagen remodelling and the secretion of growth factors that accelerate resolution of the inflammatory phase (Enoch et al., 2008; Mak et al., 2009; Glim et al., 2013). Third, the non porous synthetic or natural matrix results in poor fibroblast infiltration and migration even when the fibroblasts were incorporated (Moharamzadeh et al., 2008).

Collagen is the major structural component of the ECM where its main role is in mechanical integrity (Rajan et al., 2006). Therefore, it has been used as a scaffold for oral mucosa engineering either as pure collagen (Masuda, 1996) or as compound collagen−based matrices such as collagen−chitosan (Ma et al., 2003) and the collagen−glucosaminoglycan matrix (Ojeh et al., 2001). Recently, extracellular protein-based scaffolds such as fibrin and plasma have been used to construct autologous oral mucosa equivalents. The results showed a reasonable outcome for intraoral grafting with good handling characteristics and no contraction (Llames et al., 2014; Peña et al., 2010; Peña et al., 2012). However, the epithelium showed only monolayered keratinocytes and negative expression of the proliferation marker, ki67, which indicates poor differentiation.

Synthetic scaffolds such as polycarbonate membranes are used in commercially available partial thickness epithelium (SkinEthic and MatTek tissue models). These synthetic matrices have good mechanical properties with no risk of disease transmission. A hybrid scaffolds, on the other hand, may provide controlled biodegradability and good biocompatibility such as for scaffolds made of benzyl esters of hyaluronan (Zacchi et al., 1998).

1.5.2.3. Culture environment of EOM

Usually, EOM is cultured in Green's medium supplemented with serum (Rheinwald and Green, 1975). However, in order to eliminate the xenogenetic components present in serum and irradiated mouse 3T3 fibroblast feeder layers from human grafts, a tissue−engineered oral mucosa equivalent was developed and characterised (Izumi et al., 2000). In addition, various methods have been utilised to induce keratinocyte differentiation in 3D models, including the addition of calcium, concomitant use of serum and calcium, and the use of lower incubation temperatures (Borowiec et al., 2013).

1.5.3. Applications of EOM

1.5.3.1. Clinical applications

EOM has been developed for both intra and extraoral clinical applications. An oral mucosa equivalent of 15 cm^2 has been produced using a seeding density of 3 × 1 0^5 cells/cm^2 oral keratinocytes in AlloDerm with a thickness of 508.0 µm (Kato et al., 2015). Success in the fabrication of EOM in such a large and reproducible way has enabled its use in grafting of many congenital and acquired intraoral defects. For example, hemifacial microsomia and ankyloglossia are facial congenital anomalies that have been treated by the grafting of autologous EOM, although re-grafting was required due to post−operative wound shrinkage and the recurrence of ankyloglossia (Llames et al., 2014). Likewise, the engineering of palatal mucosa−like human tissue using a collagen matrix was achieved as a potential graftable tissue for cleft palate augmentation (Luitaud et al., 2007; Liu et al., 2008). Satisfactory results have been clinically achieved using oral mucosa equivalents in both minor and extensive oral reconstructive surgery. Augmentation of mucogingival defects with *ex vivo*−produced EOM was demonstrated in clinical trial, and was assessed in terms of efficacy, safety, rapid integration, and vascularization (Izumi et al., 2013). Similarly, optimal functional and aesthetic outcomes have been obtained using EOM prelaminated with a fibula flap in the treatment of a severely atrophic maxilla or extensive mandibular defects following mandibulectomy (Sieira Gil et al., 2015).

Extra orally, it was found that re−epithelisation of a severely burned cornea can be enhanced by oral mucosa epithelial transplants, although the long-term survival of the graft largely depends on the stem cells in the basal layer (Chen et al., 2009). The suitability of an oral mucosa epithelial sheet was also investigated for the treatment of an oesophageal ulcers after endoscopic submucosal dissection, and the findings indicated the possibility of using the

epithelial sheet to promote wound healing and re−epithelialisation, and to prevent oesophageal stenosis (Takagi et al., 2011). Another example is the use of engineered buccal mucosa for substitution urethroplasty in patients with long urethral strictures (Osman et al., 2015).

1.5.3.2. Experimental applications

In vitro EOM modelling is another potential use in a wide range of studies. An oral carcinogenesis model was developed by (Colley et al., 2011) to replicate the different stages of oral squamous cell carcinoma from dysplasia to early invasion. Such models may facilitate the study of the mechanisms of malignant transformation as well as *in vitro* testing of new diagnostic and treatment methods. Investigating the pathogenesis of oral infections such as *candida albicans* using normal or immortalised oral keratinocytes cultured with collagen−populated fibroblasts is another example of using EOM models to study the cellular response and host defence mechanism against infection (Yadev et al., 2011). The variation in permeability, keratinisation, and composition across different regions of EOM also makes it a suitable tool for *in vitro* assessment systemic drug delivery (Hearnden et al., 2012) and material biocompatibility (Hearnden et al., 2012; Moharamzadeh et al., 2009).

1.6. Challenges and future directions in oral and maxillofacial tissue engineering

Despite the significant progress that has been achieved in BTE, many hurdles are still ahead. Some of these limitations pertain to TE itself such as identification of reliable and scalable cell source, optimisation of scaffold properties, controlling of the *in vitro* microenvironment, and vascularisation of the engineered tissue (Spicer et al, 2014). Other restrictions are associated with commercialisation, manufacturing facilities, and governmental regulations (Ram-Liebig et al., 2015).

The presence of such difficulties may explain the lack of proved and marketable cell−based engineered bone products that can address the unmet clinical need regardless of the extensive research being conducted in this field. However, it may be worth to mention that even the availability of such products does not imply its successful application. For example, the commercially tissue engineered transplants (Oral Bone®, BioTissue, Germany), produced by seeding periosteal human cells on PLGA bone chips, was compared with autologous iliac bone graft in sinus augmentation. The outcome 3 months post operatively was not encouraging due to high resorption rate in the engineered bone that reached up to 90 % while the autologous graft showed a resorption rate of 29 % (Zizelmann et al., 2007). Such unfavorable results may pose a question regarding the long−term stability of any off the shelf cellular engineered bone and whether or not this post−operative complication can be encountered by using the current materials and techniques.

Oral mucosa engineering may share the same challenges associated with BTE. While the first FDA−approved skin product, Apligraf ® (Organogenesis, Boston, USA), was introduced in 1998 (Zaulyanov and Kirsner, 2007), the marketing of EOM has lagged behind the engineered skin. The first commercially available oral mucosa product, GINTUIT®, received FDA approval in

2012 (Charles, 2012). However, the current EOM models cannot be deemed as an identical replica of the normal oral mucosa due to manufacturing and biological challenges. Ideally, the EOM should be constructed using autologous cells. Therefore, the time elapses between biopsy and grafting entails precise coordination between clinic and laboratory to cope with the long, complicated, and expensive culture procedures. The biological challenges include the introduction of other cells such as immune cells in the lamina propria and the incorporation of the vascular components which aids in revascularisation of the construct following transplantation (Böttcher-Haberzeth et al., 2010). Moreover, more advanced fabrication technologies such as 3D bioprinting may be utilized in the future to generate oral mucosal equivalent in the same manner as skin has been recently fabricated (Cubo et al., 2017; Rimann et al., 2016).

In addition to aforementioned hurdles, engineering of composite tissues and attaching various parts in their normal anatomical relationship poses a considerable challenge particularly in OMF region where heterogenous tissues are closely related to each other in a relatively small area (Spicer et al, 2014). Although the engineering of many orofacial tissues such as bone, teeth, muscles, and cartilage have been investigated (Zaky and Cancedda, 2009; Tayebi and Moharamzadeh, 2017), only a few intricately-structured hybrid tissues have been developed such as osteochondral structure (Ruan et al., 2017) and bone−periodontal ligament complex (Park et al., 2011).

Bone and overlying mucosal tissues represent the key components in orofacial area. They comprise together with cementum and periodontal ligament the periodontal apparatus that provides anchorage and support to the teeth in dental jaws (Lang et al., 2015). In addition, alveolar bone and masticatory mucosa form the main structure of the hard palate (Nanci,

2013). Although engineering of bone and oral mucosa has been extensively investigated, a faithful replication of oral structures entails a combination of these heterogeneous tissues in a single composite construct. The more *in vitro* representation of native oral tissue arrangement, the more accurate insight in biological, physiological, and pathological conditions thereby the gap between translation and basic research is bridged, the progress toward clinical application is promoted, and the need for costly *in vivo* model is reduced. Development of an accurate and reproducible human alveolar bone-mucosal model, therefore, represents another important step in the process of achieving a utilisable tissue engineered orofacial construct.

To date, to the best of our knowledge, there are no published studies in the current literature indicating *in vitro* TE of a composite alveolar bone−mucosal model. This study was proposed to fill this gap by generating such construct using conventional and 3D printing bone scaffolding techniques.

1.7. Aims and objectives

1. To develop and assess an *in vitro,* cell line−based composite bone−mucosal model (BMM) using a conventional bone scaffold.
    - ❖ Characterise an HA/TCP scaffold for the construction of the bone component of the BMM.
    - ❖ Optimise the suitable technique for seeding ROS cells into the HA/TCP scaffold to fabricate the bone construct (BC).
    - ❖ Optimise the culture condition of the BC.
    - ❖ Assess the proliferation and metabolic activity of the cells in the BC.
    - ❖ Construct an oral mucosal model (OMM) using a collagen gel scaffold, normal oral fibroblasts, and immortalised OKF6/TERT−2 oral keratinocytes.
    - ❖ Assess the feasibility of combining BC and OMM using a fibrin−based tissue adhesive to develop the composite BMM.
    - ❖ Assess the histological morphology of BMM using decalcified paraffin embedding techniques.
    - ❖ Assess the differentiation status of the mucosal component of the BMM.
2. To develop and characterise a novel 3D composite human alveolar bone−mucosal model (ABMM) based on the conventional bone scaffold and primary cells isolated from the native human oral hard and soft tissues.
    - ❖ Isolate and characterise oral−derived gingival and bone cells, namely keratinocytes, fibroblast, and osteoblasts.
    - ❖ Develop and characterise a human alveolar BC of the planned ABMM using an HA/TCP scaffold.

- ❖ Develop and characterise a normal human cell−based oral mucosa model (OMM).
- ❖ Assess the histological features of ground sections taken from the ABMM.
- ❖ Analyse the proteins and genes expression of cells within the ABMM using suitable markers of cells typically found within bone.

3. To construct and characterise a composite ABMM using the 3D printed bone scaffold.
    - ❖ Prepare an injectable β−TCP paste and assess its rheological properties.
    - ❖ Optimise the printing parameters for printing the β−TCP paste.
    - ❖ Print a bi−layered β−TCP scaffold that replicates the cortico−cancellous alveolar bone architecture.
    - ❖ Characterise the printed scaffold in terms of microstructure, morphology, surface topography, phase composition, mechanical and biological properties.
    - ❖ Assess the printing−based ABMM qualitatively and quantitatively.
4. To examine the relevance of the printing-based ABMM in the modelling of oral cancer at different progression stages.
    - ❖ Generate tumour cell spheroids.
    - ❖ Incorporate tumour spheroids in the ABMM at three distinct anatomical, namely epithelium (carcinoma in situ), epithelium and connective tissue layers, and connective tissue and bone interface.

Chapter 2: Development of a cell line–based 3D tissue engineered composite bone–mucosal model: a feasibility study

NB: The work described in this chapter has been published in:

Almela, T., Brook, I. M. & Moharamzadeh, K. 2016. Development of three-dimensional tissue engineered bone-oral mucosal composite models. *Journal of Materials Science: Materials in Medicine,* 27(4)**,** pp 1-8.

2.1. Introduction

Composite TE constitutes a new avenue particularly in the OMF area where a variety of tissues are closely associated with each other. Engineering of bone (Ferracane et al., 2014b; Seong et al., 2010) and oral mucosa (Moharamzadeh, 2017) has been thoroughly investigated using different cell types and biomaterials. Although the use of human primary cells in TE is relevant clinically and produce more predictive data experimentally, the difficulties of cell sourcing, inherent donor−to−donor variations, and limited proliferative capacity of native cells may restrict their usefulness (Olson et al., 2011). To circumvent these ever−presenting problems, a plethora of bone cell lines typically isolated from cancerous tissues or derived by immortalisation of primary cells are often used (Czekanska et al., 2012; Kartsogiannis and Ng, 2004). Although the phenotype expressed by cell lines such as rat osteosarcoma (ROS) (Machida et al., 1995), human osteosarcoma (SaOs-2) (Rodan et al., 1987a) and mouse cell line (MC3T3-E) (Wang et al., 1999) may not accurately reflect the true phenotype of normal osteoblasts, these cells are generally easier to culture, have a long lifespan and high proliferation rate, and have higher phenotypical stability comparing to primary cells (Czekanska et al., 2012).

Immortalised human cells can divide indefinitely due to the expression of telomerase reverse transcriptase (TERT), a cellular ribonucleoprotein which compensates for the inevitable telomer shortening thereby preventing growth arrest, and maintains the cell phenotype (Jerry and Woodring, 2000; Lee et al., 2004). OKF6/TERT-2 constitutes an example of normal epithelial cells immortalised by forced expression of telomerase (Dickson et al., 2000) and provides a valuable alternative to primary human oral keratinocytes in TE of the oral mucosal equivalent (Dongari-Bagtzoglou and Kashleva, 2006a, Dongari-Bagtzoglou and Kashleva, 2006b).

Aforementioned cell types have emerged to tackle the surge in research related to bone and soft tissue engineering and to compensate, to some degree, the unsustainable supply of primary human cells. Many studies have been conducted in the development of cell line−based TE of bone (Choi et al., 2016; Neufurth et al., 2017b; Sobhani et al., 2017) and oral mucosa equivalents (Jennings et al., 2016; Dongari-Bagtzoglou and Kashleva, 2006a; Buskermolen et al., 2016), however, the combination of these two entities in a single composite construct still needs to be addressed. This work examined the feasibility of developing an *in vitro* TE composite BMM using immortalised epithelial cells and malignant bone cells to approximate the natural anatomical structure of alveolar bone with an overlying oral mucosa.

2.2. Aim

To develop and assess an *in vitro*, cell line- based, composite bone−mucosal model.

2.3. Materials and methods

2.3.1. Routine cell culture conditions

2.3.1.1. 2D cell expansion

Three types of cells, namely osteoblast−like rat osteosarcoma (ROS) cells, normal human oral fibroblasts (NHOFs), and human telomerase-immortalised oral epithelial cells (OKF6-TERET-2) were used to construct BMM. Each cell type was cultured in cell culture flasks (Greiner Bio-one, Gloucestershire, UK) with its specific media and incubated at 37 ˚C with 5 % CO_2 in a humidified incubator. Cell morphology and growth were monitored by light microscopy and the medium was changed every other day until cells reached 80 % confluency when they were either passaged or maintained as stock cultures.

ROS cell line

ROS cells were obtained from liquid nitrogen storage in the School of Clinical Dentistry, University of Sheffield, UK. This cell line was used due to its availability, ease of culture, the culture parameters of this cell line had been already optimised by coresearcher, and the high proliferation potential which yields large cell number in short period compared to the lengthy and costly culture of primary bone cells. In addition, ROC cells exhibit an osteoblastic characteristic in terms of osteogenic markers expression and calcified matrix formation (Kartsogiannis and Ng, 2004). Cells were cultured in high glucose Complete Dulbecco's Modified Eagles Medium supplemented with L−ascorbic acid 2 phosphate (CDMEM-LAA) (Table 2.1.).

Table 2. 1. Culture medium of bone cells. Table lists the volume and final concentration (conc.) of each component required to prepare CDMEM−LAA medium that supports the growth of bone cells (Helfrich and Ralston, 2012).

Component	Volume/amount	Final conc.
Dulbecco's Modified Eagles Medium (DMEM) + GlutaMAX™ (Gibco, Paisley, UK)	444 ml	89 %
Foetal bovine serum (FBS) (Sigma Aldrich, Dorset, UK)	50 ml	10 % (v/v)
Penicillin/Streptomycin (P/S) (Sigma Aldrich, Dorset, UK)	5 ml	100 IU/ml:100 µg/ml
Amphotericin B (Sigma Aldrich, Dorset, UK)	1.25 ml	0.625 µg/ml
L-ascorbic acid 2-phosphate (LAA) (Sigma Aldrich, Dorset, UK)	25 mg	50 µg/ml

NHOFs

NHOFs were obtained from liquid nitrogen storage in the School of Clinical Dentistry, the University of Sheffield, UK (Sheffield Research Ethics Committee (REC:04/Q2305/78)). Cells were cultured in CDMEM (Table 2.2.).

Table 2. 2. CDMEM culture medium. Table lists the volume and final concentration of each component required to prepare CDMEM used for culture NHOFs.

Component	Volume/amount	Final conc.
DMEM + GlutaMAX™	444 ml	89 %
FBS	50 ml	10 % (v/v)
P/S	5 ml	100 IU/ml:100 µg/ml
Amphotericin B	1.25 ml	0.625 µg/ml

OKF6-TERET-2

OKF6-TERET-2 cells were kindly provided by Brigham and Women's Hospital, Harvard Institute of Medicine, USA. This cell line was chosen to overcome the shortage of resected gingival tissue and the donor-to-donor variations thereby it produces a valuable and reproducible model of normal oral epithelial cells. OKF6-TERET-2 were cultured in Green's medium (Table 2.3.). The individual stock solutions were prepared as follows:

1. Adenine

0.5 g Adenine powder (Sigma Aldrich, Dorset, UK) was mixed with 70 ml distilled water. 1 M hydrochloric acid (HCL) was added to the mixture until the powder dissolved completely. The solution was made up to 80 ml with distilled water (dH_2O) to give a final concentration of 6.25 µg/ml, filter sterilised and stored aliquots at −20 °C.

2. Insulin

10 mg recombinant human insulin (Sigma Aldrich, Dorset, UK) was added to 1 ml of 0.01 M HCL. Once dissolved 9 ml of dH_2O is added to give a final concentration of 1 mg/ml, filter sterilised and stored aliquots at -20 °C.

3. 3, 3, 5- Tri-iodothyronine (T3)/Apo-Transferrin

13.6 mg of T3 (Sigma Aldrich, Dorset, UK) was dissolved in a minimum volume of 0.02 M sodium hydroxide. Once dissolved the solution was made up to 100 ml with dH_2O. 250 mg apo−transferrin (Sigma Aldrich, Dorset, UK) was dissolved in 30 ml of phosphate buffer saline (PBS). 0.5ml of the T3 solution was added to 30 ml of the apo−transferrin solution and the volume was made up to 50 ml with PBS, filter sterilised and stored aliquots at -20 ^{o} C.

4. Hydrocortisone

Dissolve 25 mg hydrocortisone (Sigma Aldrich, Dorset, UK) in 10 ml PBS. Stored at 4 °C.

5. Epidermal growth factor (EGF)

100 µg of EGF (Thermofisher, USA) was reconstituted in 1 ml of PBS. Aliquoted and stored at −20 °C.

Table 2. 3. Green's medium. Table lists the volume and final concentration of each component required to prepare Green's medium. Adapted from (Hearnden, 2011).

Component	Volume	Final Conc.
DMEM + GlutaMAX™	330 ml	66 %
Nutrient Mixture F12 medium (Hams F12) (Gibco,Paisley, UK)	108 ml	21.6 %
P/S	5 ml	100 IU/ml:100 µg/ml
Amphotericin B	1.25 ml	0.625 µg/ml
FBS	50 ml	10 % (v/v)
Adenine	2 ml	0.025 µg/ml
Insulin	2.5 ml	5 µg/ml
3, 3, 5-Triiodothyronine (T3)	0.5 ml	136 ng/ml
Apo-transferrin	0.5 ml	5 µg/ml
Hydrocortisone	80 µl	4 µg/ml
EGF	25 µl	5 ng/ml

2.3.1.2. Cell passaging

Cells were passaged by removing media and washing twice with calcium and magnesium free PBS before incubation with 0.25 % (v/v) trypsin/ 0.02 % (v/v) ethylene diamine tetra acetic acid (EDTA) (Sigma Aldrich, Dorset, UK) at 37 °C, 5 % CO_2 for 5 minutes to detach the monolayer from the flask surface. CDMEM was added at a 1:1 (v/v) ratio to inhibit further enzymatic activity of trypsin. Cells were centrifuged at 190 × g for 5 minutes, resuspended in the appropriate cell culture medium at the required seeding density (Table 2.4.) into tissue culture flasks.

Table 2. 4. 2D seeding densities of cells used in cell line-based BMM

Cell type	Seeding density
ROS	13×10^3 /cm^2
NOFs	7×10^3 /cm^2
OKF6-TERET-2	13×10^3 /cm^2

For cell counting, 20 µl of cell suspension was diluted with the viability stain trypan blue (Thermofisher, USA) and viable cells were counted using a Neubauer hemocytometer (Weber Scientific International, Middlesex, UK) using the equation:

$$\% \text{ of viable cells per milliliter} = \frac{\text{Number of live cells counted}}{\text{Number of Squares counted}} \times 10{,}000 \times \text{dilution factor}$$

Higher than 90 % viable cells were used in each experiment.

2.3.1.3. Cell freezing and cryopreservation

For long−term storage, cells were passaged and resuspended at 1.5−2 × 10^6 cells/ml in cryoprotectant freezing medium which consisted of 90 % FBS (v/v) with 10 % dimethyl sulfoxide (DMSO) (v/v) (Sigma Aldrich, Dorset, UK). One ml of cell suspension was added to each cryovial (Greiner bio-one, Gloucestershire, UK) which placed in Mr. Frosty™ freezing container (Thermo Scientific, Leicestershire, UK) to achieve a cooling rate of 1°C per minute to −80 °C. After 24 hours in −80, cryovials were transferred to liquid nitrogen storage for optimal long−term cell preservation.

2.3.1.4. Resuscitation of frozen cells

When required, frozen cells were thawed and rapidly resuspended in appropriate cell culture media, centrifuged at 190 × g for 5 minutes to remove DMSO, then pellet resuspended in media and seeded into tissue culture flask.

2.3.2. Authentication of human cell line

An accurate data interpretation depends on unambiguous identity of a cell line relative to its original source. Contamination, mutation, and misidentification of human cell cultures leads to spurious results; therefore, authentication of human cell lines adds confidence to the scientific study. Short-tandem-repeat (STR) DNA profiling provides an accurate, reliable, and standardized method for authentication of human identity (Nims et al., 2010). Authenticity of OKF6-TRET was performed by STR profiling (Appendix I). For that, the DNA was extracted using QIAamp DNA Mini Kit (Qiagen) according to the manufacturer's instructions. The concentration of DNA was measured using a NanoDrop 1000 Spectrophotometer (ThermoScientific) at 260/280 nm. ABI 3730 DNA analyzer (ThermoFisher, UK) was used to run samples.

2.3.3. Development of cell-line based bone construct (BC)

2.3.3.1. Microstructural analysis of bone scaffold using micro−computed tomography (μ−CT)

HA/TCP (60 %/40 %) scaffolds of 20 mm × 3 mm dimension fabricated by conventional aqueous gel−casting method were used (Ceramisys LTD, UK). The microstructural characteristics of the scaffolds were quantified by a high resolution μ−CT scanner (SkyScan 1172; Bruker, Belgium) with a source voltage of 100 Kilovoltage (kV) and current of 90 MicroAmpere. For scanning, each HA/TCP disc was covered by polystyrene, placed on the sample holder, and scanned with a filter of 0.5 mm aluminum at a rotation step of 0.7° and rotation angle of 180°. Images were taken using Skyscan 1172 Control software (version 1.0. ×) and all the resulted 2D and 3D cross-sectional images were reconstructed using NRecon (version 1.6.10.4, Skyscan) software. For image analysis (CTAn, version 1.13.2.1, Skyscan software), a region of interest (RIO) with a diameter of 9 mm and a height of 1.8 mm was

chosen to exclude the peripheral irregularities of the scaffold. Closed and open porosity, interconnectivity as well as the other basic features were determined.

2.3.3.2. Optimisation of 3D seeding method

Seeding efficiency is defined as the percentage of the cells retained in the scaffold with respect to the total amount of cells (Zhao and Ma, 2005). Two different seeding techniques were compared to evaluate cell seeding efficiency; static and dynamic seeding (Burg et al., 2000). Prior to seeding, the scaffolds were autoclaved and pre-wet with CDMEM for 4 hours.

In static seeding, scaffolds were placed in 12 well plate (Greiner Bio-one, UK) and 1×10^6 of ROS cells suspended in 15 µl of CDMEM−LAA media were slowly distributed on top of each scaffold and allowed to adhere for 2 hours after which 2 ml of culture media were added to each well. Spinning seeding technique was performed using spinner bioreactor (Stem stirrer, UK). The bioreactor consisted of dual side arm cylinder and rubber cover pierced by a 22 gauge needle on which scaffolds were threaded and separated 5 mm apart by silicon tubes. Subsequently, 3×10^6 ROS cells suspended in 50 ml CDMEM−LAA media were added to the spinner which was stirred at 30 rpm under incubation conditions.

All cell−scaffolds constructs were incubated for 24 hours to give the cells enough time to adhere to and establish themselves in the scaffolds. Following that, the number of non adherent cells in each group was quantified by cell counting. For the well plate, the culture medium was removed, the wells were washed with PBS, and cells attached to wells were trypsinized using 0.25 % trypsin/EDTA solution. For the spinners, 20 µl of the culture medium was taken from each spinner. Following cell counting, seeding efficiency was calculated based on the following equation (Hong et al., 2014):

Cell seeding efficiency % =

$$\frac{\text{initial seeded cells to scaffold} - \text{non adherent cells}}{\text{initial seeded cells to scaffold}} \times 100$$

2.3.3.3. Optimisation of 3D culture technique

Scaffolds were statically seeded as mentioned previously (see section 2.3.3.2.). To promote a robust cell attachment, cell−scaffold constructs were maintained in an initial static period of 24 hours before transferring them to a dynamic environment. This time was recommended by many authors to prevent initial cell detachment and death (Hewitt et al., 2011; Teixeira et al., 2014). Following 24 hours, constructs were cultured under two different conditions; statically in 12 well plate or dynamically in spinner flask (Sikavitsas et al., 2002). The culture was carried out in CDMEM−LAA for one month with the refreshment of medium every other day. Sample assessment was performed at 1, 7, 14, 21, 30 days for cell viability using PresoBlue (PB) live assay.

2.3.3.4. Cell viability assessment using PresoBlue (PB) live assay

The assessment of cell viability was performed using PB assay (Invitrogen, USA). This new, simple, and extremely fast assay is a resazurin-based compound which is converted to the reduced form by mitochondrial enzymes of viable cells and, consequently, exhibits a colour change that can be quantified by fluorometric or spectrophotometric approach (Boncler et al., 2014).

At each time point, samples were placed in 12 well plate and washed with PBS. Then, a mixture of 900 µl of CDMEM and 100 µl of PB reagent was added to each well. Three acellular discs were included as a control (ctrl). Culture plates were wrapped in aluminum foil and incubated at 37 °C and 5 % CO_2 for 3 hours. The incubation time of PB reagent had been optimised by taking readings at different time points namely; 1, 2, 3, and 4 hours. After incubation, 200 µl

aliquot of test and control samples were transferred to a white opaque 96 well plate (Greiner Bio-one, UK) in triplicate. Subsequently, the fluorescence values were measured (excitation/emission: 560/590 nm) using spectrophotometric plate reader (Infinite® M200, TECAN, USA). For calculation, the average fluorescent values of negative ctrl (scaffolds without cells) were subtracted from the averaged sample readings.

2.3.3.5. Preparation of BC

BCs were prepared according to the technique described by (Sikavitsas et al., 2002). In brief, 10 autoclaved scaffolds were pre−wet in CDMEM 4 hours prior to cell seeding. In 12 well plate, 2×10^6 ROS cells suspended in 15 µl CDMEM-LAA were dropwise seeded in each scaffold. Following 2 hours, BCs were submerged with 2 ml of CDMEM-LAA and incubated for 24 hours after which they were suspended 5 mm apart in a spinner bioreactor spun at a rate of 30 rpm (Figure 2.1.). Spinner was filled with 150 ml of CDMEM-LAA refreshed every 3 days until the end of the culture period.

Figure 2. 1. The dynamic culture of BCs in spinner bioreactor. Figure shows ROS cells−seeded HA/TCP scaffolds threaded in spinner before the addition of CDMEM−LAA and transferring to the incubator.

2.3.4. Development of OMM

Collagen hydrogel−based OMMs were constructed using the protocol adapted from (Dongari-Bagtzoglou and Kashleva, 2006a). Briefly, keeping everything on ice, rat tail collagen (R & D biosystems, UK) was mixed with 10 × DMEM, reconstitution buffer (22 mg/ml sodium bicarbonate and 20 mM 4-(2-hydroxyethyl)-1-piperazineethanesulfonic acid (HEPES), FBS, L-glutamine (Table 2.5.). Before the addition of 0.2×10^6 NHOFs per model, this mixture was neutralised to pH 7.4 by addition of 1 Molar sodium hydroxide (NaOH) (All Sigma Aldrich, Dorset, UK).

Table 2. 5. The components added to collagen to prepare collagen hydrogel−based OMM

Component	Final Conc.
10 × DMEM	13.8 mg/ml
Sodium bicarbonate	2.25 mg/ml
HEPES	2 mM
NaOH	6.3 mM
FBS	8.5 % (v/v)
L-Glutamine	2.1 mM

Then, 2 ml of the resultant fibroblast-collagen mixture was poured into 30 mm diameter cell culture transwell inserts (0.4µm pore size, Millipore) in 6 well plate (Greiner Bio-one, UK) and incubated at 37 ^{o}C in a 5 % CO_2 incubator for 2 hours allowing the collagen hydrogels to set. Once the hydrogels had set, they were completely submerged in 2 ml of CDMEM for 3 days. Following that, 1×10^6 OKF6−TERET−2 suspended in 30 µl of Green's media were seeded on top of each model and allowed to adhere for 2 hours after which 2 ml of CDMEM and Green's

media were added to outside and inside of the insert, respectively. After a further 4 days of culture, OMMs were raised to an air-to-liquid interface (ALI) using a 6 well plate and perforated metal grids. 6 ml of Green's media was added to each well and refreshed every 2 days for 10 days (Figure 2.2.).

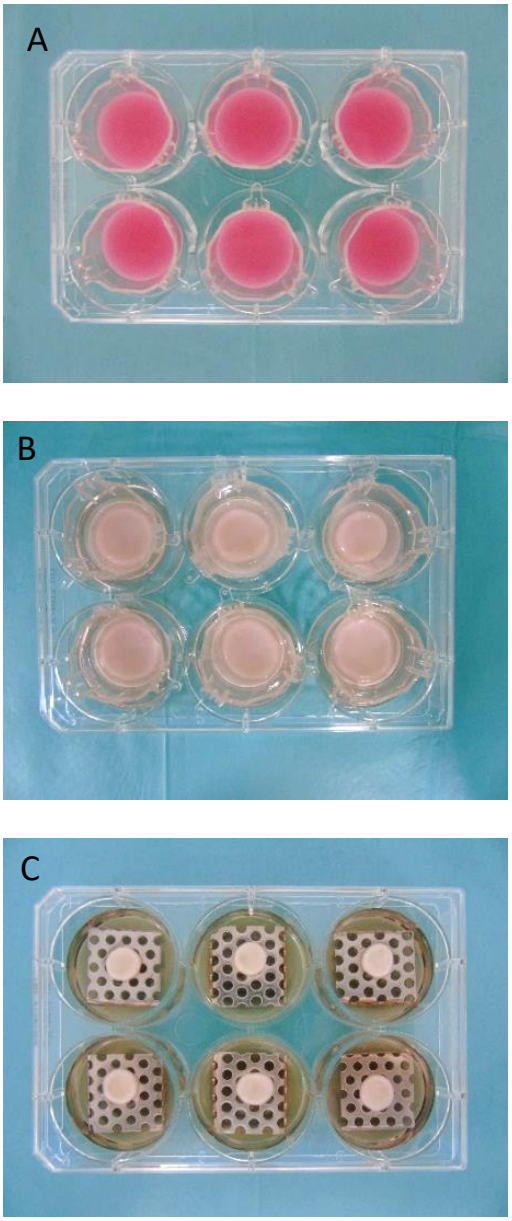

Figure 2. 2. Main steps of OMM construction. (A) Collagen embedded−fibroblasts immediately after pouring in the inserts to be cultured in CDMEM; **(B)** OMMs following the addition of OKF6−TERET−2 to be cultured in submerged condition for 4 days with CDMEM and Green's medium; **(C)** OMM at ALI culture which lasted for 10 days in Greene's medium only.

2.3.5. Development of composite BMM

Once the culture of BCs and OMMs had completed, both models were combined to construct the composite BMMs. Briefly, BC was placed on a sterile culture plate containing 10 ml CDMEM. Then, a biocompatible fibrin-based adhesive sealant (ARTISS, Baxter, UK) (Table 2.6.) was prepared in a pre−filled syringe according to manufacturer's instructions, and a thin layer of the mixed fibrinogen-thrombin sealer applied to the non-epithelial side of OMM. OMM was then immediately attached to the surface of BC and held in the desired position with gentle compression for a minimum of 60 seconds to ensure that adhesive material had completely set and both models were firmly adhered to each other (Figure 2.3.). The resultant BMMs were then further cultured at static ALI for 5 days, after which the analyses were performed.

Table 2. 6. The main constituents of fibrin sealant

Fibrinogen Solution	Fibrinogen	67−106 mg/ml
	Fibrinolysis Inhibitor (Synthetic)	2250−3750 kallikrein inhibitor units (KIU)/ml
Thrombin Solution	Thrombin (Human)	2.5−6.5 units/ml
	Calcium Chloride	36−44 µmol/ml

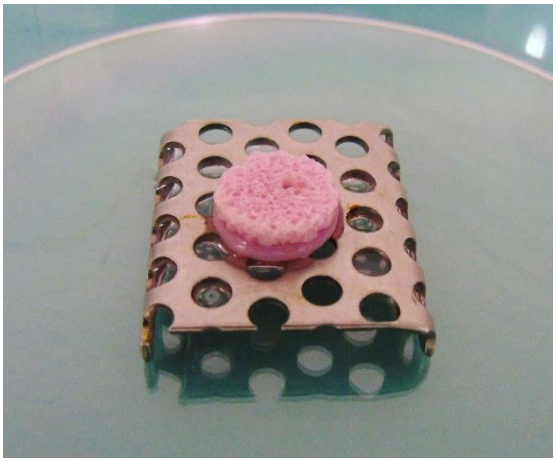

Figure 2. 3. BMM after the adhering of OMM and BC with fibrin adhesive. OMM was inverted for fibrin addition on the connective tissue side then BC was placed on the top and held in its position for 1 minute under gentle pressure. The final BMM was further cultured at ALI for 5 days.

2.3.6. Assessments

BCs were assessed monthly by scanning electron microscopy and histological examination. BMMs were examined histologically at the end of the culture period.

2.3.6.1. Scanning electron microscopy (SEM) examination

SEM assessment was performed to observe cell attachment and proliferation. Following collection from the spinner, BCs were rinsed with 5 ml of 0.1 cacodylate buffer, fixed with 3 % of glutaraldehyde for 3 hours, and then rinsed again with cacodylate buffer. Osmium tetroxide was added to cover the material surface and left for 2 hours. Then, the samples were washed with buffer and dehydrated gradually with the increasing concentration of ethanol solutions (75 %, 95 %, and 100 %) for 15 minutes each. Samples were air dried overnight, mounted onto 20 mm diameter stubs and sputter−coated with gold (~20 nm). Cell attachment and distribution were imaged at an acceleration voltage of 15 kV using a scanning electron microscope (Philips XL-20, USA). Preparation of samples for imaging was performed by Chris Hill, Department of Biomedical Science, University of Sheffield.

2.3.6.2. Histological examination

Formalin−fixed paraffin−embedded (FFPE) sections were prepared to examine the tissue morphology of OMM, BC, and BMM. Samples were fixed in 10 % (v/v) PBS−buffered formalin for 24 hours, decalcified with formic acid for the same period, and processed overnight using a Leica TP1020 benchtop tissue processor (Leica TP1020 benchtop tissue processor, Leica Microsystems, Germany; Table 2.7.). Samples were then embedded in paraffin wax using a Leica EG1160 embedding centre (Leica Microsystems). Sections of 10 µm thickness were prepared (Leica RM2235 microtome, Leica Microsystems, Germany), floated onto a paraffin section mounting bath (Barnstead Electrothermal, Staffordshire, UK), mounted onto superfrost plus micro slide (VWR, West Sussex, UK), and placed in an oven for 30 minutes at 55°C.

Table 2. 7. Dehydration and embedding schedule for FFPE tissue. Table shows solutions and length of time the tissue spent in each solution.

Solution	Time (hours)
10 % (v/v) neutral buffered formalin	1
70 % alcohol	1
80 % alcohol	1
90 % alcohol	1
Absolute alcohol I	1
Absolute alcohol II	1
Absolute alcohol III	1
Xylene	1.5
Xylene	1.5

Paraffin wax I	2
Paraffin wax II	2

Haematoxylin and eosin (H&E) staining was performed (Leica ST4040 Shandon Linear Stainer, Leica Microsystems, Germany; Table 2.8.). Following staining, slides were mounted with Dibutyl phthalate, polystyrene, xylene (DPX) and covered with an appropriate coverslip. Images were captured using an Olympus BX51 microscope and colour view Illu camera with associated Cell^d software (Olympus soft imaging solutions, GmbH, Münster, Germany).

Table 2. 8. H&E staining schedule of FFPE sections. The table describes the order and solutions used for staining. Each step lasted for 45 seconds. Industrial denatured alcohol (IDA).

Order	Solution
1	Xylene
2	Xylene
3	Xylene
4	99 % IDA
5	99 % IDA
6	99 % IDA
7	Distilled water
8	Distilled water
9	Harris' haematoxylin (Shandon)
10	Harris' haematoxylin (Shandon)
11	Harris' haematoxylin (Shandon)
12	Harris' haematoxylin
13	Running tap water
14	0.1 % acid alcohol
15	Running tap water
16	Scott's tap water substitute

17	Running tap water
18	Eosin Y−aqueous (Shandon)
19	Eosin Y−aqueous (Shandon)
20	Eosin Y−aqueous (Shandon)
21	Running tap water
22	99 % IDA
23	99 % IDA
24	99 % IDA
25	Xylene
26	Xylene
27	Xylene
28	Xylene

2.3.7. Statistical analysis

All data were presented in terms of mean ± standard deviation (SD). The statistical significance of differences within each group was evaluated by one−way analysis of variance (ANOVA) complemented by Tukey's post−test while two−way ANOVA with Sidak's post−test was used to determine the difference between groups. Comparison between two groups was performed using Unpaired two−tailed t−test. Statistical analysis was performed using GraphPad Prism software v7.0 (GraphPad Prism software, CA, USA), and differences were considered significant when $p < 0.05$.

2.4. Results

2.4.1. µ–CT analysis of HA/TCP scaffold

2D cross-sectional views of scanned scaffolds showed interconnected, randomly distributed pores of different sizes (Figure 2.4.). µ–CT analysis revealed an open porosity (total porosity) of 78.9 % compared with 0.01 % closed porosity. Similarly, the volume of closed pore space showed a negligible value of 0.002 mm^3 in comparison with 90.7 mm^3 open pore volume. The averaged trabecular separation (pore diameter) was 0.24 mm (240 µm) while the value of trabecular thickness (pore wall) was 0.05 mm. The interconnectivity was 68487.6 (Table 2.9.).

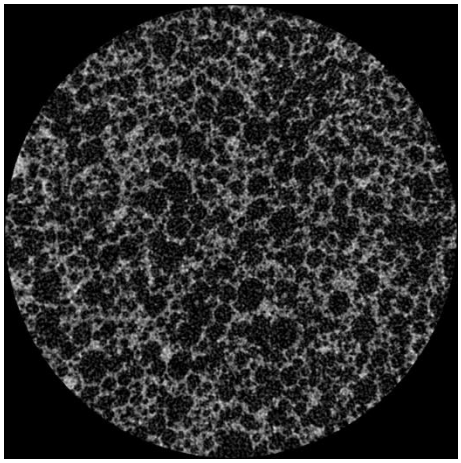

Figure 2. 4. µ–CT image of HA/TCP scaffold. Representative µ–CT image illustrating the 2D cross–sectional architecture of the conventional ceramic scaffold used for the construction of the bone component of BMM. The area represents a region of interest (RIO) with a diameter of 9 mm and a height of 1.8 mm. Note the random distribution of multi-size, open and interconnected pores.

Table 2. 9. µ–CT scan measurement of HA/TCP scaffold. Table summarising the main characteristic features of HA/TCP bone scaffold. Data are representative of mean ± SD of three independent experiments (n=3) performed in triplicate.

	Feature	Unit	Mean ± SD
1	Volume of closed pores	mm^3	0.002 ± 0.001
2	Volume of open pores	mm^3	90.71 ± 3.31
3	Closed porosity	%	0.01 ± 0.005
4	Open porosity	%	78.9 ± 2.88
5	Trabecular thickness	mm	0.05 ± 0.01
6	Trabecular separation	mm	0.24 ± 0.04
7	Trabecular number	1/mm	3.93 ± 0.42
8	Surface density	1/mm	14.78 ± 1.6
9	Connectivity density	$1/mm^3$	595.71 ± 116.81
10	Connectivity	-	68487.6 ± 13429.14

2.4.2. Assessment of cell seeding efficiency

The results of cell seeding efficiency are presented in Figure (2.5.). The efficiency of static seeding (97.23 ± 0.96 %) was significantly higher than spinning seeding (92.08 ± 2.08 %).

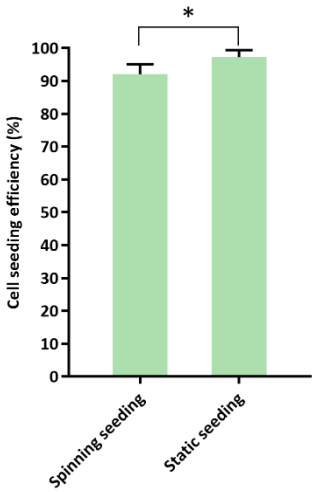

Figure 2. 5. Assessment of cell seeding efficiency of ROS cells in HA/TCP scaffold. Bar chart to show difference efficiency between two methods of cell seeding; spinning and static. In static seeding, ROS cells were added drop-wise to each HA/TCP scaffold while in the spinning method the cell suspension was added to the spinner and allowed to attach to the threaded scaffolds. Data represent mean ± SD of three independent experiments (n=3) performed in triplicate. Statistical significance was determined using an unpaired two-tailed *t*-test (* = $p < 0.05$).

2.4.3. Viability of BCs in static and dynamic conditions

Before the assessment of BCs viability in static and dynamic culture, the optimal incubation time of BC in PB reagent was performed. The optimisation showed a significant difference in the metabolic activities during the 1st, 2nd, and 3rd hour of incubation. However, after 3 hours there was no significant change in metabolic activity values (Figure 2.6.). Therefore, in this thesis, 3 hours incubation period was used in all PB assessments of BC.

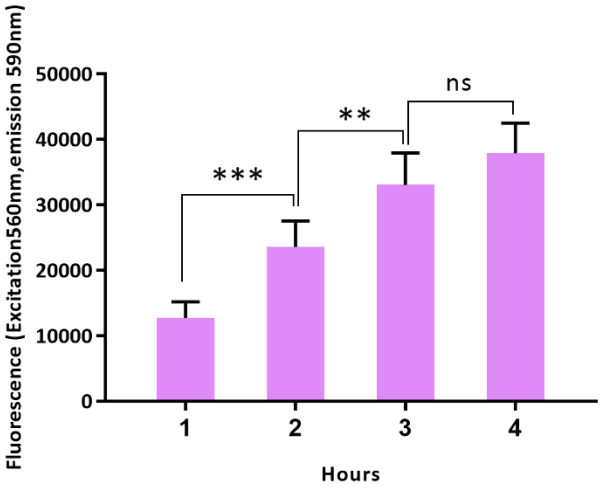

Figure 2. 6. Optimisation of PB assay incubation time. The graph to show fluorescent readings of PB assay at different time points when incubated with ROS cell−seeded scaffolds. The graph demonstrated a significant increase in the metabolic activities during the 1st, 2nd, and 3rd hour of incubation while after 3 hours there was no significant change in metabolic activity values. Data represent mean ± SD of a single experiment (n=1) performed in triplicate. Statistical significance was determined using one-way ANOVA with Tukey's post-test (** = $p<0.01$, *** = $p<0.001$).

With regard to the comparison between the static and dynamic culture, our results showed that the metabolic activities of BCs cultured statically were not significantly different from those cultured in the spinner in the 1st, 2nd, and 3rd week. Conversely, in the 4th week, the spinning culture yielded significantly higher metabolic activity values than the static environment (Figure 2.7.).

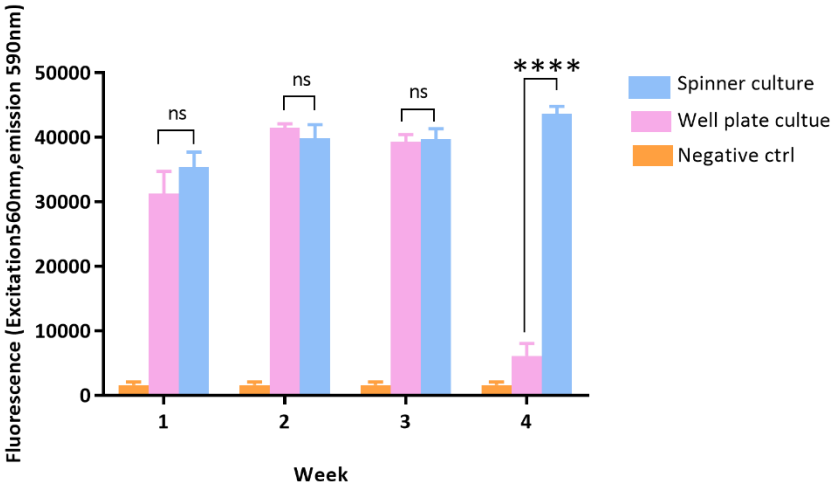

Figure 2. 7. Comparison of the static and dynamic culture of ROS within 3D scaffold. Bar graph to show the vitality of ROS−seeded scaffolds following 28 days culture in either well plate or under spinner bioreactor conditions. The graph demonstrated no significant difference in the metabolic activities of BCs cultured statically in well plate and dynamically spinner in the in the 1st, 2nd, and 3rd week. However, in the 4th week, the dynamically-cultured BCs yielded significantly higher metabolic activity values than those cultured in the static environment. Data represent mean ± SD of a single experiment (n=1) performed in triplicate. Statistical significance was determined using two-way ANOVA with Sidak's post-test (**** = $p<0.0001$).

2.4.4. Attachment, distribution, and morphology of ROS cells

SEM micrographs of the surface regions of acellular HA/TCP scaffold showed a porous microstructure with pores of different sizes (Figure 2.8. A and B). Examination of the BCs surface following one day of culturing demonstrated sparse ROS cells which had a flat irregular morphology attached to the surface and occupied numerous pores (Figure 2.8. C and D). After one month of culturing, the adherent cells had proliferated and arranged into dense aggregates covering the entire scaffold surface and filling the pores. The growing cells established a plump, rounded morphology with a thin layer of secreted matrix appearing in few areas (Figure 2.8. E and F). In the 2nd month (Figure 2.8 G and H) and 3rd month (Figure 2.8. I and J), however, the cells revealed a shrunk degenerative appearance at the surface.

Some areas were devoid of cells whereas in other areas a mineral deposition within the scaffold pores was observed.

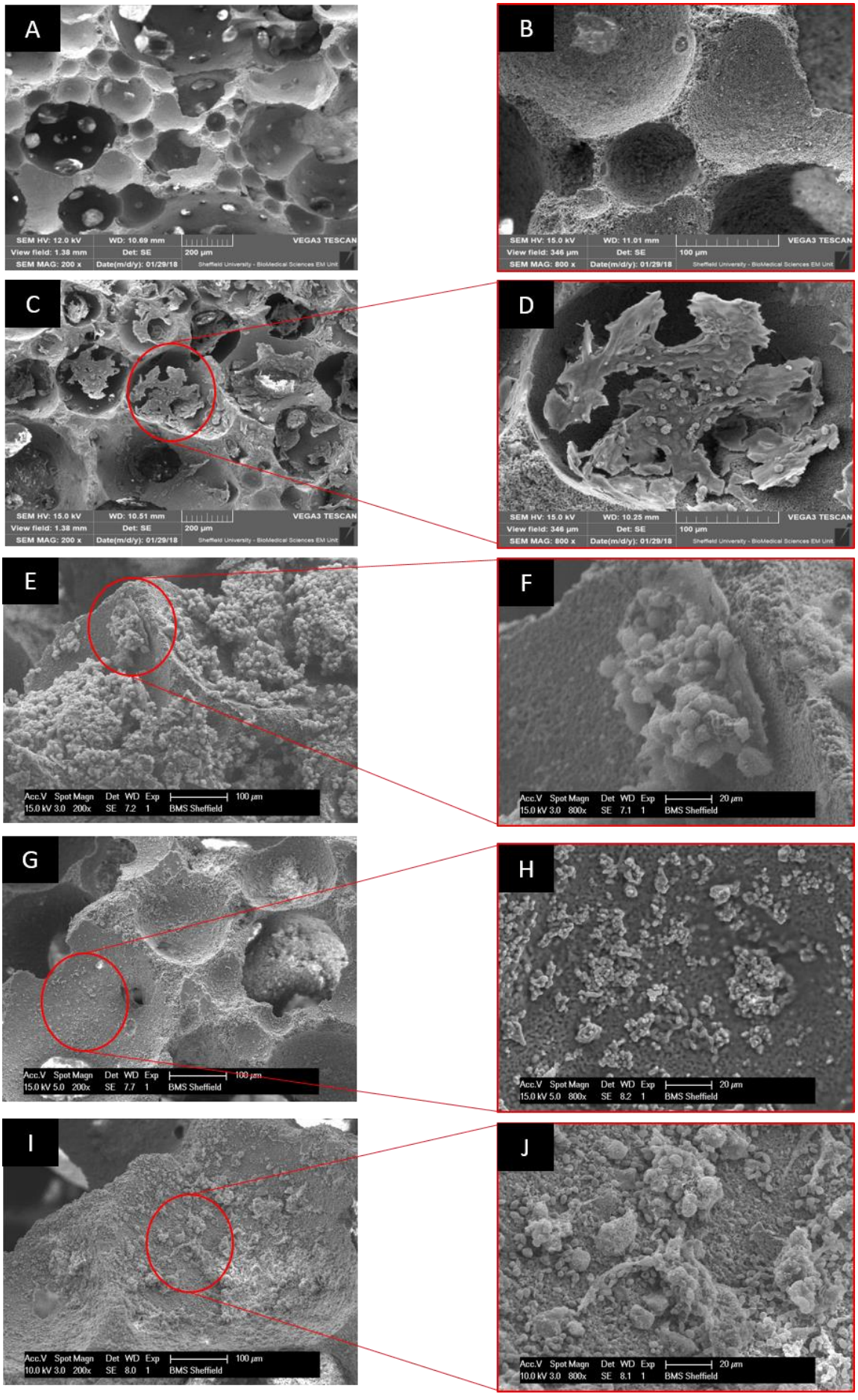
A
SEM HV: 12.0 kV
WD: 10.69 mm
VEGA3 TESCAN
View field: 1.38 mm
Det: SE
200 µm
SEM MAG: 200 x
Date(m/d/y): 01/29/18
Sheffield University - BioMedical Sciences EM Unit
B
SEM HV: 15.0 kV
WD: 11.01 mm
VEGA3 TESCAN
View field: 346 µm
Det: SE
100 µm
SEM MAG: 800 x
Date(m/d/y): 01/29/18
Sheffield University - BioMedical Sciences EM Unit
C
SEM HV: 15.0 kV
WD: 10.51 mm
VEGA3 TESCAN
View field: 1.38 mm
Det: SE
200 µm
SEM MAG: 200 x
Date(m/d/y): 01/29/18
Sheffield University - BioMedical Sciences EM Unit
D
SEM HV: 15.0 kV
WD: 10.25 mm
VEGA3 TESCAN
View field: 346 µm
Det: SE
100 µm
SEM MAG: 800 x
Date(m/d/y): 01/29/18
Sheffield University - BioMedical Sciences EM Unit
E
Acc.V Spot Magn Det WD Exp 100 µm
15.0 kV 3.0 200x SE 7.2 1 BMS Sheffield
F
Acc.V Spot Magn Det WD Exp 20 µm
15.0 kV 3.0 800x SE 7.1 1 BMS Sheffield
G
Acc.V Spot Magn Det WD Exp 100 µm
15.0 kV 5.0 200x SE 7.7 1 BMS Sheffield
H
Acc.V Spot Magn Det WD Exp 20 µm
15.0 kV 5.0 800x SE 8.2 1 BMS Sheffield
I
Acc.V Spot Magn Det WD Exp 100 µm
10.0 kV 3.0 200x SE 8.0 1 BMS Sheffield
J
Acc.V Spot Magn Det WD Exp 20 µm
10.0 kV 3.0 800x SE 8.1 1 BMS Sheffield

Figure 2. 8. SEM micrographs of ROS cell–seeded scaffold. Representative SEM micrographs of HA/TCP scaffold before and after ROS cells seeding and culturing for 3 months. **(A and B)** Scaffold without cells showed the porous structure with pores of various sizes and random distribution. **(C and D)** BC after 24 hours of dynamic culture demonstrated flat irregularly shaped cells scattered on the scaffold surface and occupied many pores. **(E and F)** BC after one month of culturing demonstrated the proliferated cells arranges into dense clusters covering the entire scaffold surface and filling the pores. Note the change of cell morphology from flat at day one to a plum, rounded shape with a thin shell of the secreted matrix appeared in few areas. **(G and H)** and **(I and J)** The construct after 2 and 3 months of culture, respectively. Cells showed a degenerative cell pattern with spherical minerals appearing in the scaffold surface (Scale bars: A, C, E, G =200 μm; B, D, F, H, J = 800 μm). Preparation of samples for imaging was performed by Chris Hill, Department of Biomedical Science, University of Sheffield according to the method described in section (2.3.6.1).

4.4.5. Histological examination of BCs

Decalcified histological section of the acellular scaffold is presented in the (Figure 2.9. A). From day one (Figure 2.9. B) to day 30 (Figure 2.9. C), cells were distributed in the scaffold and became densely packed with a high degree of mitotic figures and even distribution. However, there was a gradual decrease in cellular density in the 2nd and 3rd month (Figure 2.9. D and E, respectively).

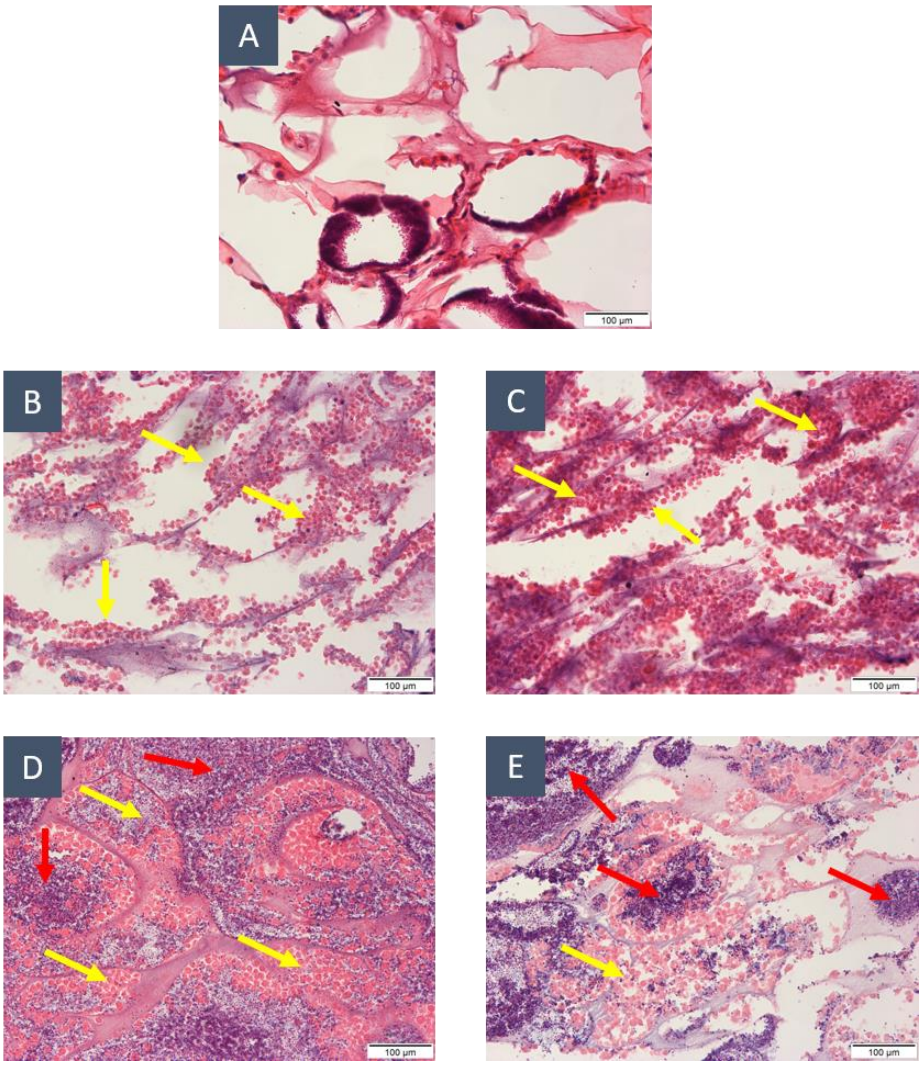

Figure 2. 9. H&E histological sections of decalcified BC. (A) HA/TCP scaffold without cells. **(B)** BC after 24 hours of culture in spinner demonstrated the cells scattered on the residual scaffold material. **(C)** The cells showed proliferation after 1 month of culture. **(D)** BC in the 2nd month of culture demonstrated a decreased cell number and increasing the dissolved scaffold minerals. **(E)** The cell number decreased further at the end of 3rd month. The yellow arrows indicating the ROS cells while the red arrows indicating the degraded scaffold material (Scale bars = 100 µm).

2.4.6. Histological examination of BMM

Examination of the composite BMM revealed a tri−layered structure comprising equivalents of epithelium, connective tissue, and a bony layer. Mucosal part demonstrated a relatively differentiated parakeratinised epithelial tissue with 6−8 cell layers of OKF6/TRET−2 and

evenly distributed fibroblasts within the connective tissue layer. The bone−mucosa interface displayed a thin band of fibrin sealant adhering the soft and hard tissue interface, with many cells populated beneath the sealant and scattered around residual mineral from the decalcified HA/TCP scaffold (Figure 2.10.).

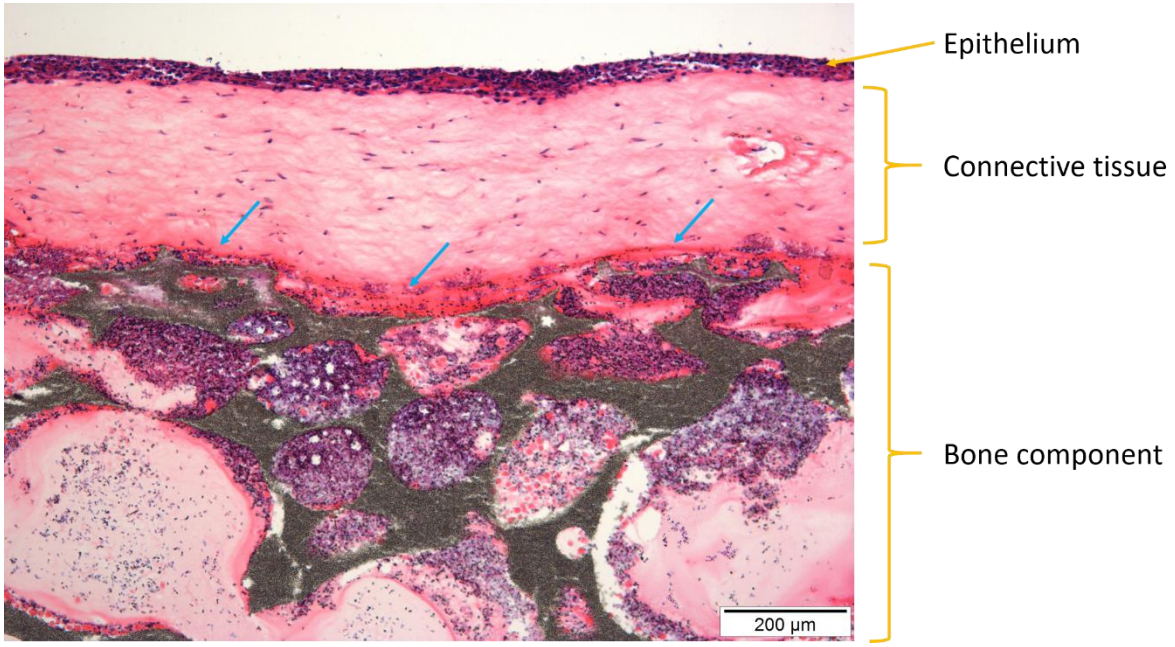

Figure 2. 10. H&E section of the composite cell line−based BMM. Image shows the decalcified section of BMM consisted of mucosal and bone components. The mucosal part was comprised of a relatively stratified epithelial layer formed by immortal OKF6 and a connective tissue layer which demonstrated an evenly distributed fibroblasts within the collagen gel. The bone mucosal interface revealed a thin band of fibrin sealant (blue arrows) at the interface between the soft and hard compartment. Many cells populated beneath the sealant and scattered around residual mineral from the decalcified HA/TCP scaffold (Scale bars =200 µm).

2.5. Discussion

2.5.1. Effect of scaffold structure on BTE

Porous ceramic scaffolds that mimic trabecular bone are receiving particular attention in the rapidly evolving BTE domain. An optimisation of many features such as geometry, composition, and mechanical properties of the scaffold is essential to ensure its functionality in tissue formation. For that, efficient and rapid methods for quantitative assessment of scaffold design are essential (Peyrin, 2011).

In the study of the morphological and architectural characteristics of the scaffold, several techniques have commonly been used, including gravimetric, liquid displacement, SEM, and mercury intrusion porosimetry. Although the first two methods are quantitative, simple, and fast, they are inaccurate and only give an approximation of actual scaffold porosity (Guarino et al., 2008; Nazarov et al., 2004). SEM, on the other hand, provides high resolution of surface topography and can quantify the pore size and number of interconnections (Murphy et al., 2002). However, the 2D measurement on a relatively small area presents a weakness of this method because it is difficult to envisage the internal structure. Similarly, mercury intrusion porosimetry can measure the porosity, pore size, and distribution of the whole scaffold, but it cannot detect the isolated and deep pores. In addition, both SEM and mercury intrusion porosimetry result in sample destruction (Ho and Hutmacher 2006). A high−resolution X−ray μ−CT scan, by contrast, can easily represent specimen in 2D and 3D formats and can analyse the interconnection between pores (Moore et al., 2004). In addition, it is highly accurate, non-destructive, requires minimal sample preparation, and enables visualisation of the internal architecture (Tuan and Hutmacher, 2005; Ho and Hutmacher, 2006). Moreover, it can be employed in the quantification of newly formed bone, neovascularisation, and bone matrix (Peyrin, 2011).

Scaffold acts as synthetic ECM that largely influences cell behaviour and the rate of bone ingrowth through its architectural features, including porosity, pore size, and interconnectivity (Thavornyutikarn et al., 2014). Porosity is defined as the ratio of the volume of void space to the total solid volume (León Y León, 1998). *In vivo*, porosity enhances the mechanical interlock between the implanted scaffold and recipient site; thereby providing an interface mechanical stability (Story et al., 1998). In addition, a high porosity with a high interconnectivity between the pores is essential to permit recruitment and penetration of cells from the surrounding tissue, vascular ingress, and nutrient and waste diffusion (Kuboki et al., 1998).

Although different porosity percentage ranges between 35−90 % were indicated in the previous studies, there is a consensus among the literature that favours increasing the porosity of bone scaffold to enhance osteogenesis (Karageorgiou and Kaplan, 2005). This effect is likely due to the higher adsorption of bone−inducing factors and exchange of ions due to the larger surface area (Hing, 2004; Hing, 2005). Conversely, only a limited number of studies showed no effect of porosity on bone apposition (Fisher et al., 2002; Kujala et al., 2003). The absence of any report in the literature indicating the beneficial effect of minimal porosity solidifies the importance of highly porous scaffold in tissue regeneration. However, increasing porosity often compromises the mechanical property of the scaffold (Scott, 2006). Hence, a balance between the mass transport and mechanical function of the scaffold should exist for an optimal outcome.

Pore size formed by the trabecular separation between struts is another determining factor in bone formation. Generally, pores are either micro (<5 μm pores) or macro (>100 μm pores) (Karageorgiou and Kaplan, 2005). Too small pores limit cell migration and lead to cellular capsule formation in the scaffold periphery, which compromises nutrient diffusion and causes

necrosis in the interior part of the construct. Too large pores, by contrast, decrease cell attachment (Yannas, 1992). To date, the optimal pore size is still controversial. In general, scaffolds with microporosity (<10 µm pores) and macroporosity (>100 µm pores up to 800 µm) have been used in BTE applications and yielded different results (Karageorgiou and Kaplan, 2005). For instance, a study conducted by (Hulbert et al., 1970) in which a calcium aluminate scaffold implanted in dog femoral bone showed that pores of 100 µm−150 µm resulted in substantial bone growth, pores of 75 µm−100 µm showed unmineralized bone, while fibrous tissue was formed in scaffold with pores of 10 µm−75 µm. The author concluded that 100 µm is the minimum recommended pore size for the significant bone formation and correlated this with normal Haversian systems that have an approximate diameter of 100−200 µm. Although these findings were confirmed by other successive studies (Eggli et al., 1988; Flatley et al., 1983), growing evidence has shown that pore size exceeding 300 µm is needed for optimal osteogenesis and vasculogenesis (Murphy et al., 2010; Karageorgiou and Kaplan, 2005; Liu, 1997). However, the role of microporosity in bone formation should not be ignored because it increases the surface area and surface roughness, which in turn enhances protein adsorption and biodegradability (Jeon et al., 2014). The importance of heterogeneous pore size may have led to the emergence of the concept of “gradient scaffold” that incorporates different pore sizes in one construct to exhibit similar structural complexity as the native bone tissue (Di Luca et al., 2016; Andrea Di et al., 2016).

Another important structural parameter of scaffold design is the interconnectivity, which refers to the connection and communication between pores (Li et al., 2003); in other words, the volume of pores accessible by cell divided by the total volume of all pores (Lemon et al., 2012). The pores may be either interconnecting or may contain “dead−ends” (Blokhuis et al. 2000). Several studies demonstrated that interconnectivity is as important as porosity for

effective fluid permeation, cell migration, and mass transfer (Salerno et al., 2017). Connectivity density, on the other hand, is defined as the maximum number of trabecular connection that must be broken in order to break the scaffold (Tellis et al. 2009). Therefore, it correlates more to the scaffold's mechanical properties and may act as an estimator for bone stiffness when it undergoes remodelling (Kabel et al., 1999).

Based on the previously mentioned literature, it appeared that the conventional HA/TCP scaffold used in this study reasonably provided the required features for BTE. However, for ideal bone scaffolding characteristics (see Table 1.1.) further optimisation in terms of structure and composition is needed.

2.5.2. Influence of the seeding technique on seeding efficiency

In this study, ROS cell line was chosen for the fabrication of BC. This cell line was first derived in the late 1970s from the spontaneous tumour in rat. The cells exhibit an osteoblastic characteristic such as ALP expression, OC secretion, and calcified matrix formation when cultured in a dynamic environment (Kartsogiannis and Ng, 2004; Shteyer et al., 1986).

The first step in TE of any construct is seeding of the scaffold. This step often affects the success of tissue-engineered products because it determines the initial number of cells as well as their spatial distribution throughout the construct, which, consequently, provides the basis for cell proliferation, migration, and uniform ECM secretion (Li et al., 2001). Many investigators demonstrated that the optimal initial cellularities of the construct are desirable because they resulted in high proliferation, increased osteogenic gene expression, and more bone tissue formation (Yassin et al., 2015; Zhou et al., 2006). Therefore, researchers have relied on different seeding methods to improve the affinity of cells to the substrate.

Generally, these methods can be divided into two approaches: static and dynamic seeding techniques (Li et al., 2014; Van Den Dolder et al., 2003). A static method is either surface

seeding which is simply performed by pipetting the cell suspension on to the scaffold surface (Wan et al., 2005) or direct injection inside the scaffold (Hofmann et al., 2003). Dynamic methods, on the other hand, involve movement of the cell solution through and/or around the scaffold using a spinner flask (Vunjak-Novakovic et al., 1998), a perfusion bioreactor (Zhao and Ma, 2005), an orbital shaker, or centrifugation (Li et al., 2014).

Several comparative studies between dynamic and static seeding highlighted the advantage of dynamic seeding in achieving high cellular yield and distribution. (Burg et al., 2000) compared the effect of the perfusion bioreactor, the spinner flask, and static seedings using rat aortic endothelial cells on polyglycolide fibrous mesh. They found that static seeding produced the poorest distribution and a low yield, as determined on the basis of cellular metabolic activity, attachment, and proliferation. Similarly, (Van Den Dolder et al., 2003) evaluated the effect of static and rotating seeding on the culturing of rat bone marrow cells into titanium fibre mesh, and concluded that high initial cell number and the osteogenic capacity of the scaffold can be promoted with the dynamic seeding technique. Another comparison performed among static, centrifugal and cycling methods demonstrated that 63.1 % of cells were seeded on the scaffold with the cycling technique, which was higher compared to 61.9 % and 53.2 % for centrifugal and static seeding, respectively (Li et al., 2014). However, the study showed that static seeding provides a more reproducible and uniform seeding in comparison with the other methods, which showed extreme statistical variance. In addition, cell damage and death were lower in static seeding, which showed 5.08 % compared with 6.11 % and 9.31 % for centrifugal and cycling method, respectively.

Other studies, by contrast, are in agreement with our findings in showing that higher seeding efficiency can be obtained with static seeding. (Wendt et al., 2003) monitored seeding efficiency and spatial uniformity of perfusion, static, and spinner systems. They showed that

the difference between perfusion (87 %) and static (85 %) seeding is not statistically significant, whereas both systems produced a significantly higher efficiency than spinner flask (71 %). Similarly, (Thevenot et al., 2011) investigated the seeding efficiency of static, orbital shaker, and centrifuge using a poly (lactide-co-glycolide) (PLGA) scaffold. They found no statistical difference between various cell seeding methods although the cell viability assessment showed 100 % viability with the static method while a cell death of 25 % and 50 % resulted from the shaking and centrifugation methods, respectively. Other studies demonstrated that seeding efficiency using droplet static seeding can reach up to > 90 % (Rajan et al., 2014; Hong et al., 2014; Buizer et al., 2014).

The variations found in the literature regarding static seeding performance may be attributed to several reasons. First, the non optimal ratio of cell number to the surface area of the scaffold may contribute towards increasing the unattached cells, which are miscalculated as un-efficient seeding. (Holy et al., 2000) used initial seeding concentrations that varied from 0.5 to 10×10^6 cells/cm^3 on a PLGA scaffold. They reported that a plateau of 1.5×10^6 cells/cm^3 (25 % of initially seeded cells) was reached regardless of the increasing initial cell concentration. Second, the efficiency of the seeding method varies according to the chemical composition and spatial architecture of the scaffold. Porosity percentage, pore dimetre, pore geometry, surface area, and wettability can lead to different seeding results (Hong et al., 2014). With regard to our results, the high seeding efficiency associated with droplet static may be explained by the proper cell/suspension volume ratio. It is likely that static seeding of 1×10^6 cells loaded in 15 µl promoted more cell attachment in the scaffold than the spinning of 3×10^6 cells suspended in 50 ml. In addition, the hydrodynamic forces such as shear stress produced by the spinner flask may cause detrimental cell damage. Therefore the number of viable attached cells was reduced (Mohd-Zulhilmi et al., 2014).

2.5.3. Effect of static *versus* dynamic culture environment on BTE

In 3D cell culture, cell viability and activity are largely influenced by a culture environment that promotes mass transfer and nutrient delivery. Cell viability can be assessed by a variety of methods, including the measurement of mitochondrial activity, analysis of lactate dehydrogenase, and determination of adenosine triphosphate cell content as the indicators of cellular necrosis and apoptosis (Miret et al., 2006). The monitoring of alterations in mitochondrial activity is particularly popular and can be detected with the use of MTT (3- (4,5-dimethylthiazol-2-yl)-2,5-diphenyltetrazolium bromide) and resazurin (7-hydroxy-10-oxidophenoxazin-10-ium-3-one) (Ansar Ahmed et al., 1994). Although MTT is economic and widely utilized, it is cytotoxic; allowing only one measurement to be made at a single time point (Boncler et al., 2014). Resazurin−based reagents are dependent on the ability of viable, metabolically active cells to reduce resazurin, a water-soluble dye compatible with phenol red, to resorufin that can be detected either colorimetrically or fluorometrically (Ansar Ahmed et al., 1994). AlamarBlue and PrestoBlue are resazurin-based compounds that are considered superior to MTT because they are not toxic to the cells. Therefore, continuous monitoring of cell viability in cultures over time is possible. In addition, these reagents are more sensitive than MTT because they can detect 1,000 cells after 1 hour of incubation while MTT is able to detect 5,000 cells after 3 hours of incubation (Xu et al., 2015).

In BTE, the reproduction of the body dynamic environment is essential because it maintains an efficient mass transfer as well as providing physical stimulation to the differentiating tissue (Szpalski et al., 2013). In 2D and thin 3D tissues, the passive diffusion provided by the continuous contact between cells and the culture medium is sufficient to maintain the cells. However, as the tissue becomes thicker, cells existing at a distance greater than 100−200 µm from the medium would undergo hypoxia and death due to insufficient nutrition/oxygen

supply and waste removal (Mekala et al., 2014). The ceramic-based bone model required a dynamic flow to improve nutrient and waste diffusion because the static culture is only sufficient to nourish the thin superficial layer contacting the medium (Rouwkema et al., 2008). As the cells increase in number, so does their metabolic demand and the build-up of waste products. In addition, once the cells start to secrete their ECM, another diffusion barrier is formed by the matrix components such as proteins and proteoglycans. These are relatively larger molecules with low diffusion coefficients, which may further hinder nutrient diffusion. Consequently, the deeper cells in the tissue interior can be deprived of an oxygen and nutrient source in long-term static culture conditions (Martin and Vermette, 2005; Kihara et al., 2013). Moreover, oxygen transport is linked to its concentration, which is approximately 220 mM in the fully oxygenated culture medium compared with 8699 mM in oxyhaemoglobin. The low oxygen concentration in media limits the diffusion to the outer cell rim and deprives the core cells of oxygen and a nutritional supply (Bhumiratana et al. 2013).

Manipulation of the mechanical force that stimulates growing bone is another important benefit of fluid flow provided by a dynamic culture system. Indeed, native bone is constantly subjected to mechanical stimulation by movement and muscular contraction which lead to bone modelling. In addition, the applied physical forces cause a change in the shear stress, hydrostatic pressure, and electrical fields (Rubin and Lanyon, 1984).

In order to address the previously described limitations associated with static culture, different bioreactor systems have been widely used in BTE (Martina and Giuseppe Maria de, 2014). A spinner flask is a simply designed bioreactor that showed a positive osteogenic effect through increasing the levels of cell proliferation, mineralization, ALP, and OC secretion (Ichinohe et al., 2008; Kim et al., 2007; Sikavitsas et al., 2002). (Sikavitsas et al., 2002) compared bone marrow seeded PLGA scaffolds cultured in static, spinner, and rotating wall

vessels for 21 days. Their weekly assessment revealed an increased cell proliferation at all time points and a higher calcium content in the spinner culture than those encountered in static and rotating wall vessels. Another comparative study was conducted for 21 days between static, orbital shaker, and spinner cultures of rat bone marrow cells seeded in polyethylene terephthalate fibre. The extent of cell proliferation, osteogenic differentiation, ALP activity and mineral density were higher in the spinner culture (Ichinohe et al., 2008). Similar results were obtained when human adipose-derived stem cells were combined with cancellous bone scaffold in the spinner and traditional static culture. Following 2 weeks of culture, ECM secretion, ALP expression, and cell vitality, metabolism, and distribution were much better in the spinner group (Kedong et al., 2014).

Our findings were in agreement with the aforementioned studies in showing that the spinner flask could mitigate the mass transport limitation and promote cells' vitality. We demonstrated that the static culture could not support the model viability for 1 month although the vitality in static and dynamic culture was the same in the first 3 weeks. Cell survival throughout 3 weeks in static culture may be attributed to the nature of cancer cells to withstand the hypoxic environment. In addition, cells can easily gain nutrition as long as they are on the surface of the scaffold where they are in contact with the medium. By contrast, the sharp decline or approximately the complete loss of the models' viability at the end of the 4^{th} week may be because the cells deeply infiltrated inside the scaffold and became isolated. Consequently, the passive diffusion in the static culture was insufficient to provide the highly proliferative cancer cells with their nutrition and oxygen need. In this regard, perhaps it is noteworthy to mention that the non-significant difference between static and spinning culture during the 3 weeks does not necessarily indicate a similar proliferation rate because PrestoBlue assay does not quantify the cell number; rather, it assesses the overall

metabolic cellular activity. It reflects the state of cellular well-being because it assesses the mitochondrial activity which indicates any shift in the aerobic metabolism (Burg et al., 2000).

2.5.4. Qualitative assessment of BC

Our study revealed the feasibility of culturing BC in the spinner bioreactor for 3 months, which is considered to be a relatively long period. A similar long study was performed by Kim et al. (2007) in which hMSC were seeded in silk scaffold and were cultured in a spinner flask for 84 days. They showed that by using the spinner culture not only cell viability was maintained, but all the osteogenic outcomes were progressively enhanced. Perhaps the logical explanation for these results is that the distribution of the nutrients/oxygen within the constructs and the efficacy of cell metabolites are improved by liquid flow in the spinner. Therefore the deeper cell could be reached (Kedong et al., 2014; Mekala et al., 2014).

The qualitative SEM and histological assessments were consistent in showing the distribution and proliferative pattern of ROS cells in HA/TCP scaffold, which was higher during the 1st month and progressively declined towards the end of the experiment. Such a trend in decreased cellularity over time may indicate necrotic cell death, which is explained by the fact that cancer cells have a higher proliferation rate and nutritional demand than normal primary cells. This can result in the deprivation of nutrients and cell death that was noticed in this study during the 2nd and 3rd months of the culture. Furthermore, cell necrosis can be attributed to the limitation of the spinner bioreactor itself because it promotes convection mass transfer at the construct surface while the dominant nutrient exchange within the construct remains by diffusion (Mekala et al., 2014). Meinel et al. (2004) cultured hMSCs on a collagen scaffold of 3 mm and 1.5 mm thickness for 5 weeks. They showed that, in spite of the porosity and minimal thickness of the scaffold, the spinner culture did not adequately

support mass transport. The penetration depth appeared to be 1 mm or less, resulting in bone formation in the exterior and cell death in the centre.

The change in the ROS cells' morphology observed by SEM between the 1st day and the 30th day may be attributed to the differences in cell shape, population, and behaviour in 2D and 3D culture. Cells after only 24 hours of seeding still behaved as in monolayer growth, where cells are usually flatter than they would appear in a 3D environment (Edmondson et al., 2014). Finally, it might be noteworthy to consider that the morphological features observed in this *in vitro* model, which is based on ROS cell line, do not reflect the typical features of bone tissue formation. Not surprising if we generally accepted the fact that malignant cells express the differentiated features of the tissue of origin but do not represent the functional properties in terms of cellular products and response, which are often species-specific (Rodan et al., 1987b).

2.5.5. Qualitative assessment of BMM

In respect of OMM, various types of synthetic and naturally derived scaffolds have been reported such as polycarbonate, PLGA, collagen, and acellular dermis (Moharamzadeh et al., 2007). Collagen comprises the main constituent of the natural oral mucosa. It was first used by (Masuda, 1996) to develop an *in vitro* full thickness OMM by seeding normal keratinocytes in bovine skin collagen gel containing fibroblasts. The resulting model showed well-differentiated mucosal tissue comparable to the native oral mucosa histologically. In this study, growing OMM in a static culture raised no problem due to the hydrophilic, high water−containing networks of collagen hydrogel that enhance permeability for oxygen, nutrients and water−soluble metabolites (Peppas et al., 2006). In addition, collagen provides a suitable template where the fibroblasts proliferate, produce ECM, and provide a condition for keratinocyte proliferation and differentiation better than any artificial matrix (Maruguchi

et al., 1994). However, the dimensional instability and gel contraction presented a problem in this study due to the positive correlation we observed between the number of the contractile fibroblasts and the amount of contraction. This contraction could be minimized by adjusting the number of fibroblasts to $0.2x10^6$, which generated a well-populated connective tissue and proper matrix deposition that appeared as pink staining in the lamina propria component of the model (Fischer et al., 2008).

Oral epithelial cell line immortalised by forced expression of telomerase (OKF6/TERT- 2) was used in this study. The use of cell line helps to reproduce and standardize the model as well as overcome the disadvantages of primary keratinocytes such as limited biopsy resources, patient-to-patient variations, short lifespan, and limited propagation (Southgate et al., 1987; Dongari-Bagtzoglou and Kashleva, 2006b). The choice of this cell line was based on the evidence that it resembles normal keratinocytes in several aspects and was successfully used in the construction of *in vitro* OMM (Dongari-Bagtzoglou and Kashleva, 2006b; Dongari-Bagtzoglou and Kashleva, 2006a). In addition, these cells retain their growth control in culture because telomerase expression rescues cells from the mechanism of senescence without affecting major growth behaviour. Therefore, these cells can be easily cultured for several passages (Dickson et al., 2000). However, in our model, the epithelial layer was not terminally differentiated, which may be attributed to a high passaged number.

The selection of fibrin to glue bone and mucosal tissues was based on imitating the normal physiological phenomenon occurring *in vivo*. When a wound occurs, adhesive fibrin protein is formed to seal the wounded edges as well as to plug blood vessels and prevent blood loss (Miloro et al., 2004). The role of fibrin adhesive in surgery has been recognized since 1972 when it was used in digital nerve repair (Matras et al., 1972). The application of fibrin glue in the field of oral and maxillofacial surgery was first described in 1982 for nerve injury (Matras,

1982); then for soft tissue injuries (Matras, 1985). In addition to its hemostatic, biocompatibility, and biodegradability, fibrin can promote osteogenesis and vasculogenesis due to its pro−angiogenic properties, which make it a suitable candidate for BTE (Khodakaram-Tafti et al., 2017).

This study demonstrated the feasibility of combining the soft and hard tissues in one construct using fibrin sealant, with no detachment cases being reported. However, the major challenge of this study was to preserve the integrity of the model structure during histological processing. The decalcification of BMMs often resulted in complete dissolution of the HA/TCP scaffold and loss of the model's structure due to the absence of a sufficient matrix that could support the residual mineral following decalcification.

Finally, it may be speculated that an alternative method of generating BMM would be by growing the soft tissue directly over the bone component.This approach may be technically impossible due to the lack of universal media formulations suitable for different types of cells in a single culture. In addition, this technique may raise the question of how long the cells, particularly in the air lifted epithelium, can survive in the presence of bone that may prevent adequate delivery of a medium that is not directly contacted to the oral mucosa substitute. Although our composite model revealed that epithelial cells survived for an additional 5 days after final assembly of the full-thickness model, it must be emphasized that this finding should be interpreted with caution because it does not necessarily represent human primary cells.

In summary, the present work demonstrated that *in vitro* engineering of a bone mucosa model resembling native oral tissue structure could be established. The use of fibroblast−populated collagen gel for oral mucosa assembly and employing a biocompatible fibrin−based adhesive to combine the constructed soft and hard tissues appear to be successful approaches in TE of a composite osteo-mucosal system. The current findings

provided primitive proof of the concept to fabricate a well-characterized composite model. In the next chapter, optimization of this newly developed model by using primary human oral cells will be addressed.

Chapter 3: Development and characterisation of tissue engineered human alveolar bone–mucosal model using conventional scaffolds

NB: The work described in this chapter has been published in:

Almela, T., Al-Sahaf, S., Bolt, R., Brook, I. M. & Moharamzadeh, K. 2018. Characterisation of Multilayered Tissue-Engineered Human Alveolar Bone and Gingival Mucosa. *Tissue Engineering Part C: Methods*, 24 (2), pp 99-107.

3.1. Introduction

Currently, there is an exceedingly high demand for bone substitutes in the United State (US) and other countries worldwide. In the US, more than 500,000 patients receive bone defect repairs annually, and the prevalence of bone disorders is expected to double globally by 2020 (Baroli, 2009). Restoration of defects following trauma, excision of pathology, and in the correction of developmental deformities, poses a great challenge due to the lack of suitable donor sites for harvesting grafts capable of accurately replicating the missing tissues. Whilst the need for anatomically-accurate grafting materials offers a niche that could be filled using refined tissue engineered constructs, it also imposes a considerable challenge to current composite TE techniques in order to create and attach the numerous tissue types required to replicate the normal anatomy (Lanza et al., 2014). Despite this challenge, 3D *in vitro* screening systems, based on human cells and tissues, have already attracted significant attention, as they offer more robust and predictive experimental data compared to 2D or animal models (Rouwkema et al., 2011). Limitations of 2D models include the loss of a natural 3D environment, which is in turn reflected in cell behaviour (Khoruzhenko, 2011), and additionally, the absence of a 3D environment excludes important factors such as hypoxic gradients and drug penetration. Furthermore, animal studies may mislead due to interspecies molecular and physiological differences (van der Worp et al., 2010). Therefore, the short−term need for anatomically representative 3D models of the oro-facial region is assured. Future development of these models beyond experimental analysis furthermore offers potential to achieve the longer−term goal of establishing tissue engineered grafting materials capable of improving and simplifying the reconstruction of surgical defects in the orofacial region.

Over the last few decades, there has been a substantial amount of innovation and progress in the engineering of various tissues found in the orofacial region, such as cartilage, bone, mucosa, and periodontium (Pallua and Suschek, 2010). This has encouraged researchers to develop more intricately−structured hybrid tissues that differ in the characteristics of their constituent parts yet comprise a single functional unit. To date, only a few examples of composite tissues have been engineered which replicate the orofacial region. Recent successes include the engineering of osteochondral components of the temporomandibular joint, which comprises both articular cartilage and subchondral bone (Sun et al., 2016; Ruan et al., 2017), and the engineering of a ligamentous interface between tooth and alveolar bone to replicate the bone-periodontal ligament complex (Park et al., 2011).

The three key components of the majority of orofacial tissues are that of bone, fibrous connective tissue, and an overlying epithelium. Development of an accurate alveolar bone-mucosal model, therefore, represents another important step in the process of achieving a clinically utilizable tissue engineered orofacial construct. In Chapter 2, the feasibility of developing 3D composite bone mucosal model was demonstrated using cancer and immortal cell lines. In this chapter, the development of a primary human alveolar bone mucosal model (ABMM) based on the conventional scaffold is presented.

3.2. Aims

1. To develop a novel 3D composite ABMM based on primary cells isolated from the native human oral hard and soft tissues.

2. To characterise the ABMM qualitatively and quantitatively, and to examine whether it accurately replicates the normal tissues in terms of histology, ultrastructural appearance, differentiation and phenotype characteristics.

3.3. Materials and methods

3.3.1. Surgical removal of biopsies

Gingival and bone biopsies were obtained with written, informed consent from patients undergoing elective oral surgery at Charles Clifford Dental Hospital, Sheffield, UK, under appropriate ethical approval from National Research Ethics Services Committee (number 15/LO/0116) (Appendix III).

3.3.2. 2D cell culture conditions of normal human alveolar gingival and bone cells

3.3.2.1. Isolation and cultivation of normal human oral keratinocytes (NHOKs)

Irradiated 3T3 (i3T3) murine fibroblast cells were used as a feeder layer for NHOKs cultivation. 3T3 (NIH/3T3 (ATCC® CRL-1658™) were cultured in DMEM supplemented with 100 IU/ml:100 µg/ml P/S, 10 % FBS, and 2 Mm L-Glutamine. For irradiation of 3T3, cells were exposed to 60 Grays using a cobalt 60 source irradiator to arrest cell growth (Hearnden, 2011). i3T3 were cryopreserved and resurrected when required.

NHOKs were isolated from normal oral mucosa (NOM) biopsies as previously described (Colley et al., 2011). Briefly, biopsies were collected and kept for 4-5 hours at 4 ^{o}C in transport medium which is comprised of DMEM-GlutaMAX™ supplemented with 100 IU:100 mg/ml P/S

and 0.625 µg/ml amphotericin B. Then, biopsies were incubated at 4 °C in 0.25 % trypsin-EDTA solution for 16 hour. Following enzymatic digestion, the epithelium was removed from the connective tissue by gentle scraping with a scalpel blade (Figure 3.1.). NHOKs were centrifuged at 190 g for 5 minutes and cultured with an equal number of i3T3 (Table 3.1.) in Green's medium (see Table 2.3.) (Rheinwald and Green, 1975) which refreshed every day until confluency. NHOKs were used at passage 2 or cryopreserved.

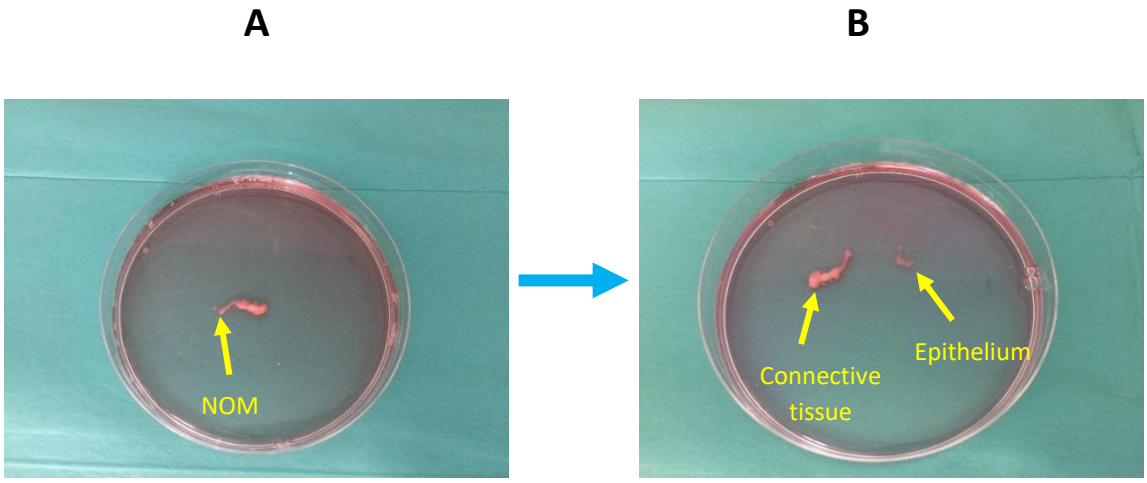

Figure 3. 1. The separation of epithelium from the connective tissue layer of the oral mucosal biopsy. Image shows; **(A)** normal oral mucosa (NOM) biopsy in the transporting medium; **(B)** the epithelial layer was separated from connective tissue by gentle scraping after incubation for 16 hours in trypsin and each layer was cultivated separately.

Table 3. 1. 2D seeding densities of primary human alveolar gingival and bone cells.

Cell type	Seeding density
NHOKs	6×10^4 /cm^2
NHOFs	7×10^3 /cm^2
HAOBs	13×10^3 /cm^2

3.3.2.2. Isolation and cultivation of normal human oral fibroblasts (NHOFs)

NHOFs were isolated from gingival and buccal mucosa biopsies as previously described (Colley et al., 2011). Following incubation with 0.25 % trypsin-EDTA solution for 16 hour at 4 ^{o}C and separation from the epithelium, connective tissue was finely minced and incubated in 0.05 % (w/v) collagenase type I (Gibco, USA) at 37 ^{o}C for 4 hours. NHOFs were collected by centrifugation at 190 g for 5 minutes and plated with appropriate seeding density (Table 3.1) in CDMEM (see Table 2.2.) which refreshed every other day until confluency. NHOFs used at passage 2 or cryopreserved.

3.3.2.3. Isolation and cultivation of primary human alveolar osteoblasts (HAOBs)

HAOBs were isolated from bone chips collected in a sterilised bone trap during the preparation of dental implant sites (Mailhot and Borke, 1998; Jonsson et al., 1999). Following collection in the transport medium, bone fragments were extensively rinsed in PBS and vortexed to remove blood components. Tissue was cultured as explant in CDMEM−LAA (see Table 2.1.) and left undisturbed for 7 days because any dislodgment of explants may impede cell outgrowth. The medium was replaced 2−3 times/week until the culture attained confluency. Cells were passaged, plated with appropriate seeding density (Table 3.1), and used in passage 3 or cryopreserved.

3.3.3. Characterisation of intraoral-derived cells.

3.3.3.1. Characterisation of bone-derived cells.

The main function of bone cells is secretion and mineralisation of ECM (Neve et al., 2011). Therefore, to verify the osteogenic phenotype of the bone-derived cells, the secretion of one major specific osteogenic protein, OC, and the calcium deposition were examined.

3.3.3.1.1. Determination of protein secretion by immunofluorescent (IF) staining

Isolated cells were grown at density 7 × 10^3 /cm^2 on sterilized glass coverslips placed in 24 well plate. After 48 hours, IF labeling with antibodies was performed according to the manufacturer's instructions. Briefly, medium was removed, cells were washed with PBS (1 × 3, 5 minutes each), fixed with 4 % paraformaldehyde (PFA) (Sigma Aldrich, Dorset, UK) (5 minutes), permeabilized with 0.1 % Triton X−100 (Sigma Aldrich, Dorset, UK) (1 × 3, 5 minutes each), and then blocked with 1 % bovine serum albumin (BSA) (Sigma Aldrich, Dorset, UK) in 0.1 % PBS−Tween (Sigma Aldrich, Dorset, UK) for 30 minutes. After removing of blocking solution, primary antibody was added and incubated for 1 hour after which cells were washed with PBS (1 × 3, 5 minutes each) and fluorescein isothiocyanate (FITC) conjugated secondary antibody was added and incubated for 45 minutes. Finally, cells were washed with PBS (1 × 3, 5 minutes each) and mounted using 4',6-diamidino-2-phenylindole (DAPI)-containing, anti-fade mounting medium (Thermofisher, UK). Visualisation was performed using Carl Zeiss microscope and colour view QI click camera with associated image pro plus 7.0.1 software (Zeiss Ltd, Germany). Human leukocyte antigen antibody (HLA) and an appropriate isotype were used as positive and negative ctrl, respectively. Ctrls were used with the dilutions and incubation times identical to that used for the primary antibodies (Table 3.2.).

Table 3. 2. Antibodies used for IF staining of bone-derived cells

Marker	Dilution	Catalogue no.	Vendor
OC	1:100	ab13420	Abcam
HLA	1:100	H1650	Sigma
Mouse IgG isotype	1:100	02-6502	ebioscience
FITC-conjugated goat anti-mouse secondary antibody	1:200	ab150113	Abcam

3.3.3.1.2. Determination of mineralisation by alizarin red stain (ARS).

Quantitative assessment of mineralisation was performed using calcium-bounded ARS (Sigma Aldrich, Dorset, UK) at day 1,7,14,21, and 28. For that, bone-derived cells were cultured on sterilized glass coverslips in 24 well plate at seeding 5×10^3/ cm^2. A standard ARS in a concentration range from 1000 to 0 µg/ml was prepared by serial dilutions with 5 % (v/v) perchloric acid (Sigma Aldrich, Dorset, UK). At each time point, samples were washed with deionized water, submerged with 500 µl of ARS stock solution, and incubated for 30 minutes. Next, the stain was removed and samples were washed repeatedly every 5 minutes with deionized water in a gentle orbital shaker until water remained clear. Then, 500 µl of 5 % (v/v) perchloric acid was added and left for 15 minutes in the orbital shaker. 150 µl of standard and sample solutions were transferred into transparent 96 well plate in triplicates and absorbance was read at 405 nm (Infinite® M200, TECAN, USA). Following subtracting the blank value (0 µg/ml) from all values, the concentration of bounded ARS in samples was determined using the equation defined by the standard curve. Blank solution was used as a negative ctrl.

3.3.3.2. Characterisation of gingival-derived cells.

Cytokeratin 13 (CK13) reacts with suprabasal non keratinised epithelium (Reibel et al., 1989) while fibroblasts surface protein (FSP) is predominately expressed in fibroblasts but not in epithelial cells in the tissue undergoing remodelling such as skin (Frank et al., 1995). These markers were selected for characterisation of NHOKs and NHOFs, respectively. Staining was performed according to the method described in section (3.3.3.1.1.) and the antibodies used for the staining are listed in the Table (3.3.).

Table 3. 3. Antibodies used for IF staining of gingival cells.

Antibodies for IF staining of NHOKs			
Marker	**Dilution**	**Catalogue No.**	**Vendor**
CK13	1:100	ab198584	Abcam
HLA	1:100	H1650	Sigma
Rabbit IgG isotype	1:100	ab172730	Abcam
FITC-conjugated goat anti-rabbit secondary antibody	1:200	ab150083	Abcam
Antibodies for IF staining of NHOFs			
FSP	1:50	Ab11333	Abcam
HLA	1:50	H1650	Sigma
Mouse IgM isotype	1:50	14-4752-81	ebioscience
FITC-conjugated goat anti-mouse secondary antibody	1:200	ab150117	Abcam

3.3.4. Construction of human alveolar bone construct (ABC).

ABC was constructed and characterised prior to its utilization in the composite model. The construction of ABC construct was performed according to the method described in section (2.3.3.5.).

3.3.5. Characterisation of ABC

ABCs were cultured for a month during which the following qualitative and quantitative assessments were carried out every 10 days.

3.3.5.1. SEM examination (see section 2.3.6.1.).

3.3.5.2. Cell viability assessment (see section 2.3.3.4.).

3.3.5.3. Proliferation assessment

Cell proliferation was estimated by measuring total DNA content using ultrasensitive Quant-iT™ PicoGreen® dsDNA reagent kits (ThermoFisher, USA). For that, lysed samples were first prepared then proliferation assessment was carried out.

3.3.5.3.1. Preparation of lysed samples

At each time point, samples were washed with PBS, grinded-frozen in liquid N_2 with pestle and mortar into a fine powder which then transferred to Eppendorf tube. Then, on the ice, 500 µl of lysis buffer consisting of 0.1 % (v/v) Triton in TE buffer (10 mM Tris-HCL, 1 mM EDTA, pH 7.5) was added with the vortex. Following three freeze−thaw cycles, lysed samples were centrifuged at 800 g for 5 minutes at 4 ^{o}C (Thermoscientific, Germany) (de Peppo et al., 2013). The supernatant lysates were collected and kept on ice to be used or kept in −80 until required.

3.3.5.3.2. Assessment of total DNA content

Standard solutions were prepared according to the manufacturer's instructions, using serial dilutions of stock DNA with TE buffer to obtain a concentration ranged from 25 to 0 (blank) ng/ml. 10 µl aliquots of lysed samples were incubated with 90 µl of TE buffer. Then, 100 µl of PicoGreen working reagent was added to standard and sample solutions. 200 µl of standard and diluted lysed sample solutions were transferred into a transparent 96 well plate in triplicates and incubated for 5 minutes protected from light after which fluorescence was read with excitation 480 nm, emission 520 nm (Infinite® M200, TECAN, USA). For calculation, the mean fluorescence value of the blank was subtracted from the averaged sample and standard readings, then a standard curve of known concentrations of DNA was used to convert fluorescence to total DNA content. Blank assay buffer solution was used as a negative ctrl.

3.3.5.4. Total protein content assessment

To quantify the deposited ECM, total protein content was measured using the BCA protein assay kit (ThermoFisher, USA). Standard solutions were prepared according to the manufacturer's instructions, by serial dilution of stock BSA with assay buffer to obtain a final BSA concentration ranged from 2000 to 0 (blank) µg/ml. Then, 25 µl of standard solutions and lysed sample (see section 3.3.5.3.1.) were transferred into a transparent 96 well plate in triplicates and incubated with 200 µl of working reagent for 30 minutes at 37 ^{o}C after which absorbance was read at 562 nm (Infinite® M200, TECAN, USA). For calculation, the mean absorbance value of the blank was subtracted from the averaged sample and standard readings, then protein concentration was determined using a standard curve of known concentrations of BSA. Blank assay buffer solution was used as a negative ctrl.

3.3.5.5. ALP activity assessment

Differentiation of HAOBs was investigated by colorimetric ALP assay (Abcam, UK) according to the manufacturer's instructions. *p*−nitrophenyl phosphate (*p*NPP) was used as a phosphatase substrate which turns yellow when dephosphorylated by ALP enzyme. Standard was prepared by serial dilution of stock *p*NPP with assay buffer to obtain a final concentration ranged from 20 to 0 (blank) nmol/well. Then, in duplicates, 10 µl of ALP enzyme was added to 120 µl *p*NPP standard whereas 10 µl of the lysed sample (see section 3.3.5.3.1.) were diluted with 70 µl of assay buffer and added to 50 µl of *p*NPP. During incubation at room temperature for 60 minutes protected from light, the enzyme converted *p*NPP substrate to an equal amount of coloured p−Nitrophenol. Finally, 20 µl of stop solution was added to sample and standard wells and the quantity of *p*NP produced was measured spectrophotometrically at 405 nm (Infinite® M200, TECAN, USA). For calculation, the mean absorbance value of the blank was subtracted from the averaged sample and standard readings and the concentration of ALP was calculated as:

$$ALP\ (U/ml) = (A/V)\ /T$$

Where **A** is the amount of calculated pNP, **V** is the sample volume, and **T** is the reaction time. Blank assay buffer solution was used as a negative ctrl.

3.3.5.6. Quantitative real−time polymerase chain reaction (qRT-PCR) examination

3.3.5.6.1. Total RNA isolation

Tissue−engineered models were grinded frozen with pestle and mortar in liquid N_2 then the total RNA was isolated from the tissue powder using isolate II RNA Mini Kit (BioLine, UK) according to manufacturer's instructions. Briefly, the grinded tissue was lysed and filtered by centrifugation for at 11,000 g for 1 minute. Then, 70 % ethanol was added to homogenise the

lysate and improve binding of the RNA to the silica-based membrane of the spin column following centrifugation at 11,000 g for 30 seconds. DNA digestion was achieved by incubation with DNase I for 15 minutes followed by washing of column−bound RNA three times and elution in RNase/nuclease−free water. The concentration and purity of RNA were measured using a NanoDrop 1000 spectrophotometer (ThermoScientific, UK) and only high purity RNA (A260/A280 ratio) equal to or more than 2.0 was used for qRT−PCR analysis.

3.3.5.6.2. Complementary DNA (cDNA) preparation

cDNA was prepared from total RNA using a high capacity cDNA reverse transcription kit (Applied Biosystems) according to the manufacturer's instructions. In this protocol, 500 ng of total RNA was reverse transcribed per reaction containing the reagents shown in Table (3.4.). Samples were then loaded in a thermal cycler (MJ Research PTC-200 Thermo Cycler, UK). The reverse transcription reaction consisted of 10 minutes at 25 ^{o}C followed by 2 hours at 37 ^{o}C, then 5 minutes at 85 ^{o}C, after which the sample was stored at −20 ^{o}C until used.

Table 3. 4. The components used to synthesize cDNA. Table shows the reagents of high capacity cDNA reverse transcription kit and their volume which were mixed into MicroAmp Fast reaction tubes (applied biosystem).

Reagent	Volume (µl)
10 × RT buffer	4.0
25 × dNTP	1.6
10 × RT random primer	4.0
Multiscribe reverse transcriptase	2.0
RNase inhibitor	2.0
Nuclease-free water	6.4
Total volume per reaction	**20**

3.3.5.6.3. Gene expression analysis

Quantitative detection of target genes was achieved using pre-designed TaqMan primers (Applied biosystems) (Table 3.5.). 0.5 µl cDNA was added to 9.5 µl qRT−PCR master mix (All Applied Biosystems) to give a total volume of 10 µl (Table 3.6).

Table 3. 5. TaqMan primers used for characterisation of ABM. Asterisked genes were used to analyse the epithelial component of the composite ABMM.

Gene	Marker	Assay ID
ALPL	Alkaline phosphatase (ALP)	HS01029144
Secreted phosphoprotein-1 (SPP1)	Osteopontin (OP)	HS00959010
Secreted protein acidic and rich in cysteine (SPARC)	Osteonectin (ON)	HS00234160
Bone gamma-carboxyglutamic acid-containing protein (BGLAP)	Osteocalcin (OC)	HS01587814
COL1A1	Collagen1 (COL1)	HS00164004
KRT10*	Cytokeratin 10 (CK10)	HS01043114-G1
KRT13*	Cytokeratin 13 (CK13)	HS02558881-S1
B_2M	B-2-microglobulin	HS00187842-M1

Table 3. 6. The reagents used in TaqMan qPCR.

Reagent	Volume (µl)
Taqman master mix	5
B_2M	0.5
Primer	0.5
Water	3.5
cDNA	0.5
Total volume per reaction	**10**

Each sample was run in triplicate and the following thermocycle settings were used:

Initial hold at 95 ^{o}C for 10 minutes, followed by 40 cycles of Annealing and Extension at 95 ^{o}C for 10 seconds, 60 ^{o}C for 45 seconds, respectively (Rotor-Gene Q, QIAGEN, Germany). B_2M was used as the reference control gene. The threshold cycle (C_T) values provided by the QIAGEN Software (QIAGEN, Germany) were imported into a spreadsheet of Microsoft Excel (version 2016) and ΔC_T was calculated as follows;

$$\Delta C_T = C_T \text{ target gene} - C_T \text{ reference gene}$$

where C_T target gene is gene under investigation while C_T reference gene is C_T for B_2M measured in the same well. The quantification of gene expression was calculated either by using delta threshold cycle (ΔCT) value to calculate fold change using the 2ΔCt equation or by calculating gene expression relative to the reference ctrl.

3.3.5.7. Enzyme-linked immunosorbent assay (ELISA).

Following 24 hours incubation of models in serum-free conditioned medium, ELISA was used to measure the level of collagen (COL1) (R&D systems, UK), osteonectin (ON) (R&D systems, UK), and osteocalcin (OC) (Abcam, UK) in the conditioned medium according to the manufacturer's instructions. For measuring COL1 and ON, conditioned medium was diluted to (1:200), (1:20), respectively. Then, 96 well plate was coated with the recommended concentration of captured antibody and incubated overnight at room temperature. The following day, wells were washed and nonspecific binding sites were blocked with 1 % BSA in PBS before the standard and samples were incubated for 2 hours. Then, unbound protein was washed and the recommended concentration of biotinylated detection antibody was incubated for 2 hours. Finally, streptavidin conjugated to horseradish peroxidase was added and incubated for 20 minutes followed by TMB substrate. For OC measurement, simple step

ELISA kit was used in which sample, standard, and antibody cocktail (capture and detector antibody) were added to antibody−coated wells and incubated for 1 hour at room temperature on a plate shaker. Following washing, TMB substrate was added and incubated for 10 minutes. All colorimetric reactions were measured spectrophotometrically using microplate reader (Infinite® M200, TECAN, UK) at an absorbance wavelength of 450 nm and 570 nm for correction. Data were imported and into a spreadsheet of Microsoft Excel (version 2016) for analysis. The concentration of target protein was determined using a standard curve of known protein concentrations. Conditioned media of monolayer cultured HAOBs was used as a positive ctrl while media without cells was the negative ctrl.

3.3.6. Development of composite human alveolar bone mucosal model (ABMM).

Construction of ABMM involved the simultaneous construction of ABC (see section 2.3.3.5.) and OMM (see section 2.3.4.). When the culture of OMM completed at day 17th, it was combined with ABC according to the method described in section (2.3.5.) to form a composite ABMM which further cultured for additional 5 days in static ALI condition (Figure 3.2.).

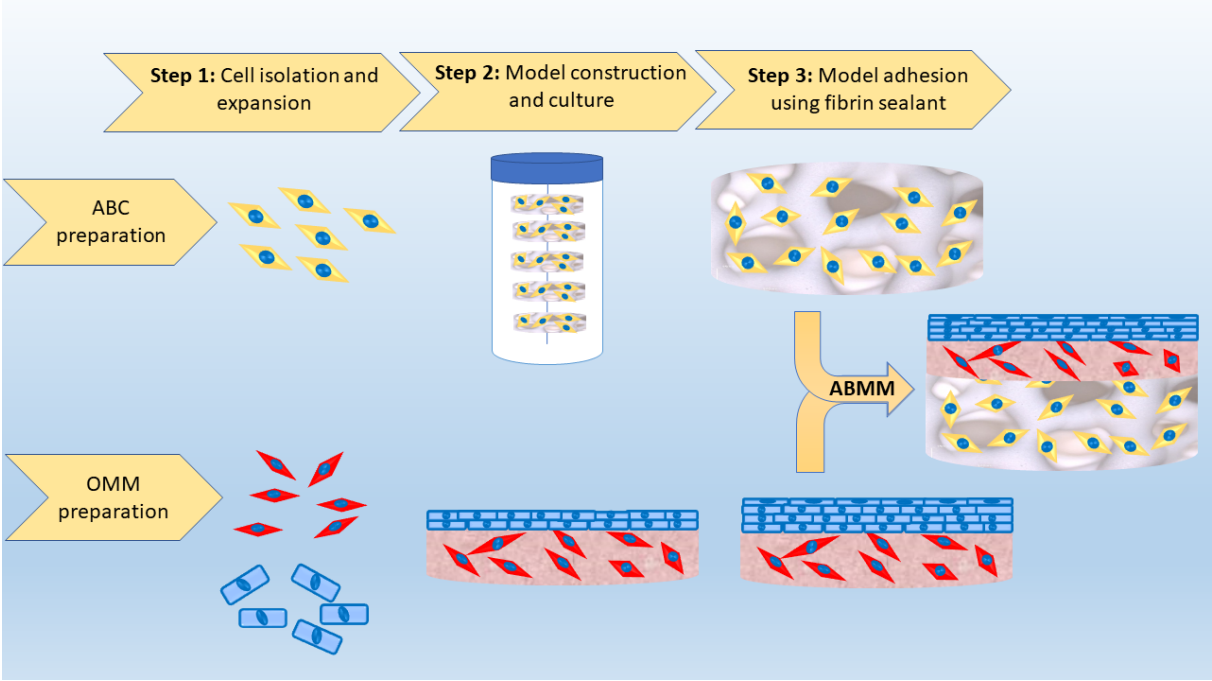

Figure 3. 2. Schematic illustration of the preparation of ABMM. The procedure involved 3 main steps. First; HAOBs, NHOFs, and NHOKs were isolated from oral tissues and cultivated in monolayer culture. Second; ABMs were prepared by seeding HAOBs in HA/TCP scaffold and cultured in spinner bioreactor while OMMs were prepared from fibroblast–embedded collagen gel and ALI cultured oral keratinocytes. Third; the combination of ABC and OMM using adhesive fibrin to form ABMM.

3.3.7. Characterisation of ABMM

3.3.7.1. Histological examination of mucosal part

For histological examination, frozen sections were prepared as previously described (Kriegebaum et al., 2012). OMMs were fixed with 4 % PFA for 24 hours, incubated overnight in 18 % sucrose solution (Sigma Aldrich, Dorset, UK), then frozen in optimal cutting temperature compound (Thermofisher, UK). Sections of 14 µm thickness were prepared (Microm, Germany) and mounted onto superfrost plus micro slide (VWR, West Sussex, UK). Some sections were stained with H&E (See Table 2.8.) and imaged using an Olympus BX51 microscope and Colour view IIIu camera with associated Cell^D software (Olympus Soft Imaging Solutions, GmbH, Münster, Germany). Other sections were subjected to IF staining.

3.3.7.2. IF staining of mucosal part

For characterisation, sections of OMM were stained with cytokeratin 10, 13, and 14, which are the markers of keratinised epithelium, non-keratinised epithelium, and actively dividing basal keratinocytes, respectively (Kinikoglu et al., 2009; Jennings et al., 2016; Kriegebaum et al., 2012). For that, sections were washed with PBS (× 3, 5 minutes each), permeabilised with 0.2 % Triton x-100 (× 2, 15 minutes each), and then blocked with 1% BSA in 0.1 % PBS-Tween for 1 hour. Following aspiration of blocking solution, sections were incubated with primary antibodies or IgG isotype overnight in a humidified chamber at 4 ^{o}C (Table 3.7.) then washed with PBS (× 3, 5 minutes each). Sections with conjugated antibodies were mounted using DAPI−containing, anti−fade mounting medium (Thermofisher, UK), while those with un conjugated antibodies or with isotype control were incubated with secondary antibodies for 1 hour at room temperature then washed with PBS (× 3, 5 minutes each) and mounted. Images were captured using Carl Zeiss microscope and colour view QI click camera with associated image pro plus 7.0.1 software (Zeiss Ltd, Germany).

Table 3. 7. Antibodies used for IF staining of OMM.

Marker	Dilution	Catalog no.	Company
CK10	1:50	ab9025	Abcam
CK13	1:100	ab198584	Abcam
CK14	1:100	ab192055	Abcam
Mouse IgG Isotype	1:50	02-6502	ebioscience
Rabbit IgG Isotype	1:100	ab172730	Abcam

Gout anti-mouse secondary antibodies	1:200	ab150117	Abcam
Gout anti-rabbit secondary antibodies	1:200	ab150083	Abcam

3.3.7.3. Transmission electron microscopy (TEM) of mucosal part

TEM assessment was performed to demonstrate the presence of epithelial cell ultrastructures such as desmosome and hemidesmosome which provide interepithelial and epithelial-connective tissue connection, respectively (Nanci, 2013). For that, 4 mm of OMM were fixed in 3 % glutaraldehyde in 0.1 M sodium cacodylate buffer overnight, washed with 0.1 molar sodium cacodylate buffer, and post-fixed in 2 % aqueous Osmium Tetroxide for 2 hours. Following rinsing with water, samples were dehydrated with 70 %, 95 %, and 100 % ethanol (×2, 10 minutes each) then cleared in epoxypropane and infiltrated in 50:50 araldite resin: epoxypropane mixture overnight on a rotor. This mixture was replaced with two changes over 8 hours with fresh araldite resin mixture before being embedded and cured in a 60 ^{o}C oven for 48-72 hours. Finally, ultrathin sections of 85 nm thick were cut on ultramicrotome (Leica UC 6, Leica microsystem, Germany) onto 200 mesh copper grids and stained for 30 mins with saturated aqueous Uranyl Acetate followed by Reynold's Lead Citrate for 5 minutes. Visualization was performed using a transmission electron microscope (FEI tecnai 12 Bio-twin, 120Kv TEM) at an accelerating voltage of 80 Kv. Electron micrographs were recorded using a Gatan Orius 1000 digital camera and Gatan Digital Micrograph software. Preparation and sectioning of samples for imaging was performed by Chris Hill, Department of Biomedical Science, University of Sheffield.

3.3.7.4. Histological examination of ABMM.

3.3.7.4.1. Preparation of undecalcified resin embedded block

Technovit 7100 (Heraeus Kulzer, Wehrheim, Germany), a plastic embedding system based on 2-hydroxyethyl methacrylate, also known as GMA (Glycolmethacrylate), was used according to manufacturer's instructions (Gerrits and Horobin, 1996). Briefly, the embedding procedure consisted of four major steps:

Fixation and dehydration

At the end of the incubation period, specimens were washed with PBS, fixed in 4 % PFA for 24 hours, then rinsed with PBS before dehydration in graded ethanol series 75 %, 95 %, 100 % for at least 2 hours with two changes for each solution.

Prefiltration

After dehydration, the specimens were immersed in a prefiltration solution consisting of equal parts of Technovit 7100 basic solution and 100 % ethanol overnight on a rotating mixer.

Infiltration

Specimens were infiltrated with infiltration solution consisting of 100 ml Technovit 7100 basic solution and 1 g Hardener 1 for 2 days on a rotating mixer.

Polymerisation

Finally, samples were polymerized in a suitable mold in premixed 15ml infiltration solution plus 1 ml Hardener 2. Polymerisation completed in around 2 hours at room temperature or 1 hour at room temperature in a vacuum embedder.

3.3.7.4.2. Ground sectioning

Cutting-grinding technique was carried out to prepare the resin embedded slides (Chai, 2011). Resin block was first sectioned into 100-150 µm thickness with a cutting machine (IsoMet® 1000 precision saw, Buehler UK Ltd, UK). Sections were then adhered onto superfrost plus micro slide using cyanoacrylate adhesive (Loctite® glass bond UV curing, UK). Thickness was then further reduced to 35−40 µm by grinding the sections with silicon carbide papers of P800 and P1200 roughness in a grinder-polisher machine (Buehler ™ Metaserv, UK). Subsequently, ground sections were stained by H&E staining according to the manufacturer's instructions (Table 3.8.) (Leica ST4040 Shandon Linear Stainer, Leica Microsystems, Germany). Slides were mounted with DPX and covered with a coverslip. Finally, images were taken using an Olympus BX51 microscope and colour view Illu camera with associated Cell^d software (Olympus soft imaging solutions, GmbH, Münster, Germany).

Table 3. 8. H&E staining schedule for resin embedded section. Table describes the order, solutions used for staining, and time the tissue spent in each solution. Industrial denatured alcohol (IDA).

Order	Solution	Time (minutes)
1	Harris' haematoxylin (Shandon)	15
2	Running tap water	1
3	Scott's tap water substitute	10
4	Running tap water	1
5	Eosin Y – aqueous (Shandon)	20
6	Running tap water	1
7	70 % IDA	1
8	95 % IDA	1
9	100 % IDA	1

10	Xylene	1

3.3.7.5. qRT−PCR examination (see section 3.3.5.6.).

3.3.7.6. ELISA (see section 3.3.5.7.).

3.3.8. Statistical analysis

All data were presented in terms of mean ± SD of three independent experiments performed in triplicate. One−way ANOVA complemented by Tukey's post-test was performed using GraphPad Prism software v7.0. (GraphPad Prism software, CA, USA). Differences were considered significant when $p < 0.05$.

3.4. Results

3.4.1. 2D expansion and phenotypic characterisation of intraoral-isolated cells

Regarding intraoral derived bone cells, with the exception of a small number of detached cells from the bone surface, the first evidence of cellular outgrowth from the explants was observed within 7−10 days of plating. After 2 weeks, cells started to migrate from the tissue onto the flask surface (Figure 3.3. A). Avoiding explant dislodgment during feeding helped to anchor the explant to the flask and prevent disturbance of cell outgrowth. The proliferated cells had polygonal or spindle shape morphology. No differences in growth characteristics or cell morphology were observed among individual explant cultures. Culture generally attained confluency after 4−5 weeks after initiation of culture and achieved cell yields 2,860,000 ± 597285.5 cells/ 75 cm^2 flask.

With respect to the growth of NHOKs, by 4^{th} to 5^{th} day, small colonies of 10-15 cells were visible between i3T3. In 10−14 days, the colonies matured, lateral expansion ceased, and the cells were desquamated from the surface. The culture yielded 3,000,000 ± 163299.3 cells / 25

cm^2 flask (Figure 3.3. B). Contaminating NHOFs were seen on few occasions which scrapped off to obtain a pure culture. NHOFs outgrowth from the connective tissue pieces began in 4−6 days and the confluent culture gave 3766666.7 ± 251661.1 cells / 75 cm^2 flask (Figure 3.3. C).

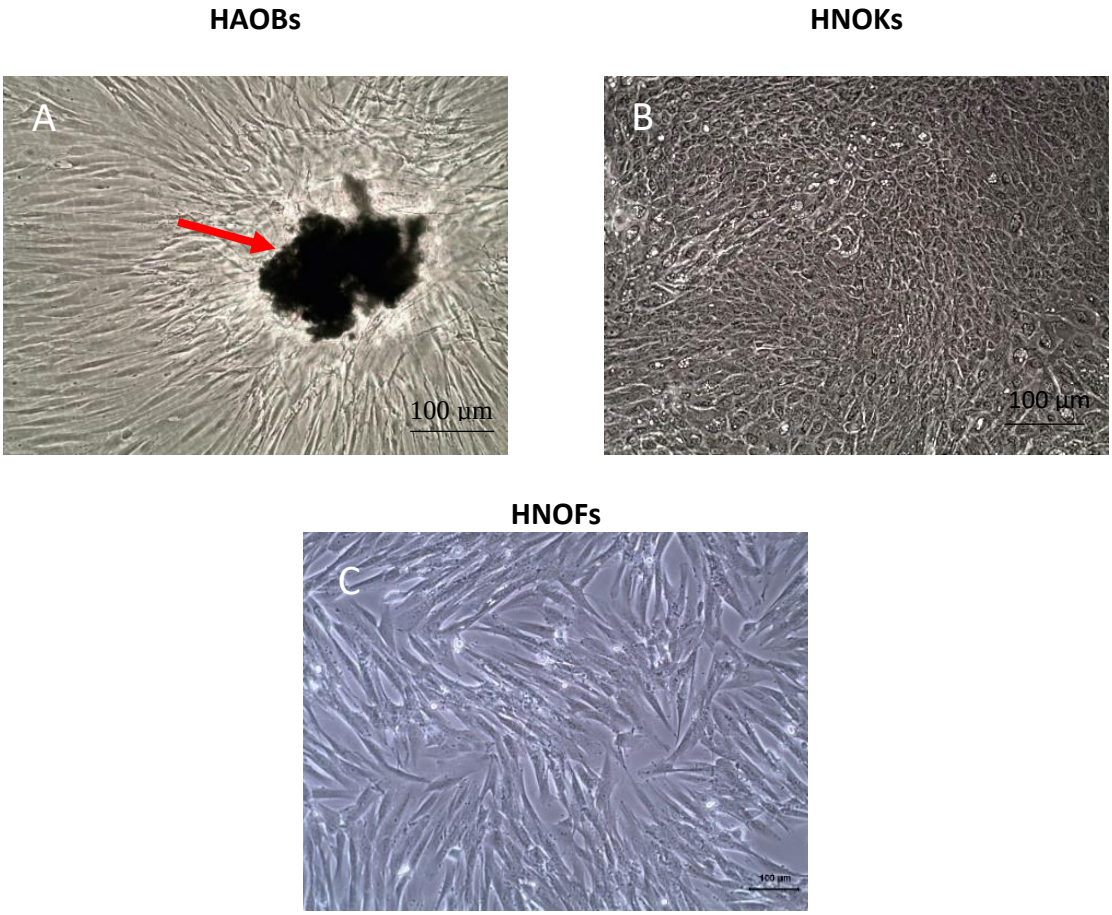

Figure 3. 3. Inverted lens microscopy of 2D cultured HAOBs, NHOKs, and NHOFs isolated from oral biopsies. Image shows **(A)** The outgrowth of bone−derived cells from the explanted oral cancellous bone (red arrow). The migration of cell started after 2 weeks of explant plating and the confluency was reached at 4^{th}–5^{th} week. The derived cells exhibited a polygonal or spindle shape which reflects the osteoblastic morphology. **(B)** A confluent layer of epithelial cells attained after 10−14 days of culture with an i3T3 feeder layer in Green's medium. The culture gave rise to apparently pure keratinocyte outgrowths except for few cases where the keratinocytes were mixed with the fibroblasts. The shape of keratinocytes was remarkably homogenous and area of intense mitotic activity was noticed before the coalescence of outgrowth and formation of the confluent culture. **(C)** The outgrowth of cells isolated from the connective tissue began 4-6 days after establishment in primary culture. The culture shows elongated fibroblasts proliferating in irregular bands (Scale bars = 100 µm).

In addition to the morphological observation, the bone, epithelial, and connective tissue-derived cells characterised by immunofluorescent labelling demonstrated a positive immunoreactivity for OC (the major non collagenous osteogenic protein), CK13 (epithelial differentiation marker) and FSP, respectively. These findings confirmed that the isolated cells had the normal phenotypical features associated with HAOBs, NHOKs, and NHOFs, as well as they showed the purity of the culture (Figure 3.4.).

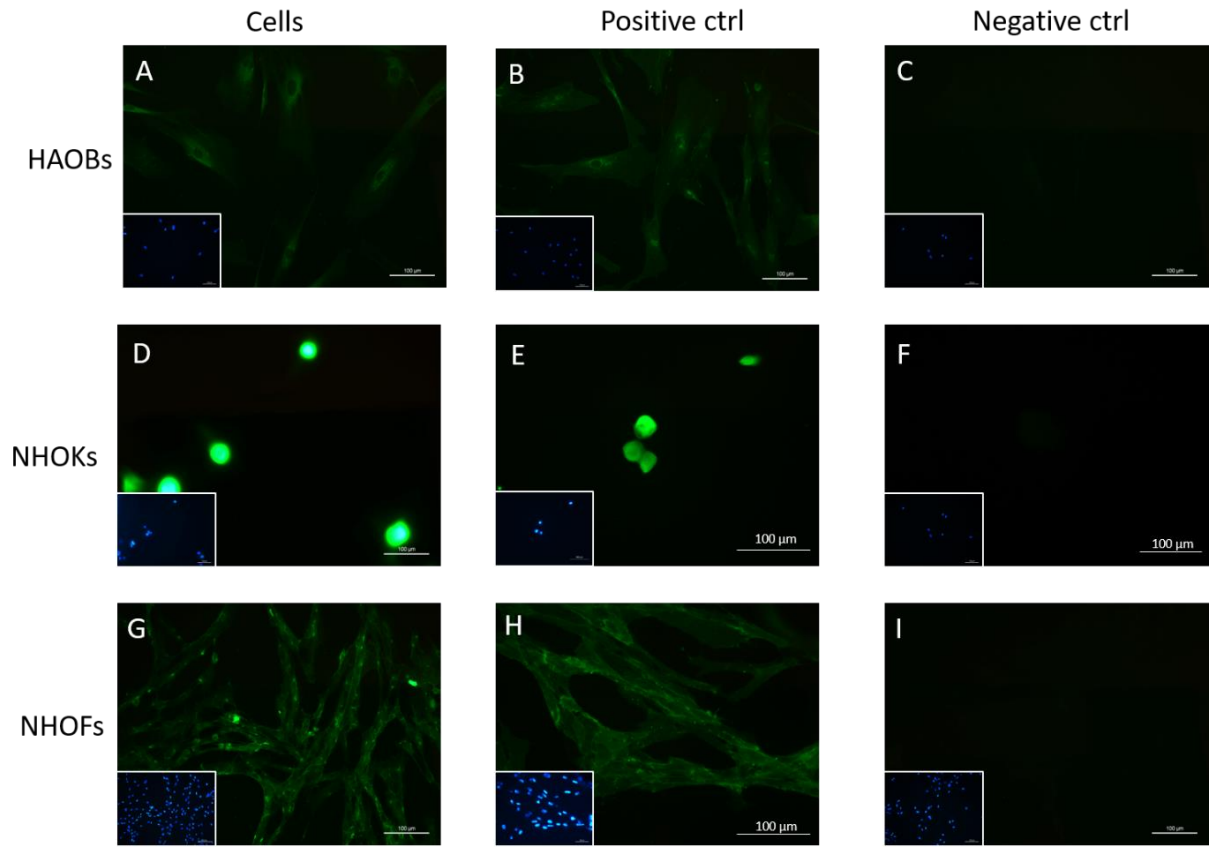

Figure 3. 4. Representative images of immunofluorescent stained HAOBs, NHOKs, and NHOFs. Images show positive immunoreactivity (green) of **(A)** HAOBs; **(D)** NHOKs; and **(G)** NHOFs with OC, CK13, and FSB, respectively. **(B, E, H)** depict positive ctrls stained with HLA and secondary antibodies. **(C, F, I)** depict negative ctrls incubated with Ig isotype and secondary antibodies. Inset images include DAPI overlay to demonstrate cell nuclei (blue) (Scale bars = 100 µm).

The capacity of bone−derived cells for mineralisation was quantified by ARS at days 1, 14, 21, and 28 of culture. Figure (3.5.) indicates that mineral deposition was significantly high at day 14 ($p=0.0006$) and continued to increase at day 21 and 28 ($p<0.0001$) compared with day 1.

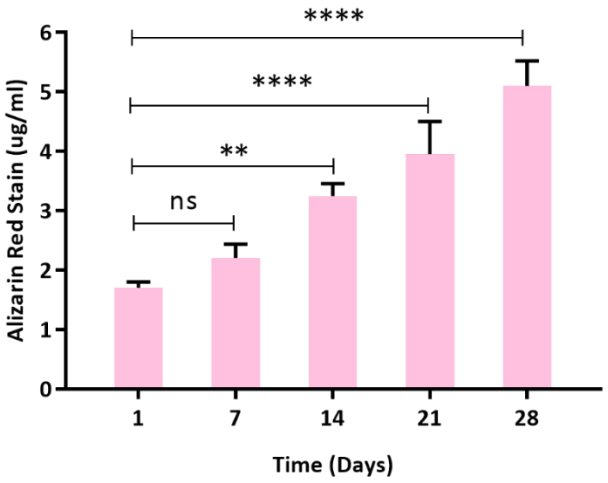

Figure 3. 5. Determination of matrix mineralisation by HAOBs using ARS. Graph shows the concentration of calcium bounded ARS at day 1,7,14,21, and 28 of culture period of HAOBs cultured in monolayer. Data represent mean ± SD of three independent experiments (n=3) performed in triplicate. Statistical significance was determined using results from a one-way ANOVA followed by Tukey's post-test (** = $p<0.001$, **** = $p<0.0001$). Asterisks above the horizontal line are relative to the two bars at the ends of the line.

3.4.2. Evaluation of ABC

3.4.2.1. SEM examination

Cell adhesion, proliferation, and distribution were qualitatively assessed by SEM. SEM observation allowed to determine sparse HAOBs well adhered to HA/TCP scaffold surface after 1 day of culture (Figure 3.6. A). At day 10, proliferated cells were being able to deeply infiltrate the pores and span across them which demonstrated the adequacy of the pore size range (Figure 3.6. B). By 20 days, it was possible to observe a higher degree of colonization occluding most of the scaffold pores (Figure 3.6.C). Additionally, it was possible to observe

what seems to be ECM fibers produced by proliferated cells (Figure 3.6. D). At the end of the month, HAOBs had massively colonized the scaffolds and occluding the scaffold bars and pores (Figure 3.6. E).

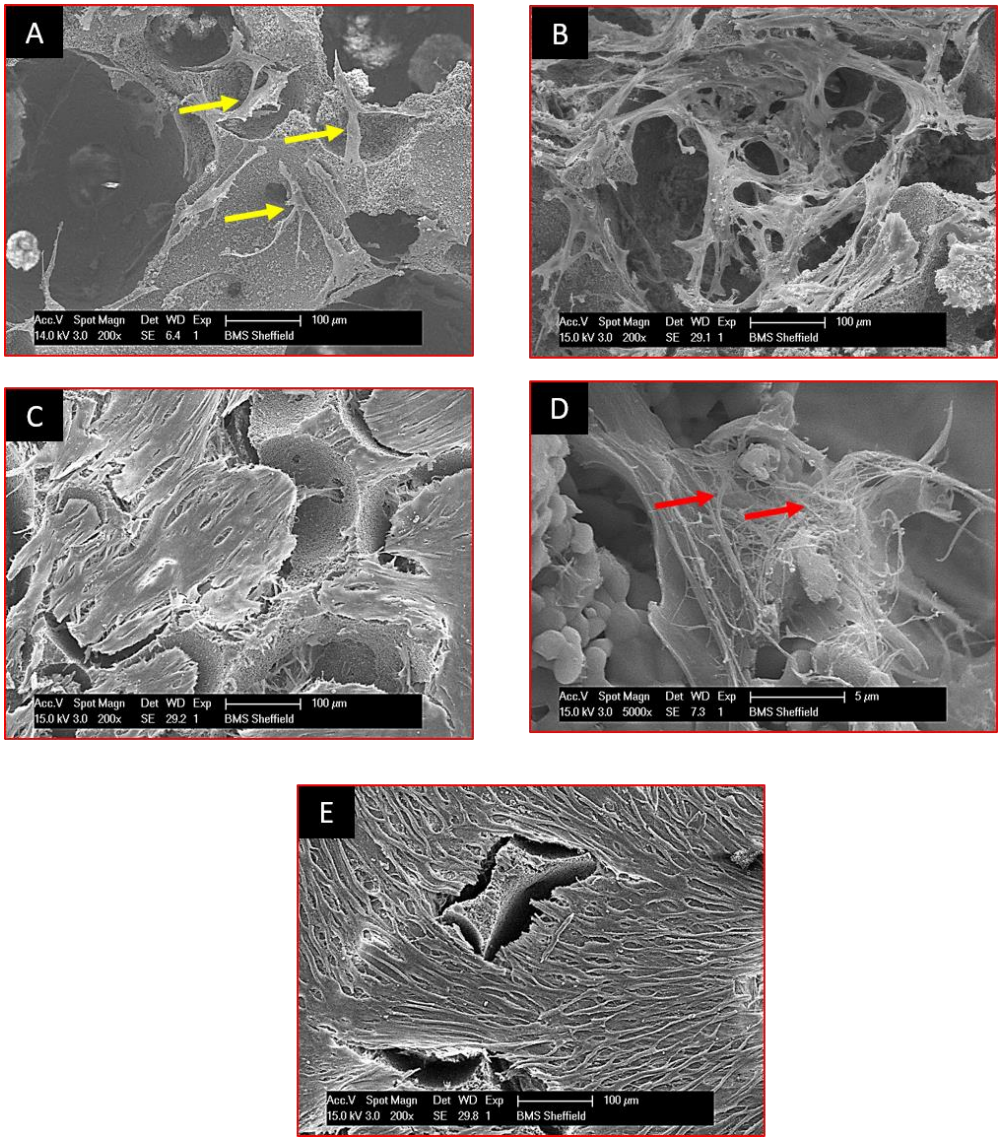

Figure 3. 6. SEM micrographs of ABC. Image shows HAOBs cultured on HA/TCP scaffold at; **(A)** day 1, HAOBs were attached and scattered on the scaffold (yellow arrows); **(B)** day 10, the cells demonstrated a proliferation and infiltration of the pores; **(C)** day 20, showed an increased cell number that covered most of the scaffold surface and **(D)** possibly the secreted ECM fibres (red arrows); **(E)** day 30, the proliferated cells expanded on the scaffold forming a membrane-like layer covering scaffold pores and bars (Scale bars: A, B, C, E = 200 µm; D = 5000 µm). Preparation of samples for imaging was performed by Chris Hill, Department of Biomedical Science, University of Sheffield according to the method described in section (2.3.6.1).

3.4.2.2. Cell vitality

Viability assessment of ABC at day 10, 20, and 30 presented a significant increase in signal intensity compared to day 1 ($p<0.0001$). The highest metabolic activity reached at day 20 which was significantly higher than that noticed at day 10 ($p=0.0038$) while no difference was observed between day 20 and 30 ($p=0.1464$) (Figure 3.7.).

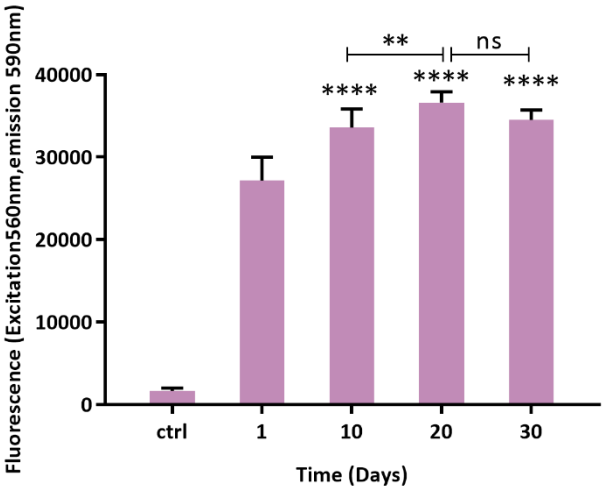

Figure 3. 7. The viability of HAOBs within the ABC. Graph shows the viability of HA/TCP bone constructs cultured in spinner bioreactor for one month. The metabolic activity of HAOBs within the construct demonstrated a gradual increase that reached the maximum level by day 20 while no significant difference was observed afterward. Data represent mean ± SD of three independent experiments (n=3) performed in triplicate. Statistical significance was determined using one-way ANOVA followed by Tukey's post-test (** = $p<0.01$, **** = $p<0.0001$). Asterisks directly above the bar are relative to the day 1 (baseline) and above the horizontal line are relative to the two bars at the ends of the line.

3.4.2.3. Cell proliferation

Total DNA content, which indicates to cell proliferation, reflected approximately the same trend observed with the cell activity assessment. The cell number demonstrated a progressive significant increase at 10 ($p= 0.0017$), 20 ($p<0.0001$), and 30 ($p=0.8073$) compared with day

1. The proliferation at day 20 was significantly high in comparison with the previous time point (0.0014) while no difference was reported between day 20 and 30 (Figure 3.8).

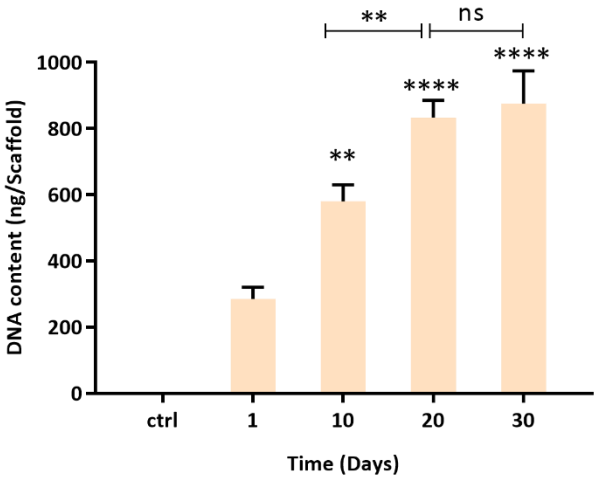

Figure 3. 8. Total DNA content in ABC. Graph shows the proliferative pattern of HAOBs cultured in HA/TCP scaffold along the entire duration of culture in the spinner. The number of HAOBs within the construct demonstrated a gradual increase that reached the highest level by day 20 and 30 which were not significantly different. Data represent mean ± SD of three independent experiments (n=3) performed in triplicate. Statistical significance was determined using one-way ANOVA with Tukey's post-test (** = $p<0.01$, **** = $p< 0.0001$). Asterisks directly above the bar are relative to the day 1 (baseline) and above the horizontal line are relative to the two bars at the ends of the line.

3.4.2.4. Total protein secretion

The concentration of protein progressively increased at day 10 ($p=0.0223$), 20 ($p<0.0001$), and 30 ($p<0.0001$) compared with day 1. The protein level at day 20 was significantly higher in comparison with day 10 ($p=0.0037$) while no significant difference was observed afterward ($p=0.9362$) (Figure 3.9.).

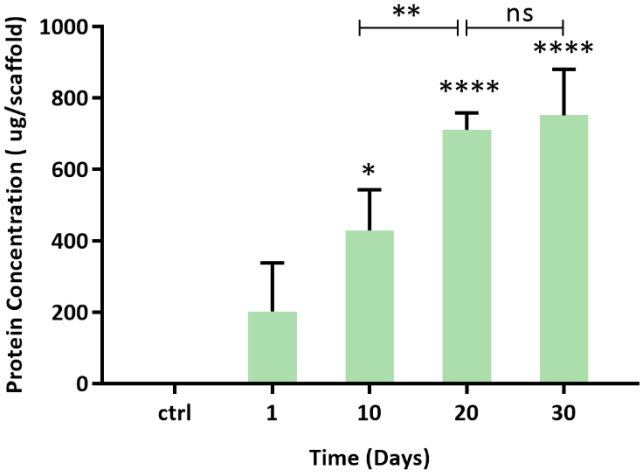

Figure 3. 9. Protein content in ABC. Graph shows the protein content in HAOBs−HA/TCP constructs along the entire duration of culture in the spinner. The total protein content within the construct demonstrated a progressive increase that reached the highest level by day 20 and 30 which were not significantly different. Data represent mean ± SD of three independent experiments (n=3) performed in triplicate. Statistical significance was determined using one-way ANOVA with Tukey's post-test (* = $p< 0.05$, ** = $p<0.01$, **** = $p< 0.0001$). Asterisk(s) directly above the bar is relative to the day 1 (baseline) and above the horizontal line are relative to the two bars at the ends of the line.

3.4.2.5. ALP assessment

The osteogenic differentiation was investigated by measuring the ALP activity. The data presented in Figure (3.10) demonstrated that the constructs of HAOBs were positive for ALP from day 1 and reached the maximum level by day 30. Compared to day 1, cells produced a significantly higher amount of ALP at day 10 ($p=0.0005$), 20 ($p<0.0001$), and 30 ($p<0.0001$). The level of ALP at day 20 was significantly higher than that reported at day 10 ($p<0.0001$) and lower than the level at day 30 ($p=0.0004$).

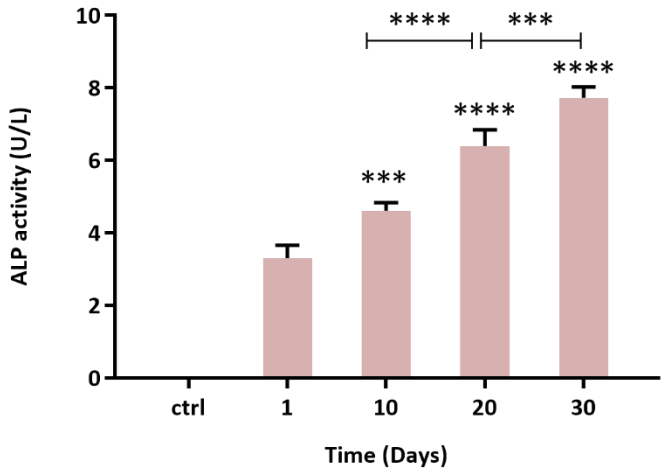

Figure 3. 10. ALP activity for ABC. Graph demonstrates the progressive differentiation of HAOBs cultured in HA/TCP scaffold for one month. HAOBs within the construct demonstrated a progressive increase in ALP expression that reached its highest level at day 30. Data represent mean ± SD of three independent experiments (n=3) performed in triplicate. Statistical significance was determined using one-way ANOVA with Tukey's post-test (*** = $p<0.001$, **** = $p< 0.0001$). Asterisks directly above the bar are relative to the day 1 (baseline) and above the horizontal line are relative to the two bars at the ends of the line.

3.4.2.6. qRT-PCR assessment

To obtain a complete insight into the phenotypic profile of ABCs during differentiation, the changes of osteogenic genes at 10 days interval over 30 days were analysed. Gene expression for osteoblast−specific markers was evaluated and made relative to the expression of these genes in the construct at day 1. ALPL displayed comparable levels from day 1 to 30 with no significant changes in the expression at day 10 ($p>0.9999$), 20 ($p=0.6531$), and 30 ($p=0.9977$) compared to day 1 (Figure 3.11. A). Similarly, the levels of COL1A1 at day 10 ($p=0.7662$), 20 ($p=0.3751$), and 30 ($p=0.5856$) were not observed to be significantly higher compared with day 1 although the expression slightly increased (Figure 3.11. B). Conversely, SPARC expression was significantly upregulated 2 fold and 3.9 fold at day 20 ($p= 0.0076$) and 30 ($p<0.000$), respectively (Figure 3.11. C). The expression of SPP1 at day 10 was generally comparable with

day 1 (p=0.8817) then the level increased steeply 3 fold at day 20 (p=0.0049) and 30 (p=0.0060) (Figure 3.11. D). BGLAP, unlike other genes, was found to be significantly decreased 0.5, 0.6, and 0.4 fold by day 10 (p=0.0015), 20 (p=0.0039), and 30 (p=0.0002), respectively in comparison with day 1 (Figure 3.11. D).

A

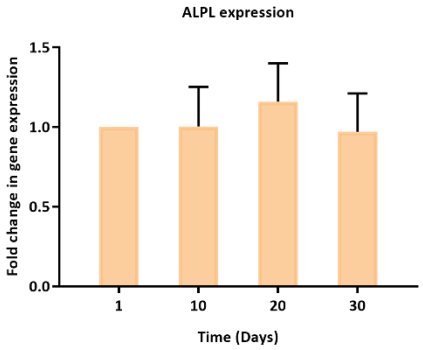

B

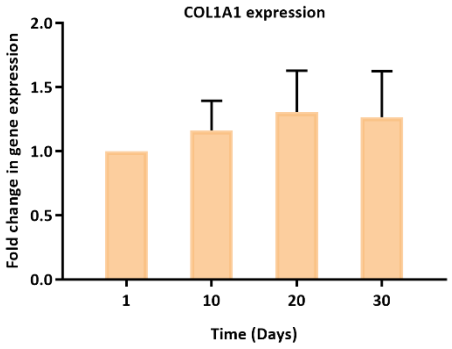

C

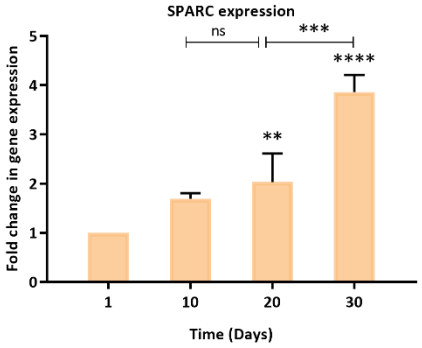

D

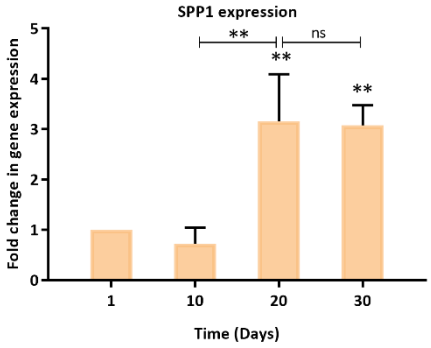

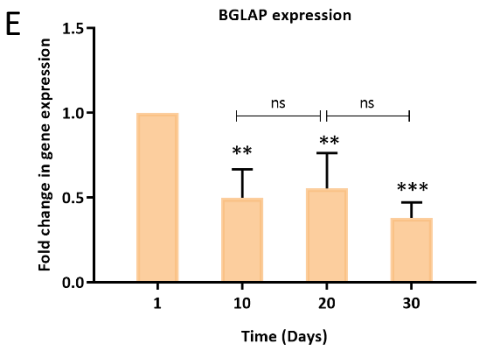

Figure 3. 11. qRT−PCR gene expression analysis of ABC. Image shows the expression level of **(A)** ALPL; **(B)** COL1A1; **(C)** SPARC; **(D)** SPP1; **(E)** BGLAP in ABC cultured in spinner bioreactor for one month. Data represent mean ± SD of three independent experiments (n=3) performed in triplicate. Statistical significance was determined using one-way ANOVA with Tukey's post-test (** = $p<0.01$; *** = $p<0.001$; **** = $p<0.0001$). Asterisks directly above the bar are relative to the day 1 (baseline) and above the horizontal line are relative to the two bars at the ends of the line.

3.4.2.7. ELISA

Quantitative analysis of COL1, ON, and OC released into the serum−free conditioned medium of ABC were assessed by ELISA every 10 days for a month and evaluation was made in comparison with protein level at day 1. Generally, the concentration of COL1 and ON reflected the same trend of their encoding genes; COL1A1 and SPARC, respectively. COL1 level tended to be steady and demonstrated no significant change at different time points (Figure 3.12. A). Conversely, ON was progressively upregulated at day 10, 20, and 30 ($p<0.0001$) and reached the maximum level at day 20 when compared with day 10 ($p=0.0014$) and 30 ($p=0.9040$) (Figure 3.12. B). In contrast with its encoding gene profile (BGLAP), OC displayed a fluctuant level compared with day 1. The trend demonstrated by a sharp increase at day 10 ($p=0.0014$) followed by a decline at day 20 although it was not significantly different ($p=0.0720$) then the level increased again significantly in day 30 ($p=0.0038$) (Figure 3.12. C).

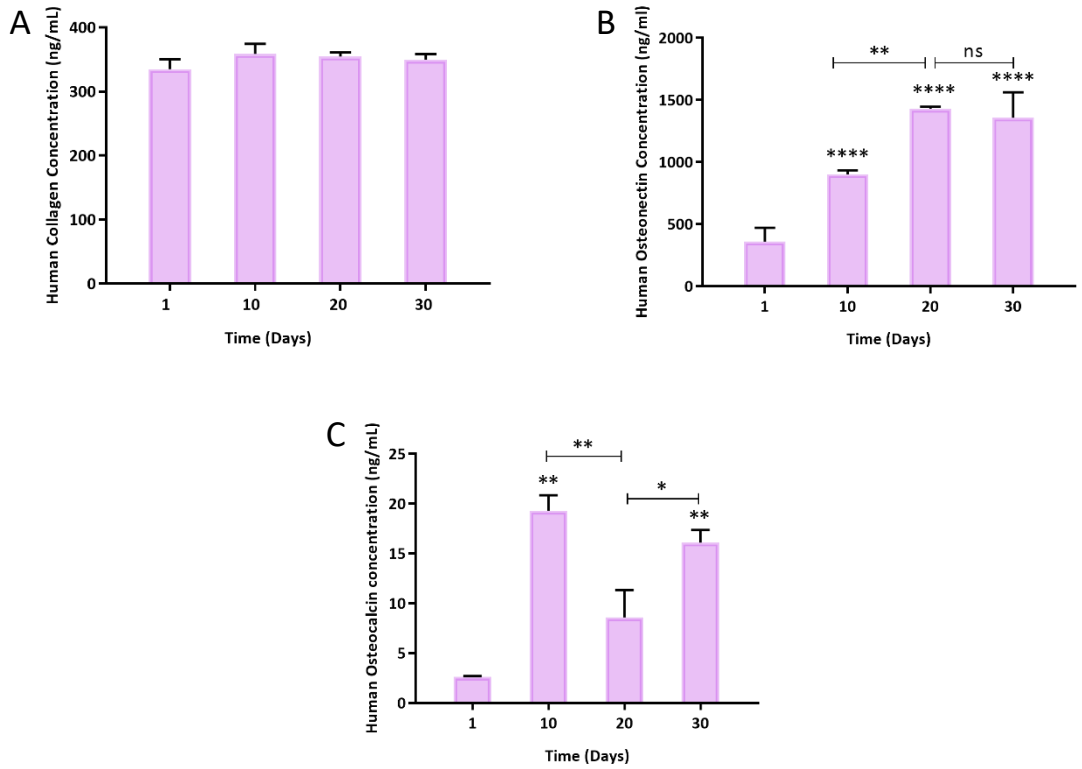

Figure 3. 12. ELISA assessment of ABC. Image shows the secreted **(A)** collagen I; **(B)** osteonectin; **(C)** osteocalcin in ABM. Data represent mean ± SD of three independent experiments (n=3) performed in triplicate. Statistical significance was determined using one-way ANOVA with Tukey's post-test (* =p<0.05, ** = p< 0.01, **** = p<0.0001). Asterisk(s) directly above the bar is relative to the day 1 (baseline) and above the horizontal line are relative to the two bars at the ends of the line.

3.4.3. Assessments of the composite ABMM

3.4.3.1. Histological examination of OMM

Figure (3.13.) show the histological appearance of the mucosal part of ABMM. OMM demonstrated a proliferating basal layer and well−differentiated stratified squamous oral epithelium of 12−14 NHOKs thickness, which resembled the NOM. The epithelium consisted of distinct layers that included equivalents to basal, intermediate, and superficial cells, respectively. No stratum corneum was observed, as in the case of nonkeratinized native oral mucosa. The uppermost aspect of the superficial layer had cells of a flattened appearance, while cells in the basal layer remained rounded. Glycogen granules were occasionally observed in the intermediate layer. NHOFs were found dispersed homogeneously in the connective tissue.

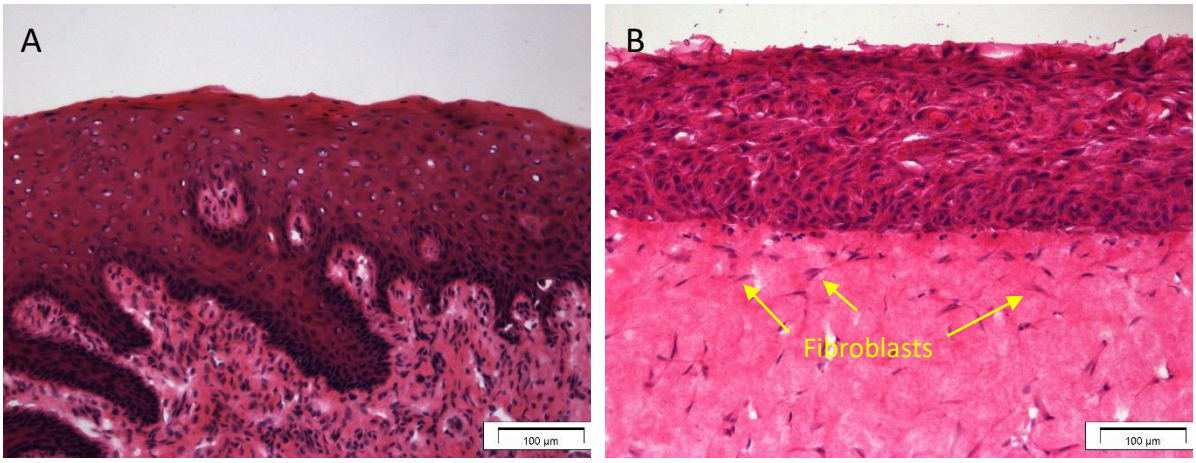

Figure 3. 13. H&E−stained histological sections of OMM. (A) NOM; and **(B)** OMM showing a well−differentiated stratified squamous epithelial layer with fibroblasts (yellow arrows) scattered in the connective tissue layer (Scale bars = 100 µm).

3.4.3.2. Immunohistochemical examination of OMM

Figure (3.14.) shows the keratin expression of NOM and OMM, as assessed by immunofluorescent staining for CK10, CK13, and CK14. OMM showed very mild expression of CK10 (Figure 3.14. A) and strong expression of CK13 throughout the entire epithelium (Figure 3.14. D). CK14 was strongly expressed in the basal layer while it downregulated in the intermediate layer and disappeared in the superficial layer (Figure 3.14. G). NOM (positive ctrl) demonstrated similar results regarding the expression of CK10, CK13, and CK14, respectively (Figure 3.14. B, E, H). All markers were negatively expressed in OMM stained with IgG isotype and secondary antibody (negative ctrl) (Figure 3.14.C, F, I).

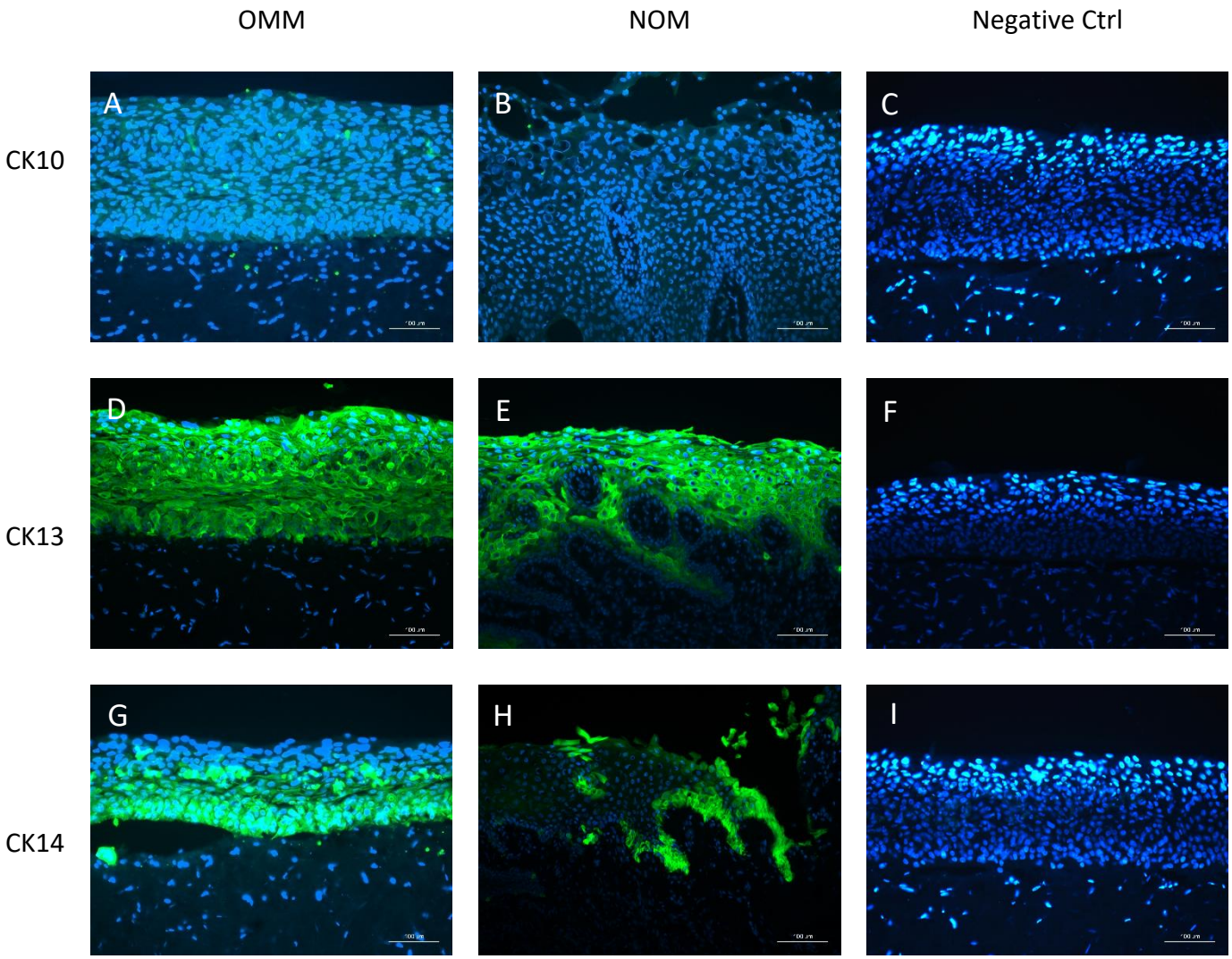

Figure 3. 14. Immunofluorescent labelling of OMM with CK10, CK13, and CK14. Image demonstrates the Immunolabelling of CK10 (keratinized epithelium marker), CK13 (non-keratinised epithelium marker), and CK14 (basal epithelial layer marker) in the epithelial layer of NOM and OMM. OMM showing **(A)** negative staining with CK 10; **(D)** strong expression of CK13 in suprabasal layers; **(G)** expression of CK14 in basal and intermediate layers. The same results were obtained in NOM (positive ctrl) for CK10 **(B)**, CK13 **(E)**, and CK14 **(H)**. **(C, F, I)** OMM stained with isotype control and secondary antibody were used as negative ctrl for CK10, CK13, and CK14, respectively. Positive immunolabelling are shown in green while cell nuclei are shown in blue (Scale bars = 100 µm).

3.4.3.3. TEM examination of OMM

Ultrastructural analysis of the OMM demonstrated the presence of numerous desmosomes between adjacent epithelial cells (Figure 3.15. A and B). A continuous and intact basement membrane was formed on the lamina propria equivalent all along the interface between the epithelium and connective tissue anchoring the epithelium firmly to the connective tissue by means of hemidesmosomal attachments (Figure 3.15. C). In the sup−epithelial layer, a high amount of newly synthesised collagen was observed (Figure 3.15. D).

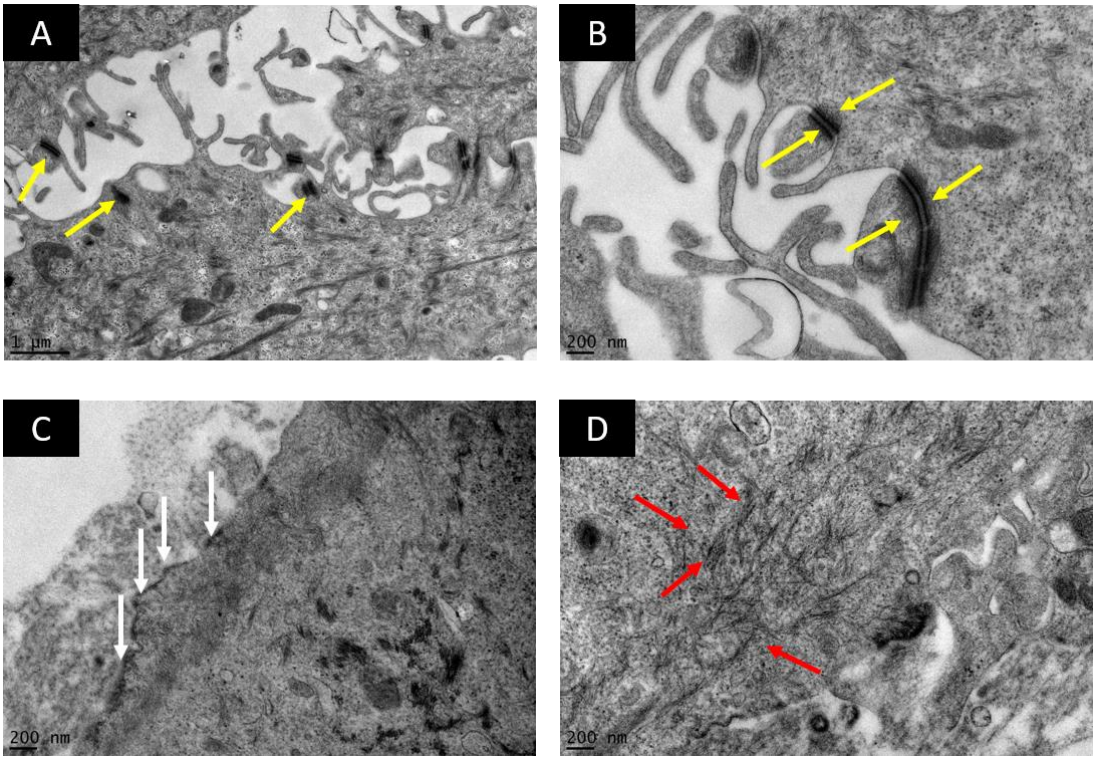

Figure 3. 15. Ultrastructural analysis of the OMM by transmission electron microscopy. Image demonstrating; **(A)** numerous desmosomes between adjacent epithelial cells (yellow arrows); **(B)** a desmosome at higher magnification; **(C)** basement membrane formed all along the interface between the epithelial cell and connective tissue with the presence of hemidesmosomes (white arrows); **(D)** newly synthesised collagen I fibrils in the connective tissue (red arrows) (Scale bars: A = 1 µm; B, C, D = 200 nm). Preparation and sectioning of samples for imaging was performed by Chris Hill, Department of Biomedical Science, University of Sheffield according to the method described in section (3.3.7.3.).

3.4.3.4. Histological examination of ABMM

Histological observation revealed that the ABMM had a structure consisting of epithelial, connective tissue and bony layers which were comparable to the histological architecture of the soft and hard tissues of the oral cavity (Figure 3.16. A). The model's surface displayed a continuous stratified epithelial layer, and a connective tissue layer densely populated with viable fibroblasts (Figure 3.16. B). The hard-soft tissue interface showed a thin band of cell−infiltrated sealant adhering both layers (Figure 3.16. C). Viable cells evenly populated the scaffold porosities with a secreted matrix partially or completely filling the pores of the scaffold (Figure 3.16. D).

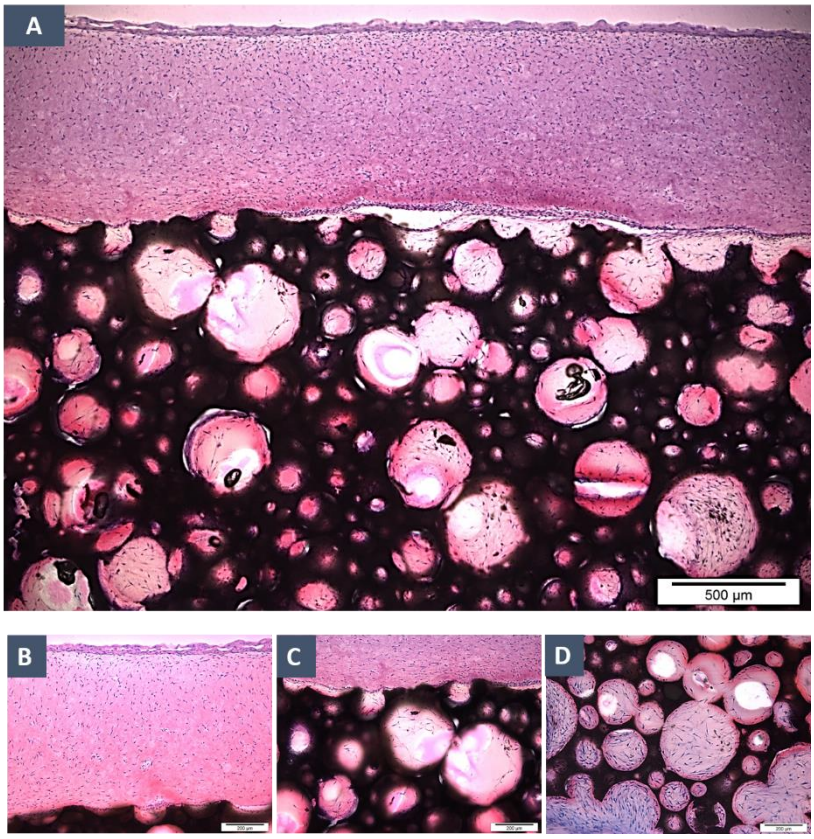

Figure 3. 16. H&E stained sections of ABMM. Representative images showing **(A)** full thickness multi−layered bone and mucosa; and magnified images of **(B)** oral mucosa part; **(C)** bone−mucosal interface; and (D) bony part showing the pores of the scaffold populated with spindle−shaped cells (Scale bars: A = 500 µm; B, C, D = 200 µm).

3.4.3.5. qRT-PCR assessment

Figure (3.17.) summarises gene expression for the composite model, including both HAOB and NHOK cell components. Bone−specific genes such as ALPL, BGLAP, SPARC, and SPP1 were detected. Mucosal genes encoding KRT10 and KRT13 were expressed. The trend of gene expression in ABMM was observed in the osteoblasts (positive ctrl) although the expression of OC and OP was minimal. Undetectable OC and OP, as well as the negligible amount of ALP (0.0002) in the mucosal part of the model (negative ctrl), indicated the osteogenic specificity of these markers. Conversely, COL1 and ON were detected in mucosa which demonstrated that these markers can be expressed by cells other than bone cell.

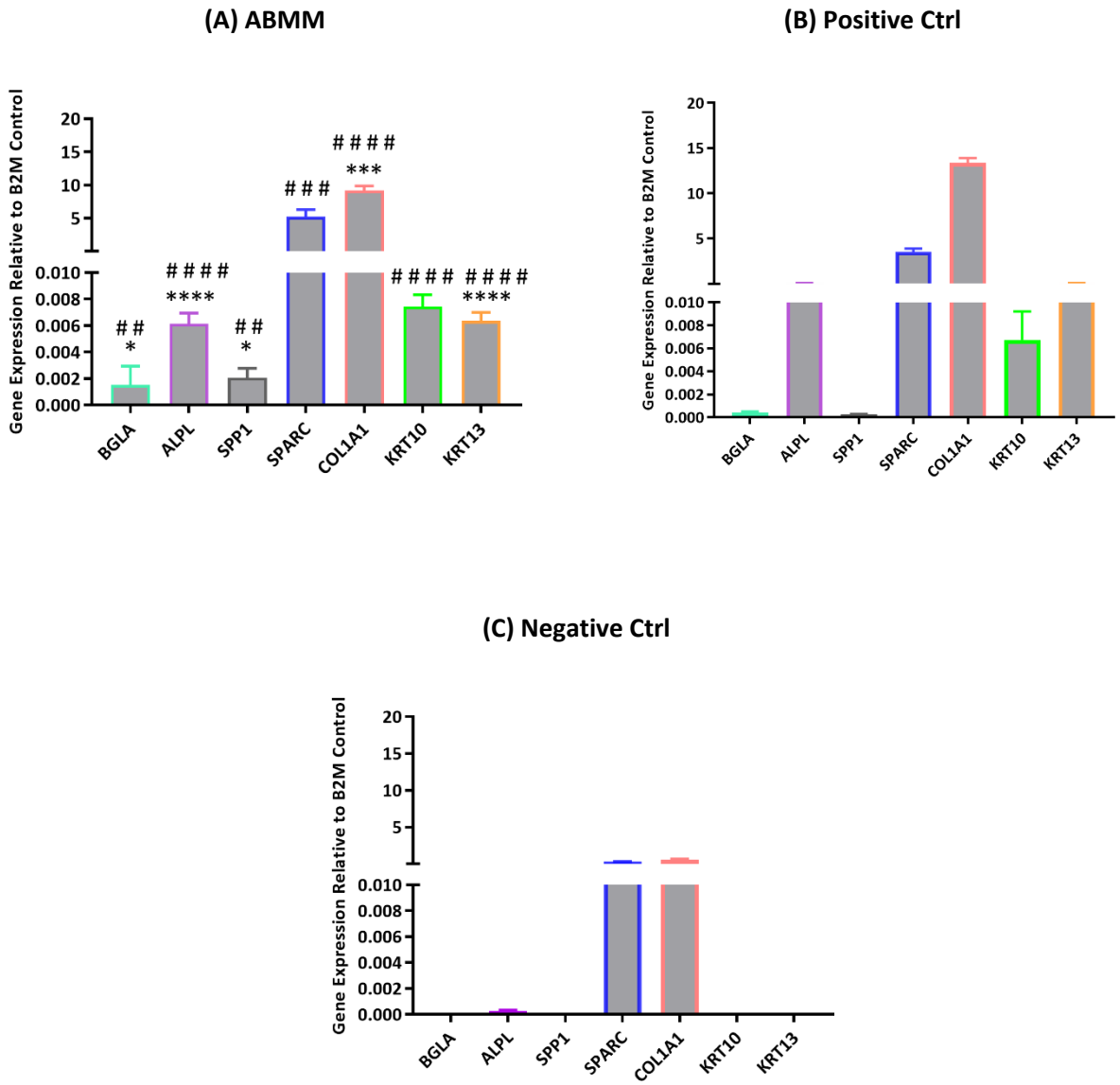

Figure 3. 17. qRT–PCR analysis of the osteogenic and epithelial gene expression in ABMM. (A) The osteogenic genes; BGLA, ALPL, SPP1, SPARC, and COL1A1 as well as the epithelial genes; KRT10 and KRT13 were detected in the composite ABMM. The expression of SPARC and COL1A1 in ABMM demonstrated the same trend found in the positive ctrl although the expression of COL1A1 was significantly lower. BGLA and SPP1 showed high level compared with the positive ctrl while the expression of ALP and KR13 was lower. All the detected genes were significantly higher than their level in the negative ctrl. **(B)** Positive ctrl were HAOBs and NHOKs for bone and epithelial components, respectively. **(C)** Negative ctrl for bone was OMM while no cDNA sample was used for epithelium. Data represent mean ± SD of three independent experiments (n=3) performed in triplicate. Statistical significance was determined using one-way ANOVA with Tukey's post-test. *: compared to positive ctrl: # compared to negative ctrl. (* = p<0.05, ## = p< 0.01, *** or ### = p<0.001, **** or #### = p<0.0001).

3.4.3.6. ELISA

ELISA results for COL1, ON, and OC demonstrated the same trend observed with their gene expression profile. All proteins in ABMM were significantly higher than that found in positive ctrl (Figure 3.18.).

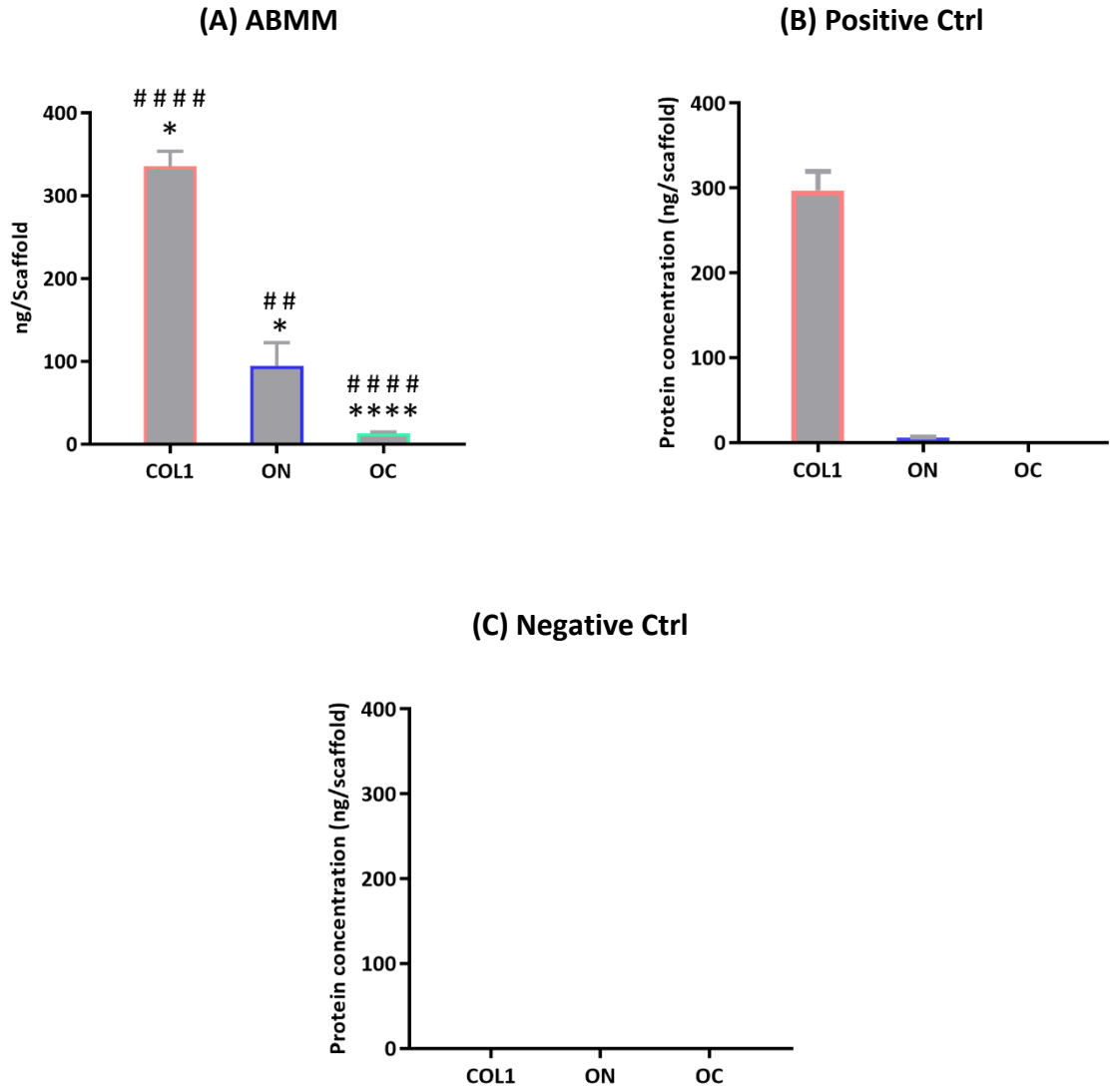

Figure 3. 18. ELISA assessment of proteins expressed in ABMM. Image shows the levels of COL1, ON, and OC produced in; **(A)** ABMM; **(B)** HAOBs which was used as a positive ctrl, and **(C)** serum-free medium represented the negative ctrl. Data represent mean ± SD of three independent experiments (n=3) performed in triplicate. Statistical significance was determined using one-way ANOVA with Tukey's post-test. *: compared to positive ctrl: # compared to negative ctrl. (* = $p<0.05$, ## = $p< 0.01$, **** or #### = $p<0.0001$).

3.5. Discussion

3.5.1. Isolation, growth, and characterisation of alveolar bone and gingival cells.

Cells constitute the main element in any engineered tissue. Therefore, identification of a reliable cell source and expansion of the harvested cells to an appropriate *quantity* while preserving the fundamental *quality* such as identity, purity, potency, functionality, and genetic stability are of utmost importance in TE. Parameters related to the cell itself such as the biological properties and nature of original tissue or related to culture conditions, including initial seeding density and passage number and length, are all crucial in determining normal cell function (Melero-Martin et al., 2009).

In bone tissue, it is well established that matrix formation and subsequent mineralisation are organised by osteoblasts through a complex process, including cell migration, proliferation, differentiation, and expression of growth factors and structural proteins (Neve et al., 2011). Several studies indicated that alveolar bone can be used as a source to isolate mesenchymal cells that have the potential to undergo osteogenic differentiation when cultured in appropriate conditions (Clausen et al., 2006; Malicev et al., 2008; Pradel et al., 2008). Interestingly, previous work suggested that cells originating from alveolar bone exhibit distinct differentiation properties *in vivo* and *in vitro* (Akintoye et al., 2006) as well as different drug responses compared to the cells derived from long and iliac bones (Marolt et al., 2012; Stefanik et al., 2008). These studies clearly indicate that bone cell populations at different anatomical locations have different physiological characteristics. As such, primary human alveolar bone cells might uniquely represent a physiologically relevant model for *in vitro* studies related to the OMF region.

Explant culture or enzymatic treatment by collagenase are the main reported methods for isolating human bone cells. However, previous studies showed no difference in phenotypical

characteristics between cells harvested from both methods (Jonsson et al., 1999; Marolt et al., 2014). The morphology of bone cells, as demonstrated by a light microscope, revealed predominantly a polygonal or spindle appearance, which is postulated by some investigators as a typical osteoblastic shape (Clausen et al., 2006; Murata et al., 2004). The absence of major morphological variations in bone−derived cells can be explained by the fact that young cells of early passage were used in this study while subculturing to a high passage number might reveal shape differences (Kassem et al., 1997).

Many non-osseous cell types such as periodontal and gingival cells that have similar morphology to osteoblasts are present in bone biopsies and may multiply along with or preferentially relative to osteoblasts and osteoprogenitors. Therefore, definite characterization cannot be made based on morphological features. In our study, cells isolated from an intraoral osseous explant were characterised by OC, which is one of the major non-collagenous proteins produced exclusively by cells of osteoblastic lineage (Allori et al., 2008b). Another essential indicator for osteogenesis is the formation of mineralised ECM. Mature osteoblasts produce a collagen I−rich matrix which consequently calcified (Neve et al., 2011). Our findings are correlated with other studies in showing that bone-derived cells have the capacity to deposit calcium mineral within 2 weeks of culture, and the deposition increased with time (Wang et al., 2006; Birmingham et al., 2012).

The validity of the oral mucosal tissues as a cell source for oral tissue engineering was proved by the morphological appearance, the purity of culture, and the positive immunoreactivity of NHOKs and NHOFs to CK13 and FSP, respectively. The former protein is the epithelial differentiation marker predominately secreted by non keratinised epithelial cells (Reibel et al., 1989), while FSP is a fibroblast−specific protein (Frank et al., 1995). Considering the generally accepted fact that, the more the cells are passaged, the more they change and their

health declines, leading to variable results, early passaged primary cells should be used. For human primary bone cells, studies indicated that the 4th passage is more likely to be the turning point after which cell dedifferentiation begins (Pradel et al., 2008; Kwist et al., 2016). Oral keratinocytes, on the other hand, can be used at Passage 2 (Taichman et al., 1979) up to Passage 5 (Zhou et al., 2001). The reason for the decrease in lifespan with the progressive passage may be related to keratinocyte terminal differentiation induced by serum in the medium or by a change in calcium level due to repeated exposure to EDTA in trypsin that reduces cell mitotic activity (Borowiec et al., 2013).

3.5.2. Characteristics of ABC

To date, BTE has been extensively studied for both clinical and research purposes using different cell types. While several osteogenic cell lines were established and well characterised, primary human osteoblasts remain the "gold standard" with which other cells are compared (Czekanska et al., 2014). The developmental sequence of osteogenesis *in vitro* is described by three phases: proliferation with matrix secretion, matrix maturation, and matrix mineralisation (Lian and Stein, 1995; Owen et al., 1990). The current study assessed these phases in the BC before its utilisation in the composite model. We, therefore, identified the behaviour of 3D cultured bone cells in dynamic conditions, and to what extent these cells can survive and reproduce the phenotypic differentiation and maturation of cell*s in vivo.*

SEM images of HAOBs grown in an HA/TCP scaffold clearly showed the proliferative cells expanded on the surface and within the pores, forming a continuous layer of cells and their matrix fibres. This finding was confirmed by the quantitative vitality assessment, which revealed a marked progressive increase in cell signal in the first 20 days. However, the PrestoBlue measurement is based on the metabolic activity of cells and may not accurately

reflect the cell number. For this reason, another method was used in this study in order to precisely quantify cell number.

Cell proliferation can be estimated using different methods, including quantification of nucleic acid by measuring the absorbance at 260 nm. However, the relative insensitivity, the interference caused by contaminants commonly found in nucleic acid preparations, and the inability to distinguish between DNA and RNA are major disadvantages of this technique. PicoGreen®, by contrast, is a fluorochrome that selectively binds dsDNA and quantitates as little as 25 pg/mL of dsDNA with minimal fluorescence contribution of RNA and single-stranded DNA. The proliferative pattern was consistent with the vitality as well as with the matrix protein figures in showing the progressive increase in cell activity, number, and total protein secretion during the first 20 days, and all these parameters remained steady afterward. These findings may be attributed to the normal lifespan of osteoblasts, which is approximately 1−3 months through which the cells can continue their proliferation, differentiation, and matrix protein secretion (Franz-odendaal et al., 2006).

In addition, our observations are in the line with other studies in showing that dynamic culture can enhance bone formation by the effect of fluid flow and the convective transport of nutrients to the scaffold in spinner flask culture (Meinel et al., 2004; Sikavitsas et al., 2002). Furthermore, the spinning exposes cells on the surface to shear stress, which was found to enhance cell differentiation (Wang et al., 2009; Ichinohe et al., 2008). This may explain the persistent increase in ALP expression, the early differentiation bone marker, throughout the entire culture period. Such increased ALP expression in response to shear stress was reported by another study, which showed that the BCs cultured in spinner exhibited higher ALP compared with static culture, and this expression became significantly higher in the perfusion bioreactor (Hosseinkhani et al., 2005). Collectively, these findings showed that the

dynamically cultured HAOBs reflected the osteogenic stages of proliferation, differentiation, and matrix secretion.

In order to track the process of osteogenesis in the ABC, the expression of key osteoblast−specific markers that regulate bone formation was analysed. ALPL/ALP and COL1A1/COL1 can be described as early bone formation markers and can be detected *in vitro* after approximately 2 weeks of culturing under osteogenic conditions (Donahue et al., 2000). SPP1/osteopontin and SPARC/osteonectin are mid-stage markers and are involved in the initiation of crystal nucleation. BGLAP/ OC is considered a late−stage marker that is expressed in bones and teeth and plays an important role in regulating mineralisation (Setzer et al., 2009).

Normally, ALPL is expressed at the early phase during the matrix synthesis stage and it is upregulated in the stage of matrix mineralization. It hydrolyses pyrophosphate and provides inorganic phosphate to promote calcification (Orimo, 2010). Many *in vitro* studies examined the differentiation of human osteoblasts and showed a positive expression of ALPL in a time−dependent manner (Czekanska et al., 2014; Marolt et al., 2014). Other studies demonstrated the enhancing effect of the dynamic culture environment on the ALPL expression (de Peppo et al., 2013a; Hosseinkhani et al., 2005). Our results, however, showed a steady expression of ALPL throughout the experiment with no significant changes compared to Day 1. This profile would suggest an insufficient matrix maturation and would preclude the beginning of the calcification process because ALPL activity usually increases many times between the cell growth phase and the mineralisation phase (Collin et al., 1992).

The expression profile of COL1A1/COL1 that coincided with the similar ALPL trend may be attributed to the same reason. Type I collagen is the predominant collagen isoform found in bone ECM and is essential for HA formation, osteoblast function, and proper fibril formation

with the subsequent physiological matrix maturation (Gehron Robey, 1989). The absence of a significant upregulation in COL1A1, which is highly upregulated in the stage prior to matrix mineralisation, may indicate the immature collagenous matrix (Lian and Stein, 1995).

SPARC is localised to mineralised bone trabeculae and accounts for approximately 23 % of total non collagenous protein. Interestingly, the protein encoded by SPARC, osteonectin, can be demonstrated in active osteoblasts and osteoprogenitor cells as well as in young osteocytes, but not in aged, quiescent osteocytes. The protein, therefore, may be a reliable marker of functional osteoblasts (Jundt et al., 1987). Osteonectin selectively binds to COL1, and the resultant osteonectin−collagen complexes initiate mineral phase deposition by binding synthetic apatite crystals and free calcium ions (Termine et al., 1981). Our results that showed the significant upregulation in SPARC expression at Day 20 onwards may accord with the role of SPARC/osteonectin in the initiation and enhancement of mineralization. Many studies indicated that calcium mineral deposition *in vitro* can be detected from Day 7 and increased significantly at Day 21 (Ferracane et al., 2014a; Czekanska et al., 2014).

SPP1 that encodes osteopontin is another bone marker that is known to be secreted by osteoblasts (Weinreb et al., 1990; Merry et al., 1993), as well as osteoclasts (Tezuka et al., 1992). It has been found that osteopontin is markedly upregulated in osteoblasts following fracture, which suggests that it is involved in immediate cell recruitment, bone formation and resorption (Denhardt and Guo, 1993; Sandberg et al., 1993). Our findings supported other previous research indicating the upregulation of SPP1 in intramembranous ossification (Denhardt and Noda, 1998) and osteoblastic differentiation and proliferation (Zohar et al., 1998).

BGLAP encoded osteocalcin is considered a late osteoblast cell marker and it is upregulated in late mineralisation rather than in early matrix deposition (Rutkovskiy et al., 2016). Although osteocalcin is identified as an osteoblast−specific gene, it may not be considered critical for bone formation, and its precise role within the bone matrix remains unclear (Murshed et al., 2005; Hollinger, 2005). Previous investigations indicated that BGLAP/OC acts as a regulator of mineralization by inhibiting spontaneous mineral precipitation and HA crystal growth (Romberg et al., 1986; Desbois and Karsenty, 1995). Other studies, however, showed that BGLAP/OC is upregulated during the mineralisation phase (Price et al., 1981; Collin et al., 1992). In our study, BGLAP, unlike other genes, displayed a significant decrease in expression. Similar results were previously reported by other authors; demonstrating that bone cells underwent a significant decrease in expression of BGLAP/OC when cultured under dynamic conditions (Bjerre et al., 2008; Mygind et al., 2007). The downregulation observed with BGLAP may be caused by the mechanical stresses associated with the dynamic conditions, and optimising the load applied to the cells may result in stimulating the expression of the gene (de Peppo et al., 2013). The lack of specific gene promoters involved in the regulation of OC expression, such as the AP−1−related protein and the bone−restricted Cbfa1/AML3 transcription factor may account for another reason for OC gene downregulation (Lian et al., 1998). However, it was demonstrated that OC-deficient mice showed increased bone formation and mineralization, which indicated that a low expression of OC gene may be desirable during bone formation (Patricia et al., 1996).

Although gene expression is a standard mechanism to evaluate cell characteristics and to quantify changes induced by culture environment, this method does not entirely reflect cell function in terms of matrix production (Cote et al., 2016); a central point of directed osteogenesis (Datta et al., 2005). Quantification of ECM components provides a more

comprehensive evaluation of cell behaviours than genetic analysis alone (Ortega et al., 2004). Therefore, our gene analysis was supported by ELISA assessment of the major three components of ECM: COL1, ON, and OC. The data obtained from the quantification of COL1 and ON was consistent with their encoding gene analysis and approximately reflected the same trend. The pattern of OC secretion, however, showed inconsistency with its gene expression profile. Such a rebound pattern in OC secretion was observed in MG−63 and MC3T3 cell lines. The authors attributed this trend in OC secretion to an unknown regulatory mechanism (Czekanska et al., 2014). Presumably, the poor correlation between the protein and gene levels may be attributed to the many complicated transcriptional and translational mechanisms involved in turning mRNA into protein. In addition, the mRNA may degrade following translation while the half−life of its corresponding protein remained high due to a reduced degradation rate (Greenbaum et al., 2003).

3.5.3. Characteristics of composite ABMM

In Chapter 4, the culture of cell-line based BCs was extended for 3 months. This study, however, was modified to involve a simultaneous construction of ABC and OMM that were cultured separately for 17 days followed by 5 days' culture of the composite constructs. Although it is appreciated that the total culture period of 22 days is relatively short compared to the *in vivo* implantation studies that are usually extended for months, such experimental design was necessary. First, finite lifespan and limited proliferative potential of primary cells impede culture for a long time because the cells undergo apoptosis (Jilka et al., 1998). Second, the composite model is cultured at a static ALI condition after the incorporation of the soft and hard tissues on the final days. Extended static culture may deprive the deeper tissue of oxygen and nutrients, causing cell death and tissue necrosis.

We have shown that the histological structure and expression of key markers associated with stratification, differentiation, and keratinization in the OMM were comparable to those of its normal tissue counterpart. Our findings were consistent with other studies which characterised EOM (Buskermolen et al., 2016; Kinikoglu et al., 2009). Similar to other oral mucosal equivalents (Chai et al., 2010; Kinikoglu et al., 2009), the model used in this study showed the characteristics of a para−keratinised epithelium, as demonstrated by the weak expression of CK10 and the strong expression of CK13: two established biomarkers of suprabasal cells in keratinised and non keratinised stratified epithelium, respectively (Reibel et al., 1989). In contrast, other studies have revealed the strong expression of CK10 in superficial layers (Moharamzadeh et al., 2008; Tra et al., 2012). Such differences between these oral mucosal models may be attributed to the fact that oral keratinocytes appear to maintain the properties of their original donor epithelium, which may be either keratinised (gingiva and palate) or non keratinised (buccal mucosa) (de Luca et al., 1990).

The control of keratinocyte's proliferation and differentiation is multifactorial. Several studies have confirmed the role of fibroblasts in epithelial development through the stimulation of keratinocyte proliferation, migration, and keratin expression (Okazaki et al., 2003; Rakhorst et al., 2006). Fibroblasts establish such growth promoting roles through paracrine cross−talk between NHOFs and NHOKs via cytokines such as heparin-binding epidermal growth factor, Interleukin 1 alpha, and transforming growth factor beta 1 (Wang et al., 2012). This function requires an optimal fibroblast density because the presence of either excessive or inadequate numbers of fibroblast will adversely affect epithelium morphogenesis; leading to differentiation markers being inappropriately expressed (El-Ghalbzouri et al., 2002). In our models, we found that the optimised fibroblast seeding density of 2×10^5 per model could support an anatomically representative epithelial layer. Keratinocyte senescence may also

impact on the capacity to achieve well-developed epithelia in tissue culture models. Sequential subculturing may restrict the capacity of keratinocytes to divide once seeded into a 3D model due to sustained telomerase expression within primary cells, and therefore it is recommended that the use of keratinocytes in tissue substitute constructs is limited to Passage 3 or less (Ng et al., 2009).

The proper functionality of keratinocytes is important not only for epithelial layer formation but also for epithelial−connective tissue attachment and cell−cell adhesion, which are essential for achieving an accurate, functional mucosal substitute. Our data, consistent with data from other studies, has confirmed that cells within the 3D models actively synthesized the ultrastructural components, including desmosomes, hemidesmosomes, and the basement membrane required for this structural stability (Tra et al., 2012; Chai et al., 2012b).

In Chapter 4, standard decalcified FFPE sections were prepared for the histological examination of the composite model. The major disadvantage of paraffin embedding is that it requires sample decalcification that eliminates essential information about the tissue structure. Decalcifying the specimen for paraffin sectioning resulted in the total dissolution of the HA/TCP scaffold and poor−quality histological sections. Plastic embedding resin such as GMA, by contrast, preserves the structural integrity of the sample better than paraffin. It eliminates the need for demineralisation of the sample and the removal of resin from section prior to staining; thereby preventing the distortion of tissue elements. However, the polymerisation of GMA is exothermic, and high temperatures can result from the dibenzoyl peroxide that decomposes, producing free radicals, which act as initiators of the polymerisation (Gerrits and Horobin, 1996). The polymerisation temperature of this resin ranged between 40−45^{o}C, which results in the denaturing of proteins and impedes immunological staining. Therefore, the undecalcified resin-embedded sections were chosen

to examine the histological morphology of the composite construct, while the mucosal part was separately characterised by immunostaining.

The overall histological appearance of the ABMM replicated the structure of the native oral bone mucosal arrangement. However, the major challenge of this study was to prepare specimens for a bone-mucosal interface without disturbing the soft mucosal component. The cutting and grinding procedure is known to be labour intensive and technically challenging, particularly with soft tissue, which posed a difficulty in obtaining an intact histological section without losing the epithelium. It was observed that the epithelium within composite models was generally less stratified compared with the OMM that detached from the composite model before the resin embedding. We hypothesized that this difference resulted from two different embedding methods used for the OMM and ABMM. The OMMs were minimally handled for cryosectioning. Therefore, the epithelial layer remained intact and never rubbed off, as happened with the composite construct where the mucosa was subjected to surface abrasion during grinding and polishing.

Regarding gene expression, although all the marker-encoded genes were detected, a relatively high level of COL1A1/COL1 was expressed in our model. This may be for a number of reasons. First, this marker constitutes the most abundant component of bone ECM (90 % of the organic component), and it is upregulated during bone formation (Allori et al., 2008a). Second, ascorbic acid was added as a component of the culture medium in order to maintain the osteoblastic phenotype of bone-derived cells; ascorbic acid is known to stimulate cell growth and collagen synthesis in osteoblasts (Choi et al., 2008). The hydroxylation of proline residues of procollagen is increased to approximately 40 % by ascorbate, which is known to stabilize the collagen triple helix (Berg and Prockop, 1973). Third, Type I collagen is not only secreted by osteoblasts but it is also produced in abundance by fibroblasts (Kishimoto et al.,

2013; Schwarz, 2015). Therefore, the fibroblastic component of the model may have contributed to the collagen levels observed.

The main role of SPARC and its encoding ON in active bone mineralisation is to selectively bind newly-secreted collagen fibrils with apatite crystals. Therefore, it is frequently associated with tissues with high rates of collagen turnover such as bone (Termine et al., 1981). By implication, the presence of ON suggests that an abundant collagenous matrix was concomitantly secreted. Although SPARC/ON is considered a bone-specific marker (Termine et al., 1981; Jundt et al., 1987), its expression in the oral cavity has been localised in the fibroblasts in collagen-rich tissues such as periodontal ligament (Trombetta and Bradshaw, 2010) and dermal fibroblasts (Rentz et al., 2007).

ALPL is synthesised by osteoblasts and has been used to assess osteoblast phenotype and matrix mineralisation (Masrour Roudsari and Mahjoub, 2012). However, like COL1A1, it is expressed by cells other than osteoblasts such as gingival fibroblasts (Abe et al., 1996; Gomes and Resende, 2010). Present data accorded with previous studies in showing the expression of COL1A1, SPARC, and ALPL in the non-bony tissue (the mucosal component of the composite model), while OC and OP were absolutely absent.

The expression of all osteoblast-associated molecules varies over the different stages of bone development. Therefore, the expression profiles observed in our models, which were cultured over a relatively short period compared to that of normal human bone turnover, may vary to that found *in vivo*. For example, ALP increases during the initial stages of bone formation but decreases as mineralisation progresses, while OP is first detected in young bone and OC appears towards the end of the mineralisation process (Kim et al., 2015).

In conclusion, this study showed that the tissue-engineered tri−layered model based on HAOBs' BC adhered to the collagen-based mucosal model was able to mimic the native alveolar bone and overlaying full−thickness mucosal structures. The composite hard and soft tissue model may provide scope to act as a valuable alternative to 2D and animal models for various *in vitro* and potential *in vivo* applications.

Chapter 4: Tissue engineering of human alveolar bone–mucosal model using 3D printed bone scaffold

NB: The work described in this chapter has been published in:

Almela, T., Brook, I. M., Khoshroo, K., Rasoulianboroujeni, M., Fahimipour, F., Tahriri, M., Dashtimoghadam, E., El-Awa, A., Tayebi, L. & Moharamzadeh, K. 2017. Simulation of cortico-cancellous bone structure by 3D printing of bilayer calcium phosphate-based scaffolds. *Bioprinting,* 6, pp 1-7.

Almela, T., Al-Sahaf, S., Brook, I. M., Khoshroo, K., Rasoulianboroujeni, M., Fahimipour, F., Tahriri, M., Dashtimoghadam, E., Bolt, R., Tayebi, L. & Moharamzadeh, K. 2018. 3D printed tissue engineered model for bone invasion of oral cancer. *Tissue and Cell,* 52, pp 71-77.

4.1. Introduction

BTE owes most of its advances to the improvements in novel biomaterial−based technologies that can accurately replicate the heterogeneous nature of native tissue. However, many challenges remaine to be addressed in order to progress this field. Fabrication of an ideal bone scaffold is one of the on-going medical challenges due to the complex hierarchical structure of bone.

Ideally, scaffold intended for osteogenesis should mimic the bone composition, morphology, structure, and function in order to optimise integration into the surrounding tissues. In terms of composition, calcium phosphates have been the primary focus for synthetic bone substitutes because of their osteoconductivity, biocompatibility, bioresorbability and chemical similarity to the inorganic phase of the bone (Boccaccini et al., 2014). The structure of bone has an inner trabecular layer which creates a porous environment with 50−90 % porosity (Karageorgiou and Kaplan, 2005) and an outer cortical layer with 3−12 % porosity. These two layers vary in their characteristics in terms of porosity, interconnectivity, pore size, mechanical properties, and surface area (Cooper et al., 2004; Nanci, 2013).

The factors that govern the scaffold design are complex and include considerations of matrix architecture, pore size, morphology, mechanics versus porosity, surface topography and degradation products (Do et al., 2015). Conventional scaffold manufacturing methods such as particulate leaching (Park and Park, 2015), freeze-drying (Offeddu et al., 2015), and foam replication (Baino and Vitale-Brovarone, 2014) have been used extensively. Although high porosity can be achieved by these methods, the internal structure of the scaffold is difficult to control. Random and disconnected pores significantly decrease nutrient transportation,

cell migration, and cell survival, especially in the centre of a bulky scaffold (Thavornyutikarn et al., 2014).

Recently, advances in computational design and additive manufacturing (AM) have enabled quick and accurate fabrication of 3D porous scaffolds with well-controlled architectures (Cox et al., 2015). Three−dimensional printing (3DP) is an innovative technique that offers an entirely new method of reconstructing complex tissues comprising intricate 3D microarchitectures, such as bone, cartilage, heart tissue, and blood vessels. It has been used to create physiologically relevant *in vitro* models which can be applied as an alternative to conventional 2D and animal models in a number of research settings, such as disease modeling and drug screening (Pati et al., 2016).

In contrast with current conventional scaffold fabrication methods, 3DP facilitates precise production of 3D scaffolds with defined shape, size, porosity and pore size distribution which can have a significant impact on cell proliferation, differentiation, and vascularization (Wang et al., 2015; Shrivats et al., 2014; Ferlin et al., 2016; Cavo and Scaglione, 2016). In addition, it enables mimicking bone's hierarchy, that is not possible to be reproduced by conventional methods, through construction of multiscale scaffolds with small and large pores and high interconnectivity which in turn directly related to scaffold performance since it influences bone growth and strength (Do et al., 2015; Egan et al., 2017). Moreover, 3DP enables the use of various materials including polymers, ceramics, or composites to construct a hybrid scaffold (Inzana et al., 2014; Neufurth et al., 2017a). Several studies have used different printing methods to fabricate bone scaffolds (Bose et al., 2012; Wen et al., 2017). Many of these studies, however, have produced scaffolds with a single homogenous structure which do not simulate the bilayer cortico−cancellous structure of bone in most parts of the body

and in the maxillofacial region. The aim of this study was to exploit the advantage of 3D printing to fabricate a bilayer ceramic scaffold that replicates the cortico−cancellous alveolar bone architecture and using the printed scaffold in TE of the composite human alveolar bone mucosal model.

4.2. Aims

1. To fabricate a bi−layered β−TCP-based scaffold that replicates the cortico−cancellous alveolar bone architecture using 3D printing technique.
2. To characterise the structural, morphological, mechanical, and biological properties of the printed scaffold.
3. To construct and characterise the composite ABMM using the printed bone scaffold.

4.3. Materials and methods

4.3.1. Scaffold design and fabrication

4.3.1.1. Preparation of printable β−TCP paste

An injectable β−TCP paste was formulated by mixing 1 g Sodium Tripolyphosphate ($Na_5P_3O_{10}$) (Alfa Aesar, US), 0.15 g Carboxymethylcellulose Sodium salt (Alfa Aesar, US), and 30 g β-TCP powder (Sigma, US) in 10 ml deionised, filtered water. The paste was mixed and defoamed for 10 and 3 minutes, respectively at 2000 rpm using a centrifugal mixer (THINKY, Japan) and loaded into the plotting cartridge (Nordson, USA) for printing.

4.3.1.2. Rheological assessment of β−TCP paste

The rheological measurements were performed using a shear rheometer (Kinexus, Malvern, UK) with a stainless steel parallel plate geometry with a diameter of 20 mm. The paste was placed on the lower plate and the upper plate was lowered until it gently touched the surface of the sample at a gap distance of 0.5 mm and excess material was removed. Measurements

were performed at different temperatures from 30 ^{o}C to 15 ^{o}C with a scanning interval of 5 ^{o}C. At each temperature, the rheological evaluation consisted of two consecutive shear cycles with no rotational pre-shear step. The shear rate varied linearly in ramp mode from 0 to 100 s^{-1} with 10 s^{-1} intervals in 2 min and then back to 0 s^{-1}. The total testing time was 12 minutes.

4.3.1.3. 3D plotting of β−TCP scaffolds

The scaffolds were fabricated using the 3D bio plotting system (EnvisionTec, Germany) (Figure 4.1.). First, the printed scaffold was designed using computer-aided design (CAD) software. Then, the digital model was converted to a standard tessellation language file format that represents the surface geometry of the 3D scaffold. The model was virtually sliced into sequential 2D layers using the bioplotter software. The printing machine then used those layers to create the necessary tool-path along the X and Y directions for direct manufacturing. Finally, each layer was processed one on top of the other to form a 3D part. This process was performed by applying the optimised parameters as listed in Table (4.1.), β−TCP paste extruded from a cartridge through a plotting needle (Nordson, USA) having an inner diameter of 400 um. The printer head deposited strands of the paste in a layer−by−layer fashion on the building platform forming a disc of 10 mm x 2 mm thickness. Scaffolds were air−dried overnight and then sintered. The temperature of the furnace (Vulcan, USA) was raised to 600 ^{o}C at the uniform rate of 3^{o}/min, held for 1 hour in 600, then raised from 600 ^{o}C to 1100 ^{o}C at a rate of 5^{o}/min and remained at 1100 ^{o}C for 4 hours.

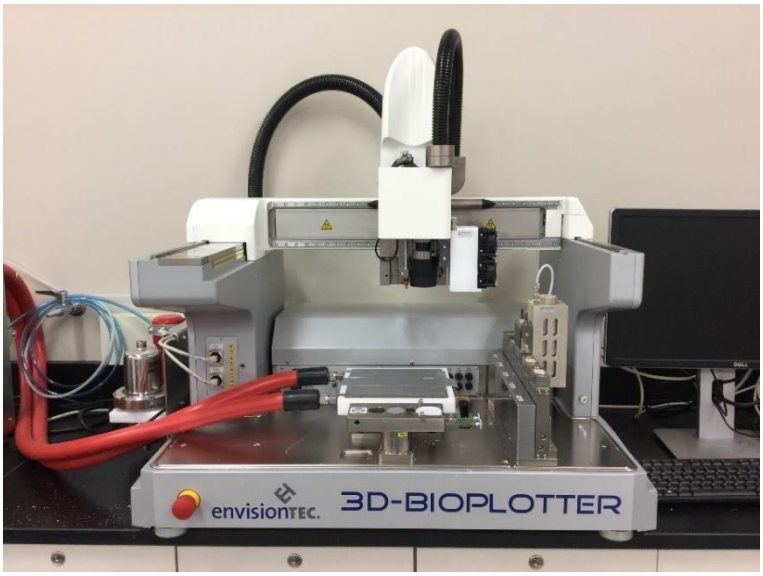

Figure 4. 1. 3D bio-plotter system used in the fabrication of 3DP bone scaffold.

Table 4. 1. The optimised parameters for printing β−TCP scaffold

Parameter	Measurement
Pressure	1.5−1.7 bar
Speed	5 mm/s
Material temperature	23 ^{o}C
Platform temperature	Room temperature
Distance between strands	0.6 mm & 0.8mm
Lay down pattern	0^{0}, 60^{0}, 120^{0}
Slice width	150 µm

4.3.2. Scaffold characterisation

4.3.2.1. Structure, morphology, and surface topography

Evaluation of the scaffold's, structure, morphology, and surface roughness was conducted by 3D laser scanning digital microscope (Olympus LEXT OLS 4000, Japan). Scaffolds were randomly selected to measure the roughness, morphology, dimension of the pores, distance between strands, and thickness of strands on both sides of scaffolds using the software (LEXT OLS 4000).

4.3.2.2. Microstructural characterisation by μ–CT scanner (see section 2.3.3.1.).

4.3.2.3. X–ray diffraction (XRD)

XRD was carried out for the scaffold powder and pure β–TCP from which the paste was prepared. Sintered scaffolds were ground using an agate mortar and pestle (Fisher Scientific, UK). The powder was then sieved to 150 μm particles (Endecotts, UK). XRD patterns were recorded between 5^o and 70^o 2θ at a step of 0.4/s using D_2 phaser diffractometer (Bruker, UK) equipped with a Cu Kα radiation source of (30) KV and (10) mA. Diffraction data was analysed by ICDD PDF-4+ software (2015 edition).

4.3.2.4. Mechanical properties

The Young's modulus and ultimate compressive strength of the scaffolds were measured using a mechanical testing machine (Shimadzu, Japan) with a 5kN load cell, and a cross–head speed of 1.0 mm min^{-1}. The sintered cylindrical samples with a diameter of 10 mm and a height of 20 mm were compressed in Z direction until they fractured. The data obtained was used to calculate the mean compressive strength and modulus.

4.3.2.5. Biological properties of 3DP scaffolds

The scaffolds were autoclaved and pre-incubated in the culture medium for 4 hours, followed by cell seeding and culture for 1 month as described in chapter 2 (see section 2.3.8.). Every 10 days, the following assessments were performed:

4.3.2.5.1. Cell viability assessment (see section 2.3.3.4.).

4.3.2.5.2. Proliferation assessment (see section 3.3.5.3.).

4.3.2.5.3. SEM examination (see section 2.3.6.1.).

4.3.3. Construction of printed ABMM (see section 3.3.6.).

4.3.4. Characterisation of printed ABMM

4.3.4.1. Histological examination of mucosa (see section 3.3.7.1.).

4.3.4.2. IF staining of mucosa (see section 3.3.7.2.).

4.3.4.3. TEM of mucosa (see section 3.3.7.3.).

4.3.4.4. Histological examination of printed ABMM (see section 3.3.7.4.).

4.3.4.5. qRT-PCR examination (see section 3.3.5.6.).

4.3.4.6. ELISA (see section 3.3.5.7.).

4.3.5. Statistical analysis

All data were presented in terms of mean ± SD of three independent experiments performed in triplicate. One−way ANOVA complemented by Tukey's post−test was performed using GraphPad Prism v7.0 (GraphPad Software, La Jolla, CA). Differences were considered significant when $p < 0.05$.

4.4. Results

4.4.1. Rheological assessment of β−TCP paste

The viscosity assessment of the β−TCP paste indicates that the viscosity is strongly dependent on both shear rate and temperature. Figure (4.2. A) shows that at 15 ^{o}C the dependence of viscosity to shear rate is considerable for a shear rate of 10 s^{-1} to 70 s^{-1}, while it remained constant at shear rates higher than 70 s^{-1}. On the other hand, the effect of shear rate on viscosity is not significant when the temperature is above 15 ^{o}C. Regarding the temperature, Figure (4.2. B) shows that the decline in the viscosity started at 15 ^{o}C and ended at 20 ^{o}C. Increasing temperature up to 30 °C had no significant effect on the viscosity. The viscosity seems to be independent of the temperature for temperatures higher than 20 ^{o}C at a specific shear rate. Figure (4.2. C) shows shear stress versus shear rate for the prepared paste at 20−30 ^{o}C. The paste seems to be a Bingham plastic material with yield stresses of 58.12, 47.05 and 39.75 Pa at 20, 25 and 30 ^{o}C, respectively. A linear correlation between shear stress and shear rate was found for all the examined temperatures where all the coefficients of determination (r-squared) were found to be greater than 0.99. The dependence of viscosity on temperature and shear rate influences the printing parameters i.e. cartridge temperature and printing pressure, respectively. The pressure applied to the material for printing dictates the material's flow rate from the needle which in turn could be related to the shear rate.

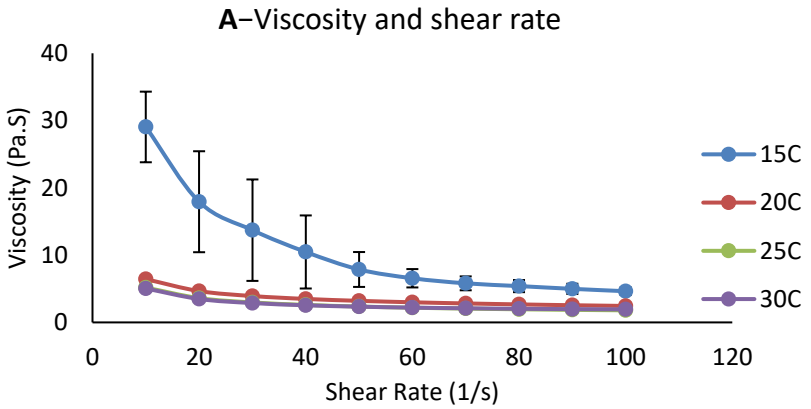
A–Viscosity and shear rate
Viscosity (Pa.S)
40
30
20
10
0
0
20
40
60
80
100
120
Shear Rate (1/s)
15C
20C
25C
30C

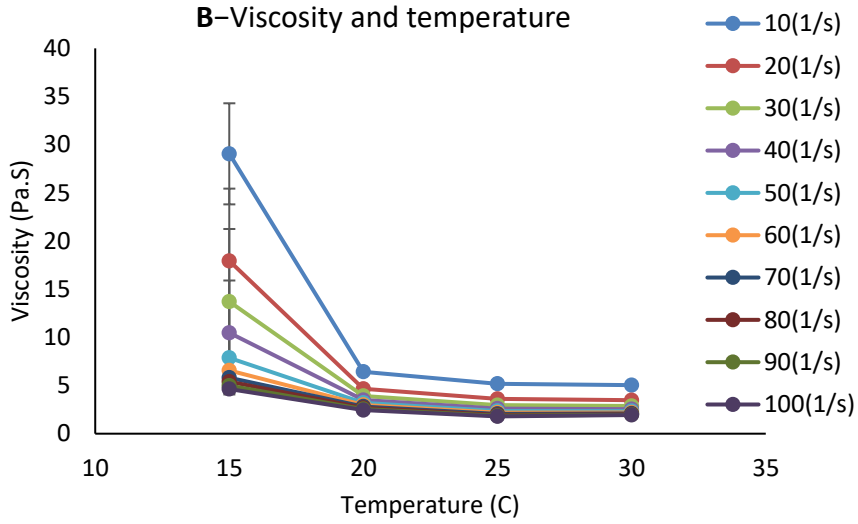
B–Viscosity and temperature
Viscosity (Pa.S)
40
35
30
25
20
15
10
5
0
10
15
20
25
30
35
Temperature (C)
10(1/s)
20(1/s)
30(1/s)
40(1/s)
50(1/s)
60(1/s)
70(1/s)
80(1/s)
90(1/s)
100(1/s)

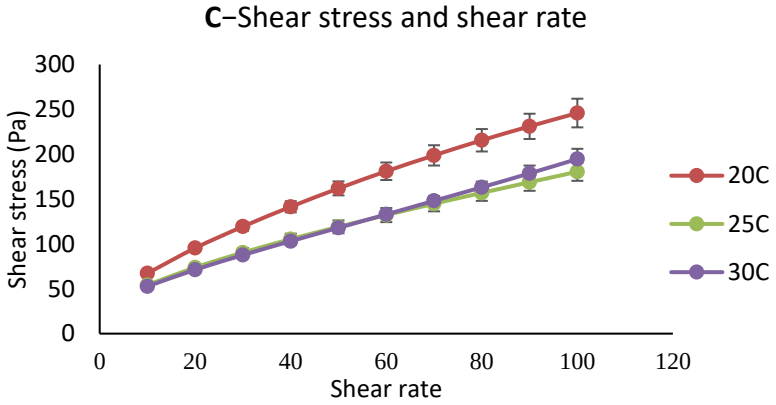
C–Shear stress and shear rate
Shear stress (Pa)
300
250
200
150
100
50
0
0
20
40
60
80
100
120
Shear rate
20C
25C
30C

Figure 4. 2. The rheological assessment of TCP paste. (A) The dependence of viscosity on shear rate at 15 ^{o}C is considerable for a shear rate of 10 s^{-1} to 70 s^{-1}. The viscosity remained constant at shear rates higher than 70 s^{-1}. No significant effect of shear rate on viscosity was observed when the temperature is above 15 ^{o}C. **(B)** The decline in the viscosity started at 15 ^{o}C and ended at 20 ^{o}C. Increasing temperature higher than 20 ^{o}C at a specific shear rate had no significant effect on the viscosity. **(C)** A linear correlation between shear stress and shear rate was found at 20, 25 and 30 ^{o}C. The prepared paste had yield stresses of 58.12, 47.05 and 39.75 Pa at the examined temperature, respectively (Pa=Pascal, S=second).

4.4.2. Characterisation of 3DP scaffold

4.4.2.1. Structural morphology and surface roughness of 3DP scaffold

3D laser microscopy examination revealed the morphology and geometrical accuracy of scaffold structure. It showed smooth continuous strands as well as clearly revealed the differences between both sides of 3DP scaffold (Figure 4.3.). For the compact side, the measurements of pore diameter, strands thickness and the distance between strands were 242.2 ± 24.3 µm, 516.8± 28.1 µm, and 214.5± 19.1 µm, respectively while the dimensions in the cancellous side were 410.5± 27.9 µm, 447.1± 46.7 µm, and 502.1± 46.9 µm. Figure (4. 4. A) presents the 2D laser scanning of the single printed layer at X and Y direction while Figure 4.4. B) shows the compact layers in Z directions. The value of surface roughness (*R*a) was found to be 1.1 ± 0.2 µm.

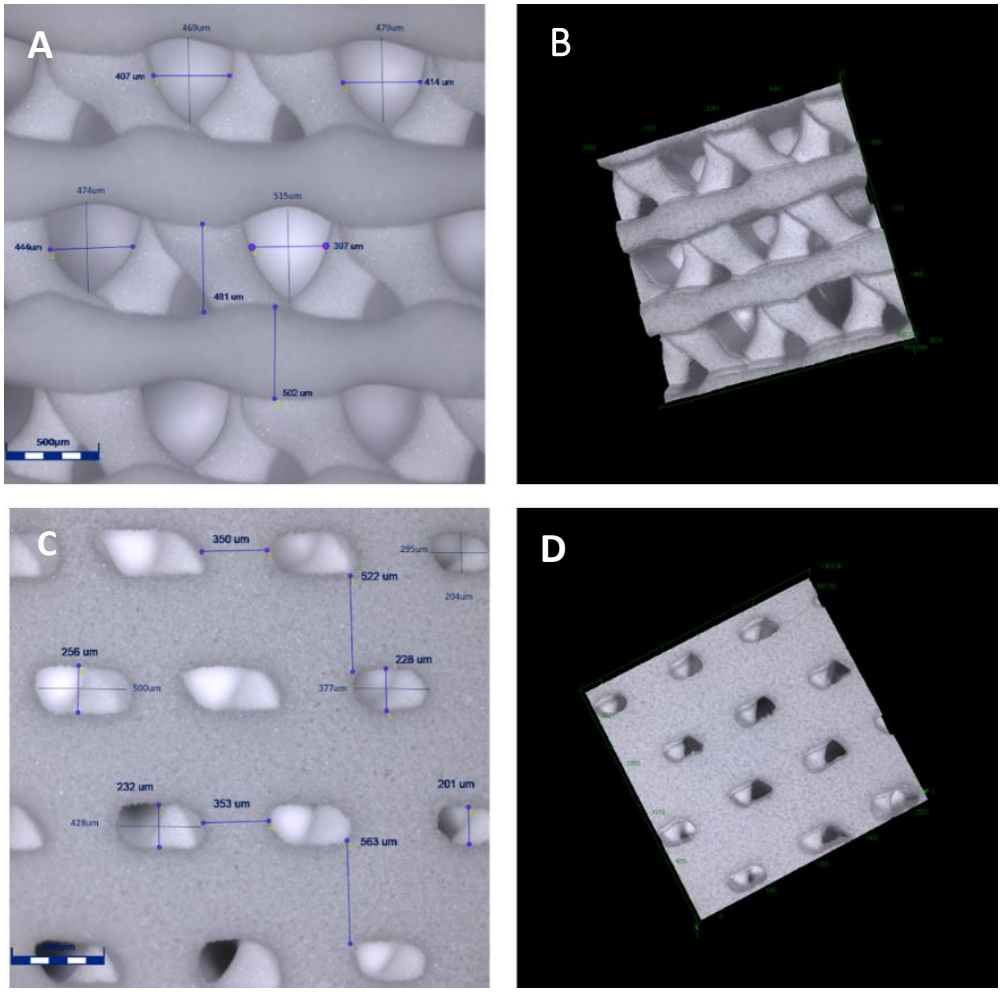

Figure 4. 3. Representative 2D and 3D laser scanning images of the bilayered printed scaffold. Image showing; **(A)** The measurements of pore size and the distance between strands in the cancellous side; **(C)** The compact side that is in contact with the substrate. The pore shape is parallelogram because of the angle of printing in the second layer. **(B and D)** Representing the 3D views of cancellous and compact sides, respectively (Scale bars = 500 µm).

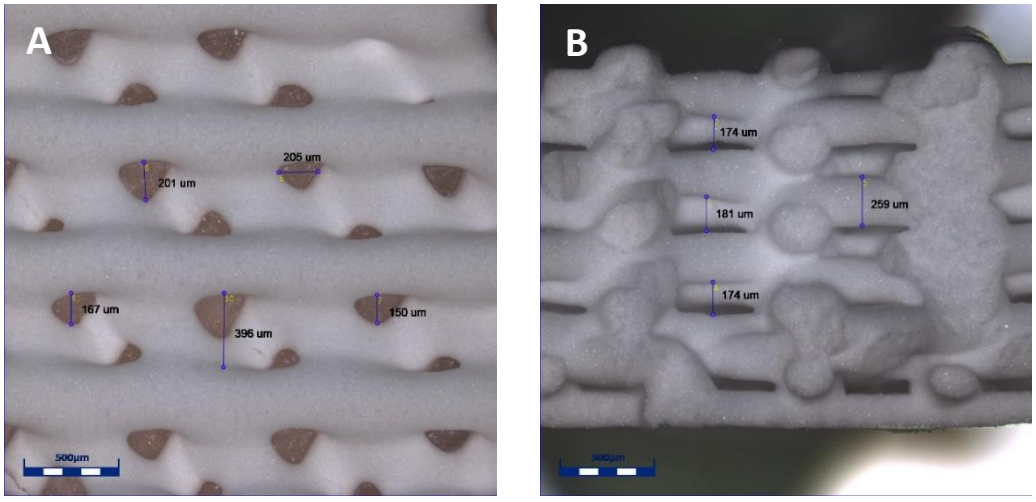

Figure 4. 4. 2D laser scanning of the single and compact printed layer(s) in X, Y, and Z directions. Image shows; **(A)** The pore dimensions in X and Y directions for the printed cortical part that is not in contact with the substrate (platform); **(B)** The spaces between printed layers at Z direction (Scale bars = 500 µm).

It was noticed that these consistent values were obtained after optimisation of printing parameters (see Table 4.1.). Changes in these variables or utilizing unoptimised printing resulted in many problems such as clogging of dispensing needle, disconnection of the plotted strands (Figure 4.5. A), and even cracking of the scaffold after sintering (Figure 4.5. B).

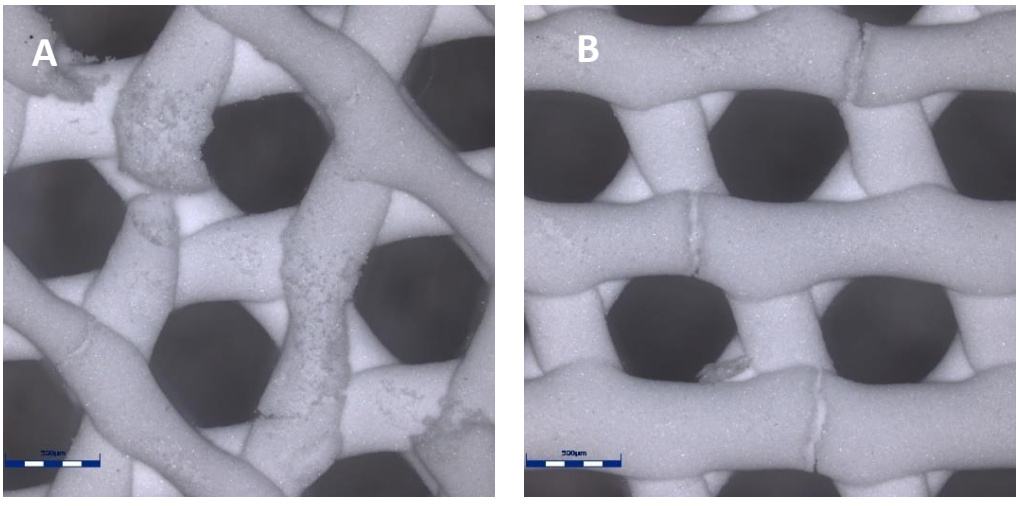

Figure 4. 5. 2D laser scanning images of the faulty 3DP scaffold. Image shows examples of inappropriate β−TCP scaffolds when they were printed with un optimised plotting parameters. **(A)** Incomplete and uneven strands; **(B)** microcracking in the sintered scaffold (Scale bars = 500 µm).

4.4.2.2. Phase analysis by X−ray diffraction (XRD).

Figure (4.6.) shows the XRD patterns of β−TCP from which the scaffolds were prepared and the crushed scaffolds after sintering. As it can be seen in this figure, the crystalline structure of β−TCP was a major phase. XRD patterns of sintered and unsintered β−TCP exhibited approximately the same characteristic peaks. No secondary phase, organic residue or crystallographic substitution was detected.

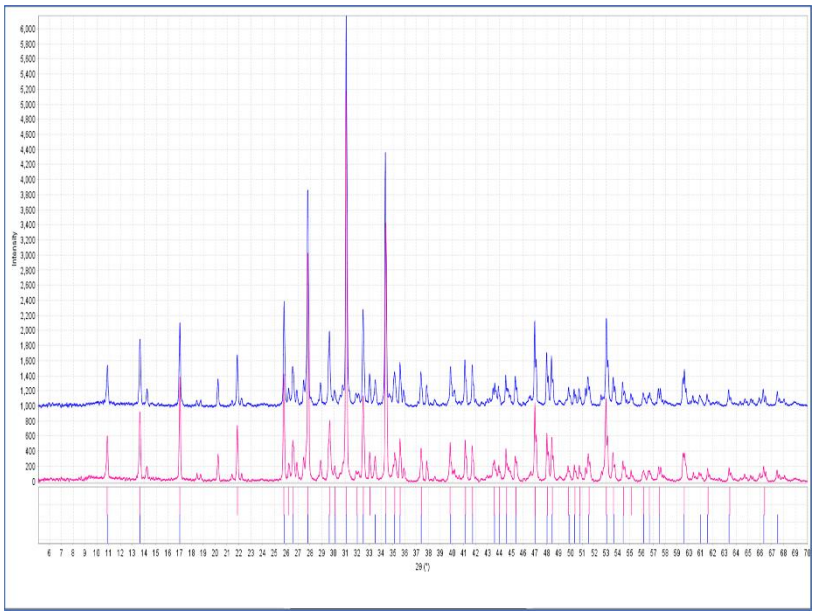

Figure 4. 6. XRD patterns of β−TCP powders. The unsintered powder (pink) and powder of scaffold sintered at 1100 °C for 4 hours (blue) are displayed. Both patterns demonstrated approximately the same characteristic peaks.

4.4.2.3. µ−CT scan assessment

The basic properties of the scaffolds determined by µ−CT scanning are shown in Table (4.2.). 3DP scaffold had 61.8 % open porosity (total porosity) while the closed porosity was 0.003 %. The volume of closed pores (0.002 mm^3) was approximately negligible compared with 71.1. mm^3 open pores volume. Scaffold demonstrated high interconnectivity and connectivity density.

Table 4. 2. µ CT-scan measurement of 3DP scaffold

	Feature	Unit	Mean ± SD
1	Volume of closed pores	mm3	0.0342 ± 0.0064
2	Volume of open pores	mm3	71.1 ± 1.6
3	Closed porosity	%	0.04 ± 0.041
4	Open porosity	%	61.8 ± 1.4
5	Trabecular thickness	mm	0.05 ± 0.007
6	Trabecular separation	mm	0.2 ± 0.02
7	Trabecular number	-	7.47 ± 0.95
8	Surface density	1/mm	24.11 ± 2.6
9	Connectivity density	1/mm3	1815.4 ± 455.8
10	Connectivity	-	208707.5 ± 52405.1

4.4.2.4. Mechanical properties

The compressive strength of the scaffolds was found to be 10.0 ± 2.4 MPa while the modulus was 55.5 ± 5.7 MPa.

4.4.3. Characterisation of printed ABC

4.4.3.1. Cell viability

The results obtained from this assay are presented in Figure (4.7.). It shows that cells remained alive and their metabolic rate was significantly higher on day 10 and afterward compared with day 1 ($p<0.0001$).

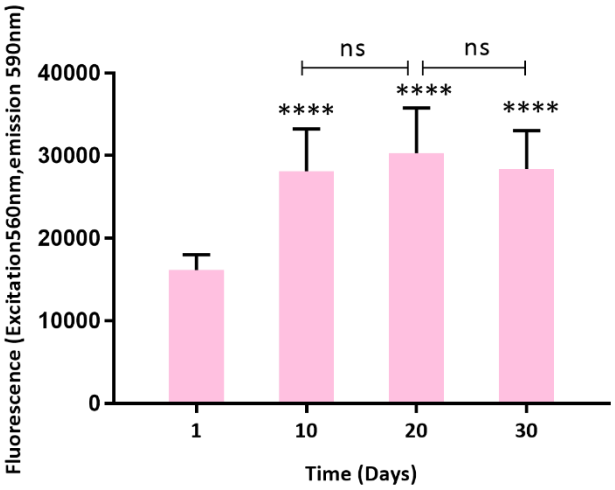

Figure 4. 7. The viability of 3DP bone constructs. Graph shows the viability of 3DP bone constructs cultured in spinner bioreactor for one month. The metabolic rate of HAOBs was significantly higher on day 10 and afterward compared with day 1 (baseline) with no significant increase was observed on day 20 and 30. Data represents mean ± SD of three independent experiments (n=3) performed in triplicate. Statistical significance was determined using one-way ANOVA with Tukey's post-test (****= $p<0.0001$). Asterisks directly above the bar are relative to day 1 (baseline) and above the horizontal line are relative to the two bars at the ends of the line.

4.4.3.2. Cell proliferation

Proliferation assessment demonstrated a detectable but not significant increase in cell number from day 1 to 10 ($p=0.0641$) while a significant proliferation was found at day 20 ($p=0.0126$) and 30 ($p<0.0001$) (Figure 4.8.). day 30 showed a decrease in cell number although it was not significant compared to day 20.

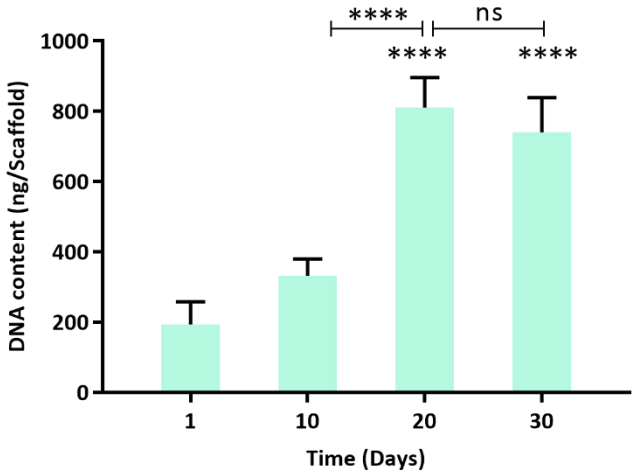

Figure 4. 8. Total DNA content 3DP bone constructs. Graph shows the proliferative pattern of HAOBs cultured in 3DP scaffold in spinner bioreactor for one month. The number of HAOBs within the construct demonstrated no significant difference on day 10 compared to day 1 while the cell number remarkably increased on day 20 followed by slight non significant decrease on day 30. Data represents mean ± SD of three independent experiments (n=3) performed in triplicate. Statistical significance was determined using one-way ANOVA with Tukey's post-test (**** = $p<0.0001$). Asterisks directly above the bar are relative to the day 1 (baseline) and above the horizontal line are relative to the two bars at the ends of the line.

4.4.3.3 Assessment of cell attachment and spatial distribution

SEM observation of cell morphology revealed normal osteoblastic polygonal shaped cells attached to the rough scaffold surface (Figure 4.9.). The macroporous scaffold structure supported the cell adhesion, penetration, and ingrowth on both surfaces of the scaffold throughout 30 days of dynamic culture (Figure 4.10.). The attached cells showed even distribution as well as elongation and orientation along the scaffold strands which indicates that the osteoblasts spread and align along the surface microstructures. On day 20, both surfaces were densely covered by interconnected growing cells which formed stacked and crusted layers. Pores in the compact side approximately occluded and completely sealed by

cellular matrix at the end of the month while some open pores were observed in the porous side at the end of the experiment.

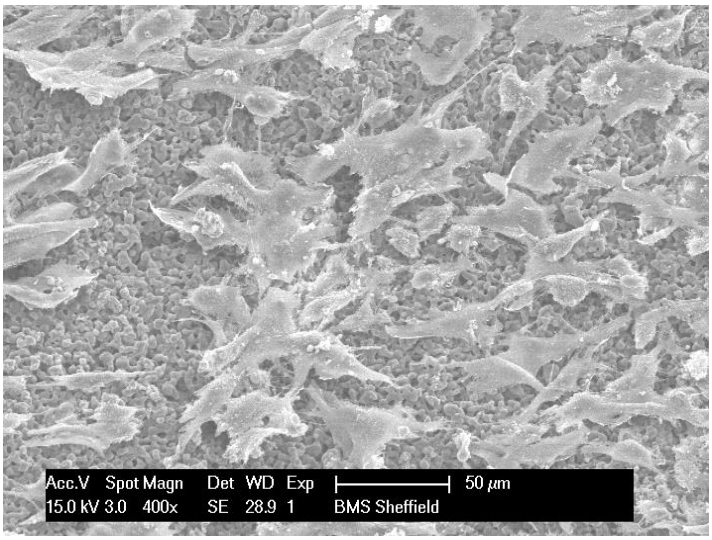

Figure 4. 9. SEM micrograph of HAOBs attached to 3DP scaffold after 24 hours of seeding (Scale bar = 50 µm).

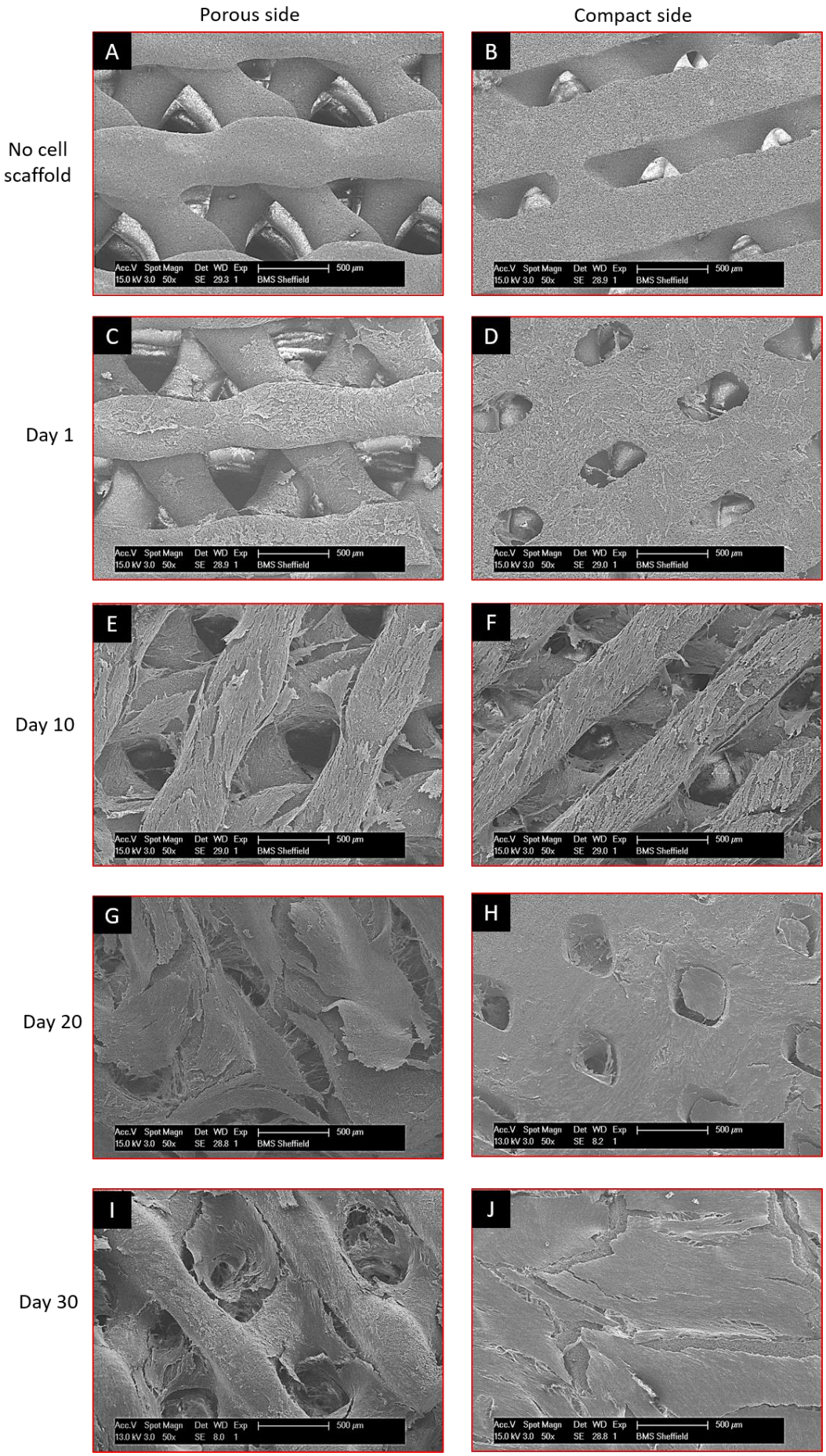
Porous side
Compact side
No cell scaffold
Day 1
Day 10
Day 20
Day 30
A
B
C
D
E
F
G
H
I
J

Figure 4. 10. SEM micrographs of HAOBs cultured in 3DP scaffold. Image shows the attachment, distribution, and ingrowth of HAOBs on both surfaces of 3DP scaffold during 30 days of dynamic culture. **(A and B)** non cellular porous and compact sides, respectively. **(C-I)** and **(B-J)** show porous and compact sides of the constructs, respectively at 1, 10, 20, and 30 days (Scale bars = 500 µm). Preparation of samples for imaging was performed by Chris Hill, Department of Biomedical Science, University of Sheffield according to the method described in section (2.3.6.1).

4.4.4. Assessment of printed ABMM

4.4.4.1. Histological examinations of mucosa

As expected, OMMs displayed the same histological obtained in chapter 3. A well−developed stratified squamous epithelium overlying collagen−populated fibroblasts in a way mimicking NOM was demonstrated (Figure 4.11. A and B).

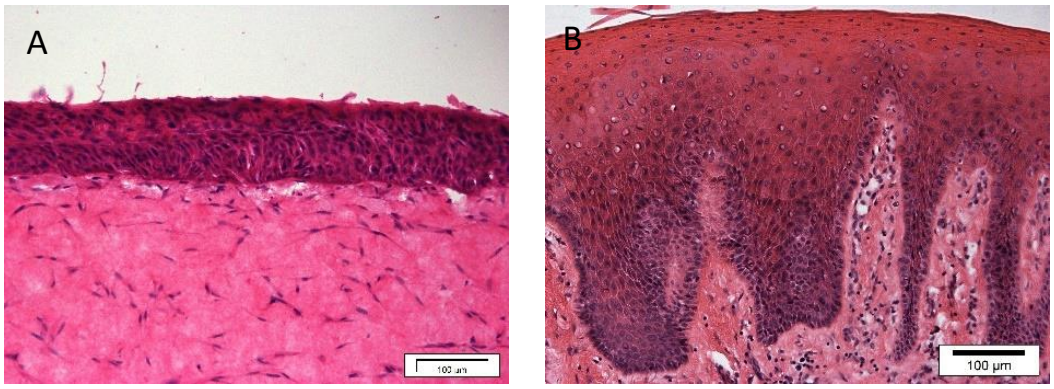

Figure 4. 11. H&E representative image compared the mucosal part (OMM) of the printed composite model with normal oral mucosa (NOM). (A) shows OMM with a well−differentiated oral epithelium overlying collagen−populated fibroblasts. **(B)** NOM (Scale bars = 100 µm).

4.4.4.2. IF characterisation of mucosa

IF staining of OMM revealed strong expression of CK13 throughout the entire epithelium (Figure 4.12. A) and CK14 expression in basal layer (Figure 4.12. D). The expression was comparable to that found in NOM (Figure 4.12. B and E).

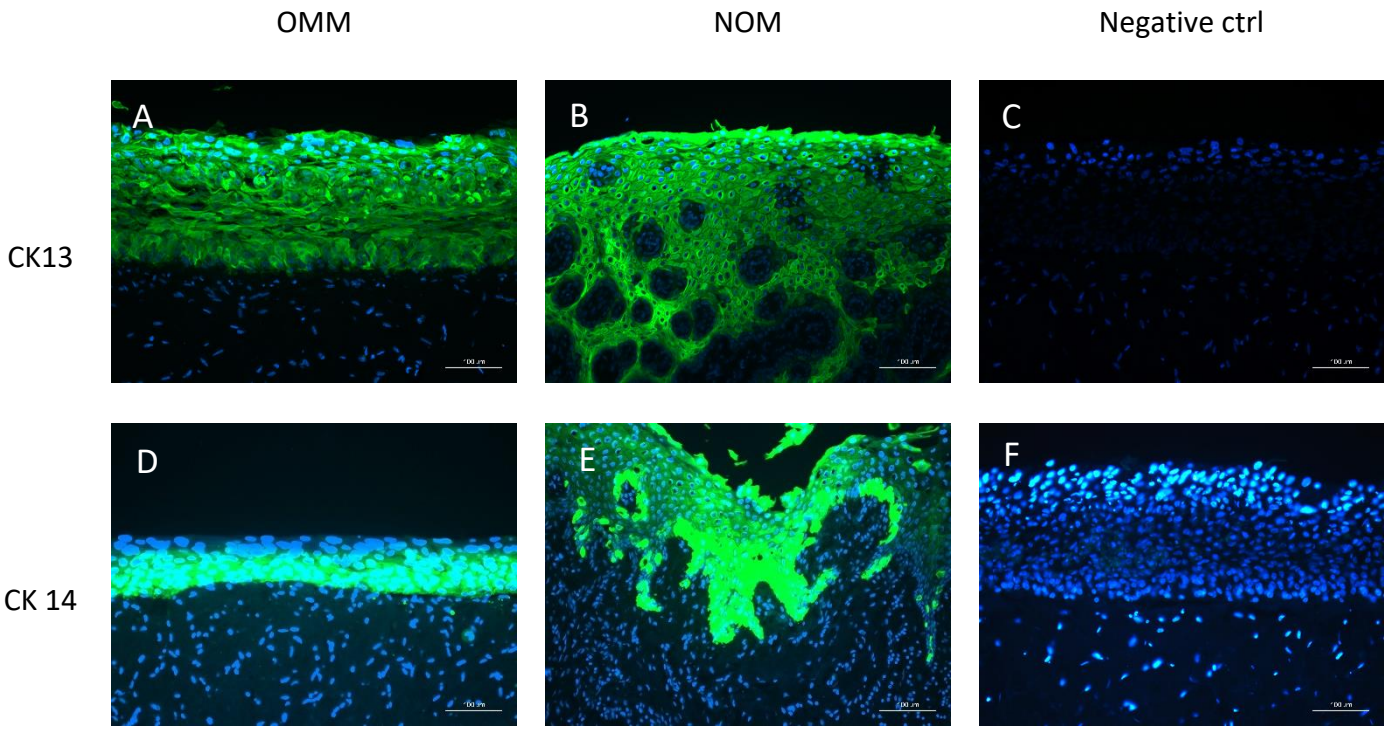

Figure 4. 12. Representative images compared the cytokeratin expression in mucosa part (OMM) of the printed composite model with normal oral mucosa (NOM). OMM displays cytokeratin expression profile similar to NOM. Image demonstrates; **(A and D)** Immunofluorescent labelling shows the positive expression of cytokeratin (CK) 13 and 14, respectively in OMM. Similar CKs expression was found in NOM (positive ctrl) for CK 13 **(B)** and CK14 **(E)**. **(C and F)** represent OMM stained with isotype control and secondary antibody (negative ctrl) for CK13 and CK14, respectively. Positive immunolabelling are shown in green while cell nuclei are shown in blue (Scale bars = 100 µm).

4.4.4.3. Histological assessment of printed ABMM

Printed ABMM demonstrated a histological structure consisting of oral mucosa adhered to the underlying bone scaffold (Figure 4.13. A), simulating the native oral hard and soft tissues. The uppermost surface displayed a continuous stratified epithelium covering a quite fibroblast−populated dense connective tissue. Oral mucosa−bone interface revealed a thin band of cell infiltrated fibrin attaching both layers. The pores of 3DP scaffold containing two apparently viable cell layers; a central mass of fusiform cells partially aligned with each other,

and a separate mural monolayer of rounded cells within a more eosinophilic matrix (Figure 4.13. B). Such cellular alignment was noticed in native oral bone (Figure 4.13. C).

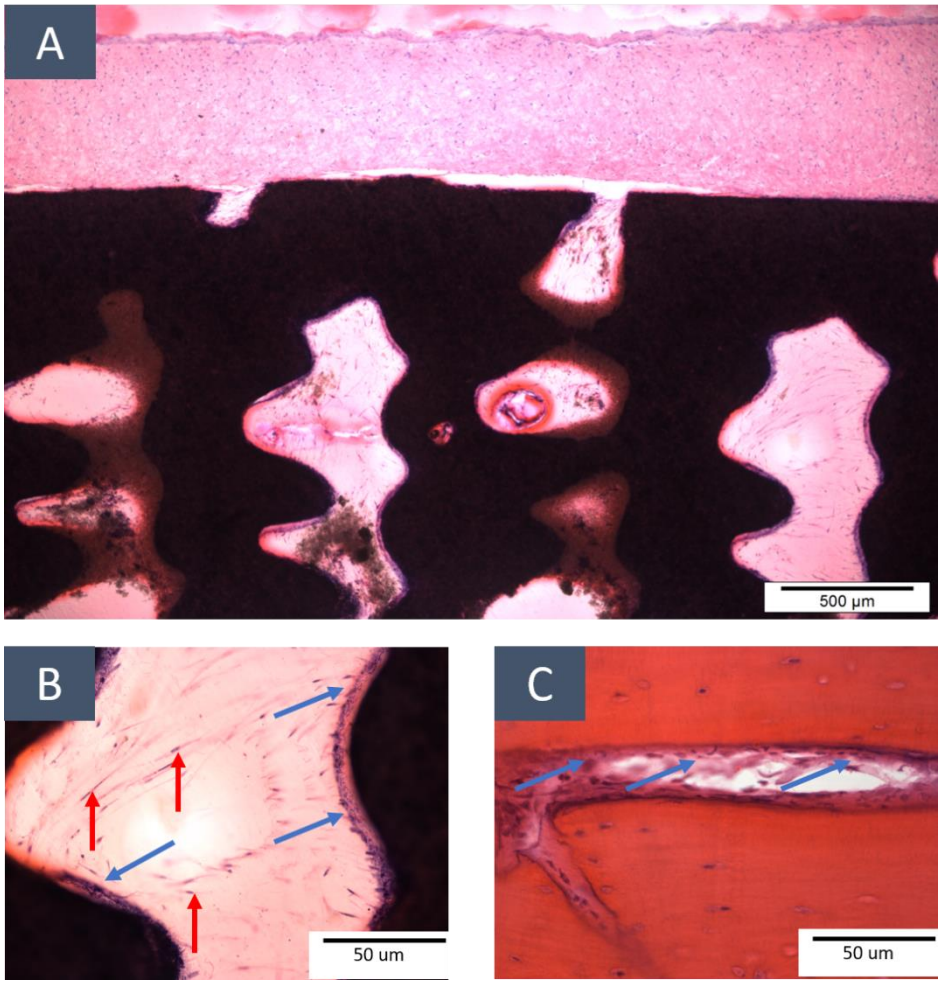

Figure 4. 13. H&E stained histological ground section of 3DP ABMM. Image showing **(A)** full−thickness, multi−layered 3DP bone mucosal construct consisting of a stratified oral epithelium, connective tissue layer adherent to the underlying 3DP bone. **(B)** The bony part showing the pores of the scaffold containing two apparently viable cell layers; a central mass of fusiform cells partially aligned with each other (red arrows), and a separate mural monolayer of rounded cells (blue arrows). **(C)** Similar cellular alignment was noticed in natural alveolar bone (Scale bars: A = 500 µm; B and C = 50 µm).

4.4.4.4. qRT–PCR assessment

Figure (4.14.) demonstrates the osteogenic and epithelial genes expressed in the printed ABMM.

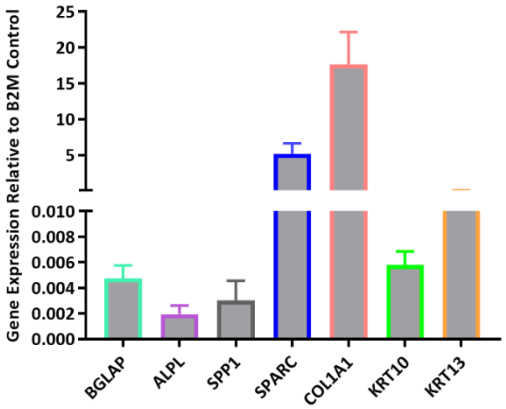

Figure 4. 14. qRT–PCR analysis of the osteogenic and epithelial genes expressed in printed ABMM. Data represents mean ± SD of three independent experiments (n=3) performed in triplicate.

4.4.4.5. ELISA

Quantification of COL1, ON, and OC proteins was consistent with their gene profile. COL1 demonstrated an increased protein concentration in comparison to ON and OC. OC, in turn, showed the lowest level (Figure 4.15.).

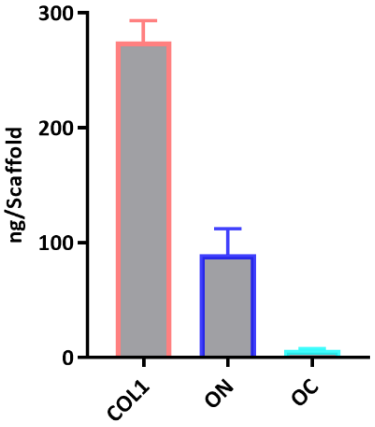

Figure 4. 15. Protein expression of COL1, ON, and OC in the printed ABMM analysed by ELISA. Data represents mean ± SD of three independent experiments (n=3) performed in triplicate

4.5. Discussion

An important prerequisite for successful BTE is the utilization of a suitable scaffold that satisfies the physical and chemical requirements of the native bone. TCP is a well−established bone substitute material that has been used in different techniques of scaffold fabrication such as leaching and foaming (Ginebra et al., 2010). AM techniques enable a more controlled construction of scaffold architecture and shape than using conventional scaffold fabrication methods (Lode et al., 2014). Therefore, it provides advantages from both clinical and experimental standpoints. While it allows fabrication of a precise, patient−specific construct for therapeutic purposes, a tissue model with more reproducibility and replication of native tissue can be obtained for research applications. In this study, we have described the use of 3D printing technology to fabricate TCP scaffolds with dual layers, including compact and porous.

Optimisation of the prepared paste and extrusion parameters have an impact on the fabrication and characteristics of the TCP-based scaffold. The flow rate of the dispensing material is a crucial aspect of the 3D printing technique. This factor is known to affect line width, fabrication time, and geometry resolution (Li et al., 2009). Our results indicated that the viscosity of the TCP paste is dependent on the shear rate and temperature to a certain extent. The prepared TCP paste, like many other ceramic slurries, has non-Newtonian behaviour and is a Bingham plastic material, which means that the flow rate is directly proportionate to the shear stress and inversely proportionate to the viscosity (resistance to flow) (Liu et al., 2006; Qi et al., 2008). This feature can be advantageous in adjusting the viscosity of the dispensing paste by controlling the temperature; thereby increasing the flow rate and shortening the fabrication time. However, the high dispensing speed may compromise the geometrical resolution. Particle size may comprise a contributing factor in

the flowability and printability of the material. A too small particle size can compromise flowability due to the agglomeration of the particles, while too large particles easily flow but do not pack sufficiently. This leads to interlayer instability that compromises binding and geometrical accuracy. A 10-50 µm particle size is generally considered optimal (Butscher et al., 2012; Inzana et al., 2014; Zhou et al., 2014b).

The bonding solution, which is usually a sacrificial polymer such as tripolyphosphate or an aqueous solution like diluted phosphoric acid, may constitute a factor that determines the solidification process. While the polymer binder pyrolyzed during sintering, the acidic binder initiates a dissolution−precipitation reaction within the powder to fuse the particles. The resultant scaffolds may have different mechanical and biological properties. TCP scaffolds printed with high temperature (i.e. heat sintered) usually have enhanced mechanical properties, enabling them to be structurally sound, particularly in load bearing areas. The low-temperature method, on the other hand, allows direct printing of living cells and/or biological factors with the printed paste, which is hardened by cement reaction or UV light (Trombetta et al., 2017).

The importance of the structural and morphological features of bone scaffold was detailed in Chapter 2 (see section 2.6.1.). In this study, it was possible to adjust the structural parameters to be close to the optimised desirable values. Porosity (pore size, pore shape, and porosity percentage) and interconnectivity are two critical parameters that have a strong impact on cell behaviour. Previous studies have shown that the optimum pore size for the bone is 400 µm (Bai et al., 2010; Feng et al., 2011), whereas the critical size is considered to be 100 µm due to cell size, migration, and nutrition (Rouwkema et al., 2008). A study conducted on the printed TCP scaffold with a pore size of 1,000, 750, and 500 µm showed that decreasing the macro porosity from 1,000 to 500 µm resulted in increasing the osteoblasts' proliferation

(Tarafder et al., 2013). In the same study, the obtained total open porosity was between 42 % and 63 %, which is very close to our findings. Human cancellous bone demonstrates a total porosity between 30 % and 90 %. Therefore, a scaffold construct containing a porosity within this range is considered to be suitable for bone regeneration (Karageorgiou and Kaplan, 2005).

Strand thickness and the distance between the strands on the porous scaffold layers were tailored to be around or within the range of the trabecular struts in the cancellous bone, which are approximately 100−300 µm thick and have spaces equal to 300−1,500 µm (Bueno, 2011). The compact bone is denser than the cancellous bone, therefore, a plotter with higher resolution is required to obtain a concentric ring similar to Haversian canals, which are approximately 50 µm in diameter (Burr and Allen, 2014).

With regard to surface roughness, it has been established that surface topography can have positive effects on cellular functions by increasing wettability and surface area. This results in a favourable cellular response in terms of protein secretion, adhesion, proliferation, and differentiation (Zhao et al., 2015). Wu et al. (2015) investigated the influence of different degrees of roughness on bone cells and found that the optimum average roughness of 0.80−1.00 µm could be a key factor in determining the morphological and functional cell responses. However, the cells exhibited a less activated proliferation when the surface roughness was above the critical point (Ra=1.00 µm).

Although all the aforementioned factors are fundamentals for bone regeneration, a balance should be struck between these factors and maintaining proper mechanical properties. Mechanical strength is affected by pore volume and distribution as well as layer thickness and printing orientation (Farzadi et al., 2014). These factors yield mechanical properties close to the cancellous bone, which ranged between 1.8−10.2 MPa and 10−2,000 MPa for

compressive strength and modulus, respectively. These properties are lower than those of the compact bone, which has a compressive strength of 133−195 MPa and Young's modulus of 11.7−18.2 GPa (Bueno, 2011). To counteract the poor mechanical properties, many methods have been used to reinforce ceramic-based scaffolds, including the infiltration of the bioactive glass with a tough Polycaprolactone polymer (Eqtesadi et al., 2016), reinforcement with hydroxyapatite whiskers (Feng et al., 2014), or compositing with collagen (Zhou et al., 2014a). Recently, Roohani-Esfahani et al. (Roohani-Esfahani et al., 2016) developed a 3D printed bioactive ceramic scaffold with a high compressive strength comparable to compact bone (90−110 MPa at 70 % porosity). The authors attributed this result to the hexagonal architecture of the pores, which resulted in a higher contact area between the printed struts, leading to an enhanced load transfer.

Another method of scaffold consolidation is through sintering technique and temperature. (Tarafder et al., 2013) compared microwave and conventionally sintered TCP printed scaffold at different temperatures. They obtained a maximum compressive strength of 10.95 ± 1.28 MPa and 6.62 ± 0.67 MPa in microwave and conventional furnaces, respectively, for scaffolds with 500 µm pores sintered at 1250 ^{o}C. However, this improvement in the mechanical feature was at the expense of total porosity, which dropped from 69 % to 46 % due to the marked shrinkage associated with microwave sintering. In another study, when a mixture of tetracalcium phosphate/β−TCP was sintered at 1400 ^{o}C, the strength of the 3DP scaffold was increased, while sintering a tetracalcium phosphate/calcium sulphate dihydrate composite compromised the strength due to water release (Khalyfa et al., 2007).

Voids volume is another factor that should be considered when a scaffold is fabricated in a layer−by−layer manner. Voids volume influences the strength of interlayer bonds, leading to the propagation of cracks along the boundaries between layers due to the weakness and

brittleness of these bonds under parallel compression load (Cox et al., 2015). Perhaps this problem is signified when the printed material itself is brittle, as is the case in all ceramic material, including β−TCP. Taking these data together, the printed scaffold in this study may be deemed appropriate in terms of porosity and mechanical properties compared with many studies that achieved porosity ranges between 30 % and 54 % and compressive strength between 3.8 and 6.6 MPa (Khalyfa et al., 2007; Tarafder et al., 2013).

Undoubtedly, for regenerative applications, it is necessary to determine the biocompatibility of the 3D printed scaffold. The cell-scaffold biological interaction, as evaluated by cell vitality, DNA content, and adhesion, all showed a significant increase in the cell activity, proliferation, and exponential growth of HAOBs on a 3DP scaffold. Together these findings indicated that the biomimetic β−TCP printed scaffold possessed biocompatibility, and structural features facilitated cellular growth *in vitro.* These results are in the line with many investigations which found that printing calcium phosphate with different patterns favourably supports cell behaviour. A comprehensive systematic review by (Trombetta et al., 2017) described different 3DP approaches of calcium phosphate and the evidence of its *in vivo* and *in vitro* efficacy.

In bone, collagen fibres and apatite crystals are preferentially self-assembled according to the bone's anatomical position, which in turn has its own impact on the mechanical properties. The alignment and spreading of osteoblasts in different degrees of orientation along the scaffold's strands suggest that the newly produced bone matrix may exhibit an anisotropic microstructure similar to bone microstructure (Nakano et al., 2014).

With regard to the printed ABMM, the characteristic features were comparable to those found in composite constructs fabricated by the conventional scaffold. A discussion of the characteristics features of the composite model was provided in Chapter 3 (see section

3.4.3.). The trends relating to gene expression and protein secretion in the printed models were generally similar to those observed in conventional counterparts, logically, due to the same reasons explained in Chapter 3. Such similarities in the expression of major ECM markers, which are known to be upregulated in osteogenesis, confirmed the biocompatibility of the printed scaffold and its ability to support bone tissue formation. In addition, the higher gene expression found in the printed model compared with the conventional one can be supported by many studies, indicating that osteogenic proliferation and differentiation are favourably enhanced by printed design (Ferlin et al., 2016; Cavo and Scaglione, 2016; Zhang et al., 2017). However, in this study, the quantitative comparison between printed and conventional models may be not feasible due to patient-to-patient variations.

Further to the results pertaining to the engineered composite models, the differences in scaffold fabrication using conventional and printing methods should be considered. In addition to the accuracy, consistency, reproducibility, and minimum labour efforts provided by the robotic printing system, two other factors should be highlighted: time and cost. The speed of manufacture when using 3D printing is quite high. The average printing time for each scaffold was 5 minutes. This means that 144 scaffolds can be printed within 12 hours and sintered within an additional 12 hours; resulting in a significant number of scaffolds within only 24 hours.

From an economic standpoint, although the versatility in using a wide range of cheap materials makes the cost of printed material very reasonable (GBP0.04 for each scaffold used in this study), the price of a high−quality printer, a furnace, a mixer, as well as the machinery's maintenance and the energy used, might all result in a quite high final cost per scaffold.

In conclusion, this study disclosed the fabrication of a 3D printed bi-layer calcium phosphate cement-based scaffold resembling a normal cortico−cancellous bone's microstructure. The

scaffolds demonstrated optimal *in vitro* biocompatibility and biological activity, high interconnectivity, and precise pore size on both sides. We demonstrated here the *in vitro* replication of normal human alveolar bone and the mucosa relationship. Our data suggested that the composite *in vitro* model had a structure and characteristics comparable to native oral hard and soft tissues. The developed model might have the potential to provide a more reliable human cell−based alternative to 2D or animal models for various *in vitro* applications.

Chapter 5: Application of 3D printed bone–mucosal model for *in vitro* modelling of oral cancer progression

NB: The work described in this chapter has been published in:

Almela, T., Al-Sahaf, S., Brook, I. M., Khoshroo, K., Rasoulianboroujeni, M., Fahimipour, F., Tahriri, M., Dashtimoghadam, E., Bolt, R., Tayebi, L. & Moharamzadeh, K. 2018. 3D printed tissue engineered model for bone invasion of oral cancer. *Tissue and Cell,* 52, pp 71-77.

Figure (5.1. C) illustrated in this chapter has been featured on the cover of Tissue and Cell journal, Volume 52, June 2018, ISSN 0040-8166.

5.1. Introduction

One of the applications by which the advantages of 3DP can be exploited is fabrication of reproducible constructs to be used for *in vitro* disease modelling or drug screening (Vanderburgh et al., 2017). In this preliminary study, the potential application of the printed ABMM in the future study of oral cancer invasion was demonstrated.

Oral squamous cell carcinoma (OSCC) is the most common head and neck malignancy that accounts for approximately 90 % of all oral and oropharyngeal tumours (Chi et al., 2015). To date, several authors have undertaken 3D *in vitro* modelling of OSCC using soft tissue−only constructs (Kataoka et al., 2010; Colley et al., 2011; Che et al., 2006). However, OSCC frequently invades the underlying alveolar bone due to the close anatomical relationship between these two entities (Goda et al., 2010; Ebrahimi et al., 2011). Indeed, tumours of the tongue, retromolar region, and floor of mouth invade the mandible in 42 %, 48 %, and 62 % of cases, respectively (Brown et al., 2002). Therefore, the absence of a bone equivalent construct within the soft tissue models limits their validity in translating *in vitro* findings which are heavily influenced by the presence or absence of bony invasion. A suitable *3D in vitro* model which combines both soft and hard tissues is, therefore, desirable in achieving a more sophisticated model of OSCC progression.

5.2. Aim

To construct a cancerous alveolar bone mucosal model (CABMM) representing oral squamous cell carcinoma (OSCC) in three distinct anatomical levels.

5.3. Materials and methods

5.3.1. Tumour spheroid production

According to (Hearnden, 2011) “spheroid is a mass of cells which when cultured on a non adherent surface form a spherical solid mass with a well−defined border”. In this work, the cell line UPCI−SCC090 was used to produce tumour spheroids. The cells were received under Material Transfer Agreement from Professor S. Gollin, University of Pittsburgh School of Public Health, Pittsburgh. STR profiling was performed for cell type authentication (see section 2.3.2. and Appendix II). Tumour spheroids were generated from UPCI−SCC090 cells using the liquid overlay method as previously described (Carlsson and Yuhas, 1984). A 96 well plate was coated with 1.5 % type V agarose (Sigma Aldrich, Dorset, UK) (w/v in serum-free DMEM). Then, 100 µl of cell suspension containing a 1×10^4 UPCI−SCC090 were added to each well. The cells were incubated for 4 days and medium changed every 48 hours.

5.3.2. Construction of cancerous bone mucosa model (CBMMs)

To generate a cancerous bone mucosal model (CBMMs), ABMM was constructed (see section 4.3.3.). Then, 30 spheroids of UPCI-SCC090 were added at different steps of model preparation to produce three distinct levels of OSCC. Spheroids were added either to the epithelium (carcinoma in situ), epithelium and connective tissue layers, or connective tissue and bone interface. After the end of culture time, models were assessed histologically as described in chapter 3 (see section 4.3.4.4.).

5.4. Results

After 4 days of culturing UPCI−SCC090 in a well plate coated with agarose, spheroids were formed (Figure 5.1.).

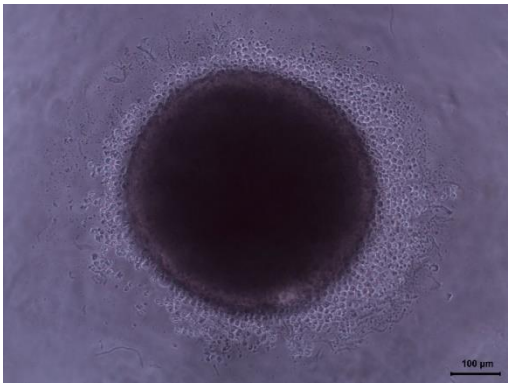

Figure 5. 1. UPCI-SCC090 spheroid formed after 4 days of culture.

The histological observation of the constructed CBMMs displayed a combined bone and oral mucosal structure with clearly visible tumour spheroids located at different depths. Figure (5.2. A) illustrates the histological pattern of OSCC in which tumour cells located in the epithelium (carcinoma in situ) while tumour cells located at the connective tissue and mucosal bone interface are demonstrated in figure (5.2. B) and (5.2. C), respectively.

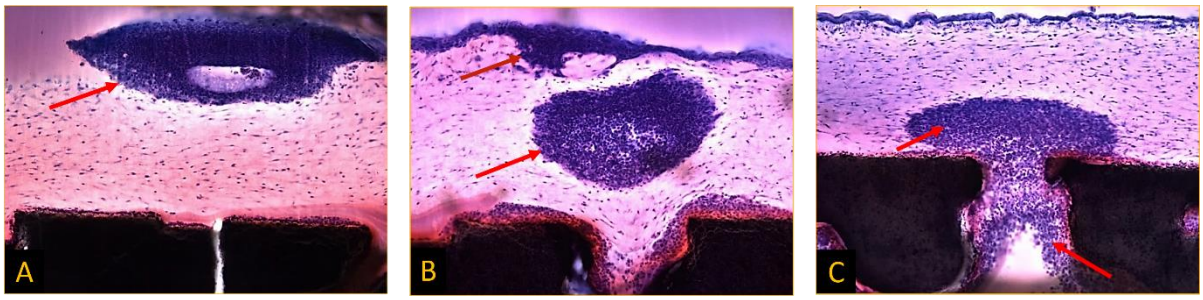

Figure 5. 2. H&E−stained histological ground sections of CBMM representing OSCC spheroids in different anatomical levels. H&E−stained histological ground sections of CBMM representing OSCC spheroids with different anatomical level. Red arrows indicate to tumor spheroids in; **(A)** epithelium; **(B)** the epithelium and connective tissue; **(C)** and connective tissue layer in direct contact with the bone (Scale bars =200 µm).

5.5. Discussion

Many studies have shown that once the OSCC has invaded the mandible, it may progress through the bone in an erosive, infiltrative or mixed pattern (Slootweg and Muller, 1989). The progression of tumour−induced bone disease has been modeled *in vitro* using 3D collagen or polymer scaffolds for metastatic prostate cancer (Fitzgerald et al., 2015), breast cancer (Mastro and Vogler, 2009), and Ewing sarcoma (Eliza Li Shan et al., 2013). These studies demonstrated that the tumour response to anticancer drugs is substantially altered in 3D microenvironment compared to 2D monolayer culture. However, these scaffolds constructed by conventional methods do not generally represent the normal bone structure which may pose a problem regarding the translation of *in vitro* findings. Similarly, OSCC has been modelled *in vitro* using soft tissue substrates (Che et al., 2006; Colley et al., 2011; Kataoka et al., 2010). The limitation of these studies, however, is the lack of bone−construct equivalent that faithfully represents the oral cancer microenvironment which often invades the bone and progress through it in an erosive, infiltrative or mixed pattern (Slootweg and Muller, 1989). This preliminary study addressed these two limitations by using the bone scaffold fabricated by the 3DP method to construct a composite bone mucosal model that might closely resemble the oral cancer microenvironment. By utilising this model, the interaction between different layers of tumor microenvironment that influence the cancer growth, progression and metastasis can be determined. However, it should be kept in mind that the size of spheroids and the length of their culture, are limited by the absence of angiogenesis; the innermost tumour cells may, therefore, become quiescent and ultimately apoptose or necrose. The lack of oxygen and nutrients, as well as the accumulation of waste products and decreased pH, can result in a central necrotic core when the spheroid's size exceeds 500−600 µm (Friedrich et al., 2007). Although present on a more macroscopic scale, changes in pH,

oxygen tension and nutrient availability also occur *in vivo* as a result of cancer growth outstripping vascular supply. Therefore, these features within our model may replicate the properties of cancer which contribute to tumour resistance to therapy and cytokine release. Accordingly, the establishment of a tissue engineered *in vitro* 3D oral cancer model by co−culturing cancer spheroids and multiple types of normal human cells within appropriate multi-layered scaffolds may represent a promising approach to simulate *in vivo* tumour microenvironment and the clinical situation as closely as possible. Therefore, the illustrated model has the potential to be further developed and characterised to be used for the assessment of novel diagnostic or therapeutic approaches to manage OSCC in the future. However, detailed and extensive analysis of the cancer model was beyond the scope of this study.

Chapter 6: Final conclusions

Several studies have demonstrated oral and dental tissue engineering using various methods in terms of the cells, scaffolds, and culture environment. While the construction of individual tissue has received significant attention, only a few studies have focused on incorporating different tissues in a single compound construct. This thesis has described the development of a 3D tissue engineered ABMM based on a ceramic bone scaffold fabricated by conventional and advanced printing techniques. Conclusions for this study can be summarized in the following points:

- *In vitro* engineering of a composite oral bone-mucosal model resembling the native histological structure of the oral tissue could be established using cancer and immortal cell line. The use of fibroblast−populated collagen gel for oral mucosa assembly and employing a biocompatible fibrin−based adhesive to combine the constructed soft and hard tissues appear to be successful approaches in TE of a tri-layered composite osteo-mucosal system. Although the development of the oral composite model using human cell lines was feasible, the construction of the model by human primary oral cells was essential for more relevant and predictive data.
- ABMM constructed from convensional scaffold and patient-sourced alveolar bone and mucosal cells demonstarted a characteristic features comparable to the native tissue in terms of histological, immunohistochemical, ultrastructural examinations, as well as the gene and protein expression. However, reconstruction of intricately stuctured scaffold mimicking the bone's hierarchy with precise measurements could not be achieved by convensional scaffolding method.

- Advanced 3DP technique disclosed the fabrication of a bi-layered bone scaffold that simulated cortico−cancellous bone structure. The characterised scaffold demonstrated optimal *in vitro* biocompatibility and biological activity, high interconnectivity, and precise pore size on cortical and porous side. This technique provided the accuracy, consistency, reproducibility, reduced time and labour effort. The printing-based ABMM demonstrated a structure and characteristic features comparable to the native tissues. However, printing with higher resolusion is needed for further optimisation of scaffold geometrie.
- The preliminary use of the printing-based CABMM demonstrated oral carcinoma at different anatomical levels, namely the epithelium, epithelium and connective tissue, or connective tissue-bone interface. This novel cancer model provides a tool to improve understanding of oral cancer progression or to be used for the assessment of novel diagnostic and therapeutic approaches in order to manage OSCC in the future. While the engineering of this multi-layered cancer construct is presented in this thesis, additional development and characterisation will provide further insight into the mechanism of oral cancer invasion.

Chapter 7: Future work

3D cell culture system has been proposed to bridge between 2D cell culture and *in vivo* animal models (Ali et al., 2006) and between animal modelling and human trials (Linda and Melody, 2006). Recently, tissue engineered models have gained increasing interest in drug discovery and disease modelling due to their evident advantages in providing more physiologically relevant information and more predictive data for *in vivo* tests. The novel ABMM demonstrated in this thesis can provide a valuable tool in many *in vitro* applications such as oral cancer and dental implant studies.

Over the last decade, there has been a growing notion of the significance of the tissue microenvironment for the initiation, progression, and suppression of cancer (Villasante and Vunjak-Novakovic, 2015). The lack of ability to replicate the complexity and heterogeneous nature of human *in vivo* oral cancer constitutes a barrier to more effective research and therapeutic targets. Recently, 3DP has found a niche in fabricating *in vitro* models with complexity approaching that of the *in vivo* tumor microenvironment (Albritton and Miller, 2017). The novel CABMM illustrated in this study may provide a representative tool to improve understanding of oral cancer progression in the future studies. Clearly, further extensive and detailed characterisation are necessary before the utilisation of this model in the testing of novel diagnostic or therapeutic approaches towards managing OSCC in the future.

Dental implant research may constitute another potential application of ABMM. Dental implants are an increasingly popular solution for edentulous people to restore appropriate masticatory functions and satisfactory aesthetic requirements. In the USA alone, it is estimated that half million implants are placed annually (Rittel et al., 2017). The implant

system is comprised of three elements; the implant itself, bone, and soft tissue. The success of implant therapy depends on the interaction between these components. Although many *in vitro* studies conducted to investigate oral mucosa-implant interface (Chai et al., 2012a; Chai et al., 2012b; Chai et al., 2013; Chai et al., 2010), the establishment of the whole implant system will provide an opportunity for new generation of dental implant with special micro−topographical, mechanical and biological features (Moradian-Oldak et al., 2006). Utilisation of ABMM in the future may include: investigating implant-soft tissue attachment, the study of implant−bone interface and osseointegration, the evaluation of biological seal, and the effects of oral bacteria on the implant−tissue interface.

Chapter 8: References

Abdollahi, S., Ma, A. C. C. & Cerruti, M. 2013. Surface transformations of Bioglass 45S5 during scaffold synthesis for bone tissue engineering. *Langmuir : the ACS journal of surfaces and colloids,* 29(5)**,** pp 1466-1474.

Abe, T., Hara, Y., Abe, Y., Aida, Y. & Maeda, K. 1996. Isolation of alkaline phosphatase-positive gingival fibroblasts from patients with chronic inflammatory periodontal disease. *Journal of Periodontal Research,* 31(4)**,** pp 285-293.

Akintoye, S. O., Lam, T., Shi, S., Brahim, J., Collins, M. T. & Robey, P. G. 2006. Skeletal site-specific characterization of orofacial and iliac crest human bone marrow stromal cells in same individuals. *Bone,* 38(6)**,** pp 758-768.

Akkineni, A. R., Luo, Y., Schumacher, M., Nies, B., Lode, A. & Gelinsky, M. 2015. 3D plotting of growth factor loaded calcium phosphate cement scaffolds. *Acta Biomaterialia,* 27, pp 264-274.

Albee, F. H. 1920. Studies in bone growth: triple calcium phosphate as a stimulus to osteogenesis. *Annals of Surgery,* 71(1)**,** pp 32-39.

Alberts, B. 2013. *Essential Cell Biology*, Fourth edition.: New York, NY : Garland Science, 2013.

Albritton, J. & Miller, J. 2017. 3D bioprinting: improving in vitro models of metastasis with heterogeneous tumor microenvironments. *Disease Models & Mechanisms, 10(1), pp.3-14.*

Ali, K., Robert, L., Jeffrey, B. & Joseph, P. V. 2006. Microscale technologies for tissue engineering and biology. *Proceedings of the National Academy of Sciences of the United States of America,* 103(8)**,** pp 2480-7.

Aljohani, W., Ullah, M. W., Zhang, X. & Yang, G. 2017. Bioprinting and its applications in tissue engineering and regenerative medicine. *International Journal of Biological Macromolecules*, 107, pp 261-275.

Allori, A., Sailon, A. & Warren, S. 2008. Biological Basis of Bone Formation, Remodeling, and Repair-- Part I: Biochemical Signaling Molecules. *Tissue Engineering Part B, Reviews,* 14(3)**,** pp 259-273.

Amrollahi, P., Shah, B., Seifi, A. & Tayebi, L. 2016. Recent advancements in regenerative dentistry: A review. *Materials Science & Engineering. C, Materials for Biological Applications,* 69, pp 1383-1390.

An, J., Teoh, J. E. M., Suntornnond, R. & Chua, C. K. 2015. Design and 3D Printing of Scaffolds and Tissues. *Engineering,* 1(2)**,** pp 261-268.

Andrea Di, L., Barbara, O., Ivan, L.-M., Antonio, L., Wojcech, S., Clemens Van, B. & Lorenzo, M. 2016. Gradients in pore size enhance the osteogenic differentiation of human mesenchymal stromal cells in three- dimensional scaffolds. *Scientific Reports,* 6(1)**,** pp 1-13.

Annabi, N., Nichol, J. W., Zhong, X., Ji, C., Koshy, S., Khademhosseini, A. & Dehghani, F. 2010. Controlling the porosity and microarchitecture of hydrogels for tissue engineering. *Tissue Engineering Part B, Reviews,* 16(4)**,** pp 371-83.

Ansar Ahmed, S., Gogal, R. M. & Walsh, J. E. 1994. A new rapid and simple non- radioactive assay to monitor and determine the proliferation of lymphocytes: an alternative to [3H] thymidine incorporation assay. *Journal of Immunological Methods,* 170(2)**,** pp 211-224.

Atesok, K., Doral, M., Karlsson, J., Egol, K., Jazrawi, L., Coelho, P., Martinez, A., Matsumoto, T., Owens, B., Ochi, M., Hurwitz, S., Atala, A., Fu, F., Lu, H. & Rodeo, S. 2016. Multilayer scaffolds in orthopaedic tissue engineering. *Knee Surgery, Sports Traumatology, Arthroscopy,* 24(7)**,** pp 2365-2373.

Avery, J. K. 2006. *Essentials of oral histology and embryology : a clinical approach*, 3rd ed., James K. Avery, Daniel J. Chiego., St. Louis, Mo.: St. Louis, Mo. : Mosby Elsevier, 2006.

Bai, F., Wang, Z., Lu, J., Liu, J., Chen, G., Lv, R., Wang, J., Lin, K., Zhang, J. & Huang, X. 2010. The correlation between the internal structure and vascularization of controllable porous bioceramic materials in vivo: a quantitative study. *Tissue Engineering Part A,*16(12)**,** pp 3791-803.

Baino, F. & Vitale-Brovarone, C. 2014. Mechanical properties and reliability of glass– ceramic foam scaffolds for bone repair. *Materials Letters,* 118, pp 27-30.

Baroli, B. 2009. From natural bone grafts to tissue engineering therapeutics: Brainstorming on pharmaceutical formulative requirements and challenges. *Journal of Pharmaceutical Sciences,* 98(4)**,** pp 1317-75.

Barré-Sinoussi, F. & Montagutelli, X. 2015. Animal models are essential to biological research: issues and perspectives. *Future Science OA,* 1(4)**,** pp FSO63.

Bastami, F., Nazeman, P., Moslemi, H., Rezai Rad, M., Sharifi, K. & Khojasteh, A. 2017. Induced pluripotent stem cells as a new getaway for bone tissue engineering: A systematic review. *Cell Proliferation*,50 (2), pp e12321.

Ben-Nissan, B., Nissan, B. B., Ben-Nissan, B. & Nissan, B. B. 2014. Advances in calcium phosphate biomaterials: Berlin : Springer-Verlag, 2014.

Benam, K. H., Dauth, S., Hassell, B., Herland, A., Jain, A., Jang, K.-J., Karalis, K., Kim, H. J., MacQueen, L., Mahmoodian, R., Musah, S., Torisawa, Y.-s., van der Meer, A. D., Villenave, R., Yadid, M., Parker, K. K. & Ingber, D. E. 2015. Engineered In Vitro Disease Models. *Annual Review of Pathology:Mechanisms of Disease,* 10, pp 195-262.

Berg, R. A. & Prockop, D. J. 1973. The thermal transition of a non- hydroxylated form of collagen. Evidence for a role for hydroxyproline in stabilizing the triple- helix of collagen. *Biochemical and Biophysical Research Communications,* 52(1)**,** pp 115-120.

Berkovitz, B. K. B. 2009. *Oral anatomy, histology and embryology [electronic resource]*, 4th ed., Edinburgh: Edinburgh : Mosby, 2009.

Berthiaume, F., Maguire, T. J. & Yarmush, M. L. 2011. Tissue Engineering and Regenerative Medicine: History, Progress, and Challenges. *Annual Review of Chemical and Biomolecular Engineering,* 2, pp 403-430.

Bhadriraju, K. & Chen, C. S. 2002. Engineering cellular microenvironments to improve cell-based drug testing. *Drug Discovery Today,* 7(11)**,** pp 612-620.

Bhagavati, S. 2015. Stem Cell Therapy: Challenges Ahead. *The Indian Journal of Pediatrics,* 82(3)**,** pp 286-291.

Bhargava, S., Chapple, C. R., Bullock, A. J., Layton, C. & MacNeil, S. 2004. Tissue-engineered buccal mucosa for substitution urethroplasty. *BJU International,* 93(6)**,** pp 807-11.

Bhumiratana, S., Bernhard, J., Cimetta, E. & Vunjak-Novakovic, G. 2014. Chapter 14 - Principles of Bioreactor Design for Tissue Engineering *In:* Langer, R. & Vacanti, J. (eds.) *Principles of Tissue Engineering (Fourth Edition).* Boston: Academic Press.

Bielby, R. C., Polak, J. M., Buttery, L. D. K. & Boccaccini, A. R. 2004. In vitro differentiation and in vivo mineralization of osteogenic cells derived from human embryonic stem cells. *Tissue Engineering,* 10(9-10)**,** pp 1518-1525.

Bigdeli, N., De Peppo, G. M., Lennerås, M., Sjövall, P., Lindahl, A., Hyllner, J. & Karlsson, C. 2010. Superior osteogenic capacity of human embryonic stem cells adapted to matrix-free growth compared to human mesenchymal stem cells. *Tissue Engineering Part A,* 16(11)**,** pp 3427-3440.

Birla, R. 2014. *Introduction to Tissue Engineering [electronic resource]:Applications and Challenges*, Hoboken: Hoboken : Wiley, 2014.

Birmingham, E., Niebur, G. L., McHugh, P. E., Shaw, G., Barry, F. P. & McNamara, L. M. 2012. Osteogenic differentiation of mesenchymal stem cells is regulated by osteocyte and osteoblast cells in a simplified bone niche. *European Cells & Materials,* 23, pp 13-27.

Biver, E., Soubrier, A.-S., Thouverey, C., Cortet, B., Broux, O., Caverzasio, J. & Hardouin, P. 2012. Fibroblast growth factor 2 inhibits up- regulation of bone morphogenic proteins and their receptors during osteoblastic differentiation of human mesenchymal stem cells. *Biochemical and Biophysical Research Communications,* 427(4)**,** pp 737-742.

Bjerre, L., Bünger, C. E., Kassem, M. & Mygind, T. 2008. Flow perfusion culture of human mesenchymal stem cells on silicate- substituted tricalcium phosphate scaffolds. *Biomaterials,* 29(17)**,** pp 2616-2627.

Blokhuis, J. T., Termaat, F. M., Den Boer, C. F., Patka, C. P., Bakker, J. T. M. F. & Haarman, J. T. M. H. 2000. Properties of Calcium Phosphate Ceramics in Relation to Their In Vivo Behavior. *The Journal of Trauma: Injury, Infection, and Critical Care,* 48(1)**,** pp 179-179.

Boccaccini, A. R., Ma, P. X. & Boccaccini, A. R. 2014. *Tissue engineering using ceramics and polymers*, Second edition / edited by Aldo R. Boccaccini and Peter X. Ma.: Amsterdam : Elsevier, 2014.

Bodner, L. & Grossman, N. 2003. Autologous cultured mucosal graft to cover large intraoral mucosal defects: A clinical study. *Journal of Oral and Maxillofacial Surgery,* 61(2)**,** pp 169-173.

Boelsma, E., Verhoeven, M. C. & Ponec, M. 1999. Reconstruction of a human skin equivalent using a spontaneously transformed keratinocyte cell line (HaCaT). *Journal of Investigative Dermatology,* 112(4)**,** pp 489-98.

Bonassar, L. J. & Vacanti, C. A. 1998. Tissue engineering: the first decade and beyond. *Journal of Cellular Biochemistry,* 30-31, pp 297-303.

Boncler, M., Różalski, M., Krajewska, U., Podsędek, A. & Watala, C. 2014. Comparison of PrestoBlue and MTT assays of cellular viability in the assessment of anti- proliferative effects of plant extracts on human endothelial cells. *Journal of Pharmacological and Toxicological Methods,* 69(1)**,** pp 9-16.

Borowiec, A.-S., Delcourt, P., Dewailly, E. & Bidaux, G. 2013. Optimal Differentiation of In Vitro Keratinocytes Requires Multifactorial External Control (Multifactorial Keratinocyte Differentiation). *PLoS One,* 8(10)**,** pp e77507.

Bose, S., Ke, D., Sahasrabudhe, H. & Bandyopadhyay, A. 2018. Additive manufacturing of biomaterials. *Progress in Materials Science,* 93, pp 45-111.

Bose, S., Roy, M. & Bandyopadhyay, A. 2012. Recent advances in bone tissue engineering scaffolds. *Trends Biotechnololgy,* 30(10)**,** pp 546-54.

Brown, J. S., Lowe, D., Kalavrezos, N., Souza, J., Magennis, P. & Woolgar, J. 2002. Patterns of invasion and routes of tumor entry into the mandible by oral squamous cell carcinoma. *Head & Neck,* 24(4)**,** pp 370-383.

Bueno, E. M. and Glowacki, J. 2011. Biologic foundations for skeletal tissue engineering.San Rafael, Calif.: San Rafael, Calif: Morgan & Claypool.

Buizer, A. T., Veldhuizen, A. G., Bulstra, S. K. & Kuijer, R. 2014. Static versus vacuum cell seeding on high and low porosity ceramic scaffolds. *Journal of Biomaterials Applications,* 29(1)**,** pp 3-13.

Burg, K. J. L., Holder, W. D., Culberson, C. R., Beiler, R. J., Greene, K. G., Loebsack, A. B., Roland, W. D., Eiselt, P., Mooney, D. J. & Halberstadt, C. R. 2000. Comparative study of seeding methods for three- dimensional polymeric scaffolds. *Journal of Biomedical Materials Research,* 51(4)**,** pp 642-649.

Burr, D. B. & Allen, M. R. 2014. Preface. *Basic and Applied Bone Biology.* San Diego: Academic Press.

Buskermolen, J. K., Reijnders, C. M., Spiekstra, S. W., Steinberg, T., Kleverlaan, C. J., Feilzer, A. J., Bakker, A. D. & Gibbs, S. 2016. Development of a Full-Thickness Human Gingiva Equivalent Constructed from Immortalized Keratinocytes and Fibroblasts. *Tissue Engineering Part C Methods,* 22(8)**,** pp 781-791.

Butscher, A., Bohner, M., Roth, C., Ernstberger, A., Heuberger, R., Doebelin, N., Rudolf Von Rohr, P. & Müller, R. 2012. Printability of calcium phosphate powders for three-dimensional printing of tissue engineering scaffolds. *Acta Biomaterialia,* 8(1)**,** pp 373-385.

Böttcher-Haberzeth, S., Biedermann, T. & Reichmann, E. 2010. Tissue engineering of skin. *Burns,* 36(4)**,** pp 450-460.

Cao, H. & Kuboyama, N. 2010. A biodegradable porous composite scaffold of PGA/β-TCP for bone tissue engineering. *Bone,* 46(2)**,** pp 386-395.

Carletti, E., Motta, A. & Migliaresi, C. 2011. Scaffolds for tissue engineering and 3D cell culture. *Methods* in *Molecular Biology,* 695, pp 17-39.

Carlsson, J. & Yuhas, J. M. 1984. Liquid-overlay culture of cellular spheroids. *Recent Results Cancer Research,* 95, pp 1-23.

Carragee, E. J., Hurwitz, E. L. & Weiner, B. K. 2011. A critical review of recombinant human bone morphogenetic protein- 2 trials in spinal surgery: emerging safety concerns and lessons learned. *The Spine Journal,* 11(6)**,** pp 471-491.

Carreira, A. C., Lojudice, F. H., Halcsik, E., Navarro, R. D., Sogayar, M. C. & Granjeiro, J. M. 2014. Bone Morphogenetic Proteins. *Journal of Dental Research,* 93(4)**,** pp 335-345.

Cavo, M. & Scaglione, S. 2016. Scaffold microstructure effects on functional and mechanical performance: Integration of theoretical and experimental approaches for bone tissue engineering applications. *Materials Science & Engineering C,* 68, pp 872-9.

Center of workforce intellegence (CWFI) (2010). Oral and Maxillofacial Surgery: CfWI medical fact sheet and summary sheet. Available at: http://www.cfwi.org.uk/publications/oral-maxillofacial-surgery-cfwi-medical-fact-sheet-and-summary-sheet-august-2010.

Chai, W. L. 2011. *Development of a tissue-engineered oral mucosa for the investigation of implant-soft tissue interfaces.* 2010.

Chai, W. L., Brook, I. M., Palmquist, A., Van Noort, R. & Moharamzadeh, K. 2012a. The biological seal of the implant–soft tissue interface evaluated in a tissue-engineered oral mucosal model. *Journal of the Royal Society Interface,* 9 (77)**,** pp 3528-3538.

Chai, W. L., Moharamzadeh, K., Noort, R., Emanuelsson, L., Palmquist, A. & Brook, I. M. 2013. Contour analysis of an implant–soft tissue interface. *Journal of Periodontal Research,* 48(5)**,** pp 663-670.

Chai, W. L., Moharamzadeh, K., Van Noort, R., Brook, I. M., Emanuelsson, L. & Palmquist, A. 2010. Development of a novel model for the investigation of implant- soft tissue interface. *Journal of Periodontology,* 81(8)**,** pp 1187-1195.

Chai, W. L., Van Noort, R., Moharamzadeh, K., Brook, I. M., Emanuelsson, L. & Palmquist, A. 2012b. Ultrastructural analysis of implant- soft tissue interface on a three dimensional tissue- engineered oral mucosal model. *Journal of Biomedical Materials Research Part A,* 100(2)**,** pp 269-277.

Charles, S. 2012. Gintuit cell therapy approval signals shift at US regulator. *Nature Biotechnology,* 30(6)**,** pp 479.

Che, Z. M., Jung, T. H., Choi, J. H., Yoon, D. J., Jeong, H. J., Lee, E. J. & Kim, J. 2006. Collagen-based co- culture for invasive study on cancer cells- fibroblasts interaction. *Biochemical and Biophysical Research Communications,* 346(1)**,** pp 268-275.

Chen, A. A., Tsang, V. L., Albrecht, D. R. & Bhatia, S. N. 2007. 3-D Fabrication Technology for Tissue Engineering. *In:* Ferrari, M., Desai, T. & Bhatia, S. (eds.) *BioMEMS and Biomedical Nanotechnology: Volume III Therapeutic Micro/Nanotechnology.* Boston, MA: Springer US.

Chen, F., Feng, X., Wu, W., Ouyang, H., Gao, Z., Cheng, X., Hou, R. & Mao, T. 2007. Segmental bone tissue engineering by seeding osteoblast precursor cells into titanium mesh–coral composite scaffolds. *International Journal of Oral & Maxillofacial Surgery,* 36(9)**,** pp 822-827.

Chen, H.-C. & Hu, Y.-C. 2006. Bioreactors for tissue engineering. *Biotechnology Letters,* 28(18)**,** pp 1415-1423.

Chen, H.-C. J., Chen, H.-L., Lai, J.-Y., Chen, C.-C., Tsai, Y.-J., Kuo, M.-T., Chu, P.-H., Sun, C.-C., Chen, J.-K. & Ma, D. H.-K. 2009. Persistence of transplanted oral mucosal epithelial cells in human cornea. *Investigative Ophthalmology & Visual Science,* 50(10)**,** pp 4660.

Chi, A. C., Day, T. A. & Neville, B. W. 2015. Oral cavity and oropharyngeal squamous cell carcinoma--an update. *Cancer Journal for Clinicians,* 65(5)**,** pp 401-21.

Cho, K. H., Ahn, H. T., Park, K. C., Chung, J. H., Kim, S. W., Sung, M. W., Kim, K. H., Chung, P. H., Eun, H. C. & Youn, J. I. 2000. Reconstruction of human hard- palate mucosal epithelium on de- epidermized dermis. *Journal of Dermatological Science,* 22(2)**,** pp 117-124.

Choi, H. J., Lee, J. J., Park, Y. J., Shin, J.-W., Sung, H.-J., Shin, J. W., Wu, Y. & Kim, J. K. 2016. MG- 63 osteoblast- like cell proliferation on auxetic PLGA scaffold with mechanical stimulation for bone tissue regeneration. *Biomaterials Research,* 20, pp 33.

Choi, K.-M., Seo, Y.-K., Yoon, H.-H., Song, K.-Y., Kwon, S.-Y., Lee, H.-S. & Park, J.-K. 2008. Effect of ascorbic acid on bone marrow- derived mesenchymal stem cell proliferation and differentiation. *Journal of Bioscience and Bioengineering,* 105(6)**,** pp 586-594.

Chung, J., Li, S., Stevens, M. M., Georgiou, T. & Jones, Jr. 2016. Tailoring Mechanical Properties of Sol- Gel Hybrids for Bone Regeneration through Polymer Structure. *Chemistry Of Materials,* 28(17)**,** pp 6127-6135.

Clausen, C., Hermund, N. U., Donatsky, O. & Nielsen, H. 2006. Characterization of human bone cells derived from the maxillary alveolar ridge. *Clinical Oral Implants Research,* 17(5)**,** pp 533-540.

Coelho, M. J. & Fernandes, M. H. 2000. Human bone cell cultures in biocompatibility testing. Part II: effect of ascorbic acid, β- glycerophosphate and dexamethasone on osteoblastic differentiation. *Biomaterials,* 21(11)**,** pp 1095-1102.

Colley, H. E., Hearnden, V., Jones, A. V., Weinreb, P. H., Violette, S. M., Macneil, S., Thornhill, M. H. & Murdoch, C. 2011. Development of tissue- engineered models of oral dysplasia and early invasive oral squamous cell carcinoma. *British Journal of Cancer,* 105 (10)**,** pp 1582.

Collin, P., Nefussi, J. R., Wetterwald, A., Nicolas, V., Boy-Lefevre, M. L., Fleisch, H. & Forest, N. 1992. Expression of collagen, osteocalcin, and bone alkaline phosphatase in a

mineralizing rat osteoblastic cell culture. *Calcified Tissue International,* 50(2)**,** pp 175-83.

Cooper, D. M., Matyas, J. R., Katzenberg, M. A. & Hallgrimsson, B. 2004. Comparison of microcomputed tomographic and microradiographic measurements of cortical bone porosity. *Calcified Tissue International,* 74(5)**,** pp 437-47.

Cote, A. J., McLeod, C. M., Farrell, M. J., McClanahan, P. D., Dunagin, M. C., Raj, A. & Mauck, R. L. 2016. Single-cell differences in matrix gene expression do not predict matrix deposition. *Nature Communications,* 7(10865).

Cox, S. C., Thornby, J. A., Gibbons, G. J., Williams, M. A. & Mallick, K. K. 2015. 3D printing of porous hydroxyapatite scaffolds intended for use in bone tissue engineering applications. *Materials Science and Engineering C: Materials for Biological Applications,* 47, PP 237-247.

Cubo, N., Garcia, M., del Cañizo, J. F., Velasco, D. & Jorcano, J. L. 2017. 3d bioprinting of functional human skin: production and in vivo analysis. *Biofabrication,* 9(1)**,** pp 015006.

Cunniffe, G., Gonzalez-Fernandez, T., Daly, A., Sathy, B., Jeon, O., Alsberg, E. & Kelly, D. 2017. Three- Dimensional Bioprinting of Polycaprolactone Reinforced Gene Activated Bioinks for Bone Tissue Engineering. *Tissue Engineering Part A,* 23(17-18)**,** pp 891-900.

Czekanska, E., Stoddart, M., Richards, R. G. & Hayes, J. 2012. In search of an osteoblast cell model for in vitro research. *European Cells & Materials,* 24(1-17).

Czekanska, E. M., Stoddart, M. J., Ralphs, J. R., Richards, R. G. & Hayes, J. S. 2014. A phenotypic comparison of osteoblast cell lines versus human primary osteoblasts for biomaterials testing. *Journal of Biomedical Materials Research Part A,* 102 (8)**,** pp 2636-2643.

Daculsi, G., Fellah, B. H., Miramond, T. & Durand, M. 2013b. Osteoconduction, Osteogenicity, Osteoinduction, what are the fundamental properties for a smart bone substitutes. *IRBM,* 34(4-5)**,** pp.

Datta, N., Holtorf, H. L., Sikavitsas, V. I., Jansen, J. A. & Mikos, A. G. 2005. Effect of bone extracellular matrix synthesized in vitro on the osteoblastic differentiation of marrow stromal cells. *Biomaterials,* 26(9)**,** pp 971-7.

Datta, P., Ozbolat, V., Ayan, B., Dhawan, A. & Ozbolat, I. T. 2017b. Bone tissue bioprinting for craniofacial reconstruction. *Biotechnology and Bioengineering,* 114(11)**,** pp 2424-2431.

de Luca, M., Albanese, E., Megna, M., Cancedda, R., Mangiante, P. E., Cadoni, A. & Franzi, A. T. 1990. Evidence that human oral epithelium reconstituted in vitro and transplanted onto patients with defects in the oral mucosa retains properties of the original donor site. *Transplantation,* 50(3)**,** pp 454-9.

de Peppo, G. M., Marcos-Campos, I., Kahler, D. J., Alsalman, D., Shang, L., Vunjak-Novakovic, G. & Marolt, D. 2013a. Engineering bone tissue substitutes from human induced pluripotent stem cells. *Proceedings of the National Academy of Sciences of the United States of America,* 110 (21)**,** pp 8680.

de Peppo, G. M., Sladkova, M., Sjövall, P., Palmquist, A., Oudina, K., Hyllner, J., Thomsen, P., Petite, H. & Karlsson, C. 2013b. Human Embryonic Stem Cell- Derived Mesodermal Progenitors Display Substantially Increased Tissue Formation Compared to Human Mesenchymal Stem Cells Under Dynamic Culture Conditions in a Packed Bed/ Column Bioreactor. *Tissue Engineering Part A,* 19(1-2)**,** pp 175-187.

Denhardt, D. T. & Guo, X. 1993. Osteopontin: a protein with diverse functions. *Faseb Journal,* 7(15)**,** pp 1475-82.

Denhardt, D. T. & Noda, M. 1998. Osteopontin expression and function: role in bone remodeling. *Journal Of Cellular Biochemistry,* 30-31(92-102).

Dermenoudis, S. & Missirlis, Y. F. 2010. Bioreactors in Tissue Engineering. *Advanced Engineering Materials,* 12(11)**,** pp B592-B608.

Desbois, C. & Karsenty, G. 1995. Osteocalcin cluster: implications for functional studies. *Journal Of Cellular Biochemistry,* 57(3)**,** pp 379-83.

Devine, J. G., Dettori, J. R., France, J. C., Brodt, E. & McGuire, R. A. 2012. The use of rhBMP in spine surgery: is there a cancer risk?. *Evidence-Based Spine-Care Journal,* 3(2)**,** pp 35.

Di Luca, A., Longoni, A., Criscenti, G., Mota, C., van Blitterswijk, C. & Moroni, L. 2016. Toward mimicking the bone structure: design of novel hierarchical scaffolds with a tailored radial porosity gradient. *Biofabrication,* 8(4)**,** pp 045007.

Dickson, M. A., Hahn, W., Ino, Y., Ronfard, V., Wu, J., Weinberg, R., Louis, D., Li, F. & Rheinwald, J. 2000. Human Keratinocytes That Express hTERT and Also Bypass a p16 super(INK4a)-Enforced Mechanism That Limits Life Span Become Immortal yet Retain Normal Growth and Differentiation Characteristics. *Molecular and Cellular Biology,* 20(4)**,** pp 1436-1447.

Donahue, H. J., Li, Z., Zhou, Z. & Yellowley, C. E. 2000. Differentiation of human fetal osteoblastic cells and gap junctional intercellular communication. *American journal of physiology. Cell Physiology,* 278 (2)**,** pp C315.

Dongari-Bagtzoglou, A. & Kashleva, H. 2006a. Development of a highly reproducible three-dimensional organotypic model of the oral mucosa. *Nature Protocols,* 1(4)**,** pp 2012-8.

Dongari-Bagtzoglou, A. & Kashleva, H. 2006b. Development of a novel three- dimensional in vitro model of oral Candida infection. *Microbial Pathogenesis,* 40(6)**,** pp 271-278.

Ebrahimi, A., Murali, R., Gao, K., Elliott, M. S. & Clark, J. R. 2011. The prognostic and staging implications of bone invasion in oral squamous cell carcinoma. *Cancer,* 117(19)**,** pp 4460-4467.

Edmondson, R., Broglie, J. J., Adcock, A. F. & Yang, L. 2014. Three- Dimensional Cell Culture Systems and Their Applications in Drug Discovery and Cell- Based Biosensors. *Assay and Drug Development Technologies,* 12(4)**,** pp 27-218.

Egan, P., Ferguson, S. J. & Shea, K. 2017. Design of Hierarchical Three- Dimensional Printed Scaffolds Considering Mechanical and Biological Factors for Bone Tissue Engineering. *Journal of Mechanical Design,* 139(6)**,** pp 061401-1- 061401-9.

Eggli, P. S., Muller, W. & Schenk, R. K. 1988. Porous hydroxyapatite and tricalcium phosphate cylinders with two different pore size ranges implanted in the cancellous bone of rabbits. A comparative histomorphometric and histologic study of bony ingrowth and implant substitution. *Clinical Orthopaedics and Related Research,* 232**,** pp 127-38.

Eke, P. I., Dye, B. A., Wei, L., Thornton-Evans, G. O. & Genco, R. J. 2012. Prevalence of Periodontitis in Adults in the United States: 2009 and 2010. *Journal of Dental Research,* 91(10)**,** pp 914-920.

El Ghalbzouri, A., Lamme, E. & Ponec, M. 2002. Crucial role of fibroblasts in regulating epidermal morphogenesis. *Cell Tissue Research,* 310 (2)**,** pp 189-199.

El Tamer, M. K. & Reis, R. L. 2009. Progenitor and stem cells for bone and cartilage regeneration. *Journal of Tissue Engineering and Regenerative Medicine,* 3(5)**,** pp 327-37.

Eliza Li Shan, F., Salah-Eddine, L.-C., Emily, B., Vandhana, R., Alexander, J. L., Kasper, F. K., Mary, C. F.-C., Deeksha, V., Elizabeth, G. D., Brian, A. M., Hesham, M. A., Antonios, G. M. & Joseph, A. L. 2013. Modeling Ewing sarcoma tumors in vitro with 3D scaffolds. *Proceedings of the National Academy of Sciences,* 110(16)**,** pp 6500.

Elsalanty, M. E. & Genecov, D. G. 2009. Bone grafts in craniofacial surgery. *Craniomaxillofacial Trauma & Reconstruction,* 2(3)**,** pp 125.

Enoch, S., Moseley, R., Stephens, P. & Thomas, D. W. 2008. The oral mucosa: a model of wound healing with reduced scarring. *Oral Surgery*, 1 (1), pp 11-21.

Eqtesadi, S., Motealleh, A., Pajares, A., Guiberteau, F. & Miranda, P. 2016. Improving mechanical properties of 13–93 bioactive glass robocast scaffold by poly (lactic acid) and poly (ε-caprolactone) melt infiltration. *Journal of Non-Crystalline Solids,* 432, Part A (111-119).

Fahimipour, F., Rasoulianboroujeni, M., Dashtimoghadam, E., Khoshroo, K., Tahriri, M., Bastami, F., Lobner, D. & Tayebi, L. 2017b. 3D printed TCP-based scaffold incorporating VEGF-loaded PLGA microspheres for craniofacial tissue engineering. *Dental Materials.,* 33(11)**,** pp 1205-1216.

Farzadi, A., Solati-Hashjin, M., Asadi-Eydivand, M. & Abu Osman, N. A. 2014. Effect of layer thickness and printing orientation on mechanical properties and dimensional accuracy of 3D printed porous samples for bone tissue engineering. *PLoS One,* 9(9)**,** pp e108252.

Feng, B., Jinkang, Z., Zhen, W., Jianxi, L., Jiang, C., Jian, L., Guolin, M. & Xin, D. 2011. The effect of pore size on tissue ingrowth and neovascularization in porous bioceramics of controlled architecture in vivo. *Biomedical Materials,* 6(1)**,** pp 015007.

Feng, P., Wei, P. P., Li, P., Gao, C. D., Shuai, C. J. & Peng, S. 2014. Calcium silicate ceramic scaffolds toughened with hydroxyapatite whiskers for bone tissue engineering. *Materials Characterization,* 97, pp 47-56.

Fennema, E., Rivron, N., Rouwkema, J., van Blitterswijk, C. & de Boer, J. 2013. Spheroid culture as a tool for creating 3D complex tissues. *Trends Biotechnolology,* 31(2)**,** pp 108-15.

Ferlin, K. M., Prendergast, M. E., Miller, M. L., Kaplan, D. S. & Fisher, J. P. 2016. Influence of 3D printed porous architecture on mesenchymal stem cell enrichment and differentiation. *Acta Biomaterialia,* 32, pp 161-169.

Ferracane, J. L., Giannobile, W. V., Guo, T., Li, Y., Cao, G., Zhang, Z., Chang, S., Czajka-Jakubowska, A., Nör, J. E., Clarkson, B. H. & Liu, J. 2014a. Fluorapatite- modified Scaffold on Dental Pulp Stem Cell Mineralization. *Journal of Dental Research,* 93(12)**,** pp 1290-1295.

Ferracane, J. L., Giannobile, W. V., Tevlin, R., McArdle, A., Atashroo, D., Walmsley, G. G., Senarath-Yapa, K., Zielins, E. R., Paik, K. J., Longaker, M. T. & Wan, D. C. 2014b. Biomaterials for Craniofacial Bone Engineering. *Journal of Dental Research,* 93(12)**,** pp 1187-1195.

Fischer, A. H., Jacobson, K. A., Rose, J. & Zeller, R. 2008. Hematoxylin and eosin staining of tissue and cell sections. *Cold Spring Harbor Protocols,* pdb.prot4986.

Fisher, J. P. 2013. *Tissue engineering : principles and Practices*, Boca Raton: Boca Raton : CRC Press, 2013.

Fisher, J. P., Vehof, J. W. M., Dean, D., Van Der Waerden, J. P. C. M., Holland, T. A., Mikos, A. G. & Jansen, J. A. 2002. Soft and hard tissue response to photocrosslinked poly(propylene fumarate) scaffolds in a rabbit model. *Journal of Biomedical Materials Research,* 59(3)**,** pp 547-556.

Fitzgerald, K. A., Guo, J., Tierney, E. G., Curtin, C. M., Malhotra, M., Darcy, R., amp, Amp, Apos, Brien, F. J. & Driscoll, C. M. 2015. The use of collagen- based scaffolds to simulate prostate cancer bone metastases with potential for evaluating delivery of nanoparticulate gene therapeutics. *Biomaterials,* 66, pp 53-66.

Flatley, T. J., Lynch, K. L. & Benson, M. 1983. Tissue response to implants of calcium phosphate ceramic in the rabbit spine. *Clinical Orthopaedics and Related Research,* (179)**,** pp 246-52.

Frank, S., Hirokazu, O., Cecilia, W. L., Theodore, D., Robert, L. C., John, E. T. & Eric, G. N. 1995. Identification and characterization of a fibroblast marker: FSP1. *The Journal of Cell Biology,* 130(2)**,** pp 393-405.

Franz-Odendaal, T. A., Hall, B. K. & Witten, P. E. 2006. Buried alive: how osteoblasts become osteocytes. *Developmental Dynamics,* 235(1)**,** pp 176-90.

Friedrich, J., Ebner, R. & Kunz-Schughart, L. A. 2007. Experimental anti-tumor therapy in 3-D: spheroids--old hat or new challenge? *International Journal of Radiation Biology,* 83(11-12)**,** pp 849-71.

Fu, Q., Saiz, E., Rahaman, M. N. & Tomsia, A. P. 2011. Bioactive glass scaffolds for bone tissue engineering: state of the art and future perspectives. *Materials Science & Engineering C,* 31(7)**,** pp 1245-1256.

Gaspar, D. A., Gomide, V. & Monteiro, F. J. 2012. The role of perfusion bioreactors in bone tissue engineering. *Biomatter,* 2(4)**,** pp 167.

Gehron Robey, P. 1989. The biochemistry of bone. *Endocrinology and Metabolism Clinics of North America,* 18(4)**,** pp 858-902.

Gerrits, P. O. & Horobin, R. W. 1996. Glycol Methacrylate Embedding for Light Microscopy: Basic Principles and Trouble- Shooting. *Journal of Histotechnology,* 19(4)**,** pp 297-311.

Gibbons, M. C., Foley, M. A., Cardinal, K. O. & Halloran 2013. Thinking Inside the Box: Keeping Tissue- Engineered Constructs In Vitro for Use as Preclinical Models. *Tissue Engineering Part B: Reviews,* 19(1)**,** pp 14-30.

Gilbert, S. F. 2010. *Developmental biology*, Ninth edition.: Sunderland, Massachusetts : Sinauer Associates, 2010.

Ginebra, M. P., Espanol, M., Montufar, E. B., Perez, R. A. & Mestres, G. 2010. New processing approaches in calcium phosphate cements and their applications in regenerative medicine. *Acta Biomaterialia,* 6(8)**,** pp 2863-2873.

Girod, D. A., Sykes, K., Jorgensen, J., Tawfik, O. & Tsue, T. 2009. Acellular dermis compared to skin grafts in oral cavity reconstruction. *Laryngoscope,* 119(11)**,** pp 2141-2149.

Glim, J. E., Egmond, M., Niessen, F. B., Everts, V. & Beelen, R. H. J. 2013. Detrimental dermal wound healing: What can we learn from the oral mucosa? *Wound Repair and Regeneration,* 21(5)**,** pp 648-660.

Goda, T., Shimo, T., Yoshihama, Y., Hassan, N. M., Ibaragi, S., Kurio, N., Okui, T., Honami, T., Kishimoto, K. & Sasaki, A. 2010. Bone destruction by invading oral squamous carcinoma cells mediated by the transforming growth factor-beta signalling pathway. *Anticancer Research,* 30(7)**,** pp 2615-23.

Goldstein, A. S., Juarez, T. M., Helmke, C. D., Gustin, M. C. & Mikos, A. G. 2001. Effect of convection on osteoblastic cell growth and function in biodegradable polymer foam scaffolds. *Biomaterials,* 22(11)**,** pp 1279-1288.

Gomes, R. & Resende, M. 2010. Isolation and characterization of gingival fibroblasts positive for alkaline phosphatase in patients with chronic periodontitis and drug-induced gingival hyperplasia. *Revista Odonto Ciencia,* 25(1)**,** pp 54-58.

Goudouri, O.-M., Vogel, C., Grünewald, A., Detsch, R., Kontonasaki, E. & Boccaccini, A. R. 2016. Sol– gel processing of novel bioactive Mg- containing silicate scaffolds for alveolar bone regeneration. *Journal of Biomaterials Applications,* 30 (6)**,** pp 740-749.

Greek R, Menache A. 2013. Systematic Reviews of Animal Models: Methodology versus Epistemology. *International Journal of Medical Sciences*, 10 (3), pp 206-221.

Greenbaum, D., Colangelo, C., Williams, K. & Gerstein, M. 2003. Comparing protein abundance and mRNA expression levels on a genomic scale. *Genome Biology,* 4(9), pp 117-117

Griffith, L. & Naughton, G. 2002. Tissue Engineering-- Current Challenges and Expanding Opportunities. *Science*, 295 (5557), pp1009-1010.

Grigoriadis, A. E., Petkovich, P. M., Ber, R., Aubin, J. E. & Heersche, J. N. M. 1985. Subclone heterogeneity in a clonally- derived osteoblast- like cell line. *Bone,* 6(4)**,** pp 249-256.

Gu, Z., Zhang, X., Liu, F., Yu, X., Li, L. & Xie, H. 2013. Application of strontium- doped calcium polyphosphate scaffold on angiogenesis for bone tissue engineering. *Journal of Materials Science: Materials in Medicine,* 24, (5), pp 1251–1260.

Guarino, V., Causa, F., Taddei, P., Di Foggia, M., Ciapetti, G., Martini, D., Fagnano, C., Baldini, N. & Ambrosio, L. 2008. Polylactic acid fibre- reinforced polycaprolactone scaffolds for bone tissue engineering. *Biomaterials,* 29(27)**,** pp 3662-3670.

Hadjizadeh, A., Ghasemkhah, F. & Ghasemzaie, N. 2017. Polymeric Scaffold Based Gene Delivery Strategies to Improve Angiogenesis in Tissue Engineering: A Review. *Polymer Reviews*, 57(3), pp 505-556.

Hearnden, V. 2011. Developing tissue engineered models of oral mucosa and oral cancer to study novel therapeutic and diagnostic techniques*.*

Hearnden, V., Sankar, V., Hull, K., Juras, D. V., Greenberg, M., Kerr, A. R., Lockhart, P. B., Patton, L. L., Porter, S. & Thornhill, M. H. 2012. New developments and opportunities in oral mucosal drug delivery for local and systemic disease. *Advanced Drug Delivery Reviews,* 64(1)**,** pp 16-28.

Helfrich, M. H. & Ralston, S. H. 2012. Bone Research Protocols *[electronic resource]*, Totowa, NJ: Totowa, NJ : Humana Press : Imprint: Humana Press, 2012.

Hench, L. L. & Polak, J. M. 2002. Third- generation biomedical materials. *Science (Washington),* 295(5557)**,** pp 1014.

Henrich, D., Wilhelm, K., Warzecha, J., Frank, J., Barker, J., Marzi, I. & Seebach, C. 2013. Human Endothelial- Like Differentiated Precursor Cells Maintain Their Endothelial Characteristics When Cocultured with Mesenchymal Stem Cell and Seeded onto Human Cancellous Bone. *Mediators of Inflammation*, 2013, pp 1-12.

Hewitt, C. J., Lee, K., Nienow, A. W., Thomas, R. J., Smith, M. & Thomas, C. R. 2011. Expansion of human mesenchymal stem cells on microcarriers. *Biotechnology Letters*, 33 (11), pp 2325-2335.

Hildebrand, H. C., Hakkinen, L., Wiebe, C. B. & Larjava, H. S. 2002. Characterization of organotypic keratinocyte cultures on de-epithelialized bovine tongue mucosa. *Histology and Histopathology* 17(1)**,** pp 151-63.

Hing, K. A. 2004. Bone repair in the twentyfirst century: biology, chemistry or engineering? *Philosophical Transactions of the Royal Society A: Mathematical, Physical and Engineering Sciences,* 362(1825)**,** pp 2821-2850.

Hing, K. A. 2005. Bioceramic Bone Graft Substitutes: Influence of Porosity and Chemistry. *International Journal of Applied Ceramic Technology,* 2(3)**,** pp 184-199.

Ho, M.-H., Kuo, P.-Y., Hsieh, H.-J., Hsien, T.-Y., Hou, L.-T., Lai, J.-Y. & Wang, D.-M. 2004. Preparation of porous scaffolds by using freeze- extraction and freeze- gelation methods. *Biomaterials,* 25(1)**,** pp 129-138.

Ho, S. T. & Hutmacher, D. W. 2006. A comparison of micro CT with other techniques used in the characterization of scaffolds. *Biomaterials,* 27(8)**,** pp 1362-1376.

Hofmann, A., Konrad, L., Gotzen, L., Printz, H., Ramaswamy, A. & Hofmann, C. 2003. Bioengineered human bone tissue using autogenous osteoblasts cultured on different biomatrices. *Journal of Biomedical Materials Research Part A,* 67(1)**,** pp 191-199.

Hollinger, J. O. 2005. *Bone tissue engineering*, Boca Raton, Fla.: Boca Raton, Fla. : CRC Press, 2005.

Holy, C. E., Shoichet, M. S. & Davies, J. E. 2000. Engineering three- dimensional bone tissue in vitro using biodegradable scaffolds: Investigating initial cell-seeding density and culture period. *Journal of Biomedical Materials Research,* 51(3)**,** pp 376-382.

Hong, M.-H., Kim, S.-M., Om, J.-Y., Kwon, N. & Lee, Y.-K. 2014. Seeding Cells on Calcium Phosphate Scaffolds Using Hydrogel Enhanced Osteoblast Proliferation and Differentiation. *The Journal of the Biomedical Engineering Society,* 42(7)**,** pp 1424-1435.

Hosseinkhani, H., Inatsugu, Y., Hiraoka, Y., Inoue, S. & Tabata, Y. 2005. Perfusion culture enhances osteogenic differentiation of rat mesenchymal stem cells in collagen sponge reinforced with poly(glycolic acid) fiber. *Tissue Engineering,* 11(9-10)**,** pp 1476-1488.

Huang, W., Shi, X., Ren, L., Du, C. & Wang, Y. 2010. PHBV microspheres – PLGA matrix composite scaffold for bone tissue engineering. *Biomaterials,* 31(15)**,** pp 4278-4285.

Huh, D. D., Kim, D.-H., Nam, K.-H., Smith, A. S. T., Lone, S. & Kwon, S. 2015. Biomimetic 3D Tissue Models for Advanced High-Throughput Drug Screening. *Journal of Laboratory Automation,* 20(3)**,** pp 201-215.

Hulbert, S. F., Young, F. A., Mathews, R. S., Klawitter, J. J., Talbert, C. D. & Stelling, F. H. 1970. Potential of ceramic materials as permanently implantable skeletal prostheses. *Journal of Biomedical Materials Research,* 4(3)**,** pp 433-56.

Hutmacher, D. W. 2000. Scaffolds in tissue engineering bone and cartilage. *Biomaterials,* 21(24)**,** pp 2529-2543.

Hyun-Wook, K., Sang Jin, L., In Kap, K., Carlos, K., James, J. Y. & Anthony, A. 2016. A 3D bioprinting system to produce human- scale tissue constructs with structural integrity. *Nature Biotechnology,* 34(3)**,** pp 312–319.

Ichinohe, N., Takamoto, T. & Tabata, Y. 2008. Proliferation, Osteogenic Differentiation, and Distribution of Rat Bone Marrow Stromal Cells in Nonwoven Fabrics by Different Culture Methods. *Tissue Engineering Part A,* 14(1)**,** pp 107-16.

Ilmarinen, T., Laine, J., Juuti-uusitalo, K., Numminen, J., Seppänen-suuronen, R., Uusitalo, H. & Skottman, H. 2013. Towards a defined, serum- and feeder- free culture of stratified human oral mucosal epithelium for ocular surface reconstruction. *Acta Ophthalmologica,* 91(8)**,** pp 744-750.

Inzana, J. A., Olvera, D., Fuller, S. M., Kelly, J. P., Graeve, O. A., Schwarz, E. M., Kates, S. L. & Awad, H. A. 2014. 3D printing of composite calcium phosphate and collagen scaffolds for bone regeneration. *Biomaterials,* 35(13)**,** pp 4026-4034.

Izumi, K. & Feinberg, S. E. 2002. Skin and oral mucosal substitutes. *Oral and Maxillofacial Surgery Clinics of North America,* 14(1)**,** pp 61-71.

Izumi, K., Feinberg, S. E., Iida, A. & Yoshizawa, M. 2003. Intraoral grafting of an ex vivo produced oral mucosa equivalent: a preliminary report. *International Journal of Oral & Maxillofacial Surgery,* 32(2)**,** pp 188-197.

Izumi, K., Neiva, R. F. & Feinberg, S. E. 2013. Intraoral grafting of tissue-engineered human oral mucosa. *International Journal of Oral & Maxillofacial Implants,* 28(5)**,** pp e295-303.

Izumi, K., Song, J. & Feinberg, S. E. 2004. Development of a tissue-engineered human oral mucosa: from the bench to the bed side. *Cells Tissues Organs,* 176(1-3)**,** pp 134-52.

Izumi, K., Terashi, H., Marcelo, C. L. & Feinberg, S. E. 2000. Development and Characterization of a Tissue- engineered Human Oral Mucosa Equivalent Produced in a Serum- free Culture System. *Journal of Dental Research*, 79(3), pp 798-805.

Jafari, M., Paknejad, Z., Rad, M. R., Motamedian, S. R., Eghbal, M. J., Nadjmi, N. & Khojasteh, A. 2017. Polymeric scaffolds in tissue engineering: a literature review. *Journal of Biomedical Materials Research Part B: Applied Biomaterials,* 105(2)**,** pp 431-459.

Jaiswal, N., Haynesworth, S. E., Caplan, A. I. & Bruder, S. P. 1997. Osteogenic differentiation of purified, culture- expanded human mesenchymal stem cells in vitro. *Journal of Cellular Biochemistry,* 64(2)**,** pp 295.

Jennings, L. R., Colley, H. E., Ong, J., Panagakos, F., Masters, J. G., Trivedi, H. M., Murdoch, C. & Whawell, S. 2016. Development and Characterization of In Vitro Human Oral Mucosal Equivalents Derived from Immortalized Oral Keratinocytes. *Tissue Engineering Part C: Methods,* 22(12)**,** pp 1108-1117.

Jeon, H., Lee, H. & Kim, G. 2014. A Surface- Modified Poly(ε- caprolactone) Scaffold Comprising Variable Nanosized Surface- Roughness Using a Plasma Treatment. *Tissue Engineering Part C: Methods,* 20 (12)**,** pp 951-963.

Jerry, W. S. & Woodring, E. W. 2000. The use of telomerized cells for tissue engineering. *Nature Biotechnology,* 18(1)**,** pp 22.

Jilka, R. L., Weinstein, R. S., Bellido, T., Parfitt, A. M. & Manolagas, S. C. 1998. Osteoblast Programmed Cell Death (Apoptosis): Modulation by Growth Factors and Cytokines. *Journal of Bone and Mineral Research,* 13(5)**,** pp 793-802.

Jin, G. z., Kim, T. h., Kim, J. h., Won, J. e., Yoo, S. y., Choi, S. j., Hyun, J. K. & Kim, H. w. 2013. Bone tissue engineering of induced pluripotent stem cells cultured with macrochanneled polymer scaffold. *Journal of Biomedical Materials Research Part A,* 101(5)**,** pp 1283-1291.

Jonsson, K. B., Ljunghall, S., Ljunggren, Ö., Frost, A. & Nilsson, O. 1999. Three isolation techniques for primary culture of human osteoblast- like cells. A comparison. *Acta Orthopaedica Scandinavica,* 70(4)**,** pp 365-373.

Juliano, R. & Haskill, S. 1993. Signal transduction from the extracellular- matrix. *Journal of Cell Biology*, 120(3), pp 577-585.

Jundt, G., Berghäuser, K., Termine, J. & Schulz, A. 1987. Osteonectin — a differentiation marker of bone cells. *Cell and Tissue Research,* 248(2)**,** pp 409-415.

Kabel, J., Odgaard, A., van Rietbergen, B. & Huiskes, R. 1999. Connectivity and the elastic properties of cancellous bone. *Bone,* 24(2)**,** pp 115-120.

Kahnberg, K. 2010. Treatment of bone-deficient ridges in implant rehabilitation. In: Andersson, L., Kahnberg, K., & Pogrel, M., A. 2010. Oral and Maxillofacial Surgery. Blackwell publishing Ltd.

Karageorgiou, V. & Kaplan, D. 2005. Porosity of 3D biomaterial scaffolds and osteogenesis. *Biomaterials,* 26(27)**,** pp 5474-5491.

Kartsogiannis, V. & Ng, K. W. 2004. Cell lines and primary cell cultures in the study of bone cell biology. *Molecular and Cellular Endocrinology,* 228(1)**,** pp 79-102.

Kassem, M., Ankersen, L., Eriksen, E. F., Clark, B. F. & Rattan, S. I. 1997. Demonstration of cellular aging and senescence in serially passaged long- term cultures of human trabecular osteoblasts. *Osteoporosis international,* 7(6)**,** pp 514.

Kataoka, T., Umeda, M., Shigeta, T., Takahashi, H. & Komori, T. 2010. A new in vitro model of cancer invasion using AlloDerm, a human cadaveric dermal equivalent: a preliminary report. *The Kobe journal of medical sciences,* 55(5)**,** pp E106.

Kato, H., Marcelo, C. L., Washington, J. B., Bingham, E. L. & Feinberg, S. E. 2015. Fabrication of Large Size Ex Vivo- Produced Oral Mucosal Equivalents for Clinical Application. *Tissue Engineering Part C: Methods,* 21(9)**,** pp 872-880.

Kawai, T., Shanjani, Y., Fazeli, S., Behn, A. W., Okuzu, Y., Goodman, S. B. & Yang, Y. P. 2018. Customized, degradable, functionally graded scaffold for potential treatment of early stage osteonecrosis of the femoral head. *Journal of Orthopaedic Research,* 36(3)**,** pp 1002-1011.

Kedong, S., Wenfang, L., Yanxia, Z., Hong, W., Ze, Y., Mayasari, L. & Tianqing, L. 2014. Dynamic Fabrication of Tissue- Engineered Bone Substitutes Based on Derived Cancellous Bone Scaffold in a Spinner Flask Bioreactor System. *Part A: Enzyme Engineering and Biotechnology,* 174(4)**,** pp 1331-1343.

Khademhosseini, A. & Langer, R. 2016. A decade of progress in tissue engineering. *Nature Protocols,* 11(10)**,** pp 1775-81.

Khalyfa, A., Vogt, S., Weisser, J., Grimm, G., Rechtenbach, A., Meyer, W. & Schnabelrauch, M. 2007. Development of a new calcium phosphate powder- binder system for the 3D printing of patient specific implants. *Official Journal of the European Society for Biomaterials,* 18(5)**,** pp 909-916.

Khan, F. & Tanaka, M. 2018. Designing smart biomaterials for tissue engineering. *International Journal of Molecular Sciences,* 19(1)**,** pp 1-14.

Khan, Y., Yaszemski, M., Mikos, A. & Laurencin, C. 2008. Tissue Engineering of Bone: Material and Matrix Considerations. *The Journal of Bone & Joint Surgery*, 90(1), pp 36-42.

Khodakaram-Tafti, A., Mehrabani, D. & Shaterzadeh-Yazdi, H. 2017. An overview on autologous fibrin glue in bone tissue engineering of maxillofacial surgery. *Dental Research Journal,* 14(2)**,** pp 79-86.

Khojasteh, A., Fahimipour, F., Jafarian, M., Sharifi, D., Jahangir, S., Khayyatan, F. & Baghaban Eslaminejad, M. 2017. Bone engineering in dog mandible: Coculturing mesenchymal stem cells with endothelial progenitor cells in a composite scaffold containing vascular endothelial growth factor. *Journal of Biomedical Materials Research Part B: Applied Biomaterials,* 105(7)**,** pp 1767-1777.

Khoruzhenko, A. I. 2011. 2D- and 3D- cell culture. *Biopolymers and Cell,* 27(1)**,** pp 17-24.

Kihara, T., Ito, J. & Miyake, J. 2013. Measurement of Biomolecular Diffusion in Extracellular Matrix Condensed by Fibroblasts Using Fluorescence Correlation Spectroscopy. *PLoS ONE,* 8(11)**,** pp e82382.

Kim, H. J., Kim, U.-J., Leisk, G. G., Bayan, C., Georgakoudi, I. & Kaplan, D. L. 2007. Bone regeneration on macroporous aqueous- derived silk 3- D scaffolds. *Macromolecular Bioscience,* 7(5)**,** pp 643.

Kim, J., Kang, J., Park, J., Choi, Y., Choi, K., Park, K., Baek, D., Seong, S., Min, H.-K. & Kim, H. 2009. Biological characterization of long- term cultured human mesenchymal stem cells. *Archives of Pharmacal Research,* 32(1)**,** pp 117-126.

Kim, M.-C., Hong, M.-H., Lee, B.-H., Choi, H.-J., Ko, Y.-M. & Lee, Y.-K. 2015. Bone Tissue Engineering by Using Calcium Phosphate Glass Scaffolds and the Avidin– Biotin Binding System. *The Journal of the Biomedical Engineering Society,* 43(12)**,** pp 3004-3014.

Kim, S., Kim, S.-S., Lee, S.-H., Eun Ahn, S., Gwak, S.-J., Song, J.-H., Kim, B.-S. & Chung, H.-M. 2008. In vivo bone formation from human embryonic stem cell- derived osteogenic cells in poly(d, l- lactic- co- glycolic acid)/ hydroxyapatite composite scaffolds. *Biomaterials,* 29(8)**,** pp 1043-1053.

Kinikoglu, B., Auxenfans, C., Pierrillas, P., Justin, V., Breton, P., Burillon, C., Hasirci, V. & Damour, O. 2009. Reconstruction of a full- thickness collagen- based human oral mucosal equivalent. *Biomaterials,* 30(32)**,** pp 6418-6425.

Kirk, R. G. W. 2017. Recovering the principles of humane experimental technique: The 3Rs and the human essence ofanimal research. *Science, Technology, & Human Values,* pp 1-27.

Kishimoto, Y., Saito, N., Kurita, K., Shimokado, K., Maruyama, N. & Ishigami, A. 2013. Ascorbic acid enhances the expression of type 1 and type 4 collagen and SVCT2 in cultured human skin fibroblasts. *Biochemical and Biophysical Research Communications,* 430(2)**,** pp 579-584.

Kokemueller, H., Spalthoff, S., Nolff, M., Tavassol, F., Essig, H., Stuehmer, C., Bormann, K. H., Rücker, M. & Gellrich, N. C. 2010. Prefabrication of vascularized bioartificial bone grafts in vivo for segmental mandibular reconstruction: experimental pilot study in sheep and first clinical application. *International Journal of Oral & Maxillofacial Surgery,* 39(4)**,** pp 379-387.

Kriegebaum, U., Mildenberger, M., Mueller-Richter, U. D. A., Klammert, U., Kuebler, A. C. & Reuther, T. 2012. Tissue engineering of human oral mucosa on different scaffolds: in vitro experiments as a basis for clinical applications. *Oral Surgery, Oral Medicine, Oral Pathology and Oral Radiology,* 114(5)**,** pp S190-S198.

Kuboki, Y., Takita, H., Kobayashi, D., Tsuruga, E., Inoue, M., Murata, M., Nagai, N., Dohi, Y. & Ohgushi, H. 1998. BMP- induced osteogenesis on the surface of hydroxyapatite with geometrically feasible and nonfeasible structures: Topology of osteogenesis. *Journal of Biomedical Materials Research,* 39(2)**,** pp 190-199.

Kujala, S., Ryhänen, J., Danilov, A. & Tuukkanen, J. 2003. Effect of porosity on the osteointegration and bone ingrowth of a weight- bearing nickel– titanium bone graft substitute. *Biomaterials,* 24(25)**,** pp 4691-4697.

Kwist, K., Bridges, W. & Burg, K. 2016. The effect of cell passage number on osteogenic and adipogenic characteristics of D1 cells. *Incorporating Methods in Cell Science International Journal of Cell Culture and Biotechnology,* 68(4)**,** pp 1661-1667.

Lang, N. P., Lindhe, J., Berglundh, T., Giannobile, W. V., Sanz, M., Giannobile, W. V. & Lang, N. P. 2015. *Clinical periodontology and implant dentistry*, Sixth edition.: Chichester, West Sussex, UK : Wiley Blackwell, 2015.

Langer, R. & Vacanti, J. 2016. Advances in tissue engineering. *Journal of Pediatric Surgery,* 51(1)**,** pp 8-12.

Langer, R. & Vacanti, J. P. 1993. Tissue engineering. *Science,* 260(5110)**,** pp 920-6.

Lanza, R. P., Langer, R. S., Vacanti, J. 2014. *Principles of tissue engineering*, Fourth edition.: Amsterdam : Academic Press, 2014.

Lauer, G. 1994. Autografting of feeder- cell free cultured gingival epithelium: Method and clinical application. *Journal of Cranio-Maxillofacial Surgery,* 22(1)**,** pp 18-22.

Lee, K., Choi, K. & Ouellette, M. 2004. Use of exogenous hTERT to immortalize primary human cells. *International Journal of Cell Culture and Biotechnology,* 45(1)**,** pp 33-38.

Leis, H. J., Hulla, W., Gruber, R., Huber, E., Zach, D., Gleispach, H. & Windischhofer, W. 1997. Phenotypic Heterogeneity of Osteoblast- like MC3T3- E1 Cells: Changes of Bradykinin-Induced Prostaglandin E 2 Production During Osteoblast Maturation. *Journal of Bone and Mineral Research,* 12(4)**,** pp 541-551.

Lemon, G., Reinwald, Y., White, L. J., Howdle, S. M., Shakesheff, K. M. & King, J. R. 2012. Interconnectivity analysis of supercritical CO2- foamed scaffolds. *Computer Methods and Programs in Biomedicine,* 106(3)**,** pp 139-149.

León Y León, C. A. 1998. New perspectives in mercury porosimetry. *Advances in Colloid and Interface Science,* 76, pp 341-372.

Li, L., Zhou, G., Wang, Y., Yang, G., Ding, S. & Zhou, S. 2015. Controlled dual delivery of BMP-2 and dexamethasone by nanoparticle- embedded electrospun nanofibers for the efficient repair of critical- sized rat calvarial defect. *Biomaterials,* 37, pp 218-229.

Li, M. G., Tian, X. Y. & Chen, X. B. 2009. A brief review of dispensing-based rapid prototyping techniques in tissue scaffold fabrication: role of modeling on scaffold properties prediction. *Biofabrication,* 1(3)**,** pp 032001.

Li, S., De Wijn, J. R., Li, J., Layrolle, P. & De Groot, K. 2003. Macroporous biphasic calcium phosphate scaffold with high permeability/ porosity ratio. *Tissue Engineering,* 9(3)**,** pp 535-548.

Li, W., Li, M., Chen, Y., Zhang, S. & Qi, N. 2014. Various seeding methods for tissue development of human umbilical- cord- derived mesenchymal stem cells in 3-dimensional PET matrix. *Biotechnology and Bioprocess Engineering,* 19(1)**,** pp 108-117.

Li, Y., Ma, T., Kniss, D. A., Lasky, L. C. & Yang, S. T. 2001. Effects of Filtration Seeding on Cell Density, Spatial Distribution, and Proliferation in Nonwoven Fibrous Matrices. *Biotechnology Progress,* 17(5)**,** pp 935-944.

Lian, J. B. & Stein, G. S. 1995. Development of the osteoblast phenotype: molecular mechanisms mediating osteoblast growth and differentiation. *The Iowa orthopaedic journal,* 15, pp 118-140.

Lian, J. B., Stein, G. S., Stein, J. L. & Van Wijnen, A. J. 1998. Osteocalcin gene promoter: Unlocking the secrets for regulation of osteoblast growth and differentiation. *Journal of Cellular Biochemistry,* 31**,** pp 62-72.

Lichte, P., Pape, H. C., Pufe, T., Kobbe, P. & Fischer, H. 2011. Scaffolds for bone healing: Concepts, materials and evidence. *Injury,* 42(6)**,** pp 569-573.

Lieberman, R. J., Daluiski, A. A. & Einhorn, A. T. 2002. The Role of Growth Factors in the Repair of Bone : Biology and Clinical Applications. *The Journal of Bone & Joint Surgery,* 84(6)**,** pp 1032-1044.

Linda, G. G. & Melody, A. S. 2006. Capturing complex 3D tissue physiology in vitro. *Nature Reviews Molecular Cell Biology,* 7(3)**,** pp 211.

Linh, N., Min, Y. & Lee, B.-T. 2013. Fabrication and in vitro evaluations with osteoblast-like MG-63 cells of porous hyaluronic acid-gelatin blend scaffold for bone tissue engineering applications. *Journal of Materials Science,* 48(12)**,** pp 4233-4242.

Liu, C., Shao, H., Chen, F. & Zheng, H. 2006. Rheological properties of concentrated aqueous injectable calcium phosphate cement slurry. *Biomaterials,* 27(29)**,** pp 5003-5013.

Liu, D.-M. 1997. Fabrication of hydroxyapatite ceramic with controlled porosity. *Official Journal of the European Society for Biomaterials,* 8(4)**,** pp 227-232.

Liu, J., Lamme, E. N., Steegers-Theunissen, R. P., Krapels, I. P., Bian, Z., Marres, H., Spauwen, P. H., Kuijpers-Jagtman, A. M. & Von den Hoff, J. W. 2008. Cleft palate cells can regenerate a palatal mucosa in vitro. *Journal of Dental Research,* 87(8)**,** pp 788-92.

Liu, J., Mao, J. & Chen, L. 2011. Epithelial- Mesenchymal Interactions as a Working Concept for Oral Mucosa Regeneration. *Tissue Engineering Part B: Reviews,* 17(1)**,** pp 25-31.

Llames, S., García, E., Meana, Á., Larcher, F., Del Río, M., Recuero, I., Romance, A., Peña, I. & Del Valle, Á. F. 2014. Tissue-engineered oral mucosa for mucosal reconstruction in a pediatric patient with hemifacial microsomia and ankyloglossia. *Cleft Palate-Craniofacial Journal,* 51(2)**,** pp 246-251.

Lode, A., Meissner, K., Luo, Y., Sonntag, F., Glorius, S., Nies, B., Vater, C., Despang, F., Hanke, T. & Gelinsky, M. 2014. Fabrication of porous scaffolds by three-dimensional plotting of a pasty calcium phosphate bone cement under mild conditions. *Journal of Tissue Engineering and Regenerative Medicine,* 8(9)**,** pp 682-93.

Luitaud, C., Laflamme, C., Semlali, A., Saidi, S., Grenier, G., Zakrzewski, A. & Rouabhia, M. 2007. Development of an engineering autologous palatal mucosa- like tissue for potential clinical applications. *Journal of Biomedical Materials Research Part B: Applied Biomaterials,* 83(2)**,** pp 554-561.

Lynch, S. E. 2008. Tissue engineering : applications in oral and maxillofacial surgery and periodontics, 2nd ed., Chicago ; London: Chicago ; London : Quintessence, c2008.

Ma, L., Gao, C., Mao, Z., Zhou, J., Shen, J., Hu, X. & Han, C. 2003. Collagen/chitosan porous scaffolds with improved biostability for skin tissue engineering. *Biomaterials,* 24(26)**,** pp 4833-41.

Macewen, W. 1881. Observations concerning Transplantation of Bone. Illustrated by a Case of Inter- Human Osseous Transplantation, Whereby over Two- Thirds of the Shaft of a Humerus Was Restored. *Proceedings of the Royal Society of London,* 32, pp 232-247.

Machida, J., Koshino, T., Yoshida, N., Hiruma, T., Miyagi, Y., Aoki, I., Watanabe, S., Kuchino, Y., Misugi, K. & Nagashima, Y. 1995. Establishment of Two Rat Osteosarcoma Cell Lines (YROS- 1 and YROS- 2) Induced by Radioactive Phosphorus. *Pathology - Research and Practice,* 191(5)**,** pp 478-485.

Mailhot, J. M. & Borke, J. L. 1998. An isolation and in vitro culturing method for human intraoral bone cells derived from dental implant preparation sites. *Clinical Oral Implants Research,* 9(1)**,** pp 43-50.

Malicev, E., Marolt, D., Kregar Velikonja, N., Kreft, M. E., Drobnic, M. & Rode, M. 2008. Growth and differentiation of alveolar bone cells in tissue- engineered constructs and monolayer cultures. *Biotechnology and Bioengineering,* 100(4)**,** pp 773-781.

Mandrycky, C., Wang, Z., Kim, K. & Kim, D.-H. 2016. 3D bioprinting for engineering complex tissues. *Biotechnology Advances,* 34(4)**,** pp 422-434.

Mangano, C., Piattelli, A., Mangano, A., Mangano, F., Mangano, A., Iezzi, G., Borges, F. L., Avila, S. & Shibli, J. A. 2009. Combining Scaffolds and Osteogenic Cells in Regenerative Bone Surgery: A Preliminary Histological Report in Human Maxillary Sinus Augmentation. *Clinical Implant Dentistry and Related Research,* 11, pp e92-e102.

Marolt, D., Cozin, M., Vunjak-Novakovic, G., Cremers, S. & Landesberg, R. 2012. Effects of Pamidronate on Human Alveolar Osteoblasts In Vitro. *Journal of Oral and Maxillofacial Surgery,* 70(5)**,** pp 1081-1092.

Marolt, D., Rode, M., Kregar-Velikonja, N., Jeras, M. & Knezevic, M. 2014. Primary human alveolar bone cells isolated from tissue samples acquired at periodontal surgeries exhibit sustained proliferation and retain osteogenic phenotype during in vitro expansion. *PLoS One,* 9(3)**,** pp e92969.

Martin, Y. & Vermette, P. 2005. Bioreactors for tissue mass culture: Design, characterization, and recent advances. *Biomaterials,* 26(35)**,** pp 7481-7503.

Martina, S. & Giuseppe Maria de, P. 2014. Bioreactor Systems for Human Bone Tissue Engineering. *Processes,* 2(2)**,** pp 494-525.

Martínez, M. E., del Campo, M. T., Medina, S., Sánchez, M., Sánchez-Cabezudo, M. J., Esbrit, P., Martínez, P., Moreno, I., Rodrigo, A., Garcés, M. V. & Munuera, L. 1999. Influence of Skeletal Site of Origin and Donor Age on Osteoblastic Cell Growth and Differentiation. *Calcified Tissue International,* 64(4)**,** pp 280-286.

Maruguchi, T., Maruguchi, Y., Suzuki, S., Matsuda, K., Toda, K. & Isshiki, N. 1994. A new skin equivalent: keratinocytes proliferated and differentiated on collagen sponge containing fibroblasts. *Plastic and Reconstructive Surgery,* 93(3)**,** pp 537-44.

Masrour Roudsari, J. & Mahjoub, S. 2012. Quantification and comparison of bone- specific alkaline phosphatase with two methods in normal and paget's specimens. *Caspian Journal of Internal Medicine,* 3(3)**,** pp 478.

Mastro, A. M. & Vogler, E. A. 2009. A three-dimensional osteogenic tissue model for the study of metastatic tumor cell interactions with bone. *Cancer Research,* 69(10)**,** pp 4097-100.

Masuda, I. 1996. An in vitro oral mucosal model reconstructed from human normal gingival cells. *Kōkūbyō Gakkai zasshi. The Journal of the Stomatological Society, Japan,* 63(2)**,** pp 334.

Matras, H. 1982. The use of fibrin sealant in oral and maxillofacial surgery. *Journal of Oral and Maxillofacial Surgery,* 40(10)**,** pp 617-622.

Matras, H. 1985. Fibrin seal: The state of the art. *Journal of Oral and Maxillofacial Surgery,* 43(8)**,** pp 605-611.

Matras, H., Dinges, H. P., Lassmann, H. & Mamoli, B. 1972. Suture-free interfascicular nerve transplantation in animal experiments. *Wien Med Wochenschr,* 122(37)**,** pp 517-23.

Mazzoli, A. 2013. Selective laser sintering in biomedical engineering. *Medical &Biological Engineering & Computing,* 51(3)**,** pp 245-56.

McCauley LK, Somerman MJ (2012). Mineralized tissues in oral and craniofacial science: biological principles and clinical correlates Ames, Iowa; Chichester: Wiley-Blackwell.

Mehrabanian, M. & Nasr-Esfahani, M. 2011. HA/ nylon 6,6 porous scaffolds fabricated by salt-leaching/ solvent casting technique: effect of nano- sized filler content on scaffold properties. *International Journal of Nanomedicine,* 6, pp 1651-1659.

Meinel, L., Karageorgiou, V., Fajardo, R., Snyder, B., Shinde-Patil, V., Zichner, L., Kaplan, D., Langer, R. & Vunjak-Novakovic, G. 2004. Bone Tissue Engineering Using Human Mesenchymal Stem Cells: Effects of Scaffold Material and Medium Flow. *Annals of Biomedical Engineering,* 32(1)**,** pp 112-122.

Mekala, N. K., Baadhe, R. R. & Potumarthi, R. 2014. Mass transfer aspects of 3D cell cultures in tissue engineering. *Asia Pacific Journal of Chemical Engineering,* 9(3), pp 318-329.

Melchels, F. P. W., Feijen, J. & Grijpma, D. W. 2010. A review on stereolithography and its applications in biomedical engineering. *Biomaterials,* 31(24)**,** pp 6121-6130.

Melero-Martin, J. M., Santhalingam, S. & Al-Rubeai, M. 2009. Methodology for optimal in vitro cell expansion in tissue engineering. *Advances in Biochemical Engineering/Biotechnology,* 112, pp 209-29.

Merry, K., Dodds, R., Littlewood, A. & Gowen, M. 1993. Expression of osteopontin mRNA by osteoclasts and osteoblasts in modelling adult human bone. *Journal of Cell Science. London, New York NY,* 104 (4)**,** pp 1013-1020.

Miloro, M., Ghali, G. E., Larsen, P. E., Waite, P. D. & Peterson, L. J. 2004. *Peterson's principles of oral and maxillofacial surgery. Vol. 1*, 2nd ed., Hamilton, Ont. ; London: Hamilton, Ont. ; London : B.C Decker Inc, 2004.

Miloro, M. & Kolokythas, A. 2012. *Management of complications in oral and maxillofacial surgery [electronic resource]*, Chichester: Chichester : Wiley-Blackwell, 2012.

Miret, S., De Groene, E. M. & Klaffke, W. 2006. Comparison of in vitro assays of cellular toxicity in the human hepatic cell line HepG2. *Journal of Biomolecular Screening,* 11(2)**,** pp 184-193.

Mino-Farina, N., Munoz-Guzon, F., Lopez-Pena, M., Ginebra, M. P., Del Valle-Fresno, S., Ayala, D. & Gonzalez-Cantalapiedra, A. 2009. Quantitative analysis of the resorption and osteoconduction of a macroporous calcium phosphate bone cement for the repair of a critical size defect in the femoral condyle. *Veterinary Journal,* 179(2)**,** pp 264-72.

Moharamzadeh, K., Brook, I., Noort, R., Scutt, A., Smith, K. & Thornhill, M. 2008. Development, optimization and characterization of a full-thickness tissue engineered human oral mucosal model for biological assessment of dental biomaterials. *Journal of Materials Science: Materials in Medicine,* 19(4)**,** pp 1793-1801.

Moharamzadeh, K., Brook, I. M., Van Noort, R., Scutt, A. M. & Thornhill, M. H. 2007. Tissue-engineered oral mucosa: a review of the scientific literature. *Journal of Dental Research,* 86(2)**,** pp 115-24.

Moharamzadeh, K., Colley, H., Murdoch, C., Hearnden, V., Chai, W. L., Brook, I. M., Thornhill, M. H. & MacNeil, S. 2012. Tissue- engineered Oral Mucosa. *Journal of Dental Research,* 91(7)**,** pp 642-650.

Moharamzadeh, K., Van Noort, R., Franklin, K. L. & Brook, I. M. 2009. Biologic assessment of antiseptic mouthwashes using a three- dimensional human oral mucosal model. *Journal of Periodontology,* 80(5)**,** pp 769-775.

Moharamzadeh, K. Oral mucosa tissue engineering. In: Tayebi, L. & Moharamzadeh, K. 2017. Biomaterials for oral and dental tissue engineering: Oxford: Woodhead Publishing, 2017.

Mohd-Zulhilmi, I., Kerry, H. & Andreas, F. 2014. Experimental Characterisation of Fluid Mechanics in a Spinner Flask Bioreactor. *Processes,* 2(4)**,** pp 753-772.

Molladavoodi, S., Gorbet, M., Medley, J. & Ju Kwon, H. 2013. Investigation of microstructure, mechanical properties and cellular viability of poly(L- lactic acid) tissue engineering scaffolds prepared by different thermally induced phase separation protocols. *Journal of the Mechanical Behavior of Biomedical Materials,* 17, pp 186-197.

Moore, M. J., Jabbari, E., Ritman, E. L., Lu, L., Currier, B. L., Windebank, A. J. & Yaszemski, M. J. 2004. Quantitative analysis of interconnectivity of porous biodegradable scaffolds with micro- computed tomography. *Journal of Biomedical Materials Research Part A,* 71(2)**,** pp 258-267.

Moradian-Oldak, J., Wen, H. B., Schneider, G. B. & Stanford, C. M. 2006. Tissue engineering strategies for the future generation of dental implants. *Periodontology 2000,* 41(1)**,** pp 157-176.

Motamedian, S. R., Hosseinpour, S., Ahsaie, M. G. & Khojasteh, A. 2015. Smart scaffolds in bone tissue engineering: A systematic review of literature. *World Journal of Stem Cells,* 7(3)**,** pp 657-68.

Murata, H., Tanaka, H., Taguchi, T., Shiigi, E., Mizokami, H., Sugiyama, T. & Kawai, S. 2004. Dexamethasone induces human spinal ligament derived cells toward osteogenic differentiation. *Journal of Cellular Biochemistry,* 92(4)**,** pp 715-722.

Murphy, C. M., Haugh, M. G., amp, Amp, Apos & Brien, F. J. 2010. The effect of mean pore size on cell attachment, proliferation and migration in collagen– glycosaminoglycan scaffolds for bone tissue engineering. *Biomaterials,* 31(3)**,** pp 461-466.

Murphy, W. L., Dennis, R. G., Kileny, J. L. & Mooney, D. J. 2002. Salt fusion: An approach to improve pore interconnectivity within tissue engineering scaffolds. *Tissue Engineering,* 8(1)**,** pp 43-52.

Murshed, M., Harmey, D., Millan, J., McKee, M. & Karsenty, G. 2005. Unique coexpression in osteoblasts of broadly expressed genes accounts for the spatial restriction of ECM mineralization to bone. *Genes & Development,* 19(9)**,** pp 1093-1104.

Muschler, G. F., Raut, V. P., Patterson, T. E., Wenke, J. C. & Hollinger, J. O. 2010. The design and use of animal models for translational research in bone tissue engineering and regenerative medicine. *Tissue Engineering Part B Reviews,* 16(1)**,** pp 123-45.

Mygind, T., Stiehler, M., Baatrup, A., Li, H., Zou, X., Flyvbjerg, A., Kassem, M. & Bünger, C. 2007. Mesenchymal stem cell ingrowth and differentiation on coralline hydroxyapatite scaffolds. *Biomaterials,* 28(6)**,** pp 1036-1047.

Nair, K., Gandhi, M., Khalil, S., Yan, K. C., Marcolongo, M., Barbee, K. & Sun, W. 2009. Characterization of cell viability during bioprinting processes. *Biotechnology Journal,* 4(8)**,** pp 1168-77.

Nanci, A. 2013. *Ten Cate's oral histology : development, structure, and function*, 8th ed. / Antonio Nanci., St. Louis, Mo.: St. Louis, Mo. : Elsevier, 2013.

Nakano, T., Matsugaki, A., Ishimoto, T., Todai, M., Serizawa, A., Suetoshi, R., Fujitani, W. 2014. Control of oriented extracellular matrix similar to anisotropic bone microstructure, *Materials Science Forum,* PP (72–77).

Navsaria, H. A., Myers, S. R., Leigh, I. M. & McKay, I. A. 1995. Culturing skin in vitro for wound therapy. *Trends Biotechnolology,* 13(3)**,** pp 91-100.

Nazarov, R., Jin, H.-J. & Kaplan, D. L. 2004. Porous 3- D scaffolds from regenerated silk fibroin. *Biomacromolecules,* 5(3)**,** pp 718-726.

Neufurth, M., Wang, X., Wang, S., Steffen, R., Ackermann, M., Haep, N. D., Schröder, H. C. & Müller, W. E. G. 2017. 3D printing of hybrid biomaterials for bone tissue engineering: Calcium- polyphosphate microparticles encapsulated by polycaprolactone. *Acta Biomaterialia,* 64, pp 377-388.

Neve, A., Corrado, A. & Cantatore, F. 2011. Osteoblast physiology in normal and pathological conditions. *Cell and Tissue Research,* 343(2)**,** pp 289-302.

Ng, M. H., Aminuddin, B. S., Hamizah, S., Lynette, C., Mazlyzam, A. L. & Ruszymah, B. H. I. 2009. Correlation of donor age and telomerase activity with in vitro cell growth and replicative potential for dermal fibroblasts and keratinocytes. *Journal of Tissue Viability,* 18(4)**,** pp 109-116.

Niemeyer, P., Fechner, K., Milz, S., Richter, W., Suedkamp, N. P., Mehlhorn, A. T., Pearce, S. & Kasten, P. 2010. Comparison of mesenchymal stem cells from bone marrow and adipose tissue for bone regeneration in a critical size defect of the sheep tibia and the influence of platelet- rich plasma. *Biomaterials,* 31(13)**,** pp 3572-3579.

Nims, R., Sykes, G., Cottrill, K., Ikonomi, P. & Elmore, E. 2010. Short tandem repeat profiling: part of an overall strategy for reducing the frequency of cell misidentification. *In Vitro Cellular & Developmental Biology - Animal,* 46(10)**,** pp 811-819.

Nishida, K., Yamato, M., Hayashida, Y., Watanabe, K., Yamamoto, K., Adachi, E., Nagai, S., Kikuchi, A., Maeda, N., Watanabe, H., Okano, T. & Tano, Y. 2004. Corneal Reconstruction with Tissue- Engineered Cell Sheets Composed of Autologous Oral Mucosal Epithelium. *The New England Journal of Medicine,* 351(12)**,** pp 1187-1196.

Obregon, F., Vaquette, C., Ivanovski, S., Hutmacher, D. W. & Bertassoni, L. E. 2015. Three-Dimensional Bioprinting for Regenerative Dentistry and Craniofacial Tissue Engineering. *Journal of Dental Research***,** 94, pp 143S-152S.

Offeddu, G. S., Ashworth, J. C., Cameron, R. E. & Oyen, M. L. 2015. Multi-scale mechanical response of freeze-dried collagen scaffolds for tissue engineering applications. *Journal of the Mechanical Behavior of Biomedical Materials,* 42, pp 19-25.

Ojeh, N. O., Frame, J. D. & Navsaria, H. A. 2001. In vitro characterization of an artificial dermal scaffold. *Tissue Engineering,* 7(4)**,** pp 457-72.

Okazaki, M., Yoshimura, K., Suzuki, Y. & Harii, K. 2003. Effects of subepithelial fibroblasts on epithelial differentiation in human skin and oral mucosa: heterotypically recombined organotypic culture model. *Plastic and Reconstructive Surgery,* 112(3)**,** pp 784.

Olson, J. L., Atala, A. & Yoo, J. J. 2011. Tissue Engineering: Current Strategies and Future Directions. *Chonnam Medical Journal,* 47(1)**,** pp 1-13.

Olszta, M. J., Cheng, X., Jee, S. S., Kumar, R., Kim, Y.-Y., Kaufman, M. J., Douglas, E. P. & Gower, L. B. 2007. Bone structure and formation: A new perspective. *Materials Science & Engineering R,* 58(3)**,** pp 77-116.

Orimo, H. 2010. The mechanism of mineralization and the role of alkaline phosphatase in health and disease. *Journal of Nippon Medical School,* 77(1)**,** pp 4-12.

Ortega, N., Behonick, D. J. & Werb, Z. 2004. Matrix remodeling during endochondral ossification. *Trends in Cell Biology,* 14(2)**,** pp 86-93.

Osman, N. I., Hillary, C., Bullock, A. J., Macneil, S. & Chapple, C. R. 2015. Tissue engineered buccal mucosa for urethroplasty: Progress and future directions. *Advanced Drug Delivery Reviews,* 82-83, pp 69-76.

Owen, T. A., Aronow, M., Shalhoub, V., Barone, L. M., Wilming, L., Tassinari, M. S., Kennedy, M. B., Pockwinse, S., Lian, J. B. & Stein, G. S. 1990. Progressive development of the rat osteoblast phenotype in vitro: reciprocal relationships in expression of genes associated with osteoblast proliferation and differentiation during formation of the bone extracellular matrix. *Journal of Cellular Physiology,* 143(3)**,** pp 420-30.

Ozbolat, I. T., Peng, W. & Ozbolat, V. 2016. Application areas of 3D bioprinting. *Drug Discovery Today,* 21(8)**,** pp 1257-1271.

Ozbolat, I. T. & Yin Yu, I. T. 2013. Bioprinting Toward Organ Fabrication: Challenges and Future Trends. *Biomedical Engineering, IEEE Transactions on,* 60 (3)**,** pp 691-699.

Pallua, N. & Suschek, C. V. 2010. Tissue engineering: from lab to clinic. London, Berlin: Springer.

Park, C. H., Rios, H. F., Jin, Q., Sugai, J. V., Padial-Molina, M., Taut, A. D., Flanagan, C. L., Hollister, S. J. & Giannobile, W. V. 2012. Tissue engineering bone-ligament complexes using fiber-guiding scaffolds. *Biomaterials,* 33(1)**,** pp 137-45.

Park, H. & Park, C. 2015. Fabrication of 3d Porous Silk Scaffolds by Particulate (salt/sucrose) Leaching for Bone Tissue Reconstruction. *Tissue Engineering Part A,* 21, pp S390-S390.

Pati, F., Gantelius, J. & Svahn, H. A. 2016. 3D Bioprinting of Tissue/Organ Models. *Angewandte Chemie International Edition,* 55(15)**,** pp 4650-65.

Patricia, D., Christelle, D., Brendan, B., Gerald, P., Beryl, S., Colin, D., Erica, S., Jeffrey, B., Steven, G., Caren, G., Allan, B. & Gerard, K. 1996. Increased bone formation in osteocalcin- deficient mice. *Nature,* 382(6590)**,** pp 448.

Pearce, A. I., Richards, R. G., Milz, S., Schneider, E. & Pearce, S. G. 2007. Animal models for implant biomaterial research in bone: a review. *European Cells & Materials,* 13, pp 1-10.

Peck, Y. & Wang, D. A. 2013. Three-dimensionally engineered biomimetic tissue models for in vitro drug evaluation: delivery, efficacy and toxicity. *Expert Opinion on Drug Delivery,* 10(3)**,** pp 369-83.

Peppas, N. A., Hilt, J. Z., Khademhosseini, A. & Langer, R. 2006. Hydrogels in Biology and Medicine: From Molecular Principles to Bionanotechnology. *Advanced Materials,* 18(11)**,** pp 1345-1360.

Petrovic, V., Zivkovic, P., Petrovic, D. & Stefanovic, V. 2012. Craniofacial bone tissue engineering. *Oral Surgery Oral Medicine Oral Pathology Oral Radiology,* 114(3)**,** pp E1-E9.

Peyrin, F. 2011. Evaluation of bone scaffolds by micro- CT. *Osteoporosis International,* 22(6)**,** pp 2043-2048.

Peña, I., Junquera, L. M., Llorente, S., de Villalaín, L., de Vicente, J. C. & Llames, S. 2012. Clinical outcomes after the use of complete autologous oral mucosa equivalents: preliminary cases. *Oral Surgery, Oral Medicine, Oral Pathology and Oral Radiology,* 113(5)**,** pp e4-e11.

Peña, I., Junquera, L. M., Meana, Á., García, E., García, V. & De Vicente, J. C. 2010. In vitro engineering of complete autologous oral mucosa equivalents: characterization of a novel scaffold. *Journal of Periodontal Research,* 45(3)**,** pp 375-380.

Pham, D. T., Dotchev, K. D. & Yusoff, W. A. Y. 2008. Deterioration of polyamide powder properties in the laser sintering process. *Proceedings of the Institution of Mechanical Engineers, Part C: Journal of Mechanical Engineering Science,* 222(11)**,** pp 2163-2176.

Pham, Q. P., Sharma, U. & Mikos, A. G. 2006. Electrospinning of polymeric nanofibers for tissue engineering applications: a review. *Tissue Engineering,* 12(5)**,** pp 1197-211.

Pinnock, A., Murdoch, C., Moharamzadeh, K., Whawell, S. & Douglas, C. W. I. 2014. Characterisation and optimisation of organotypic oral mucosal models to study Porphyromonas gingivalis invasion. *Microbes and Infection,* 16(4)**,** pp 310-319.

Polo-Corrales, L., Latorre-Esteves, M. & Ramirez-Vick, J. E. 2014. Scaffold design for bone regeneration. *Journal for Nanoscience and Nanotechnology,* 14(1)**,** pp 15-56.

Pradel, W. & Lauer, G. 2012. Tissue- engineered bone grafts for osteoplasty in patients with cleft alveolus. *Annals of Anatomy,* 194(6)**,** pp 545-548.

Pradel, W., Mai, R., Gedrange, T. & Lauer, G. 2008. Cell passage and composition of culture medium effects proliferation and differentiation of human osteoblast- like cells from facial bone. *Journal of physiology and pharmacology,* 59, pp 47-58.

Price, P. A., Lothringer, J. W., Baukol, S. A. & Hari Reddi, A. 1981. Developmental appearance of the vitamin K- dependent protein of bone during calcification. Analysis of mineralizing tissues in human, calf, and rat. *Journal of Biological Chemistry,* 256(8)**,** pp 3781-3784.

Przyborski, S. A. 2005. Differentiation of human embryonic stem cells after transplantation in immune-deficient mice. *Stem Cells*, 23(9), pp 1242-50.

Qi, X., Ye, J. & Wang, Y. 2008. Improved injectability and in vitro degradation of a calcium phosphate cement containing poly(lactide-co-glycolide) microspheres. *Acta Biomaterialia,* 4(6)**,** pp 1837-1845.

Qiu, K., Chen, B., Nie, W., Zhou, X., Feng, W., Wang, W., Chen, L., Mo, X., Wei, Y. & He, C. 2016. Electrophoretic Deposition of Dexamethasone- Loaded Mesoporous Silica Nanoparticles onto Poly(L- Lactic Acid)/ Poly(epsilon- Caprolactone) Composite Scaffold for Bone Tissue Engineering. *ACS Applied Materials & Interfaces,* 8(6)**,** pp 4137-4148.

Rajan, A., Eubanks, E., Edwards, S., Aronovich, S., Travan, S., Rudek, I., Wang, F., Lanis, A. & Kaigler, D. 2014. Optimized Cell Survival and Seeding Efficiency for Craniofacial Tissue

Engineering Using Clinical Stem Cell Therapy. *Stem Cells Translational Medicine,* 3(12)**,** pp 1495-1503.

Rajan, N., Habermehl, J., Cote, M. F., Doillon, C. J. & Mantovani, D. 2006. Preparation of ready-to-use, storable and reconstituted type I collagen from rat tail tendon for tissue engineering applications. *Nature Protocols,* 1(6)**,** pp 2753-8.

Rakhorst, H., Tra, W., Van Neck, J. W., Van Osch, G., Hovius, S., El Ghalbzouri, A. & Hofer, S. O. P. 2006. Fibroblasts Accelerate Culturing of Mucosal Substitutes. *Tissue Engineering,* 12(8)**,** pp 2321-2331.

Ram-Liebig, G., Bednarz, J., Stuerzebecher, B., Fahlenkamp, D., Barbagli, G., Romano, G., Balsmeyer, U., Spiegeler, M.-E., Liebig, S. & Knispel, H. 2015. Regulatory challenges for autologous tissue engineered products on their way from bench to bedside in Europe. *Advanced Drug Delivery Reviews,* 82-83, pp 181-191.

Rathbone, C. R., Guda, T., Singleton, B. M., Oh, D. S., Appleford, M. R., Ong, J. L. & Wenke, J. C. 2014. Effect of cell- seeded hydroxyapatite scaffolds on rabbit radius bone regeneration. *Journal of Biomedical Materials Research Part A*, 102(5), pp 1458-1466.

Reibel, J., Clausen, H., Dale, B. A. & Thacher, S. M. 1989. Immunohistochemical analysis of stratum corneum components in oral squamous epithelia. *Differentiation,* 41(3)**,** pp 237-244.

Rentz, T. J., Poobalarahi, F., Bornstein, P., Sage, E. H. & Bradshaw, A. D. 2007. SPARC regulates processing of procollagen I and collagen fibrillogenesis in dermal fibroblasts. *The Journal of biological chemistry,* 282(30)**,** pp 22062.

Rheinwald, J. G. & Green, H. 1975. Serial cultivation of strains of human epidermal keratinocytes: the formation of keratinizing colonies from single cells. *Cell,* 6(3)**,** pp 331-334.

Rimann, M., Bono, E., Annaheim, H., Bleisch, M. & Graf-Hausner, U. 2016. Standardized 3D Bioprinting of Soft Tissue Models with Human Primary Cells. *Journal of Laboratory Automation,* 21(4)**,** pp 496-509.

Rittel, D., Shemtov-Yona, K. & Korabi, R. 2017. Engineering Dental Implants. *Current Oral Health Reports,* 4(3)**,** pp 239-247.

Rodan, S. B., Imai, Y., Thiede, M. A., Wesolowski, G., Thompson, D., Bar-Shavit, Z., Shull, S., Mann, K. & Rodan, G. A. 1987a. Characterization of a human osteosarcoma cell line (Saos- 2) with osteoblastic properties. *Cancer research,* 47(18)**,** pp 4961.

Romberg, R. W., Werness, P. G., Riggs, B. L. & Mann, K. G. 1986. Inhibition of hydroxyapatite crystal growth by bone-specific and other calcium- binding proteins. *Biochemistry,* 25(5)**,** pp 1176.

Ronfard, V., Rives, J. M., Neveux, Y., Carsin, H. & Barrandon, Y. 2000. Long- term regeneration of human epidermis on third degree burns transplanted with autologous cultured epithelium grown on a fibrin matrix. *Transplantation,* 70(11)**,** pp 1588.

Roohani-Esfahani, S. I., Newman, P. & Zreiqat, H. 2016. Design and Fabrication of 3D printed Scaffolds with a Mechanical Strength Comparable to Cortical Bone to Repair Large Bone Defects. *Scientific Reports,* 6, pp 19468.

Roseti, L., Parisi, V., Petretta, M., Cavallo, C., Desando, G., Bartolotti, I. & Grigolo, B. 2017. Scaffolds for Bone Tissue Engineering: State of the art and new perspectives. *Materials Science & Engineering C,* 78, pp 1246-1262.

Ross, M. H. 2016. Histology : a text and atlas : with correlated cell and molecular biology. Seventh edition / Michael H. Ross, PhD, Wojciech Pawlina, MD, FAAA.; International edition.: Philadelphia : Wolters Kluwer, 2016.

Rosso, F., Marino, G., Giordano, A., Barbarisi, M., Parmeggiani, D. & Barbarisi, A. 2005. Smart materials as scaffolds for tissue engineering. *Journal of Cellular Physiology,* 203(3)**,** pp 465-470.

Rouwkema, J., Gibbs, S., Lutolf, M. P., Martin, I., Vunjak-Novakovic, G. & Malda, J. 2011. In vitro platforms for tissue engineering: implications for basic research and clinical translation. *Journal of Tissue Engineering and Regenerative Medicine,* 5(8)**,** pp e164-7.

Rouwkema, J., Rivron, N. C. & van Blitterswijk, C. A. 2008. Vascularization in tissue engineering. *Trends in Biotechnology,* 26(8)**,** pp 434-41.

Ruan, S. Q., Yan, L., Deng, J., Huang, W. L. & Jiang, D. M. 2017. Preparation of a biphase composite scaffold and its application in tissue engineering for femoral osteochondral defects in rabbits. *International Orthopaedics,* 1-10.

Rubin, C. T. & Lanyon, L. E. 1984. Regulation of bone formation by applied dynamic loads. *The Journal of Bone and Joint Surgery. American volume,* 66(3)**,** pp 397.

Russell, W. M. S. & Burch, R. L. 1959. The principles of humane experimental technique. London:Methuen.

Rutkovskiy, A., Stensløkken, K.-O. & Vaage, I. J. 2016. Osteoblast Differentiation at a Glance. *Medical Science Monitor Basic Research,* 22, pp 95-106.

Saintigny, G., Bonnard, M., Damour, O. & Collombel, C. 1993. Reconstruction of epidermis on a chitosan cross-linked collagen-GAG lattice: effect of fibroblasts. *Acta Dermato-Venereologica,* 73(3)**,** pp 175-80.

Salerno, A., Diéguez, S., Diaz-Gomez, L., Gómez-Amoza, J. L., Magariños, B., Concheiro, A., Domingo, C., Alvarez-Lorenzo, C. & García-González, C. A. 2017. Synthetic scaffolds with full pore interconnectivity for bone regeneration prepared by supercritical foaming using advanced biofunctional plasticizers. *Biofabrication,* 9(3)**,** pp 035002.

Samorezov, J. E. & Alsberg, E. 2015. Spatial regulation of controlled bioactive factor delivery for bone tissue engineering. *Advanced Drug Delivery Reviews,* 84, PP 45-67.

Sanan, A. & Haines, S. J. 1997. Repairing holes in the head: a history of cranioplasty. *Neurosurgery,* 40(3)**,** pp 588-603.

Sandberg, M. M., Aro, H. T. & Vuorio, E. I. 1993. Gene expression during bone repair. *Clinical Orthopaedics and Related Research,* 289**,** pp 292-312.

Santos, M. J. & Ventura-Junca, P. 2012. Bioethical aspects of basic research and medical applications of human stem cells. *Biological Research,* 45(3)**,** pp 317-26.

Scheller, E. L., Krebsbach, P. H. & Kohn, D. H. 2009. Tissue engineering: state of the art in oral rehabilitation. *Journal of Oral Rehabilitation,* 36(5)**,** pp 368-89.

Schmalz, G., Schweikl, H. & Hiller, K. A. 2000. Release of prostaglandin E2, IL-6 and IL-8 from human oral epithelial culture models after exposure to compounds of dental materials. *European Journal of Oral Sciences,* 108(5)**,** pp 442-8.

Schwarz, R. I. 2015. Collagen I and the fibroblast: High protein expression requires a new paradigm of post- transcriptional, feedback regulation. *Biochemistry and Biophysics Reports,* 3(38-44.

Scott, J. H. 2006. Porous scaffold design for tissue engineering. *Nature Materials,* 5(7)**,** pp 590.

Seebach, C., Henrich, D., Kaehling, C., Wilhelm, K., Tami, A., Alini, M. & Marzi, I. 2010. Endothelial Progenitor Cells and Mesenchymal Stem Cells Seeded onto beta - TCP Granules Enhance Early Vascularization and Bone Healing in a Critical- Sized Bone Defect in Rats. *Tissue Engineering, Part A: Tissue Engineering,* 16(6)**,** pp 1961-1970.

Seong, J. M., Kim, B. C., Park, J. H., Kwon, I. K., Mantalaris, A. & Hwang, Y. S. 2010. Stem cells in bone tissue engineering. *Biomedical Materials,* 5(6)**,** pp 062001.

Setzer, B., Bächle, M., Metzger, M. C. & Kohal, R. J. 2009. The gene- expression and phenotypic response of hFOB 1.19 osteoblasts to surface- modified titanium and zirconia. *Biomaterials,* 30(6)**,** pp 979-990.

Shah, N. J., Hyder, M. N., Quadir, M. A., Dorval Courchesne, N.-M., Seeherman, H. J., Nevins, M., Spector, M. & Hammond, P. T. 2014. Adaptive growth factor delivery from a polyelectrolyte coating promotes synergistic bone tissue repair and reconstruction. *Proceedings of the National Academy of Sciences of the United States of America,* 111(35)**,** pp 12847.

Shamblott, M., Axelman, J., Wang, S., Bugg, E., Littlefield, J. W., Donovan, P., Blumenthal, P. D., Huggins, G. & Gearhart, J. D. 1998. Derivation of pluripotent stem cells horn cultured human primordial germ cells. *Proceedings of the National Academy of Sciences of the United States of America,* 95(23)**,** pp 13726-13731.

Shrivats, A. R., McDermott, M. C. & Hollinger, J. O. 2014. Bone tissue engineering: state of the union. *Drug Discovery Today,* 19(6)**,** pp 781-786.

Shteyer, A., Gazit, D., Passi-Even, L., Bab, I., Majeska, R., Gronowicz, G., Lurie, A. & Rodan, G. 1986. Formation of calcifying matrix by osteosarcoma cells in diffusion chambers in vivo. *Calcified Tissue International,* 39(1)**,** pp 49-54.

Sieira Gil, R., Pagés, C. M., Díez, E. G., Llames, S., Fuertes, A. F. & Vilagran, J. L. 2015. Tissue-Engineered Oral Mucosa Grafts for Intraoral Lining Reconstruction of the Maxilla and Mandible With a Fibula Flap. *Journal of Oral and Maxillofacial Surgery,* 73(1)**,** pp 195.e1-195.e16.

Sikavitsas, V. I., Bancroft, G. & Mikos, A. 2002. Formation of three- dimensional cell/ polymer constructs for bone tissue engineering in a spinner flask and a rotating wall vessel bioreactor. *Journal of Biomedical Materials Research,* 62(1)**,** pp 136-148.

Slootweg, P. J. & Muller, H. 1989. Mandibular invasion by oral squamous cell carcinoma. *Journal of Cranio-Maxillofacial Surgery,* 17(2)**,** pp 69-74.

Smith, I. O., Liu, X. H., Smith, L. A. & Ma, P. X. 2009. Nanostructured polymer scaffolds for tissue engineering and regenerative medicine. *Wiley Interdisciplinary Reviews: Nanomedicine and Nanobiotechnology,* 1(2)**,** pp 226-36.

Sobhani, A., Rafienia, M., Ahmadian, M. & Naimi-Jamal, M.-R. 2017. Fabrication and Characterization of Polyphosphazene/ Calcium Phosphate Scaffolds Containing Chitosan Microspheres for Sustained Release of Bone Morphogenetic Protein 2 in Bone Tissue Engineering. *Tissue Engineering and Regenerative Medicine,* 14(5)**,** pp 525-538.

Southgate, J., Williams, H. K., Trejdosiewicz, L. K. & Hodges, G. M. 1987. Primary culture of human oral epithelial cells. Growth requirements and expression of differentiated characteristics. *Laboratory investigation,* 56(2)**,** pp 211-23.

Spector, M. 2002. Novel Cell- Scaffold Interactions Encountered in Tissue Engineering: Contractile Behavior of Musculoskeletal Connective Tissue Cells. *Tissue Engineering, 8(3), pp 351-357.*

Spicer, P., Young, S., Kurtis Kasper, F., Athanasiou, K. A., Mikos, A. G. & Eu-Kien Wong, M. 2014. Chapter 71 - Tissue Engineering in Oral and Maxillofacial Surgery A2 - Lanza, Robert. *In:* Langer, R. & Vacanti, J. (eds.) *Principles of Tissue Engineering (Fourth Edition).* Boston: Academic Press.

Stefanik, D., Sarin, J., Lam, T., Levin, L., Leboy, P. & Akintoye, S. 2008. Disparate osteogenic response of mandible and iliac crest bone marrow stromal cells to pamidronate. *Oral Diseases,* 14(5)**,** pp 465-471.

Story, B. J., Wagner, W. R., Gaisser, D. M., Cook, S. D. & Rust-Dawicki, A. M. 1998. In vivo performance of a modified CSTi dental implant coating. *Int J Oral Maxillofac Implants,* 13(6)**,** pp 749-57.

Sulaiman, S., Keong, T., Cheng, C., Saim, A. & Idrus, R. 2013. Tricalcium phosphate/ hydroxyapatite (TCP- HA) bone scaffold as potential candidate for the formation of tissue engineered bone. *The Indian Journal of Medical Research,* 137(6)**,** pp 1093-1101.

Sun, F., Zhou, H. & Lee, J. 2011. Various preparation methods of highly porous hydroxyapatite/polymer nanoscale biocomposites for bone regeneration. *Acta Biomaterialia,* 7(11)**,** pp 3813-3828.

Sun, J., Hou, X.-K. & Zheng, Y.-X. 2016. Restore a 9 mm diameter osteochondral defect with gene enhanced tissue engineering followed mosaicplasty in a goat model. *Acta Orthopaedica et Traumatologica Turcica,* 50(4)**,** pp 464-469.

Sutherland, R., Carlsson, J., Durand, R. & Yuhas, J. 1981. Spheroids in Cancer Research. *Cancer Research,* 41(7)**,** pp 2980-2984.

Szpalski, C., Sagebin, F., Barbaro, M. & Warren, S. M. 2013. The influence of environmental factors on bone tissue engineering. *Journal of Biomedical Materials Research Part B,* 101(4)**,** pp 663-75.

Taichman, L., Reilly, S. & Garant, P. R. 1979. In- vitro cultivation of human oral keratinocytes. *Archives of Oral Biology,* 24(5)**,** pp 335-341.

Takagi, R., Yamato, M., Murakami, D., Kondo, M., Ohki, T., Sasaki, R., Okano, T., Yamamoto, M., Namiki, H. & Nishida, K. 2011. Fabrication and validation of autologous human oral mucosal epithelial cell sheets to prevent stenosis after esophageal endoscopic submucosal dissection. *Pathobiology,* 78(6)**,** pp 311-319.

Tan, Y., Ooi, S. & Wang, L. 2014. Immunogenicity and tumorigenicity of pluripotent stem cells and their derivatives: genetic and epigenetic perspectives. *Current Stem Cell Research & Therapy,* 9(1)**,** pp 63-72.

Tarafder, S., Balla, V. K., Davies, N. M., Bandyopadhyay, A. & Bose, S. 2013. Microwave-sintered 3D printed tricalcium phosphate scaffolds for bone tissue engineering. *Journal of Tissue Engineering and Regenerative Medicine,* 7(8)**,** pp 631-41.

Tayebi, L. & Moharamzadeh, K. 2017. *Biomaterials for oral and dental tissue engineering*: Duxford, United Kingdom : Woodhead Publishing, 2017.

Teixeira, G. Q., Barrias, C. C., Lourenço, A. H. & Gonçalves, R. M. 2014. A Multicompartment Holder for Spinner Flasks Improves Expansion and Osteogenic Differentiation of Mesenchymal Stem Cells in Three- Dimensional Scaffolds. *Tissue Engineering Part C: Methods,* 20(12)**,** pp 984-993.

Tellis, B. C., Szivek, J. A., Bliss, C. L., Margolis, D. S., Vaidyanathan, R. K. & Calvert, P. 2009. Trabecular scaffolds created using micro CT guided fused deposition modeling. *Materials Science & Engineering C*, 28(1) pp 171-178.

Termine, J. D., Kleinman, H. K., Whitson, S. W., Conn, K. M., McGarvey, M. L. & Martin, G. R. 1981. Osteonectin, a bone- specific protein linking mineral to collagen. *Cell,* 26(1)**,** pp 99-105.

Tezuka, K., Sato, T., Kamioka, H., Nijweide, P. J., Tanaka, K., Matsuo, T., Ohta, M., Kurihara, N., Hakeda, Y. & Kumegawa, M. 1992. Identification of osteopontin in isolated rabbit osteoclasts. *Biochemical and Biophysical Research Communications,* 186(2)**,** pp 911-7.

Thavornyutikarn, B., Chantarapanich, N., Sitthiseripratip, K., Thouas, G. A. & Chen, Q. 2014. Bone tissue engineering scaffolding: computer- aided scaffolding techniques. *Progress in Biomaterials,* 3(2-4)**,** pp 61-102.

Thevenot, P., Nair, A., Dey, J., Yang, J. & Tang, L. 2011. Method to Analyze Three- Dimensional Cell Distribution and Infiltration in Degradable Scaffolds. *Tissue Engineering Part A,* 14(4):319-331.

Thomson, J., Itshovitz-Eldor, J., Shapiro, S. & Waknitz, M. 1998. Embryonic stem cell lines derived from human blastocysts. *Science (Washington),* 282(5391)**,** pp 1145-1147.

Tra, W. M. W., Van Neck, J. W., Hovius, S. E. R., Perez-Amodio, S. & Van Osch, G. J. V. M. 2012. Characterization of a three- dimensional mucosal equivalent: Similarities and differences with native oral mucosa. *Cells Tissues Organs,* 195(3)**,** pp 185-196.

Trombetta, J. M. & Bradshaw, A. D. 2010. SPARC/ osteonectin functions to maintain homeostasis of the collagenous extracellular matrix in the periodontal ligament. *Journal of Histochemistry and Cytochemistry,* 58(10)**,** pp 871-879.

Trombetta, R., Inzana, J., Schwarz, E., Kates, S. & Awad, H. 2017. 3D Printing of Calcium Phosphate Ceramics for Bone Tissue Engineering and Drug Delivery. *The Journal of the Biomedical Engineering Society,* 45(1)**,** pp 23-44.

Tuan, H. S. & Hutmacher, D. W. 2005. Application of micro CT and computation modeling in bone tissue engineering. *Computer-Aided Design,* 37(11)**,** pp 1151-1161.

Ueda, M., Hata, K.-I., Sumi, Y., Mizuno, H. & Niimi, A. 1998. Peri- implant soft tissue management through use of cultured mucosal epithelium. *Oral Surgery, Oral Medicine, Oral Pathology, Oral Radiology and Endodontology,* 86(4)**,** pp 393-400.

Uri, B.-D. & Nissim, B. 2011. The tumorigenicity of human embryonic and induced pluripotent stem cells. *Nature Reviews Cancer,* 11(4)**,** pp 268.

Vacanti, C. A. 2006. The history of tissue engineering. *Journal of Cellular and Molecular Medicine,* 10(3)**,** pp 569-576.

Van Den Dolder, J., Jansen, J. A. & Spauwen, P. H. M. 2003. Evaluation of various seeding techniques for culturing osteogenic cells on titanium fiber mesh. *Tissue Engineering,* 9(2)**,** pp 315-325.

Van Der Stok, J., Siebelt, M., Sandker, M., Waarsing, J. H., Verhaar, J. A. N., Jahr, H., Weinans, H., Wang, H., Leeuwenburgh, S. C. G., Amin Yavari, S. & Zadpoor, A. A. 2013. Enhanced bone regeneration of cortical segmental bone defects using porous titanium scaffolds incorporated with colloidal gelatin gels for time-and dose- controlled delivery of dual growth factors. *Tissue Engineering Part A,* 19(23-24)**,** pp 2605-2614.

Van der Worp, H. B., Howells, D. W., Sena, E. S., Porritt, M. J., Rewell, S., Collins, V. & Macleod, M. R. 2010. Can Animal Models of Disease Reliably Inform Human Studies? *PLoS Medicine,* 7(3)**,** pp e1000245.

Vanderburgh, J., Sterling, J. & Guelcher, S. 2017. 3D Printing of Tissue Engineered Constructs for In Vitro Modeling of Disease Progression and Drug Screening. *The Journal of the Biomedical Engineering Society,* 45(1)**,** pp 164-179.

Villasante, A. & Vunjak-Novakovic, G. 2015. Tissue-engineered models of human tumors for cancer research. *Expert Opinion on Drug Discovery,* 10(3)**,** pp 257-68.

Vunjak-Novakovic, G., Obradovic, B., Martin, I., Bursac, P. M., Langer, R. & Freed, L. E. 1998. Dynamic Cell Seeding of Polymer Scaffolds for Cartilage Tissue Engineering. *Biotechnology Progress,* 14(2)**,** pp 193-202.

Wagner, W., Horn, P., Castoldi, M., Diehlmann, A., Bork, S., Saffrich, R., Benes, V., Blake, J., Pfister, S., Eckstein, V. & Ho, A. D. 2008. Replicative Senescence of Mesenchymal Stem

Cells: A Continuous and Organized Process (Replicative Senescence of MSC). *PLoS ONE,* 3(5)**,** pp e2213.

Wan, Y., Wang, Y., Liu, Z., Qu, X., Han, B., Bei, J. & Wang, S. 2005. Adhesion and proliferation of OCT- 1 osteoblast- like cells on micro- and nano- scale topography structured poly(l- lactide). *Biomaterials,* 26(21)**,** pp 4453-4459.

Wang, D., Christensen, K., Chawla, K., Xiao, G., Krebsbach, P. H. & Franceschi, R. T. 1999. Isolation and characterization of MC3T3- E1 preosteoblast subclones with distinct in vitro and in vivo differentiation/ mineralization potential. *Journal of bone and mineral research : the official journal of the American Society for Bone and Mineral Research,* 14(6)**,** pp 893.

Wang, M. O., Vorwald, C. E., Dreher, M. L., Mott, E. J., Cheng, M. H., Cinar, A., Mehdizadeh, H., Somo, S., Dean, D., Brey, E. M. & Fisher, J. P. 2015. Evaluating 3D- Printed Biomaterials as Scaffolds for Vascularized Bone Tissue Engineering. *Advanced Materials,* 27(1)**,** pp 138-144.

Wang, T. W., Wu, H. C., Wang, H. Y., Lin, F. H. & Sun, J. S. 2009. Regulation of adult human mesenchymal stem cells into osteogenic and chondrogenic lineages by different bioreactor systems. *Journal of Biomedical Materials Research Part A,* 88(4)**,** pp 935-946.

Wang, Y. H., Liu, Y., Maye, P. & Rowe, D. W. 2006. Examination of Mineralized Nodule Formation in Living Osteoblastic Cultures Using Fluorescent Dyes. *Biotechnology Progress,* 22(6)**,** pp 1697-1701.

Wang, Z., Wang, Y., Farhangfar, F., Zimmer, M. & Zhang, Y. 2012. Enhanced Keratinocyte Proliferation and Migration in Co- culture with Fibroblasts (Keratinocyte Proliferation and Migration). *PLoS ONE,* 7(7)**,** pp e40951.

Weinreb, M., Shinar, D. & Rodan, G. A. 1990. Different pattern of alkaline phosphatase, osteopontin, and osteocalcin expression in developing rat bone visualized by in situ hybridization. *Journal of Bone and Mineral Research,* 5(8)**,** pp 831-42.

Wen, Y., Xun, S., Haoye, M., Baichuan, S., Peng, C., Xuejian, L., Kaihong, Z., Xuan, Y., Jiang, P. & Shibi, L. 2017. 3D printed porous ceramic scaffolds for bone tissue engineering: a review. *Biomaterials Science.,* 5(9)**,** pp 1690-1698.

Wen, B., Freilich, M., & Kuhn, L. Bone Tissue Engineering Around Dental Implants. In: Vishwakarma, A., Sharpe, P. T., Shi, S., Ramalingam, M. & Ajaykumar, V. 2015. Stem cell biology and tissue engineering in dental sciences, London : Amsterdam: London : Academic Press ; Amsterdam : Elsevier, 2015.

Wendt, D., Marsano, A., Jakob, M., Heberer, M. & Martin, I. 2003. Oscillating perfusion of cell suspensions through three- dimensional scaffolds enhances cell seeding efficiency and uniformity. *Biotechnology and Bioengineering,* 84(2)**,** pp 205-214.

Williams, D. F. 2008. On the mechanisms of biocompatibility. *Biomaterials,* 29(20)**,** pp 2941-2953.

Wu, C., Chen, M., Zheng, T. & Yang, X. 2015. Effect of surface roughness on the initial response of MC3T3-E1 cells cultured on polished titanium alloy. *Biomedical Materials and Engineering,* 26 Suppl 1(S155-64.

Xu, M., McCanna, D. J. & Sivak, J. G. 2015. Use of the viability reagent PrestoBlue in comparison with alamarBlue and MTT to assess the viability of human corneal epithelial cells. *Journal of Pharmacological and Toxicological Methods,* 71(1-7.

Yadev, N. P., Murdoch, C., Saville, S. P. & Thornhill, M. H. 2011. Evaluation of tissue engineered models of the oral mucosa to investigate oral candidiasis. *Microbial Pathogenesis,* 50(6)**,** pp 278-285.

Yang, H., Gao, L.-N., An, Y., Hu, C.-H., Jin, F., Zhou, J., Jin, Y. & Chen, F.-M. 2013. Comparison of mesenchymal stem cells derived from gingival tissue and periodontal ligament in different incubation conditions. *Biomaterials,* 34(29)**,** pp 7033-7047.

Yannas, I. V. 1992. Tissue regeneration by use of collagen- glycosaminoglycan copolymers. *Clinical Materials,* 9(3)**,** pp 179-187.

Yao, Y., Czymmek, K. J., Pazhianur, R. & Lenhoff, A. M. 2006. Three- dimensional pore structure of chromatographic adsorbents from electron tomography. *Langmuir,* 22(26)**,** pp 11148-11157.

Yarlagadda, P. K., Chandrasekharan, M. & Shyan, J. Y. 2005. Recent advances and current developments in tissue scaffolding. *Biomedical Materials and Engineering,* 15(3)**,** pp 159-77.

Yassin, M. A., Leknes, K. N., Pedersen, T. O., Xing, Z., Sun, Y., Lie, S. A., Finne-Wistrand, A. & Mustafa, K. 2015. Cell seeding density is a critical determinant for copolymer scaffolds-induced bone regeneration. *Journal of Biomedical Materials Research Part A,* 103(11)**,** pp 3649-58.

Yilgor, P., Tuzlakoglu, K., Reis, R. L., Hasirci, N. & Hasirci, V. 2009. Incorporation of a sequential BMP- 2/ BMP- 7 delivery system into chitosan- based scaffolds for bone tissue engineering. *Biomaterials,* 30(21)**,** pp 3551-3559.

Yoshizawa, M., Feinberg, S. E., Marcelo, C. L. & Elner, V. M. 2004. Ex vivo produced human conjunctiva and oral mucosa equivalents grown in a serum-free culture system. *Journal of Oral & Maxillofacial Surgery,* 62(8)**,** pp 980-8.

Yu, J., Smuga-Otto, K., Antosiewicz-Bourget, J., Frane, J. L., Thomson, J. A., Vodyanik, M. A., Slukvin, I. I., Tian, S., Nie, J., Jonsdottir, G. A., Ruotti, V. & Stewart, R. 2007. Induced pluripotent stem cell lines derived from human somatic cells. *Science,* 318(5858)**,** pp 1917-1920.

Yuan, X., Smith, R. J., Jr., Guan, H., Ionita, C. N., Khobragade, P., Dziak, R., Liu, Z., Pang, M., Wang, C., Guan, G., Andreadis, S. & Yang, S. 2016. Hybrid Biomaterial with Conjugated Growth Factors and Mesenchymal Stem Cells for Ectopic Bone Formation. *Tissue Engineering Part A,* 22(13-14)**,** pp 928-39.

Yusop, A. H., Bakir, A. A., Shaharom, N. A., Abdul Kadir, M. R. & Hermawan, H. 2012. Porous Biodegradable Metals for Hard Tissue Scaffolds: A Review. *International Journal of Biomaterials,* 2012, pp 1-10.

Zacchi, V., Soranzo, C., Cortivo, R., Radice, M., Brun, P. & Abatangelo, G. 1998. In vitro engineering of human skin- like tissue. *Journal of Biomedical Materials Research,* 40(2)**,** pp 187-194.

Zafar, M., Khurshid, Z. & Almas, K. 2015. Oral tissue engineering progress and challenges. *Tissue Engineering and Regenerative Medicine,* 12(6)**,** pp 387-397.

Zaky, S. H. & Cancedda, R. 2009. Engineering craniofacial structures: facing the challenge. *Journal of Dental Research,* 88(12)**,** pp 1077-91.

Zaulyanov, L. & Kirsner, R. 2007. A review of a bi- layered living cell treatment (Apligraf (R)) in the treatment of venous leg ulcers and diabetic foot ulcers. *Clinical interventions in aging,* 2(1), pp.93-98.

Zhang, X., Wang, J., Ren, M., Li, L., Wang, Q. & Hou, X. 2016. A novel collagen/ platelet- rich plasma (COL/ PRP) scaffold: preparation and growth factor release analysis. *International Journal for Banking, Engineering and Transplantation of Cells and Tissues Incorporating Advances in Tissue Banking,* 17(2)**,** pp 327-334.

Zhang, Y., Zhai, D., Xu, M., Yao, Q., Zhu, H., Chang, J. & Wu, C. 2017. 3d- printed bioceramic scaffolds with antibacterial and osteogenic activity. *Biofabrication,* 9(2)**,** pp 025037.

Zhao, F. & Ma, T. 2005. Perfusion bioreactor system for human mesenchymal stem cell tissue engineering: Dynamic cell seeding and construct development. *Biotechnology and Bioengineering,* 91(4)**,** pp 482-493.

Zhao, F., Wang, J., Guo, H., Liu, S. & He, W. 2015. The Effects of Surface Properties of Nanostructured Bone Repair Materials on Their Performances. *Journal of Nanomaterials,* 2015(

Zhenming, W., Zhefeng, W., William Weijia, L., Wanxin, Z., Dazhi, Y. & Songlin, P. 2017. Novel biomaterial strategies for controlled growth factor delivery for biomedical applications. *NPG Asia Materials,* 9(10)**,** pp e435.

Zhong, J.-J. 2010. Recent advances in bioreactor engineering. *Korean Journal of Chemical Engineering,* 27(4)**,** pp 1035-1041.

Zhou, C. C., Ye, X. J., Fan, Y. J., Qing, F. Z., Chen, H. J. & Zhang, X. D. 2014a. Synthesis and characterization of CaP/Col composite scaffolds for load-bearing bone tissue engineering. *Composites Part B: Engineering,* 62,242-248.

Zhou, H., Weir, M. D. & Xu, H. H. K. 2011. Effect of cell seeding density on proliferation and osteodifferentiation of umbilical cord stem cells on calcium phosphate cement- fiber scaffold. *Tissue engineering. Part A,* 17(21-22)**,** pp 2603.

Zhou, Y. F., Sae-Lim, V., Chou, A. M., Hutmacher, D. W. & Lim, T. M. 2006. Does seeding density affect in vitro mineral nodules formation in novel composite scaffolds? *Journal of Biomedical Materials Research Part A,* 78(1)**,** pp 183-193.

Zhou, Z., Buchanan, F., Mitchell, C. & Dunne, N. 2014b. Printability of calcium phosphate: calcium sulfate powders for the application of tissue engineered bone scaffolds using the 3D printing technique. *Materials science & engineering. C, Materials for biological applications,* 38, pp 1-10.

Zhou, Z., Zhou, H., Shang, Q. & Cao, Y. 2001. In- vitro cultivation of normal human oral keratinocytes. *Chinese Medical Journal,* 114(7)**,** pp 731-734.

Zizelmann, C., Schoen, R., Metzger, M. C., Schmelzeisen, R., Schramm, A., Dott, B., Bormann, K. h. & Gellrich, N. C. 2007. Bone formation after sinus augmentation with engineered bone. *Clinical Oral Implants Research,* 18(1)**,** pp 69-73.

Zohar, R., Cheifetz, S., McCulloch, C. A. & Sodek, J. 1998. Analysis of intracellular osteopontin as a marker of osteoblastic cell differentiation and mesenchymal cell migration. *European Journal Of Oral Sciences,* 106 (Suppl 1), 401-407.

Chapter 9: Appendices

Appendix I: Cell line STR profile report for OKF6-TRET-2

Core Genomic Facility
Medical School
University of Sheffield

Reference data for OKF6/TERT-2

Reference profile

from: OKF6/TERT-1

THO1	D21S11	D5S818	D13S317	D7S820	D16S539	CSFIPO	AMEL	vWA	TPOX
6,9.3		12,13	11,11	8,10	11,12	11,12	X,X	14,15	9,11

Sample data

Sample: OKF6/TERT-2

THO1	D21S11	D5S818	D13S317	D7S820	D16S539	CSFIPO	AMEL	vWA	TPOX
6,9.3	31.2,31.2	12,13	11,11	8,10	11,12	11,12	X,Y	14,15	9,11

Analysis:

Sample match to reference:	Matches reference cell line profile at 8 markers.
Comment:	The percentage match between TRET-OKF6 and the reference cell line is between 94 % - 100 %.

Appendix II: Cell line STR profile report for UPCI-SCC-090

Core Genomic Facility
Medical School
University of Sheffield

Reference data for UPCISCC090

Reference Profile

from: UPCI-SCC-090

THO1	D21S11	D5S818	D13S317	D7S820	D16S539	CSFIPO	AMEL	vWA	TPOX
7,7	29,31	11,12	11,11	9,10	12,13	11,12	X,Y	17,17	8,8

Sample data

Sample: UPCI-SCC-090

THO1	D21S11	D5S818	D13S317	D7S820	D16S539	CSFIPO	AMEL	vWA	TPOX
7,7	29,31	11,12	11,11	9,10	12,13	11,12	X,Y	17,17	8,8

Analysis:

Sample match to reference: Matches reference cell line profile at 10 markers.

Comments: UPCI-SCC-090 and the reference cell line have extremely similar STR profile. The percentage match between the two profiles is 100 % and the two cell lines cannot categorically distinguish by STR profiling.

Appendix III

Ref: STH18551/SH

Sheffield Teaching Hospitals NHS
NHS Foundation Trust

02 March 2015

Ian Brook
Charles Clifford Dental Hospital
76 Wellesley Road
Sheffield
S10 2SZ

Dear Mr Brook,

Project Authorisation
NHS Permission for Research to Commence

STH ref:	18551	
NIHR CSP ref:	N/A	
REC ref:	15/LO/0116	
MHRA ref:	CTA No: N/A	EudraCT No: N/A
Clinical Trial reg no:	N/A	
Study title:	Development of 3D tissue engineered bone-oral mucosa composite model.	
Chief Investigator:	T. Almela, University of Sheffield	
Principal Investigator:	I. Brook, University of Sheffield	
Sponsor:	Sheffield Teaching Hospital NHS Foundation Trust	
Funder:	N/A	
NIHR TARGET FPFV RECRUITMENT DATE	07 May 2015	

MANDATORY REPORTING OF RECRUITMENT
The Research Department is obliged to report study set up and recruitment performance for the Trust to NIHR and to report research activity for all studies to Trust Board. In order to meet these reporting requirements please be advised that it is now a ***mandatory*** condition of STH project authorisation that recruitment to ***all*** research studies* at STH is reported into EDGE (the Accrual Collation and Reporting Database). It is essential that recruitment is entered into EDGE ***real-time*** to enable directorates to accurately monitor performance. Please see item 2 of the 'Conditions of R&D Authorisation' for further details.

Please be informed that failure to report recruitment to EDGE may result in loss or delay in funding to the Trust and to the Directorate.

*Information regarding EDGE eligibility for reporting is detailed in the 'Conditions of R&D Authorisation'

Sheffield Teaching Hospitals NHS
NHS Foundation Trust

Study Number: STH18551

Patient Identification Number for this trial:

CONSENT FORM

Title of Project: **Development of a three-dimensional tissue engineered bone- oral mucosal composite model**

Name of Researchers: **Thafar Almela, Ian Brook, Keyvan Moharamzadeh**

Please initial all boxes

1. I confirm that I have read and understood the information sheet dated 25 November 2014 (version 1) for the above study. I have had the opportunity to consider the information, ask questions and have had these answered satisfactorily. ☐

2. I understand that my participation is voluntary and that I am free to withdraw at any time without giving any reason, without my medical care or legal rights being affected. ☐

3. I understand that relevant sections of my medical notes and data collected during the study, may be looked at by individuals from the University of Sheffield from regulatory authorities or from the NHS Trust, where it is relevant to my taking part in this research. I give permission for these individuals to have access to my records. ☐

4. I agree to take part in the above study. ☐

Name of Participant	Date	Signature
Name of Person taking consent.	Date	Signature

Consent form date of issue 25 November 2014 Consent form version number: **1**

Sheffield Teaching Hospitals NHS
NHS Foundation Trust

The University Of Sheffield.
School of Clinical Dentistry

PATIENT INFORMATION SHEET

Study title: Development of 3 Dimensional tissue engineered bone-oral mucosa composite model

Invitation:

As part of the treatment you are about to undergo, a small amount of surplus soft tissue or bone is often removed. Normally this is discarded. You are being invited to donate this tissue for use in a research project that forms part of a PhD programme for one of our students and need samples of cells to develop our laboratory models. No extra tissue will be removed and you will not be received any additional procedures. Before you decide it is important for you to understand why the research is being done and what it will involve. Please take time to read the following information carefully and discuss it with others if you wish. Ask us if there is anything that is not clear or if you would like more information. Take time to decide whether or not you wish to take part.

Background:

Tissue engineering is the use of a combination of cells, engineering materials, and suitable biochemical factors to create tissue or organ that can be used for various diagnostic and/or therapeutic applications. This could be achieved in the laboratory by creation an environment outside the living body that recapitulate the native tissue environment as closely as possible and support cells to survive and grow up.

This project is proposed to contribute in advancement of this field by creation a model comprise of hard bony and soft lining tissues. Development and optimization of such model are indispensable for understanding diverse responses of human body to drugs, chemicals,

pathogens, and environmental toxins. It is also considered far more representative than animal models which are costly, lengthy and often fail to predict human responses.

Purpose

We are developing 3 dimensional tissue model comprised of bone and oral mucosa using human cells isolated from surplus tissues and cultivated in the laboratory. We hope these new models can mimic the natural tissues and thereby it could be useful for future research work.

Why have I been asked?

You are having tissue removed during your treatment which would normally be discarded but could be used in our research.

Do I have to take part?

No, it is up to you to decide whether or not to donate your tissue. If you do decide to take part you will be given this information sheet to keep and be asked to sign a consent form. If you decide to take part you are free to withdraw at any time and without giving a reason. A decision to withdraw at any time, or a decision not to take part, will not affect the standard of care you receive.

What will happen to me if I take part?

Samples will be collected for research from tissue after it has been removed and before it is discarded. We will not be removing any tissue other than that required for your treatment. The sample may be stored at the Laboratories of Sheffield University for possible use in future projects.

What will happen to the tissue?

The vast majority of the work involved in the development of this model is basic laboratory research. Tissue specimens which are produced as a waste bi products from the oral surgical operation will be collected and transferred in a sealed container to the laboratory, and stored in a dedicated refrigerator until it will be processed within 48 hours of harvesting.

What will happen to the tissue after the research is finished?

At the end of our work, all the redundant or residual specimens will be disposed of lawfully in relation to the Human Tissue Act (2004).

What do I have to do?

You do not need to do anything other than normal pre and post-operative care.

Are there any side effects?

No

What are the possible benefits of taking part?

There is no intended clinical benefit to you from taking part in this study and the tissue you donate will be considered as a gift.

What if there is a problem?

If you are harmed by your participation in this study, there are no special compensation arrangements. If you are harmed due to someone's negligence, then you may have grounds for a legal action but you may have to pay for it. If you have any cause to complain about any aspect of the way in which you have been approached or treated during the course of this study, you can contact one of the following and you are not compromised in any way because you have taken part in a research study.

- National Health Service complaints mechanisms.
- Sheffield Teaching Hospital NHS Trust complaints procedure: contact the following person: Dr D Throssell, Medical Director, 8 Beech Hill Road, Sheffield Teaching Hospital NHS Trust.
- Patient Advice and Liaison Service (PALS) : 0114 271 2400 PST@sth.nhs.uk in person at B floor Royal Hallamshire Hospital.

Will my taking part in this study be kept confidential?

All information which is collected about you will be kept strictly confidential. Any information about you which leaves the dental hospital will be anonymous so that you cannot be recognised from it. No patient identifying details will be associated with the sample sent to the laboratory. The only data that will be requested to accompany the sample will be the date

of collection, the age and sex of the patient, the nature of tissue. In the laboratory each sample will be registered and issued with a number so that we know the date of collection, age and sex of the donor and the site of the sample.

What will happen to the results of the research study?

The results of this research project will be published in a PhD thesis format and will be kept in the Libraries of the University of Sheffield. The results will also be presented in national and international scientific meetings and may be published in scientific journals. You will not be identified in any report/publication. If you interested in this study and you wish to obtain further information about the progress or summary of results at the end of project you can contact the researcher:

Miss Thafar Almela
Department of Oral and Maxillofacial Surgery
School of Clinical Dentistry
University of Sheffield.
Email: tkalmela1@sheffield.ac.uk

Thank you for considering taking part **in this study.**

You will be given a copy of this form and a signed consent form to keep.